CFD Modelling of Liquid-Liquid Slug Flow in Capillaries for Biodiesel Production

Julieth Alejandra Figueroa Rosette

School of Chemical and Process Engineering

University of Leeds

Submitted in accordance with the requirements for the degree of

Doctor of Philosophy

December 2017

This thesis is dedicated to my parents

Sandra and Jose Hector

Acknowledgements

Above all I thank God for providing me with the opportunity to undertake this doctorate.

I would like to express my gratitude to my supervisor Dr Alan Burns for his continual support, patience and encouragement. His timely proof reading and feedback has fostered clarity of thought and development of my thesis.

My sincere thanks to Dr Kevin Hughes who contributed at early stages of the project. I would also like to extend my sincere appreciation to Dr Brandon Bennett and Dr Tariq Mahmud.

I thank my parents and family for their constant motivation and love.

I am also grateful to my office colleagues for facilitating an atmosphere conducive to study.

Thank you to Consejo Nacional de Ciencia y Tecnologia (CONACYT) for their financial support.

Finally I am privileged to have undertaken my Ph.D. at the University of Leeds which has provided all the facilities necessary for my work.

Abstract

The prediction of the hydrodynamics of immiscible liquid-liquid flow is essential for the accurate design of process intensification technologies using micro capillaries and packed bed systems. It is also very complex mainly because of the shear exerted between the phases and the inertial effects that are present. The aim of this work relies on the computational fluid dynamics (CFD) study of liquid-liquid slug flow in capillaries, offering insight on the effectiveness of monoliths and packed bed reactors in biodiesel production for process optimisation.

The main parameters for modelling slug flow in capillaries were investigated. An attempt to predict the terminal droplet velocity was developed by relating the drag force and the Reynolds number over a single droplet of different sizes dispersed in a continuous flow in a capillary. The results showed a significant effect of the film thickness and droplet length on the Stokes-coefficient suggesting predominance of Stokes flow for the conditions under study. Also, the motion of a droplet in pressure driven horizontal flow was investigated. The numerical predictions revealed a notable influence of the film thickness, slug and drop length on the droplet velocity. Moreover, the study of the interfacial forces in the limits of high and low viscosity ratios was developed using an alternative method to the Volume-of-Fluid method. The velocity and shear profiles across the two-phases were efficiently achieved and visualisations of the internal hydrodynamics structures in the continuous and dispersed phases were compared to similar studies from the literature.

Furthermore, an efficient predictive tool based on slug flow correlations from the literature was developed to calculate the film thickness,

droplet velocity and pressure drop in a capillary when the properties of the fluids and the inlet flow rates are known. The results are in good agreement with those predicted by CFD methods and with experimental data found in the literature. This tool can be useful for design purposes of technologies involving two-phase flows in capillaries. Also, it can be helpful for predicting initial conditions and input parameters in CFD models applied for two-phase flow in porous systems.

Finally, the first stage of a pressure drop model for liquid-liquid flow in porous media is proposed based on slug flow correlations. The model includes the influence of interfacial forces and inertial effects in porous media and can be further implemented to predict operating conditions of a packed bed reactor for biodiesel production.

Nomenclature

A	-	constant for Ergun Equation
B	-	constant for Ergun Equation
A_c	m^2	cross-sectional area of capillary
A_d	m^2	cross-sectional area of droplet
Ca	-	Capillary number, $Ca = \frac{\mu_c U_m}{\sigma}$
C_d	-	Drag coefficient
C_s	-	Stoke drag coefficient
C_N	-	Newton drag coefficient
D	m	capillary diameter
d_p	m	droplet diameter
D_p	m	equivalent spherical diameter
P	Pa	pressure drop
$Eö$	-	$Eö$tvos number
Ga	-	Galileo number
F_D	$kgms^{-2}$	drag force
f	-	friction factor
g	m/s^2	gravitational acceleration
$g^{'}$	m/s^2	effective gravitational force
k	m^2	permeability
k'_α	m^2	relative permeability
L	m	length
L^*	-	dimensionless length
L_s	m	slug length
L_d	m	droplet length
R	m	capillary radius
r_d	m	droplet radius

Re	-	Reynolds number, $Re = \frac{\rho_c U_m d}{\mu_c}$
S	m^2	Surface area
S_i	-	Saturation
T_i	-	Total stress tensor
Q_m	m^3/s	volumetric flow rate of two-phase
Q_d	m^3/s	volumetric flow rate of dispersed phase
Q_c	m^3/s	volumetric flow rate of continuous phase
u_i	m/s	local instantaneous velocity
u_i	m/s	interface velocity
u_m	m/s	mixture velocity
u_d	m/s	droplet velocity
u_c	m/s	slug velocity
u_r	m/s	relative velocity
u_∞	m/s	settling velocity
$\tilde{u}_s$	m/s	superficial velocity
We	-	Weber number
x	m	downstream distance
x_i	m	cartesian coordinate
X_i	$-$	characteristic function
z	m	cartesian coordinate

Greek

α	-	dispersed phase
β	-	continuous phase
r_i	-	volume fraction of phase i
δ	m	film thickness
Δ	-	Differential
ϵ	-	Void fraction
γ	-	porosity
σ	N/m	surface tension
λ	-	viscosity ratio, $\frac{\mu_c}{\mu_d}$
μ	kg/ms	dynamic viscosity
ν	m^2/s	Kinematic viscosity

θ	$^\circ$	Angle
ϕ	-	droplet effect parameter
ψ	-	fitting parameter
ρ	kg/m^3	fluid density
ρ_d	kg/m^3	density of dispersed phase
ρ_c	kg/m^3	density of continuous phase
ξ	-	fitting parameter
ε_j	-	local element coordinates
τ_i	Pa	viscous shear stress
J'_{ij}	-	Jacobian matrix
δ_α	-	Reduced saturation

Subscripts

c	continuous phase
d	dispersed/droplet phase
f	fluid
i	fluid phase
G	gas phase
L	liquid phase
m	two-phase
p	particle
s	slug
EG	Ethylene Glycol
Hex	Hexadecane
Dod	Dodecane
CFD	Computational fluid dynamics
STR	Stirred tank reactor
TBR	Trickle bed reactor
PBR	Packed bed reactor

Contents

List of Figures

Chapter 1

Introduction

The development of new technologies throughout the industrial sector to reduce energy consumption and environmental impacts has been a subject of great interest, mainly for the chemical industry which is the largest energy consuming industrial sub sector Harvey & Adam (2013).

Renewable energy technologies, such as solar energy, fuel cells, wind energy and bioenergy are identified as the most effective potential solutions to current environmental issues. Yet, the application of these sources at industrial level for fossil-based fuel replacement is still a big challenge Olabi (2013). In the bioenergy sector, the use of biofuel provides a promising way to reduce environmental impacts and the depletion of fossil resources Kralisch *et al.* (2013). This type of fuel is generally produced by biomass and composed by renewable raw material from agricultural products. Among this field, the use of biodiesel has been considered effective for its numerous advantages including good biodegradibility, non-toxicity, sulphur free properties and reduced pollutant during usage Dai *et al.* (2014); Qiao *et al.* (2016). Although biodiesel demands have increased quickly and new plants are opening around the world, there is a necessity to expand the range of feed-stock and improve process efficiency Burton (2007).

The design of new technologies for biodiesel production has been limited by the complex chemical process involved, since it requires a high level of mixing due to the immiscible nature of the reactants. This in turn increases operation costs which makes the overall process less efficient and not viable for industrial volumes.

The use of packed bed reactors (PBR's) in the mixing stage during the biodiesel process have proved a significant enhancement in biodiesel yields Santacesaria *et al.* (2011). This units offer advantages over conventional stirred tank reactors since they provide a higher interfacial area and uniform distribution of the phases involved. However, the flow behaviour in packed bed reactors is more complicated and difficult to predict when dealing with two-phase flows. Several studies have simplified this feature by representing the packed bed as an idealised porous media and where the flow distribution can be assumed similar to the flow in small capillaries.

The current work is focused on the hydrodynamic study of liquid-liquid slug flow in capillaries using CFD approach. This is motivated by the application of monolithic and packed bed reactors as an alternative mixing technology for biodiesel process optimisation. The novelty of this work relies on the development of an efficient CFD interface method for solving high surface tension two-flows in capillaries. The prediction of the main slug flow parameters such as film thickness, droplet velocity and pressure drop that are necessary for an accurate equipment design were achieved implementing a predictive tool based on slug flow correlations from the literature. Additionally, these correlations were used to develop a pressure drop model to study the case of immiscible liquid-liquid two-phase flow in porous media which subject has been less studied compared to gas-liquid flows and very little work has been reported in the literature, mainly for the prediction of biodiesel production in packed bed reactors.

1.1 General aspects of Biodiesel Production

Biodiesel is generally defined as fatty acid methyl esters (FAME) and is produced by reacting vegetable oil or animal fat with an alcohol, which is usually methanol or ethanol Ataya *et al.* (2008); Santacesaria *et al.* (2012b).

The dominant biodiesel production process is known as transesterification and the chemical reaction is described in Figure 1.1. Throughout this process, the presence of a catalyst is necessary to increase the reaction rate between the oil and the alcohol. The catalyst can be either an homogeneous type or heterogeneous catalyst (solid catalyst). Almost all worldwide commercial biodiesel

production is done using homogeneous catalyst technology, namely sodium or potassium hydroxide dissolved in methanol Boer (2009). Despite the advantages offered by this type of pathway, major drawbacks have been identified such as the removal of the catalyst from end products and the formation of secondary undesired reactions Liu *et al.* (2010); Santacesaria *et al.* (2012b). This aspect requires a pre-treatment stage and purification system to ensure a complete conversion and to avoid pollutants; therefore increasing process operation costs. Figure 1.2 shows a typical biodiesel process using a homogeneous catalyst and including an oil pre-treatment stage before the reactor and a product purification system.

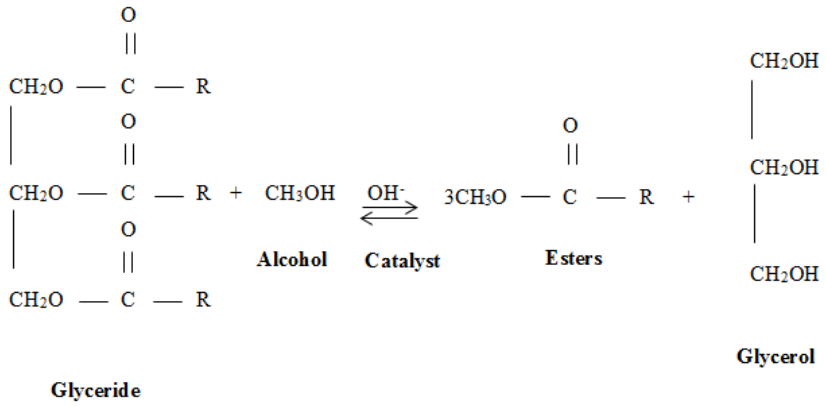

Figure 1.1: Simplified process flow chart of alkali catalysed biodiesel production Leung *et al.* (2010)

.

Across the biodiesel industry, many variations in process configuration and reactor designs have been monitored to enhance mixing between the oil and the alcohol phases. Yet, mainly conventional stirred tank reactors operating in batch or continuous mode are being used in biodiesel plants Santacesaria *et al.* (2012b). Figure 1.3 describes some of the technologies and methods used for biodiesel production.

While large amounts of biodiesel can be produced using stirred tank reactors, the performance of such units is still limited by mass transfer. The main reason for this is the variety of drop size distribution during the mixing process which affects the reaction rates at different locations in the reactor. This feature leads

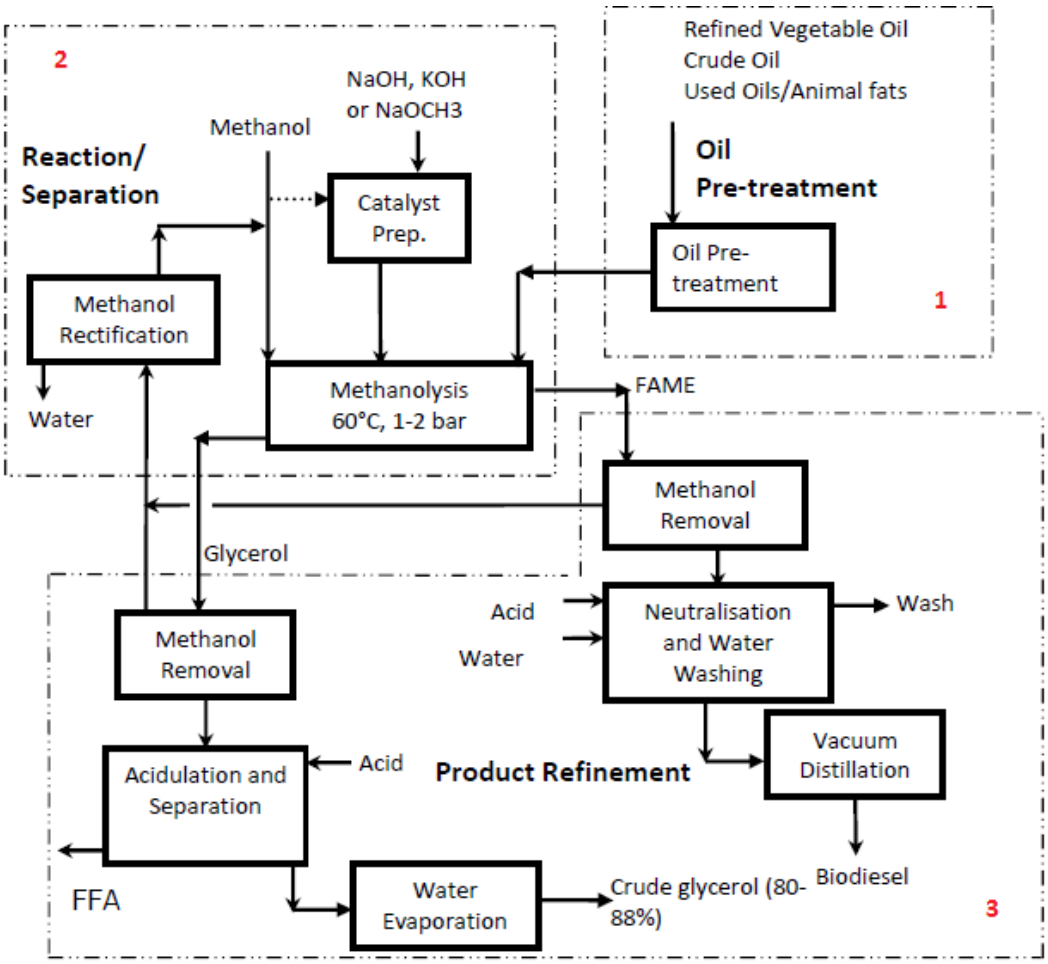

Figure 1.2: Typical Biodiesel process using alkaline homogeneous catalyst including an oil pre-treatment stage and a product purification system Boer (2009)

.

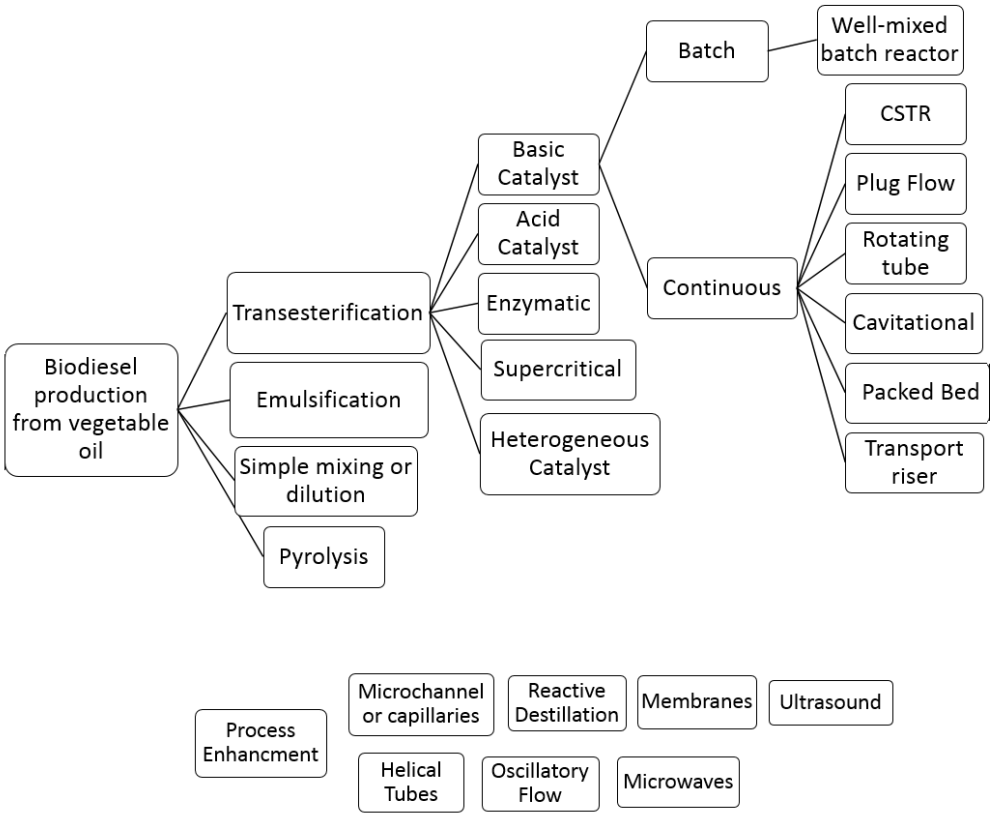

Figure 1.3: Technologies and methods used for biodiesel production found in the literature Lopez-Guajardo *et al.* (2017)

.

to a weak process control throughout the reaction and incomplete conversions to final product Jovanovic *et al.* (2010).

The cost and energy intensity related with the pre-treatment and product refinement process has led to investigate new alternatives in the production of biodiesel to make the process viable in an industrial scale. The following section describes some of the process intensification technologies recently proposed for biodiesel production.

1.2 Process Intensification Technologies

Process intensification is a new means of innovation in the chemical industry, promoting economic, environmental and social changes Harvey & Adam (2013). This technology has been developed to overcome drawbacks occurring with conventional stirred tank reactors. The main purpose is to enhance mixing between the fluids, increase reaction rates and productivity in less time and energy input Hessel *et al.* (2009). A brief summary of the process intensification technologies mainly used for biodiesel production is described below.

1.2.1 Static Mixers

Static mixers consist of a pipe or column where two immiscible liquids are introduced through two different inlets and mix as they flow through the pipe. This type of mixer for biodiesel production purposes has been only used experimentally, yet a high quality biodiesel can been obtained. Although static mixers offer the advantage of low maintenance and operating cost, very slow reaction rates are produced due to unforced molecular diffusion during the mixing process Qiu *et al.* (2010). An example of a static mixer is shown in Figure 1.4. To improve efficiency, static mixers are usually connected to other type of mixing units as they can provide a pre-mixing stage during the process Somnuk *et al.* (2013).

1.2.2 Cavitation Reactors

This type of reactor uses acoustic energy or flow energy to generate cavitation phenomena. The violent collapse of the cavities during the process are produced

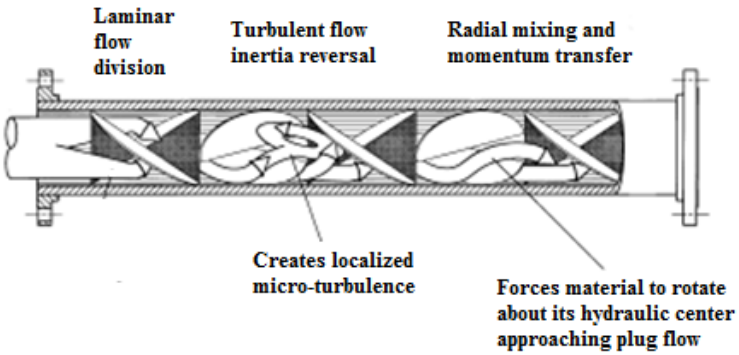

Figure 1.4: Schematic representation of a static mixer (2014 Admix, Inc)

.

by the pressure changes of the sound and flow energy. The cavitation intensifies the mass transfer rate by generating local turbulence and liquid micro circulation in the reactor. Even though fast reaction rates and mass transfer can be achieved with cavitation reactors, a precise control of the droplet size and flow distribution during operation is very difficult Qiu *et al.* (2010). Figure 1.5 shows an example of a cavitation reactor used for biodiesel production.

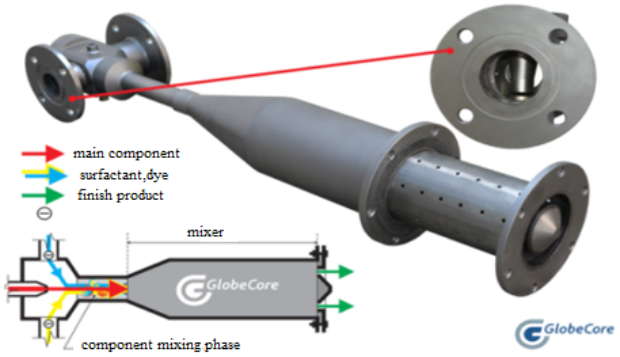

Figure 1.5: Cavitation Reactor (2010-2013 GlobeCore)

.

1.2.3 Microwave Reactors

Microwave reactors are frequently used only for small scale batch chemistry. They are units that utilise microwave irradiation to transfer energy directly into the reactants and thus accelerate the rate of chemical reaction. The advantage of microwave irradiation is its ability to heat the reactants to the required temperature more efficiently. For instance, Barnard *et al.* (2007) achieved continuous-flow preparation of biodiesel using a commercially available microwave apparatus able to produce approximately 6.1 Litres of biodiesel per minute with attainment of 99% conversion. Also, Anan & Danisman (2007) studied biodiesel production in microwave reactors and reported yields greater than 97 % with reaction times less than 2 minutes resulting more energy efficient than the conventional synthesis of biodiesel in large tank reactors. A schematic representation of a microwave reactor is shown in Figure 1.6.

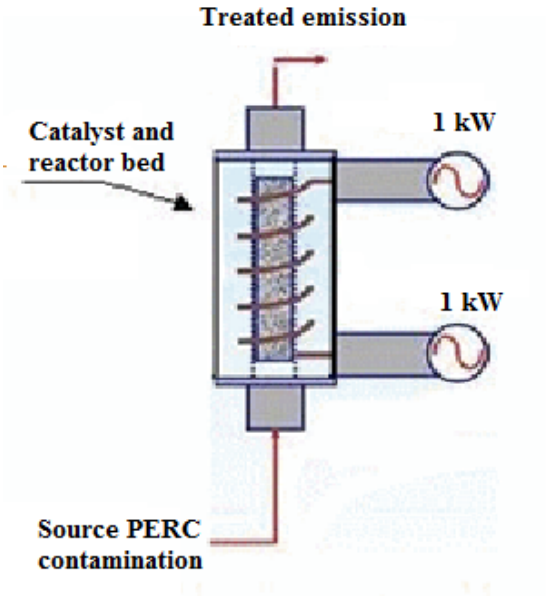

Figure 1.6: Two-KW Microwave Reactor (Chesner Engineering P.C.)

.

1.2.4 Rotating Reactors

This technology consists of an inner tube rotating rapidly within another concentric stationary tube. The reactants are introduced and mixed in the annular gap between the two tubes as shown in Figure 1.7. The two liquids are mixed instantaneously due to the high shear rate generated while moving through the thin gap and where Couette flow is induced. The thin film presents a very large interfacial contact area which enhances the reaction rate between the fluids.

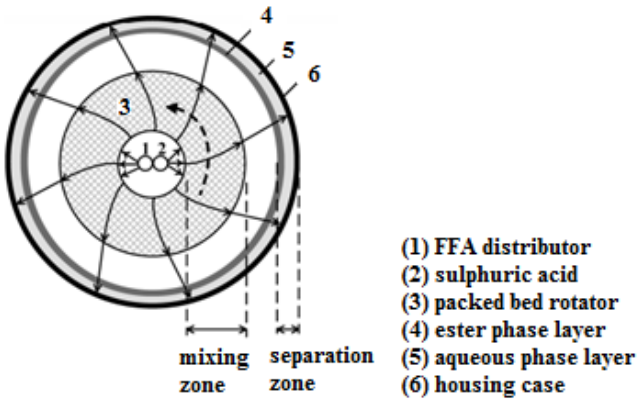

Figure 1.7: Schematic of flow pattern inside a rotating packed bed reactor Chen *et al.* (2010)

.

1.2.5 Membrane Reactors

Membrane reactors combine the separation process and the reaction into a single process. These types of reactors appear to be an excellent option to produce high purity biodiesel since the membrane role is to retain unreacted species and possible undesired secondary products. This allows the flow only of fatty methyl esters (FAME) through the pores hence a high quality product can be obtained. Dub *et al.* (2007) conducted experiments to produce biodiesel from canola oil in a 300 mL membrane reactor with a pore size of 0.05 μm and a controlled pressure at 138 kPa between the permeation side and reaction side of the membrane. The

results demonstrated the ability of the membrane reactor in removing unreacted oil from the product yielding high purity biodiesel. Although the advantages of using membrane reactors for biodiesel production, this technology is still running under non-optimal conditions for commercial operation Qiu *et al.* (2010); Shuit *et al.* (2012). A schematic of a membrane reactor used for biodiesel production is shown in Figure 1.8.

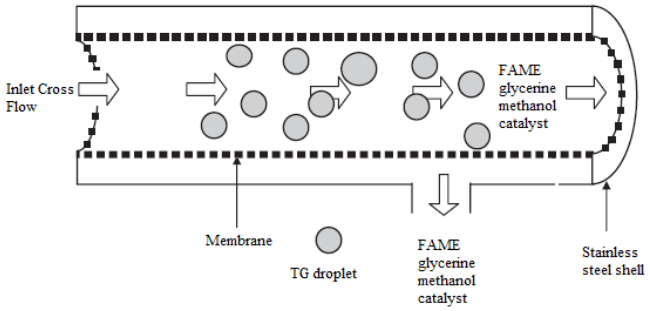

Figure 1.8: Membrane Reactor schematic for biodiesel production Cao *et al.* (2008)

.

1.2.6 Reactive Distillation

This unit operation combines the chemical reaction and product separation in one stage. Briefly, an upward flowing methanol vapour stream is used as an agitator in the reactant mixture, providing uniform mixing while it flows in the form of bubbles through the liquid phase on each plate. The main advantage of reactive distillation is the continuous in-situ product removal offering short reaction times and high productivity. Also, no excess of alcohol is required due to the equilibrium control in each plate of the system and low capital costs since no additional separation unit is required Omota *et al.* (2003); Qiu *et al.* (2010). An illustrative description of this type of technology is depicted in Figure 1.9.

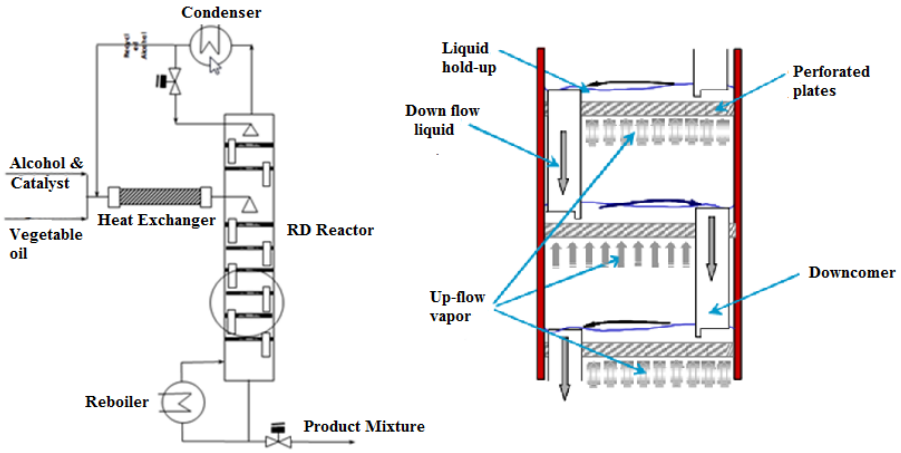

Figure 1.9: Reactive Distillation Reactor for Biodiesel production He *et al.* (2006)

.

1.2.7 Centrifugal Contactors

Centrifugal contactors involve a mixing zone where the reaction takes place and a separation zone to obtain the desired product. High yields of biodiesel can be achieved (95-96%) using centrifugal contactors, however, the intensity of the mixing and residence time inside these units is still low Kraai *et al.* (2008). Figure 1.10 shows a typical centrifugal contactor for biodiesel production.

1.2.8 Microchannel Reactors

Micro channel reactors or micro reactors are an attractive new tool for chemical engineers offering advantages over traditional reaction systems. The main characteristic of this technology is the high surface to volume ratio, which improves heat and mass transfer rates significantly Kashid *et al.* (2012). Also, an accurate process control within the system can be achieved minimising possible side reactions and generation of unstable species during the reaction process. This type of reactor can be easily scale up by increasing the number of parallel operating units which guarantees the same optimal operation during the development of the process at small scale Harvey & Adam (2013). A schematic representation of a biodiesel micro reactor is shown in Figure 1.11.

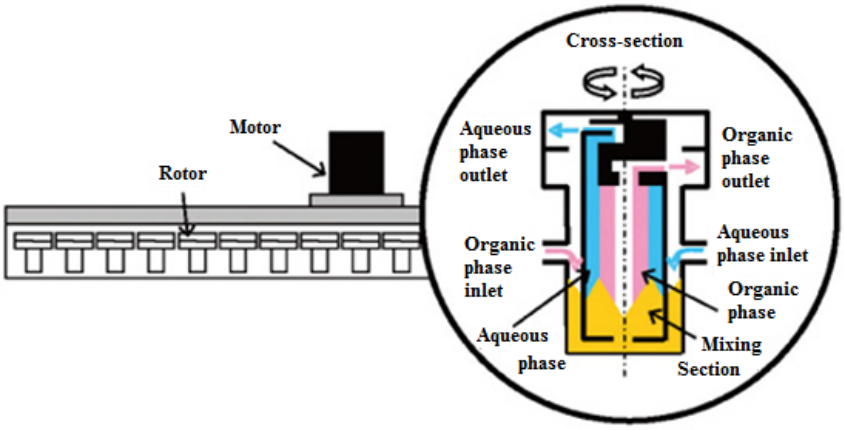

Figure 1.10: Centrifugal Contactor Nakahara & Sano (2009)

.

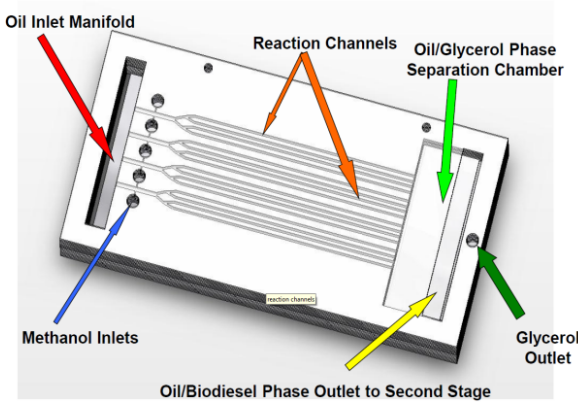

Figure 1.11: Single Stage of biodiesel microreactor (Jovanovic, 2009) Oregon State University.

1.2.9 Monolithic Reactors

Monoliths have been considered the most satisfactory structured reactors, since they provide an excellent activity and selectivity during operation Kreutzer *et al.* (2005). A monolithic reactor consist of structured arrays of parallel small channels and normally operating in the slug flow regime. A schematic representation of a monolithic reactor is shown in Figure 1.12. These units usually provide a high catalytic surface concentration and the pressure drop is very low making these systems easy to scale up and to achieve an accurate process control during operation Akbar & Ghiaasiaan (2006). However, major limitations with the mass and heat transfer have been identified due to laminar flow operation and no interconnectivity between the channels Jacob A. Moulijnn & Kapeteijn (2003).

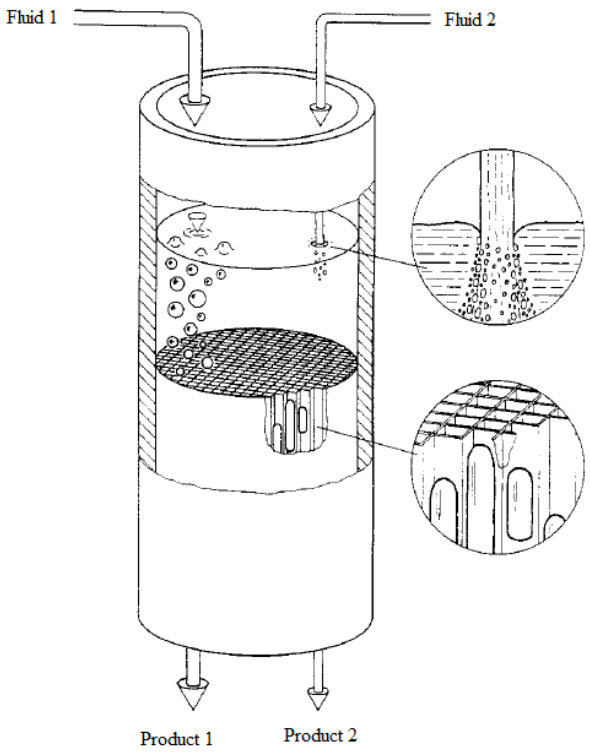

Figure 1.12: Schematic representation of a Monolithic Reactor Reinecke & Mewes (1997)

1.2.10 Packed Bed Reactors

Packed bed reactors have been recognised as the principal systems in the industry since they provide a high contact between the phases and a high conversion of the reactants can be achieved Rase (1990). Despite the existence of new types of reactors, packed bed reactors are widely used for large scale processing in petroleum industry and basic chemical industry Qiao *et al.* (2016).

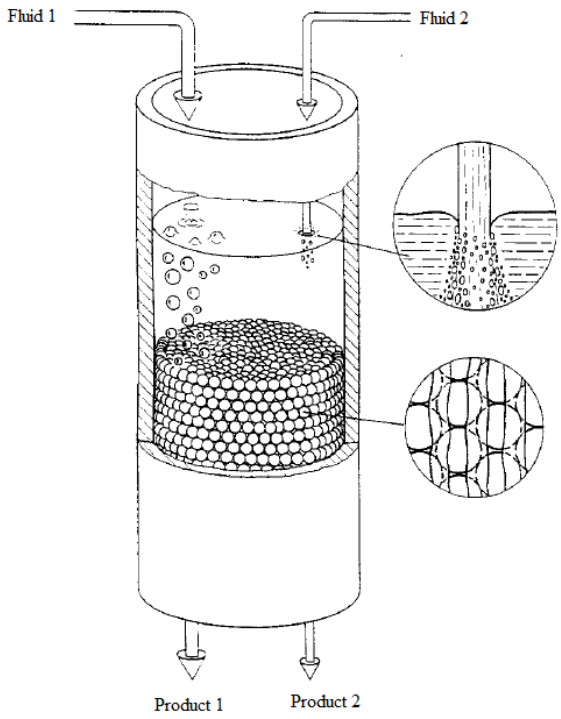

Figure 1.13: Packed Bed ReactorReinecke & Mewes (1997)

.

Packed bed reactors consist of a bed of solid spheres or pellets with the same or different diameter and random distribution inside the vessel as illustrated in Figure 1.13. The solid material can be used for two main purposes: a) to enhance mixing and area of contact between the fluid phases travelling through the void spaces formed by the random packing, b) as a solid fixed catalyst to promote a faster reaction between the fluids entering the system in addition to the high level

of mixing that can be achieved through the packed bed. An experimental study by Santacesaria *et al.* (2011), demonstrated high conversions of immiscible liquids within a short residence time in a tubular reactor filled with spheres. However, the complex flow dynamics occurring through the packed bed leads to inaccurate predictions of the pressure drop and difficulties on the characterisation of the flow regimes along the packed bed Kreutzer *et al.* (2005). Table 1.1 summarises the performance of the process intensification technologies recently used for biodiesel production.

Table 1.1: Process Intensification Technologies for biodiesel production Qiu *et al.* (2010)

Technology	Residence Time	Energy efficiency (g/J)	Current Status
Static mixer	30 min	14.9-384	Lab scale
Microchannel reactor	28 s -several minutes	0.018	Lab scale
Oscillatory flow reactor	30 min	1×10^{-4} to $2 \times 10^{-}4$	Pilot plant
Cavitational reactor	microseconds-several seconds		Commercial scale
Spinning reactor	< 1 min		Commercial scale
Microwave reactor	several minutes	0.038	Lab scale
Membrane reactor	1-3h		Pilot plant
Reactive Distillation	Several minutes	1.6×10^{-6}	Pilot plant
Centrifugal reactor	1 min		Commercial scale

This work will concentrate on the modelling of the hydrodynamics of liquid-liquid slug flow in capillaries, with a view towards the application in monolithic and packed bed reactors for biodiesel production.

1.3 Motivation and Objective of Research Project

1.3.1 Motivation

The hydrodynamics involved in a two-phase flow through a packed bed reactor is very complex due to the interaction between the flowing phases and the stationary particles. Modelling of these units is essential for an accurate equipment design and prediction of optimum operating conditions involved in a particular process. Extensive literature reviews are available describing the flow of co-current and counter-current gas-liquid systems in trickle bed reactors, as well as oil-water flow in reservoirs; however, the prediction of liquid-liquid flow through packed bed reactors is still a big challenge for engineers.

Nowadays, a similar process involving liquid-liquid flow can be found in biodiesel production, specifically at the heart of the process where the reaction takes place and the main product is obtained. A number of reactor configurations have evolved to fit the unique requirements and conditions of biodiesel production, yet, there is ongoing research to define the most efficient reactor in terms of conversion and product recovery, as well as positive environmental impact. The necessity of a new model to increase the viability of biodiesel production in large scale plants opens a wide opportunity to apply CFD modelling to approach this problem.

A common drawback of the mixing conventional equipment used for biodiesel production, such as stirred tanks, is the inability to monitor or control the droplet size precisely. This results in non-uniformities during the reaction and arises uncertainties in reactor design which imposes limitations on the optimal performance of the system. The use of packed bed reactors have been identified as an efficient alternative to overcome these drawbacks. However, the difficulty in applying CFD modelling to this particular problem centres on the complexity involved in predicting the different flow regimes and interactions occurring during the process.

Considering that micro channel reactors are powerful and economic systems for the intensification of industrial processes and that the flow structures in such units have shown similarity to the flow in packed beds, the current work suggests

the study of liquid-liquid slug flow in capillaries to provide insight into the effectiveness of pack bed reactors for a given two phase liquid-liquid system. Although plenty of experimental work has been done in multi-phase flow in micro channels, there are some large gaps in the literature about pressure drop, mass and heat transfer models in liquid-liquid slug flows.

Moreover, not enough information is available on the characterisation of multi-phase flow patterns and fluid-fluid interactions through micro channels and packed bed systems when inertial effects are present. Also, the numerical techniques available for fluid interface studies in gas-liquid and liquid-liquid systems require high computational effort and time to solve for such two-phase flow problems. Therefore an efficient interface capturing method is required that is able to reproduce parametric studies more efficiently and offering enough information for process design.

1.3.2 Objectives

The main objective of this project is to develop a CFD modelling approach to provide insight on the hydrodynamics and mass transfer mechanisms of liquid-liquid slug flow in capillaries with a view towards the application in packed bed reactors and further implementation in chemical production processes, namely biodiesel production.

1. Evaluate the effect of the drag force on the settling or rising velocities of elongated droplets of different sizes dispersed in a continuous liquid flow in a capillary based on the force balance equation.

2. Study the motion of a droplet along a capillary in a horizontal pressure driven flow and evaluate the influence of the main slug flow parameters on the droplet velocity.

3. Develop an efficient CFD model to investigate the effect of the interfacial shear forces on the flow behaviour of liquid-liquid slug flows in capillaries.

4. Develop and implement an effective tool to predict the main slug parameters such as film thickness, bubble velocity and pressure drop in liquid-liquid slug

flow through capillaries based on theoretical and empirical correlations from the literature.

5. Deep understanding of the hydrodynamics involved in liquid-liquid slug flow through capillaries to apply it in porous media systems such as packed bed reactors.

6. Develop a generalised pressure drop correlation for liquid-liquid slug flow in a porous media to be implemented mainly in bio-fuel production processes.

7. Ultimately, develop a process model where understanding of the hydrodynamics can be coupled with chemical reactions to predict the flow in micro channels and packed beds.

1.4 Thesis Structure

Chapter 2 presents a comprehensive overview of hydrodynamics studies of gas-liquid and liquid-liquid slug flow through capillaries. The review summarises the existing knowledge from both experimental and computational studies of two-phase capillary slug flow systems. Also, a review of experimental and numerical studies for two-phase flow problems involving porous domains, mainly packed bed reactors is introduced and details of important modelling parameters such as relative permeability, capillary pressure and liquid saturation are discussed. Additionally, a summary of recent applications of packed bed reactors for biodiesel production are presented in this chapter.

Chapter 3, introduces fundamental hydrodynamic concepts of a flow in circular pipes and of two-phase slug flow in capillaries. The most relevant correlations to model both, gas-liquid and liquid-liquid slug flow through capillaries are described in detail throughout this chapter. Also, the main theoretical concepts for modelling single and two phase flows in a porous media are also introduced in this chapter. The aim is to understand the transport phenomena in capillaries and incorporate it into micro-fluid systems applications, such as the flow in catalytic monoliths and multi-phase flow in porous media.

Chapter 4, presents a computational fluid dynamic (CFD) approach to model liquid-liquid slug flow in capillaries. The first part of the chapter consists of a drag force analysis over a single elongated droplet of different sizes freely rising or falling under gravity in a continuous phase through a capillary. The influence of the main slug flow parameters such as the slug length, droplet length and film thickness on the drag force coefficient are investigated and the results of the drag force analysis were used to predict the rising/settling droplet velocity. The second part of the chapter, studies the motion of a droplet in horizontal pressure driven flow. A method to calculate the droplet velocity is proposed following a moving reference approach in a single-phase framework. Simulations for high and low viscosity ratios were developed assuming a high surface tension between the two-phase flow. Finally, a two-phase flow study was developed to evaluate the the flow behaviour in a unit cell when the interfacial forces are taken into account. An alternative methodology to the Volume of Fluid is proposed to evaluate the influence of density and viscosity ratios in the flow field. Results were achieved and compared to similar studies found in the literature. Some limitations were encountered with the proposed methodology which restricted the validation with experimental data.

Chapter 5, presents an iterative method based on empirical correlations to calculate the film thickness, droplet velocity and pressure drops in a slug flow through a capillary. The algorithm predicts these parameters for known fluid properties and inlet flow rates. The results were validated with experimental and numerical data found in the literature for both gas-liquid and liquid-liquid slug flows. The model can be used as an effective tool for design purposes of systems operating under slug flow regimes.

Chapter 6, introduces the first stage of a mathematical model to predict the pressure drop of a liquid-liquid slug flow through a packed bed reactor. The proposed model includes the influence of the interfacial shear forces and inertial effects in a porous media. This model may provide insight on the hydrodynamics of liquid-liquid flows though packed bed reactors and can be further implemented in biodiesel production process. Chapter 7 summarises the main findings in each chapter and provides an overall conclusion to the thesis. Also, some suggestions for possible future work are proposed in this chapter.

Chapter 2

Literature Review

This section presents a comprehensive overview of the hydrodynamics studies for gas-liquid and liquid-liquid slug flow through capillaries over the years. The existing knowledge from both experimental and computational studies is presented. Also, the most recent studies of biodiesel production using capillaries as mixing technology are introduced in this chapter. Moreover, an overview of experimental and numerical studies for two-phase flow problems involving porous domains, mainly packed bed reactors is described. Details of important modelling parameters such as relative permeability, capillary pressure and liquid saturation are discussed. Additionally, recent applications of packed bed reactors for biodiesel production are introduced in this chapter.

2.1 Hydrodynamics of two-phase flow in capillaries

2.1.1 General Aspects

There are many industrial processes and chemical reactions in which immiscible fluids are brought into contact to give a final product. They are generally referred to as multi-phase systems and can be characterised as: gas-liquid, liquid-liquid and gas/liquid-solid systems. Recently, a great interest in the implementation of microscopic technologies for multi-phase flows has evolved significantly and has

made improvement on the efficiency of such systems. For instance, microscopic devices containing mini channels flow structures have been proposed to intensify contacting and to enhance process performance. These devices provide high mass and heat transfer rates and enable fast, continuous and safe chemical reactions Haase (2016). Also, they have been used for chemical and biocatalytic applications, as well as for extraction and absorption processes. Although the efficiency of such microscopic devices has been found to be higher than the traditional technologies, yet, their performance will greatly depend on the flow regime used during operation Yagodnitsyna *et al.* (2016). Therefore, knowledge of the hydrodynamics in these systems is essential for an adequate process design. Also, the ability to predict relevant flow features such as interfacial areas, pressure drops and mass transfer mechanisms will allow to identify the optimum operating conditions for a particular system.

The behaviour of multi-phase flows varies according to several parameters and flow conditions. For instance, a two-phase flow in a capillary presents different features compared to the flow in large pipes Angeli & Gavriilidis (2008). In a capillary the flow is dominated by surface tension forces and gravity may cause differences in the flow pattern only in specific cases Biswas *et al.* (2015); Shao *et al.* (2009). Also, the relation of surface to volume ratio is relevant in capillary flows Haase *et al.* (2016).

Extensive literature can be found for gas-liquid systems through capillaries including experimental and numerical studies Angeli & Gavriilidis (2008); Asadolahi *et al.* (2012); Aussillous & Quere (2000); Bretherton (1961); Burns & Ramshaw (1999); Dessimoz *et al.* (2008); Gupta *et al.* (2009, 2010); Kreutzer (2003); Leung *et al.* (2012); Taitel *et al.* (2000); Taylor (1961); Triplett *et al.* (1999); van Baten & Krishna (2005); Vandu *et al.* (2005). Regarding the study of liquid-liquid flows in capillaries, the information is more limited, but very recent experimental and numerical studies have provided remarkable features for modelling this type of flows Abiev & Dymov (2013); Eain *et al.* (2013, 2015); Gupta *et al.* (2013); Jovanovic *et al.* (2010, 2011a, 2012); Kashid & Kiwi-Minsker (2011); Kashid & Agar (2007); Kashid *et al.* (2005, 2007a,b, 2010a, 2011); Li & Angeli (2017); Raimondi *et al.* (2008, 2014); Tsaoulidis & Angeli (2016); Tsaoulidis *et al.* (2013).

2.1.2 Two-phase flow patterns in capillaries

Several studies have proposed gas-liquid flow regime maps which are based on dimensionless numbers Akbar & Ghiaasiaan (2006); Dessimoz *et al.* (2008); Shao *et al.* (2009). The best description of the flow regime transition maps has been considered to be the one developed by Shao *et al.* (2009), using superficial liquid and gas velocities Haase (2016). The flow patterns for gas-liquid flows in capillaries are generally classified as bubbly flow and Taylor flow, churn flow and Taylor-annular, dispersed and annular flow. Taylor flow occurs at low gas and liquid velocities, and when the liquid flow rate is increased the pattern changes to bubbly flow. At medium gas velocities and low liquid velocities Taylor-Annular flow is developed and for high liquid velocities churn flow is formed. A further increase in the gas velocity leads to annular flow which is an inertial dominated region. An experimental visualisation of different flow patterns in gas-liquid systems is shown in Figure 2.1. The main flow regimes and flow patterns for gas-liquid flow in capillaries are summarised in Figure 2.2.

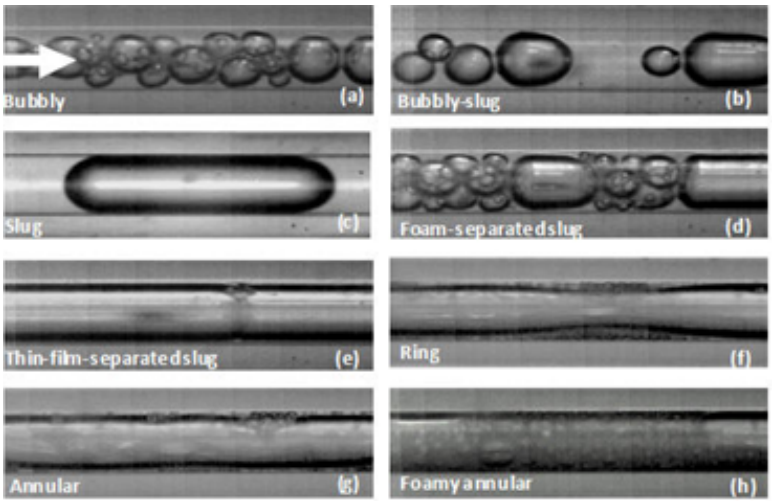

Figure 2.1: Gas-liquid flow patterns with 1000 wppm Lui (2012)

.

Compared to gas-liquid flows, the hydrodynamics in liquid-liquid flows is more complex since the interfacial shear can be significant depending on the viscosity of the dispersed phase Eain *et al.* (2015); Gupta *et al.* (2013); Raimondi *et al.*

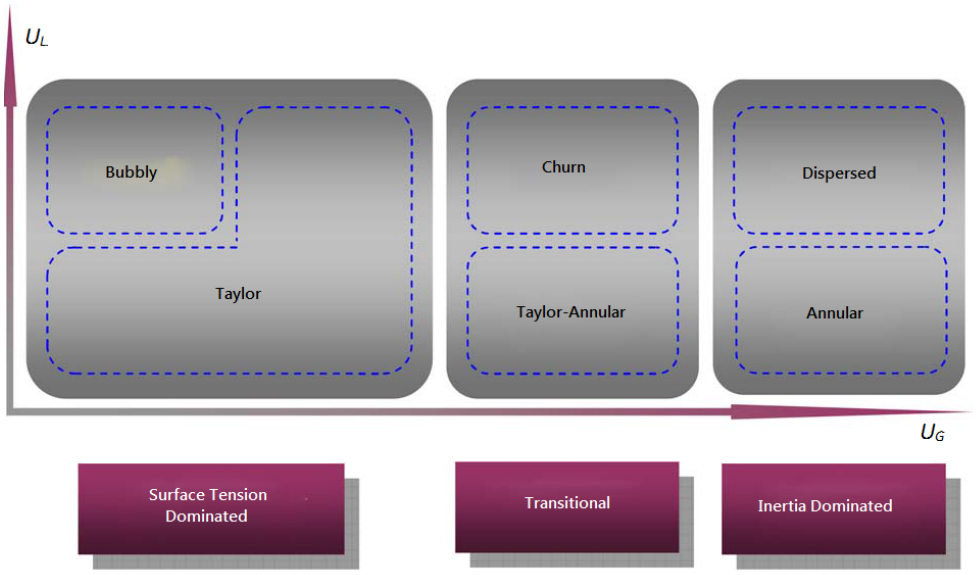

Figure 2.2: Main regimes and flow patterns for gas-liquid flow in microchannels Shao *et al.* (2009)

.

(2008). In order to classify the flow patterns in liquid-liquid flow through capillaries, experiments with different cross sections and contacting geometries were developed by Kashid & Kiwi-Minsker (2011). Similar to gas-liquid flows, three different flow patterns have been identified and classified as surface tension dominated (slug flow), transition (slug-drop and deformed interface flow), and inertia dominated (annular or parallel flow).

Kashid & Kiwi-Minsker (2011), proposed a criterion for liquid-liquid flow pattern transition in capillaries using the Capillary number and Reynolds number. Figure 2.3 (a) shows a flow pattern map indicating different flow regions while using a T shape microchannel. Figure 2.3 (b) shows a generalised flow pattern map developed for liquid-liquid systems using different contact geometries and is independent of the cross section form.

A recent study by Yagodnitsyna *et al.* (2016) presents flow pattern maps of immiscible liquid-liquid flow in a rectangular microchannel using a T-junction for fluid contacting. Different flow patterns were observed such as parallel flow, slug flow, plug flow, dispersed flow and rivulet flow for several velocity ratios.

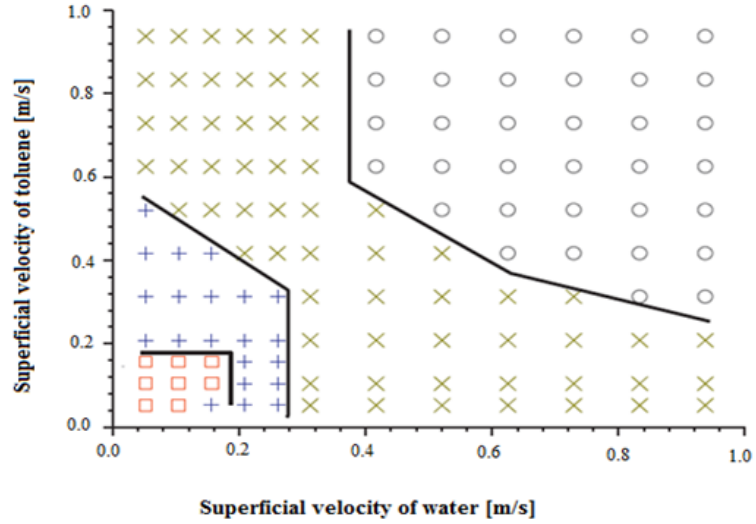

(a)

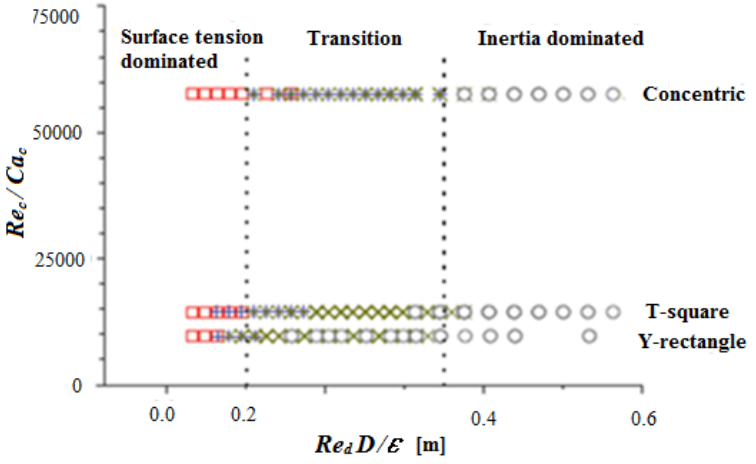

(b)

Figure 2.3: Liquid-liquid flow pattern map (a) T-shape microchannel (b) Non-dimensional Re_c/Ca_c as a function Re_d/d for different microchannels configuration (square) slug drop, (+) slug-drop, (X) deformed interface, (circle) Parallel/annular flow Kashid & Kiwi-Minsker (2011)

.

Moreover, a new flow pattern was characterised as serpentine flow which involves parallel flow with steady wavy interface. The study revealed inaccuracies in flow pattern maps based on the Weber number for different liquid-liquid systems. The author introduces a new dimensionless number known as the Ohnesorge number (Oh), which relates the viscous forces to inertial and surface tension forces, $Oh = \frac{\sqrt{We}}{Re}$. Generalised flow maps based on the parameter $We\dot{O}h$ were proposed. Figure 2.4 illustrates the flow pattern maps for three liquid-liquid systems plotted in the same axes using (a) Weber number and (b) using $We\dot{O}h$. Also, the universal flow map is displayed and compared with experimental results from Zhao *et al.* (2014) in plots (c) and (d), respectively.

Among these flow regimes, slug flow has been considered as the most important one since it provides a large interfacial area and thus enhances mass and heat transfer between the phases involved Asadolahi *et al.* (2011); Gupta *et al.* (2010). The slug flow regime has obtained a great interest for process intensification purposes, mostly in processes controlled by mass transfer mechanisms. Table 2.1 describes some of the main industrial applications where slug flow in capillaries has been implemented. Although the slug flow regime offers significant advantages for mass transfer processes, there are various parameters that may influence its performance. For instance, material properties, such as surface tension, viscosity, wall wetting properties. Also, capillary parameters such as the dimension, cross section, flow orientation and the inlet geometry configuration Rebrov (2010); Shao *et al.* (2009). The following section describes the main flow features for modelling slug flow in capillaries. The section is divided in two main categories: gas-liquid and liquid-liquid slug flows.

2.2 Slug flow in capillaries

2.2.1 Gas-liquid slug flow

Gas-liquid slug flow has been studied experimentally, analytically and using computational fluid dynamics. Some of these studies have focused on the importance of the liquid film that is formed around the bubble, and its influence on the flow behaviour and heat or mass transfer Asadolahi *et al.* (2011); Gupta *et al.* (2009);

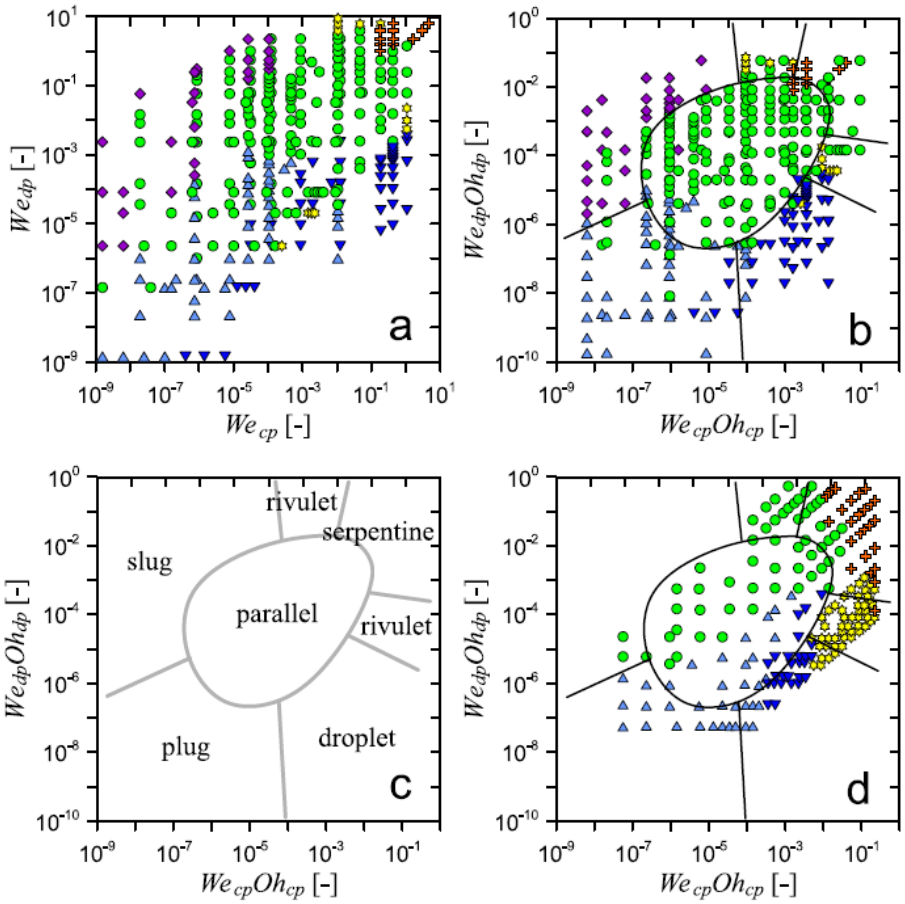

Figure 2.4: Flow pattern maps for three liquid-liquid systems using: (a) Weber number and (b) using $We\dot{O}h$. (c) universal flow map and (d) experimental results from Zhao *et al.* (2014), Yagodnitsyna *et al.* (2016)

.

Table 2.1: Industrial applications of slug flow in microchannels

Industrial Application	Application	References
Flow measurement	Measurement of liquid flow velocity	Bretherton (1961); Fairbrother & Stubbs (1935)
Chemical processing	Catalyst coating	Kolb (1991)
	Cataylitic reactors: three phase reactions	Kreutzer *et al.* (2005)
	Multiphase reactors with limited fast reactions	(Khan et al, 2004)
Biomedical	Blood flow in capillaries	Prothero (1961)
	Lung airway opening problem	Zheng (2007)
Filtration	Enhancement of microfiltration efficiency	Taha (2001)
Electronic cooling	Cooling of high density multi-chip modules in supercomputers, X-ray and diagnostic devices	Zhao (2001)
Heat exchangers	High flux in aerospace systems, cooling systems in satellites	Bao (1994)
Fuel cell	Methanol fuel cell	Buie (2009)
Oil and gas industry	Enhanced oil recovery processes	Schwartzet (1986)

Leung *et al.* (2012); Liu *et al.* (2005); van Baten & Krishna (2004); Vandu *et al.* (2005).

Furthermore, various numerical techniques for fluid interfaces are available to model two-phase flows in capillaries. For instance, Lagrangian methods such as moving mesh or front tracking, accurate resolve the shape interface and are suited to capture the thin film around moving bubbles and droplets Muradoglu & Tryggvason (2008). Also the implementation of Eulerian methods, such as the Level Set Method Yuan *et al.* (2018), Volume of Fluid method Gupta *et al.* (2010), Diffuse Interface Method Wang *et al.* (2015b) and the Lattice Boltzmann method Wang *et al.* (2015a); Yong *et al.* (2011) are commonly use for simulating multiphase flows. The advantages of these techniques are its robustness and the ability to conserve mass and reduce sharp interfaces, however these methods require high computational efforts to solve problems with large interface movements, topological changes and high surface tension flows Hoang *et al.* (2013).

The first gas-liquid slug flow studies were developed by Fairbrother & Stubbs (1935) who observed a difference between the theoretical and effective bubble velocity in capillaries and found that it was due to the presence of a liquid film near the wall, whose thickness could be correlated with the Capillary number as $Ca_b^{0.5}$. Later, Bretherton (1961) analysed the behaviour of the front and rear region of the bubble along a continuous flow and identified the dependence between the film thickness and $Ca_b^{0.5}$. Bretherton's correlation has been used in many slug flows studies and is applicable for very low Capillary numbers. A new correlation for the film thickness accounting for inertial effects was proposed by Aussillous & Quere (2000) based on the experimental data from Taylor (1961). The correlation was further improved by Han & Shikazono (2009) who introduced the inertial effect by using the Weber and Reynolds numbers.

A relationship between the Capillary number and flow velocities in vertical capillaries was proposed by Liu *et al.* (2005). The expression accounts for the effect of the liquid properties on bubble rise velocity and is applicable for circular and square cross section capillaries. The correlation was found to be restricted for only vertical flows and for specific two-phase fluid properties Abiev (2008). Thus, a model to predict the droplet velocity in upward and downward flow for a wide range of Capillary numbers was developed by Abiev (2010) and the

model was validated with the experimental data from Kreutzer *et al.* (2005); Thulasidas *et al.* (1995). The expression proposed assumes that the average gas velocity in the bubble is determined mostly by the film thickness. Additionally, Abiev (2013) introduced an expression to predict the bubble velocity considering the circulation rate dependence on slug length. This expression was based on the model elaborated in Abiev (2008) and was validated with experimental data from the literature.

The mathematical model by Abiev (2008) was developed for a gas-liquid slug flow in a capillary assuming an infinite droplet dispersed in a continuous phase. The velocity profiles in the bubble, film region and slug area were calculated with this model and showed good agreement with experimental data from the literature. A similar procedure was followed by Lac & Sherwood (2009) to study the deformation of a drop in a horizontal pressure driven flow along a capillary. They investigated the drop behaviour at high Capillary number and evaluated the limits of low and high viscosity droplets. Also, the contribution of the presence of the droplet to the overall pressure drop was investigated in their work.

Furthermore, a multi-phase modelling approach to simulate gas-liquid Taylor flow in capillaries was developed by Gupta *et al.* (2009). The work presents a methodology to predict the bubble shape using the volume-of-fluid (VOF) approach. Also, a criterion for calculating a sufficiently fine mesh to capture the liquid film around the bubble is suggested based on the Capillary number. The simulations revealed broad flow features as observed in experiments, but required a high computational cost. Anyhow, the model was extended to include heat transfer in Taylor flow from the wall to the fluid in a capillary Gupta *et al.* (2010). In order to understand the effect of slug length on flow rates and to facilitate the comparison with experiments, Asadolahi *et al.* (2011) proposed a moving domain approach to predict the bubble velocity and the pressure field of slug flow in a capillary. The configuration allowed to predict these parameters more efficiently. A similar approach for gas-liquid Taylor flow in a micro channel reactor was used by Shao *et al.* (2010) for a chemical absorption study and a new CFD model was formulated for mass transfer in Taylor flow. The effect of the bubble and slug length on the mass transfer was investigated and the results showed a significant contribution to the reactor performance. More recently, Langewisch &

Buongiorno (2015) provided a database of CFD predictions of the film thickness and bubble velocity for capillary slug flow in a range of high viscosity and density ratios. A modified film thickness correlation based on Han & Shikazono (2009) was proposed. The predictions for the bubble velocity were determined using an expression derived from the wetting fraction definition and its relation to the film thickness.

Moreover, the total pressure drop along a capillary was investigated by Bretherton (1961), who proposed a theoretical solution for the presence of a single bubble in a continuous flow. Bretherton's expression considers the changes in curvature due to the presence of the liquid film and the Laplace pressure accounted for. The expression has been widely used for slug flow studies in capillaries, however, Kreutzer *et al.* (2005); Walsh *et al.* (2009) determined that the bubble pressure drop was also affected by the slug length. They proposed a generalised expression as a function of the Capillary number, Reynolds number and slug length. Then Warnier *et al.* (2010), modified the correlation to include the bubble cross sectional area and also extended its applicability for higher Reynolds and Capillary numbers.

Since, the current work is focused mainly in the study of liquid-liquid slug flows, only a short overview of the main gas-liquid studies have been described in this section. Table 2.2 summarises relevant experimental and numerical studies of film thickness in gas-liquid slug flow in capillaries.

2.2.2 Liquid-liquid slug flow

The prediction of liquid-liquid slug flow has been less studied than gas-liquid systems Abiev & Dymov (2013); Dore *et al.* (2012); Eain *et al.* (2015); Ghaini *et al.* (2011); Gupta *et al.* (2013); Jovanovic *et al.* (2010, 2011b); Kashid & Kiwi-Minsker (2011); Kashid & Agar (2007); Li & Angeli (2017); Raimondi *et al.* (2014); Tsaoulidis *et al.* (2013); Xu *et al.* (2013). These systems are considerably more complicated, mainly because the resultant interfacial shear in the film region can have significant effects on the overall pressure drop and velocity distribution.

Immiscible liquid-liquid flows can be found in several applications such as emulsion production, nano material synthesis, nitration, extraction processes and

Table 2.2: Experimental and numerical studies of film thickness in gas-liquid slug flow in capillaries

Literature	Flow conditions	Measuring technique
Fairbrother & Stubbs (1935)	d=2.25 mm	Indicator bubble velocity
Bretherton (1961)	$10^{-4} \leq Ca \leq 10^{-2}$	Volumetry
Irandoust & Andersson (1989)	$9.5 \times 10^{-4} < Ca < 1.90$, $0.42 < Re < 860$	Light absorption
Aussillous & Quere (2000)	$10^{-3} \leq Ca \leq 1.4$	Video recording
Han & Shikazono (2009)	$0 < Ca < 0.2$, $0 < Re < 2000$	Laser meter
Howard & Walsh (2013)	$0.0059 < Ca < 1.823$, $0.72 < Re < 122.98$	Optical microscopy
Gupta *et al.* (2009)	$0.047 < We < 0.697$	CFD-Volume of Fluid
Langewisch & Buongiorno (2015)	$0 < Ca < 2$, $0 < Re < 2000$	CFD code (Gerris)

biochemical applications. The main difficulty in these systems is the lack of data correlations, allowing explicitly the prediction of flow patterns and characteristics of liquid-liquid two-phase flow in capillaries Haase *et al.* (2016). Also, there are not many studies of the influence of flow parameters such as density, viscosity and interfacial tension comparing to gas-liquid flows Yagodnitsyna *et al.* (2016).

Several experimental and numerical studies have been developed by Kashid *et al.* (2005, 2007a,b) on the hydrodynamics and mass transfer of liquid-liquid slug flows in capillaries. In their earliest experimental work, a significant effect on the circulation patterns was detected due to the presence of a thin film around the dispersed droplet. Details of this behaviour was further analysed in a single phase study using computational fluid dynamics Kashid *et al.* (2005). Then, the effect of various operating conditions on the mass transfer coefficients was investigated and the results confirmed that the presence of the thin wall film offered

3-4 times more interfacial area for mass transfer than with no film Kashid *et al.* (2007b). The influence of the fluid properties on the mass transfer with and without chemical reactions was analysed using a simplified CFD model with a fixed interface Kashid *et al.* (2007a). Furthermore, Kashid & Agar (2007) proposed a pressure drop model based on Hagen-Poiseuille flow and Bretherton's equation for a wide range of operating conditions and inlet configurations. Improvements on the CFD predictions using the volume of fluid (VOF) method to generate liquid-liquid slug flow in a capillary was achieved in their later work Kashid *et al.* (2010a). The numerical results were compared qualitatively with the experimental work by Tice *et al.* (2004) and suggested that for a well defined slug flow the Capillary number had to be less than $Ca = 0.01$ and a capillary diameter up to $d_c = 1mm$. Visualisations of a train of bubbles and a single droplet from their work are shown in Figure 2.5. It is relevant to mention that the CFD results do not show the circulatory flow inside the droplets and information regarding to the droplet velocity is not available in their work.

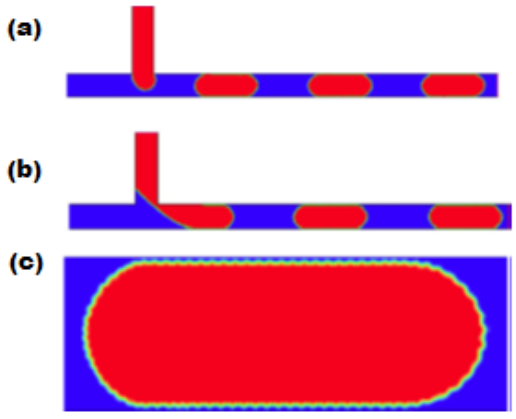

Figure 2.5: Simulated snapshot of well-defined slug flow Kashid *et al.* (2010b)

.

A recent CFD study from Gupta *et al.* (2013), investigated the hydrodynamics of vertical upward liquid-liquid slug flow using the volume-of- fluid (VOF) method and a moving reference frame. The pressure drop across the capillary was calculated using a similar pressure drop model as proposed by Jovanovic *et al.* (2011b) and the velocity profiles were compared with the analytical solution derived by

Abiev (2008). The CFD model was restricted by the droplet size, being only valid for long droplets. Flow visualisation of their work is shown in Figure 2.6. Moreover, experimental measurements of the drop velocity were performed by Dai *et al.* (2015) and CFD predictions of the film thickness were achieved for a specific liquid-liquid slug flow system. A generalised model of heat transfer in gas-liquid and liquid-liquid slug flows was developed in their work based on a combination of resistances for each interface region.

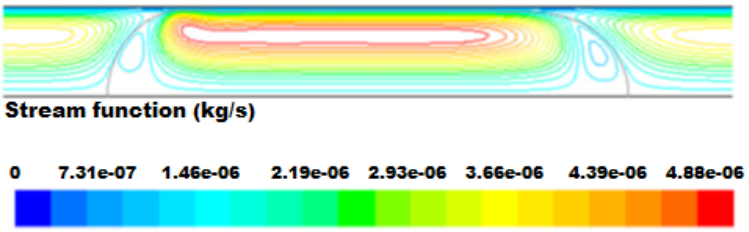

Figure 2.6: Streamlines (contours of stream function) in the slug and droplet Gupta *et al.* (2013)

.

Furthermore, Dore *et al.* (2012) developed an experimental study to investigate the mixing characteristics and circulation patterns inside a single water droplet during a water-ionic liquid slug flow. The mixing rate was quantified through a non-dimensional circulation time. The results showed a more uniform behaviour of this parameter for longer droplets. Overall, the maximum circulation velocity was found to increase linearly with the Capillary number. However, the minimum circulation time tend to decrease with increasing Capillary number for the case of sufficiently long droplets. Difficulties to determine the dependence of the minimum circulation on the Capillary number for shorter droplets were encountered and irregularities in the circulation pattern were observed. Additionally, a new film thickness correlation based on the model by Irandoust & Andersson (1989) was developed for the two-phase system under study. This expression was then used to improve the predictions of the total pressure drop for ionic-liquid flow through capillaries of different materials in Tsaoulidis *et al.* (2013).

Most recently, Li & Angeli (2017) developed an extensive experimental and CFD study of the hydrodynamic characteristics of liquid-liquid slug flow in capillaries. The main parameters such as film thickness, droplet velocity, slug and drop lengths, and total pressure drops were measured and compared against literature correlations. The CFD results were in good agreement with the experimental data and velocity profiles for ideal annular flow. Also, the numerical predictions for the pressure gradients agreed with a modified pressure drop correlation similar in form to the proposed by Kreutzer *et al.* (2005); Walsh *et al.* (2009). Some of the CFD results presented in their work for predicting the velocity distribution and internal circulations at different mixture velocities are displayed in Figure 2.7. Overall, the study offers a broad understanding of the hydrodynamics involved in capillary slug flows and provides significant improvements on the CFD modelling of slug flow in micro-fluid devices.

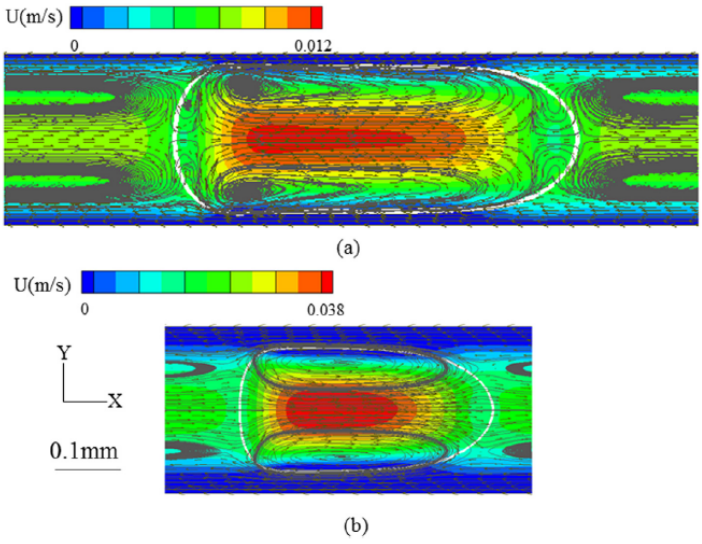

Figure 2.7: Velocity distribution and internal circulations in a droplet from CFD simulations at (a) $U_m = 0.01$ m/s and (b) $U_m = 0.03$ m/s, in a 0.2 mm ID channel Li & Angeli (2017)

.

Film thickness correlations for liquid-liquid slug flow

Recent studies dealing with liquid-liquid slug flows in capillaries have used the film thickness correlations derived for gas-liquid slug flows to describe the behaviour of their experimental results. However, the majority of these correlations have failed to accurately predict the film thickness in liquid-liquid systems. For instance, Dore *et al.* (2012) modified the film thickness correlation proposed by Irandoust & Andersson (1989) to improve the predictions for two-phase flows involving ionic liquids. Since, these types of fluids involve high density and viscosity properties, the hydrodynamics and mixing patterns were not accurately predicted by the existing film thickness correlations. Also, Abiev (2013) modified the film thickness correlation of Aussillous & Quere (2000) to fit their experimental liquid-liquid data over a wider range of Capillary numbers. Furthermore, in the work by Eain *et al.* (2013) measurements of the film thickness for different two-phase liquid-liquid systems were determined. A variation to the correlations by Aussillous & Quere (2000); Bretherton (1961) including inertial effects showed good agreements to the experimental data. The results confirmed that the film is only dependent on the Capillary number in the visco-capillary regime, similar to gas-liquid slug flow, but not during the visco-inertial regime. Additionally, a new film thickness correlation with a similar form to Eain *et al.* (2013) was proposed in the experimental work by Tsaoulidis & Angeli (2016). The correlation showed accurate predictions for the experimental ionic liquid/aqueous two-phase system in three different capillary diameters. Moreover, a recent experimental investigation of wall film renewal in liquid-liquid slug flow was developed by Arsenjuk *et al.* (2016) showed the effect of the droplet velocity, slug volume and continuous phase viscosity on the mass transfer process in the film. The results revealed that both diffusive and convective mechanisms have a significant influence on the mass transfer. This confirms that the film thickness velocity must be considered for reliable predictions of liquid-liquid slug flow systems.

Pressure drop models for liquid-liquid slug flow

There are two main pressure drop models described in the literature for liquid-liquid slug flow, both of which have been developed by Kashid & Agar (2007)

and Jovanovic *et al.* (2011b). The generic form of such models consist of three main contributions to the total pressure drop: (a) the frictional pressure drop of the continuous phase, (b) the frictional pressure drop of the dispersed phase and (c) the interfacial pressure drop.

The model by Kashid & Agar (2007) assumes that the dispersed phase makes an appreciable contribution to the total pressure drop and does not consider the film that surrounds the droplet. On the other hand, the model described by Jovanovic *et al.* (2011b) uses the theoretical solution for gas-liquid flows proposed by Bretherton (1961) to determine the interfacial pressure drop and assumes that the pressure drop caused by the non-negligible flow in the thin film is greater than that of the dispersed phase. The application of the pressure drop expressions in both models was found to be very limited and not suitable for use in the design of most systems incorporating liquid-liquid slug flow regimes Eain *et al.* (2015).

Therefore, in the recent experimental study by Eain *et al.* (2015) the validity of the existent pressure drop models for, both gas-liquid and liquid-liquid, was addressed by comparing their applicability over a wide range of viscosity ratios. The results demonstrated that the gas-liquid pressure drop models, mainly the one proposed by Walsh *et al.* (2009) can accurately predict the pressure drop of a liquid-liquid slug flow when the viscosity ratio is above 4.5. Below this threshold, none of the pressure drop models provided an accurate estimation. The closest predictions to the liquid-liquid data were obtained with the model by Warnier *et al.* (2010). Thus, a new pressure drop correlation was proposed based on this model and the results showed accurate predictions for a wide range of viscosity ratios in liquid-liquid systems. The main reason for the failing of the liquid-liquid models by Jovanovic *et al.* (2011b); Kashid & Agar (2007) was attributed to the methods used to estimate the interfacial pressure drop term, since they were limited to the cases of negligible inertial effects or no film thicknessEain *et al.* (2015).

Moreover, an important contribution on the prediction of capillary slug flow was developed by Howard & Walsh (2013) who proposed a model based on the expression derived by Abiev (2008) and allows to determine the bubble/droplet drift velocity from the material properties and relative flow rates for a given pair of fluids. The variation of the bubble velocity to the mean two-phase velocity over

a range of viscosity ratios is graphically presented in their work and is illustrated in Figure 2.8. This plot is suggested to justify whether or not an assumption of zero flow in the film can be applied.

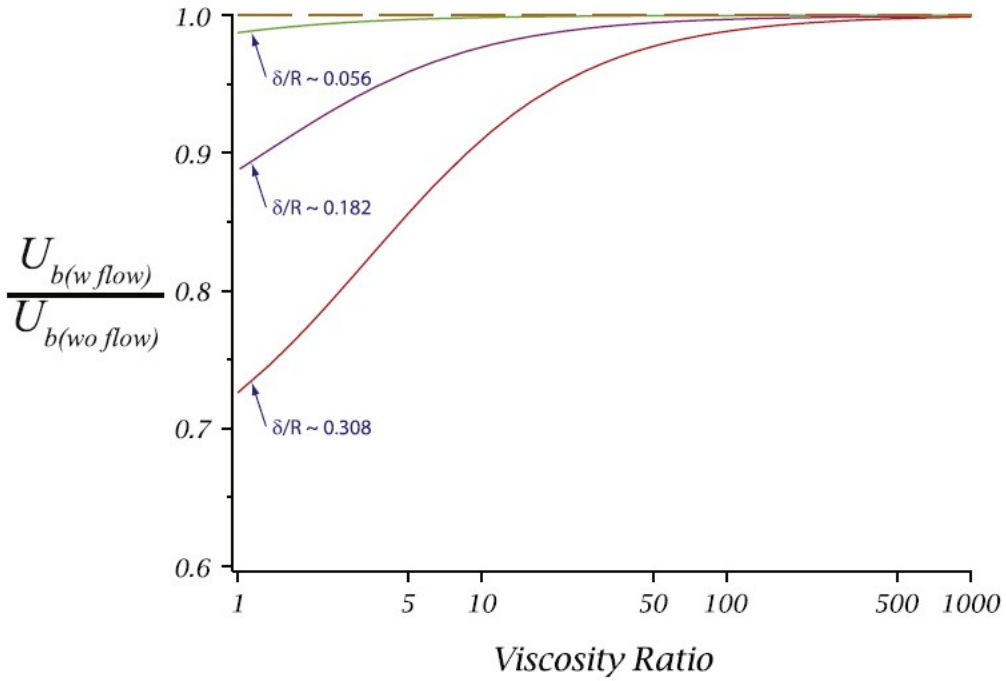

Figure 2.8: Ratio of mean bubble velocity predictions over a range of viscosity ratios from 1 to 1000 and film thickness to radius ratios from 0.056 to 0.308 Howard & Walsh (2013)

.

Furthermore, Biswas *et al.* (2015) developed experimental studies to investigate the effect of the capillary orientation in liquid-liquid slug flow. The frictional pressure gradient was significantly influenced by this feature with the maximum occurring down flow in a vertical capillary, followed by up flow and lastly horizontal orientation. The results also showed that larger droplets are formed in horizontal flows followed by up flow and down flow direction. On the contrary, the droplet frequency was highest in the downward direction and smaller in the horizontal orientation. The study of the slip ratio of the liquid phases was investigated using the mathematical model proposed by Liu *et al.* (2005) derived

for a gas-liquid system. The slip ratio was higher for down flow and minimum for horizontal flow. In general, the work suggested that down flow is the most convenient orientation for any transport process, since a higher dispersed liquid hold up is generated which enhances the residence time during the process.

Table 2.3: Studies on hydrodynamics of liquid-liquid slug flow in capillaries

Literature	Fluids Used	Relevant Results
Kashid *et al.* (2005)	water/cyclohexane	Experimental and simulation study of slug flow generation and internal circulations. Single phase and two phase simulations to predict mixing within slugs.
Kashid & Agar (2007)	Iodine/water	Micro reactors generate higher mass transfer rates than other mixing units.
Ghaini *et al.* (2010)	water/cyclohexane	Experimental study on flow regime, slug size, interfacial area, pressure drop using different Y-junction mixing. Study without film and with film.
Kashid & Kiwi-Minsker (2011)	water/toluene	Study of flow patterns with different cross sections and contacting geometries.
Ghaini *et al.* (2011)	water/ethyl acetate, water/nbutyl acetate	Experimental film thickness study and effect on the hydrodynamics and mass transfer CFD study.
Dore *et al.* (2012)	ionic liquid/aqueous	New experimental film thickness correlation.

Most of the studies described previously have explored the potential of micro channel systems in improving mass and heat transfer between immiscible fluids. However, most of these studies require a prior knowledge of the bubble velocity and this parameter is difficult or not typically measured in practical applications.

Literature	Fluids Used	Relevant Results
Jovanovic *et al.* (2011b)	water/toluene, ethylene glycol/water-toluene	Experimental slug length measurements as a function of slug velocity. Organic to aqueous flow ratio and capillary diameter. Developed two phase pressure drop model.
Gupta *et al.* (2013)	water/hexadecane	CFD and experimental study of vertically upward flow. The model was suitable for long droplet only and low viscosity ratios.
Abiev (2013)	water/vegetable oil, water/benzyl alcohol	Theoretical and experimental study and new empirical film thickness correlation.
Tsaoulidis *et al.* (2013)	ionic liquid-HNO3 solution	Flow patterns and pressure drop model.
Eain *et al.* (2013)	water/organic liquids	Experimental film thickness correlation. Study of visco-capillary and visco-inertial regimes.
Abiev (2015)	Range of Capillary number	Contact angle-hysteresis study.
Biswas *et al.* (2015)	Toluene/water	Effect of capillary orientation.
Eain *et al.* (2015)	Range of viscosity ratios	Developed new pressure drop model for liquid-liquid slug flow.
Arsenjuk *et al.* (2016)	water/kerosene	Experimental study of wall film mass transfer in function of velocity, interfacial area and wall film thickness.
Tsaoulidis & Angeli (2016)	ionic/aqueous	Experimental study and new film thickness correlation.
Li & Angeli (2017)	Ionic liquid-HNO3 solution	Experimental and CFD study main slug flow parameters. New pressure drop correlation.

A potential approach to this problem is proposed further in this work. Table 2.3 summarises recent studies on the hydrodynamics of liquid-liquid slug flow in capillaries and their main characteristics and contribution.

2.3 Biodiesel production in capillaries

The increase of biodiesel production has become of great interest in recent years due to its numerous advantages over conventional fossil fuel resources and other alternative energies. The most common way for obtaining biodiesel is through a transesterification process Demirbas (2009); Qiu *et al.* (2010). However, the main drawback of this method applied to biodiesel production is the mass transfer limitation between the reactants (oil and methanol), since a long residence time is necessary for a complete reaction and total conversion to final products. This also requires a high operation cost and energy consumption which makes the process less efficient Zelic & Bruno (2011).

Micro channel reactors have been introduced for implementation during the mixing stage of biodiesel production as a way to improve efficiency, mass transfer control and downstream process optimisation Qiu *et al.* (2010); Santacesaria *et al.* (2011, 2012a). Visualisations during the mixing and reacting stage in biodiesel process through a microchannel are displayed in Figure 2.9. The flow patterns shown in such figures are for various operating conditions, namely temperatures, methanol to oil ratios and different inlet configurations.

From Figure 2.9 (a) it can be observed that the presence of a well-defined liquid-liquid slug flow can be produced after using a T or Y type mixer at the inlet of the capillary. Also, considering several reactants molar ratios and reaction temperature, Figure 2.9 (b) shows that a well defined slug flow can be obtained at 70°C and molar ratios of 12:1 and 15:1. The residence time and reaction temperature conditions to achieve a stable slug flow can be observed in Figure 2.9 (c).

Although plenty of experiments have been developed for biodiesel production, very little work has been reported on the prediction of the flow behaviour and

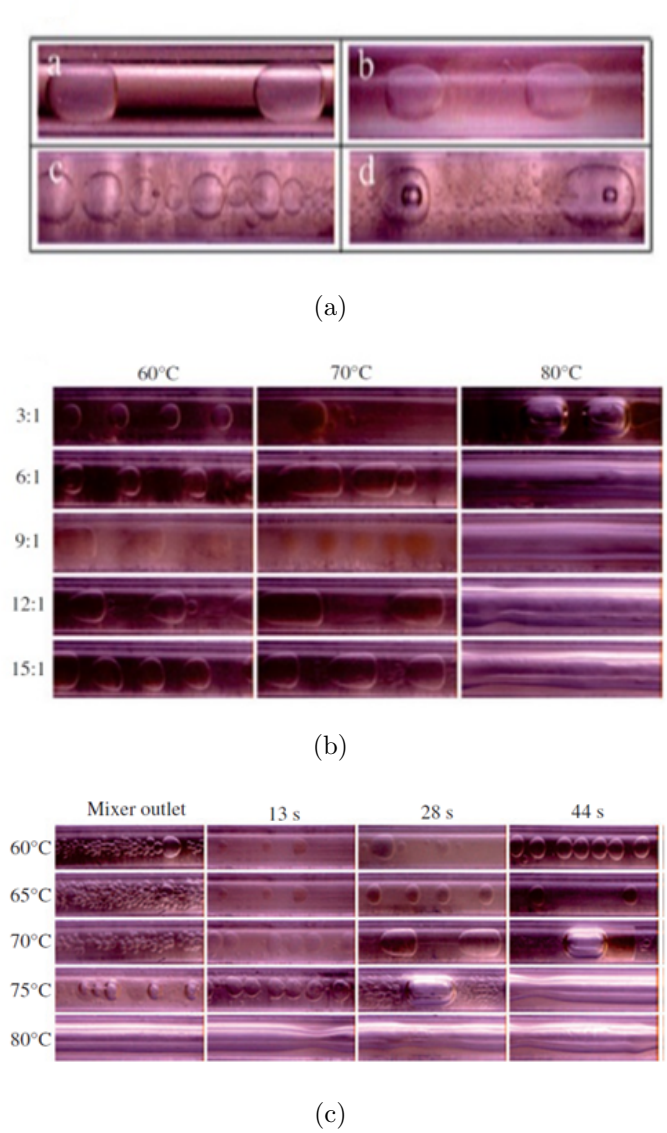

(a)

(b)

(c)

Figure 2.9: Flow patterns in transparent PVC tube during the mixing and reacting stage of biodiesel production (a) Outlet of different micromixers (b) Different methanol to oil ratios and temperatures (c) Residence time and temperatures Xie *et al.* (2012)

mass transfer during the transesterification reaction due to its complexity. Generally, the conversion of oil to FAME proceeds via three consecutive reversible reactions Boer (2009):

$$\textbf{Triglyceride + Methanol} \overset{Catalyst}{\Leftrightarrow} \textbf{Diglyceride + FAME}$$
$$\textbf{Diglyceride + Methanol} \overset{Catalyst}{\Leftrightarrow} \textbf{Monoglyceride + FAME}$$
$$\textbf{Monoglyceride + Methanol} \overset{Catalyst}{\Leftrightarrow} \textbf{Glycerol + FAME}$$

In the first stage the concentration of oil in the methanol droplets (where the majority of the catalyst resides) is low, requiring significant agitation to reach saturation levels. The rate of mass transfer between the phases in this stage is slower than the chemical rate, so mass transfer is the controlling factor. Then, during the second stage the reaction rate rapidly increases until approximately 80% conversion of the reactants is achieved. Also, the droplet size reduces as the reaction rate increases, thus the mass transfer rate increases, explaining the sudden jump in reaction rate. At this stage, a pseudo-single phase is obtained and finally after equilibrium is reached, a two-phase flow is produced consisting of biodiesel (FAME) and glycerol as a secondary product Boer (2009); Santacesaria *et al.* (2011). The three stages occurring during the reaction along a capillary were identified in the experimental work by Santacesaria *et al.* (2012a) and are presented in Figure 2.10. The graph shows the component mass fraction as a function of the degree of conversion. Although the remarkable findings in their work , the author stated that the experimental studies are not completely sufficient to explain in detail some aspects of the phenomena occurring during the reaction stage of the process, hence the necessity of a more reliable model to provide a better description of what effectively occurs in the system.

Additionally, the work developed by Wen *et al.* (2009) demonstrated that biodiesel yield is strongly dependent on the droplet size and that the mass transfer of triglyceride from the oil phase towards the methanol/oil interface limits the reaction rates and controls the kinetics at the beginning of the reaction.

Furthermore, the implementation of CFD modelling of biodiesel production in a continuous tubular reactor was carried out by Boer (2009). The dimensions of

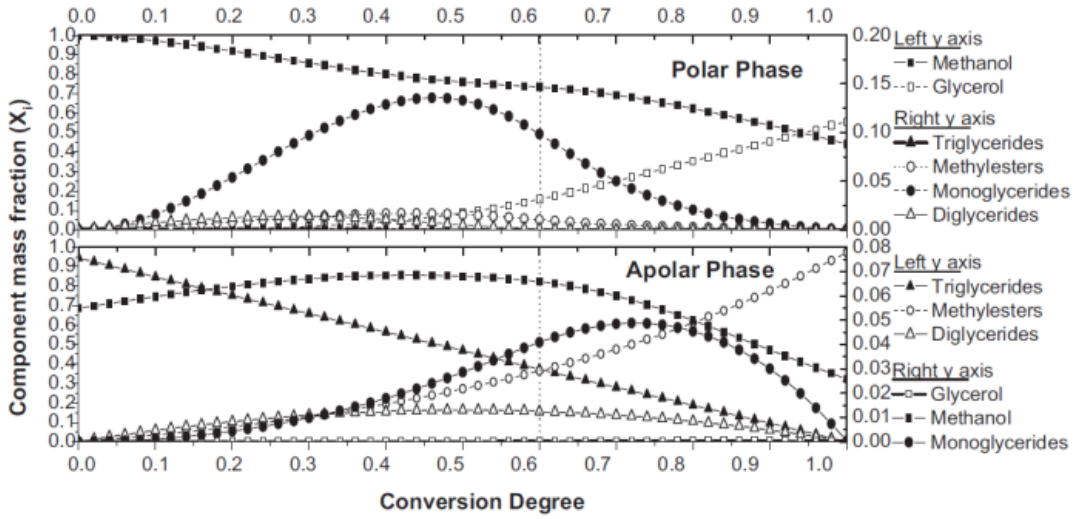

Figure 2.10: Mass fraction plot against the conversion degree related to the triglycerides for each component involved in the transesterification reaction. The upper section of the diagram is related to the polar phase, while, the lower to the apolar one. The right axis of both sections is related to: methanol and glycerol for the polar phase, triglycerides and methylesters for the apolar phase. Santacesaria *et al.* (2012a)

.

the reactor were that of their experimental set up (diameter of 11mm and length of 4m). The main feature observed in their study was the formation of stratified flow over the length of the reactor at low velocity which affected the mass transfer between the oil and methanol phases. Also, the addition of turbulent dispersion effect in the CFD model was essential to obtain an accurate representation of the flow behaviour through the reactor.

In a more recent study from Lopez-Guajardo *et al.* (2017), the production of biodiesel was carried out in a tubular micro reactor and the experimental results were analysed using computational fluid dynamics. The CFD results showed that under certain conditions a slug flow pattern can be generated and high conversion ($> 90\%$) can be reached without using high methanol-oil molar ratios. Also, the results showed that at low conversion ($< 25\%$), the internal velocity of the oil slug is the key factor related to the reactor performance. Visualisations of the

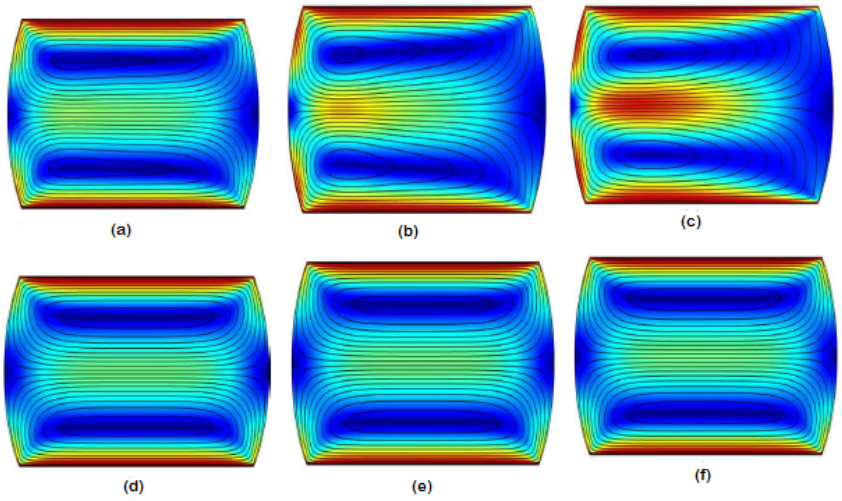

Figure 2.11: Internal circulation and velocity profiles of the methanol slug: a, b, c at 0% oil conversion 4, 1, 0.5 minutes of residence time, respectively; d, e, f at 99% oil conversion and 4, 1, 0.5 minutes of residence time, respectively Lopez-Guajardo *et al.* (2017).

internal circulation in the methanol slug and oil conversion over time are shown in Figure 2.11.

Table 2.4, shows a comparison of biodiesel production with different micro reactor configurations and a stirred tank reactor. It is relevant to mention that a fast conversion of the reactants and high yields of biodiesel can be achieved using micro-fluid devices.

Due to the mass transfer limitations occurring during the mixing and reacting stage throughout biodiesel production, there are still several challenges for an accurate prediction of the flow behaviour in these two stages. Also, the development of an efficient mixing technology is necessary for process optimisation and further scale up of such system. The current work suggests the study of slug flow in a capillary to provide insight into the effectiveness of packed bed reactors in the mixing and reaction stage in biodiesel production process.

The next section presents an overview of experimental and numerical studies for two-phase flow problems involving porous domains, mainly packed bed reactors. Additionally, recent applications of packed bed reactors for biodiesel

Table 2.4: Comparison of biodiesel production with stirred tanks Dai *et al.* (2014)

mixer type	reaction loop	catalyst amount	molar ratio	residence time	biodiesel yield (%)
stirred tank	0.25 mm	1 wt % KOH	6:1	5.89 min	99.4
stirred tank	0.5mm	1 wt % KOH	6:1	5.89 min	96.7
T-shaped	0.8 mm	4.5 wt % KOH	23:1	100 s	100
micromixer	1 mm	1 wt % KOH	23:1	112 s	100
SIMM-V2	3 mm (packed)	1 wt % KOH	8:1	17 s	99.5
T-shaped	0.24 mm (zigzag)	1.2 wt % NOH	9:1	28 s	99.5
T-shaped	1.5 mm (zigzag)	1.2 wt % KOH	8.5:1	14.+s	99.5

production are included in the following section.

2.4 Multiphase flow modelling in packed bed reactors

The implementation of packed bed reactors with one or two phases in the chemical industry can be found in diverse applications, being used as reaction, separation and purification units. Packed bed reactors are usually the first choice for economical production of large amount of product, mainly in the petroleum industry and basic chemical industry Di Serio *et al.* (2012); Iordanidi (2002). The hydrodynamics involved in a packed bed reactor is very complex, hence a good understanding of the details of the local transport processes occurring through the packing is an essential prerequisite for the performance of reliable predictive models.

2.4.1 Description of a Packed Bed Reactor

A packed bed reactor, as described briefly in Chapter 1, is an assembly of solid particles, which are randomly arranged within a vessel or tube. The fluid travels

through the gaps between the solid particles where the mixing and reaction take place. Adjacent to the solid surface the movement is slower, and this slow moving region is often assumed as a stagnant film Stanek (1994). The flow patterns of the bulk fluid through the bed are tortuous and unpredictable, since a priori knowledge of the solid particles arrangement in the bed is not possible. However, the flow is mainly characterised by the solid particle diameter and the void fraction. Also, the ratio between the diameter of the column to the particle size has a significantly effect on the flow through the packed bed Freund *et al.* (2005). Figure 2.12 illustrates schematically a typical packed bed reactor and random packing mechanism. The main aim of packed beds is to maximise the interfacial surface

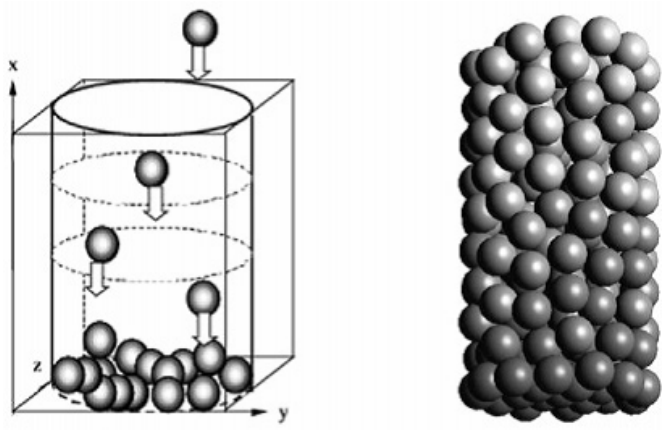

Figure 2.12: Shematic of the generation of random packing and distribution in a fixed bed system Freund *et al.* (2005)

.

area between the two-phases to improve mixing performance, reaction rates and residence time distribution.

2.4.2 Flow regimes in packed beds and porous media

Knowledge of the several flow regimes that occur in practice is indispensable in the design of packed bed reactors. These units may be operated in different flow regimes, depending on the throughput of the phases, characteristics of the packed bed and the fluid physical properties. For the flow rate of co-current two phase

flows in gas-liquid systems, it is widely accepted that four general flow regimes occur through a packed bed: the low interaction regime, also known as the trickle flow regime, pulsing flow regime, spray flow regime and the dispersed bubble flow regime Reinecke & Mewes (1997). Figure 2.13 illustrates schematically the flow regimes of a gas-liquid system through a packed bed.

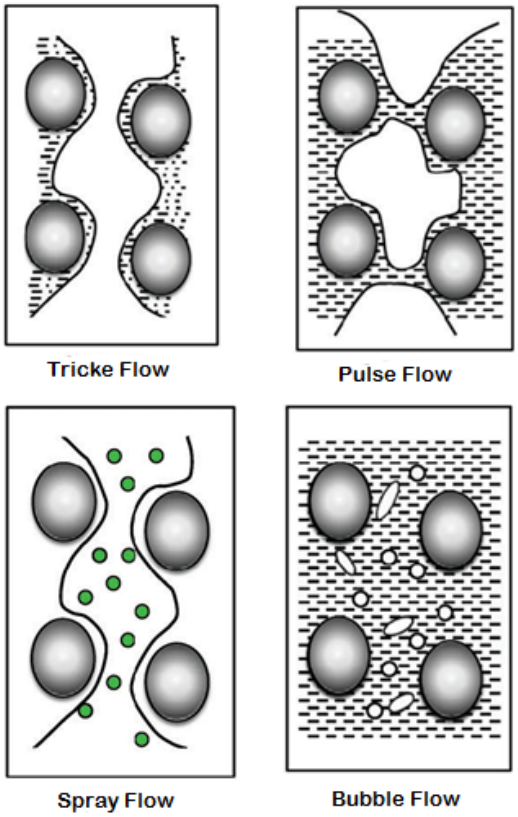

Figure 2.13: Schematic representation of gas-liquid flow regimes in a packed bed column with non-porous spherical pellets randomly distributed Reinecke & Mewes (1997)

.

Trickle flow is generated at low liquid and gas flow rates. The liquid phase flows over the solid packing in the form of streams or films while the gas phase travels in the remaining void space. In this regime a partial or total wetting of the solid particles may occur, depending on the flow rate and structures of

the liquid flow Wang *et al.* (2013). During trickle flow operation, problems such as incomplete wetting, formation of hot spots (when temperature is considered), low interaction between the gas and liquid phases and low selectivity can be encountered Kundu *et al.* (2001).

The pulsing flow regime occurs at relatively higher gas and liquid input flow rates than trickle flow. The gas and liquid flow with similar frequencies and velocities through the medium in form of pulses or slugs. Some of the advantages of this type of flow regime compared to trickle flow are the increase in mass and heat transfer rates, complete catalyst wetting and minimum stagnant liquid hold ups during operation Biardi G. (1999); Wang *et al.* (2013).

The spray flow occurs at high gas and low liquid flow rates in which the liquid phase moves along the reactor in the form of droplets entrained by the continuous gas phase Aydin & Larachi (2005); Kundu *et al.* (2001), whereas for low gas flow rates and sufficiently high liquid flow rates lead to the bubble flow regime with a continuous liquid phase which contains small spherical bubbles. The four different flow regimes in a packed bed reactor for a gas-liquid system are shown in Figure 2.14. Trickle and pulsing flow patterns are the most commonly used in industrial practice Jiang *et al.* (2001); Wang *et al.* (2013).

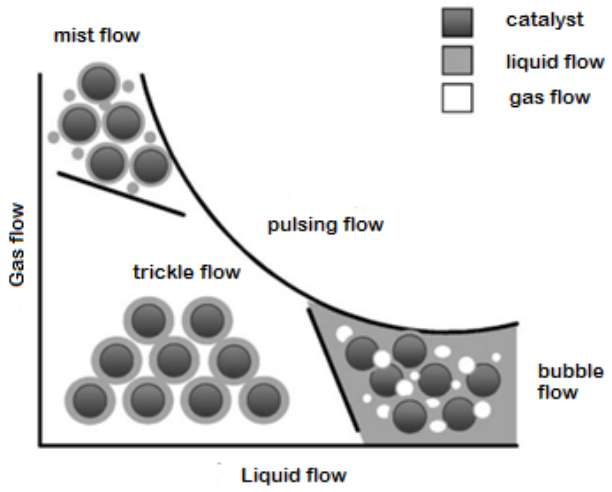

Figure 2.14: Flow regime map of gas-liquid flow in packed bed reactor Urseanu *et al.* (2005)

.

Considerable efforts have been developed to study the hydrodynamics of packed bed reactors operating in trickle flow. This type are commonly known as trickle bed reactors (TBR). A number of empirical correlations are available in the literature, including theoretical closure models based on fundamental physical basis.

The following section presents and overview of the most relevant empirical and theoretical models used for predicting two-phase flow in porous media over the past years. The review describes the main two-phase flow models that have been proposed to study the hydrodynamics of trickle flow in packed bed reactors. These models can be divided in three main categories: the relative permeability model Levec *et al.* (1986); Nemec & Levec (2005); Saez & Carbonell (1985), the slit model Aydin & Larachi (2005); Holub *et al.* (1992); Iliuta *et al.* (2000) and the fundamental force balance model Attou & Ferschneider (1999); Boyer *et al.* (2007); Narasimhan *et al.* (2002). A brief description of the most relevant models for predicting gas-liquid trickle flow in packed bed reactors is presented below.

2.4.3 Gas-liquid two phase flow models

Among the theoretical approaches, the relative permeability concept was used by Saez & Carbonell (1985) for predicting the two-phase hydrodynamics of trickle flow in packed beds. The permeability refers to a measure of the ability of a porous material to allow fluids to pass through it and is related to the porosity and to the shape of the pores in the medium. The relative permeability study considers an expression for the drag force for single phase flow and the fluid-fluid interaction was absorbed into empirical correlations for gas and liquid relative permeabilities. These are simple power-law expressions based on hold up and pressure drop data from the literature and are written as a function of the reduced liquid phase saturation and the gas saturation. Its concept was then generalised to include relative permeability in the viscous and inertial terms of the Ergun Equation Macdonald *et al.* (1979).

Later, Levec *et al.* (1986), demonstrated that the relative permeability of the liquid phase was also dependent on the liquid flow rate and proposed new power law values. The influence of the Reynolds number on the relative permeability of

the gas phase was investigated in the experimental work by Lakota *et al.* (2002) who suggested a new expression for the liquid and gas relative permeabilities. Furthermore, Nemec & Levec (2005); Nemec *et al.* (2001) modified the expressions to account for high pressure operation in trickle bed reactors. A summary of the main relative permeability models found in the literature applied to gas-liquid flow in trickle bed reactors is described in Table 2.5.

Table 2.5: Relative permeability models for atmospheric and high-pressure Trickle Bed Reactors Wang *et al.* (2013).

Literature	Liquid Phase		Gas phase
Saez & Carbonell (1985)	$k_L = \delta_L^{2.43}$		$k_G = S_G^{4.8}$
Levec *et al.* (1986)	$k_L = \delta_L^{2.9}$,	$(\delta_L \geq 0.2)$	$k_G = S_G^n (n = 3.5 - 7.5)$
	$k_L = 0.25\delta_L^{2.0}$,	$(\delta_L < 0.2)$	
	$k_L = \delta^{2.0}$		
Lakota *et al.* (2002)	$k_L = \delta_L^{2.92}$,	$(\delta_L \geq 0.3)$,	$k_G = S_G^n$,
	$k_L = 0.4\delta_L^{2.12}$,	$(\delta_L < 0.3)$	$n = x + 0.478 Re_G^{0.774}$
Nemec & Levec (2005)	$k_L = \delta_L^{2.92}$,	$(\delta_L \geq 0.3)$,	$k_G = S_G^{3.9}$
	$k_L = 0.40\delta_L^{2.12}$,	$(\delta_L < 0.3)$	$0 < S_G < 0.9$
Nemec *et al.* (2001)	$k_L = \delta_L^{2.92}$,	$(\delta_L \geq 0.3)$,	$0.40 k_G = S_G^{3.6}$
	$k_L = 0.40\delta_L^{2.12}$,	$(\delta_L < 0.3)$	$S_G^{5.5}$, $(S_G > 0.64)$

The relative permeability approach has been recognised to provide good estimations of liquid hold up and pressure drops and can also be extendible to two or three dimensions to simulate non-uniform multiphase flows Wang *et al.* (2013). Attempts in the implementation of the relative permeability approach in CFD models for trickle bed reactors have been carried out by Atta *et al.* (2007, 2010). Their results showed a reasonable prediction of the main hydrodynamics through the packed beds using this closure model.

Furthermore, Holub *et al.* (1992), proposed the slit model to predict the local flow behaviour of a two-phase flow through the packed bed. The model assumes that the liquid flows over the solid particles forming a uniform film thickness

which completely wets the particle wall, while the gas flows as a continuous phase through the remaining voids, mainly in the central core. The slit model consists of drag force expressions in the form of a modified Ergun equation. Good predictions of the liquid hold up and pressure drop based on data for atmospheric pressure were achieved in their work, however, limitations for high-pressure operations were observed. A new set of empirical velocity and shear-slip factor functions for high interaction and high pressure regimes were introduced by Al-Dahhan & Dudukovic (1994); Al-Dahhan *et al.* (1998). Further improvements to the slit model in order to account for partial and fully wetting conditions were developed by Iliuta & Larachi (1999).

In addition to the relative permeability model and the slit models, the development of physical models based on the fundamental force balance equation have been proposed by several authors Attou & Ferschneider (1999); Boyer *et al.* (2007); Narasimhan *et al.* (2002). These approaches are known as the fluid-fluid interfacial force models in which the contribution of the drag force from the particle-fluid interactions and the fluid-fluid interactions are taken into account. The drag force model by Attou & Ferschneider (1999) is the most commonly used to study the hydrodynamics of trickle flow in packed bed reactors. The model was derived from the momentum balance equation and the physical description of various interactions effects. The model assumes a two-phase annular flow in which the phases are separated by a smooth and stable interface. Also, the model includes a term for the capillary pressure gradient derived from the fluid-fluid interface in terms of the Leverett's function Leverett (1941). The interaction forces were deduced from the single phase flow equation of Kozeny-Carman, involving both the viscous and the fluid inertia contributions. The predictions of the pressure gradient and liquid saturation over a range of operating conditions showed reasonable agreement with experimental data from the literature. The accuracy of the model was significantly improved by Boyer *et al.* (2007) who generalised the tortuosity term in the closure law for two-phase flow tortuosity for a liquid film. Similar drag force models including the tortuosity concept have been tested and adopted in other studies Kundu *et al.* (2003); Narasimhan *et al.* (2002). Although the model by Attou & Ferschneider (1999) is one of the most established

drag force models the prediction of two-phase flow in packed beds, it is limited to the particular case of trickle flow regime of gas-liquid flows Wang *et al.* (2013).

Capillary Pressure correlations

The influence of the capillary forces on the flow distribution inside a trickle bed reactor has been investigated by several authors Attou & Ferschneider (2000); Grosser *et al.* (1988); Jiang *et al.* (1999); Lappalainen *et al.* (2009). The capillary pressure effects are also related to the hysteresis phenomenon occurring in the pressure drops and liquid holdups during co-current gas-liquid flow in packed beds Wang *et al.* (2013). One of the most often used capillary pressure correlation is the one proposed by Grosser *et al.* (1988) who combined the relative permeability drag force expression by Saez & Carbonell (1985) with Leverett's correlation for the capillary pressure term. The latter depends only on the liquid saturation and also exhibits hysteresis between liquid imbibition and drainage experiments Leverett (1941). A different approach was proposed by Attou & Ferschneider (1999) which is based on geometric estimates involving the Young-Laplace equation and includes an empirical factor to account for high pressure operating conditions. Furthermore, Jiang *et al.* (2002b) modified the model proposed by Grosser *et al.* (1988) to account for the particle wetting efficiency. The accuracy of the model was improved Boyer *et al.* (2005) who proposed a new modified capillary pressure model.

One of the main limitations of the capillary pressure models from Grosser *et al.* (1988) and Attou & Ferschneider (2000) is that the contact angle between the solid and the fluid is neglected. This feature has been found important in liquid spreading over a solid surface and Lappalainen *et al.* (2009) developed a new analytical capillary pressure model to describe the capillary pressure-saturation relationship. The model was found to be suitable for predicting liquid capillary and liquid saturation relations for spherical particles.

Additionally, the implementation of computational fluid dynamics (CFD) in packed bed reactors, up to now has been largely limited to the trickling-flow regime Atta *et al.* (2007, 2010); Jiang *et al.* (2002a); Lappalainen *et al.* (2011). The capillary pressure effects in CFD models have recently received attention

in efforts to properly understand the flow behaviour in such systems Solomenko *et al.* (2015); Wang *et al.* (2013). Some of the CFD results involving capillary effects can be visualised in Figure 2.15 showing the liquid dispersion of a gas-liquid flow through a packed bed reactor. Also, some studies have attempted to address the prediction of trickling-to-pulsing regime by coupling CFD approach and linear stability analysis Attou & Ferschneider (1999); Iliuta & Larachi (2004); Lopes *et al.* (2011).

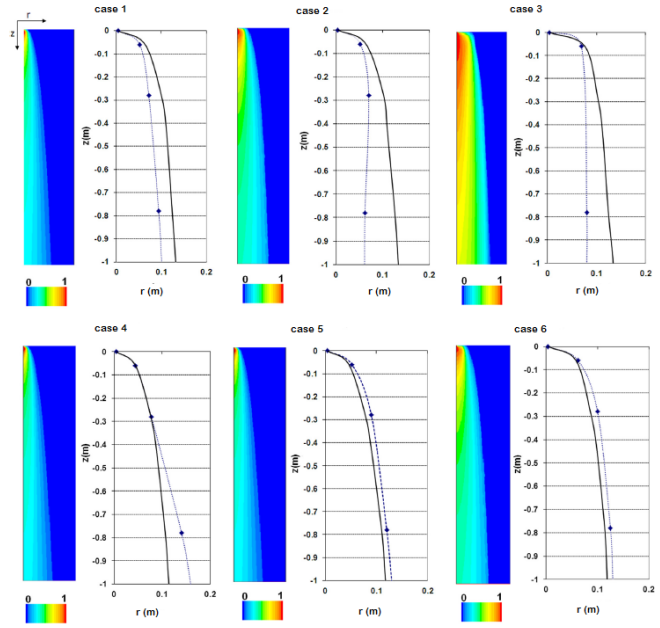

Figure 2.15: Liquid saturation fields and liquid jet contours in CFD simulations of gas-liquid flow in packed beds. Discrete points: experiments; continuous curves: CFD simulations. Case 1: Q_L=128 l/h, Q_G=45 m^3/h, d_p=1.99 mm; case 2: Q_L=128 l/h, Q_G=90 m^3/h, d_p=1.99 mm; case 3: Q_L=453 l/h, Q_G=45 m^3/h, d_p=1.99 mm; case 4: Q_L=128 l/h, Q_G=45 m^3/h, d_p=6 mm; case 5: Q_L=128 l/h, Q_G=90m^3/h, d_p=6mm; case 6: Q_L=453 l/h, Q_G=45 m^3/h, d_p=6 mm. Solomenko *et al.* (2015)

.

2.4.4 Liquid-liquid two-phase flow models

Compared to gas-liquids flows, relatively little work has been reported in the literature regarding liquid-liquid flow through packed bed reactors where porosity is higher and inertial effects are important. The traditional approaches to model these type of flows have shown limitations in the prediction of reliable flow characteristics within the porous domain. For instance, the case of fuel cells have demonstrated significant inaccuracies in prediction of moisture content Chen *et al.* (2016). Similarly, the traditional approach has shown to give rise to non-physical predictions of flooding in upward co-current liquid-liquid flows in packed bed reactors Figueroa (2013). However, a number of studies in the oil industry for flows in reservoirs have developed relevant models involving liquid-liquid flow in porous media Dake (1978) and can be gathered for the modelling of liquid-liquid flow in packed bed reactors. For instance, the relationship between the relative permeability and phase saturation for oil-water through the porous media.

The following section presents a brief overview of recent experimental and numerical studies for biodiesel production using a packed bed reactor as the mixing technology during the process.

2.4.5 Biodiesel production in packed bed reactors

The interest to increase biodiesel yields has led to investigate new alternatives for biodiesel production to make the process viable on an industrial scale. Among these, the performance of packed bed reactors have been considered as a potential alternative for process optimisation and to overcome main drawbacks found in current technologies Santacesaria *et al.* (2012b).

Nowadays, almost all worldwide commercial biodiesel production is carried out using a continuous stirred tank or tubular reactor with an homogeneous catalyst technology Boer (2009). Despite the advantages offered by this type of process, major problems have been identified such catalyst residuals and the formation of secondary undesired reactions Liu *et al.* (2006). The alternative of solid catalysts for biodiesel synthesis at industrial level has been investigated extensively Sharma *et al.* (2011). The attractiveness of solid catalysts is mainly

their ability to simplify the biodiesel process significantly, since the necessity of oil pre-treatment or product purification operations can be eliminated Boer (2009).

The performance of a packed bed reactor to produce biodiesel was evaluated using different vegetable oils and an enzyme based catalyst e Silva *et al.* (2014). The results suggested that the production from palm oil is the most favourable feed-stock to carry out a continuous packed bed reactor process. Also, Silva & Oliveira (2014) studied the behaviour of soy bean oil in a continuous non-catalytic packed bed tubular reactor using supercritical conditions. The results confirmed that higher biodiesel yields can be achieved with this type of reactor and demonstrated that the temperature, pressure, oil to ethanol molar ratio and water concentration had a positive effect on the production in the experimental range investigated.

Additionally, Gonzalez *et al.* (2011) explored the use of a packed reactor to produce micro-mixing effects among the reacting phases. Experiments were performed using different packing materials and conversion over 90% were achieved. The reaction rates were similar to those achieved while using micro-reactors and significantly higher values than with a stirred tank reactor. The packed bed reactor showed a similar performance to that observed for micro reactors, but with the potential advantage to process higher volume rates.

The current work has been developed with the aim of applying CFD in the mixing stage of biodiesel production suggesting the use of a packed bed reactor for process improvement and further scale up. The difficulty in applying CFD modelling to this particular problem centres on the complexity involved in predicting the flow regimes occurring inside the system.

2.5 Conclusions

This chapter summarised the main hydrodynamics studies found in the literature for gas-liquid and liquid-liquid slug flow through capillaries. The review covered both experimental and computational studies and was focused mainly on the case of liquid-liquid slug flow systems which subject has been less studied compared to gas-liquid systems. Also, some examples where liquid-liquid slug flow systems can be found were described namely in biodiesel production. Additionally, a summary

of two-phase flow studies in porous media such as packed beds were introduced along with recent application of these systems for biodiesel production process.

The next chapter describes fundamental concepts of the transport phenomena occurring in single and two phase flows in round capillaries. Also, the most relevant concepts for multi-phase flow modelling in porous media are introduced. The aim is to understand in detail the hydrodynamics in slug flows through capillaries and apply it to flow in porous media, such as in packed bed reactors.

Chapter 3

Theoretical Framework

This chapter introduces theoretical concepts to describe the transport properties and characteristics of single and two phase flows in circular capillaries. It is mainly focused on the study of two-phase slug flow in a capillary. The fluid dynamics corresponding to this type of flow regime is quite complex and requires a comprehensive understanding of the fundamental hydrodynamic concepts. The aim is to understand the transport phenomena in capillaries and incorporate it into microfluidic systems applications, such as the flow in catalytic monoliths and multiphase flow in porous media. Additionally, fundamental concepts for modelling single and two phase flows in a porous media are introduced in this chapter.

3.1 Dimensionless numbers

The dynamics of a flow is mainly controlled by the interaction of viscous, inertial and interfacial forces. Dimensionless numbers provide a way of quantifying the magnitude of these forces relative to each other. The relevant dimensionless numbers used to characterise the hydrodynamics of slug flow regime are described below.

Reynolds number:

The Reynolds number defines the ratio of inertial and viscous forces. It is used to characterise the flow regime as either laminar or turbulent. The Reynolds number is defined as:

$$Re = \frac{\rho_i u_i D}{\mu_i} \tag{3.1}$$

where ρ_i, μ_i, u_i and D refer to the density of the fluid i, viscosity, velocity and capillary diameter, respectively.

Capillary number:

The Capillary number is a measure of the ratio of viscous forces and the surface tension acting across an interface between two immiscible fluids. It is defined as:

$$Ca = \frac{\mu_i u_i}{\sigma} \tag{3.2}$$

where σ is the surface tension between the phases. For low Capillary numbers ($Ca < 10^{-5}$) the flow is dominated by capillary forces whereas for high Capillary number these are negligible compared to the viscous forces.

Weber number:

The Weber number represents the balance between the inertial and interfacial forces. It indicates whether the kinetic or the surface tension energy is dominant. The Weber number is the product of the Reynolds number and Capillary number defined as:

$$We = ReCa = \frac{\rho_i u_i^2 D}{\sigma} \tag{3.3}$$

Bond number:

The Bond number represents the ratio of the gravitational forces and the capillary forces as:

$$Bo = \frac{(\Delta\rho_i) g D^2}{\sigma} \tag{3.4}$$

where $\Delta\rho$ is the density difference between the immiscible fluids and g the gravitational effects. The Bond number is also known as the *Eötvös* number ($Eö$).

It is used to characterise the shape of bubbles or drops moving in a surrounding fluid.

Galileo number:

The Galileo number represents the ratio between gravity forces to viscous forces and is written as:

$$Ga = \frac{\frac{\rho_p}{\rho_f}\vec{g}d_p^3}{\nu_f^2} \tag{3.5}$$

where, ρ_p and ρ_f are the particle and fluid densities respectively, ν_f is the kinematic viscosity of the fluid,d_p the particle diameter and $\vec{g} = \frac{(\rho_p - \rho_f)}{\rho_f}$ is the reduced gravity. The Galileo number is mainly used to compute settling velocities under gravity.

3.2 Single phase flow in capillaries

The flow regime in capillaries is usually characterised by laminar flow. As the fluid flows along the capillary, a boundary layer begins to form due to the viscous forces generated between the fluid and the capillary walls. The region where the flow is developing is commonly known as the entrance region and it finishes with the merging of the boundary layers at the capillary centre-line. The entrance length is a function of the Reynolds number of the flow and for laminar flow this length is given by $L = 0.05ReD$. After this point the velocity profile develops further until it becomes parabolic, after which it maintains the same shape indicating fully developed flow. A schematic representation of the hydrodynamic boundary layer development in a laminar circular pipe flow is shown in Figure 3.1.

The velocity profile for a single phase flow in a circular capillary can be calculated by the Navier-stokes equation projected onto the x-axis in the (r, θ, x) cylindrical coordinate system as:

$$\rho\left(\frac{\partial u_x}{\partial t} + u_r\frac{\partial u_r}{\partial r} + \frac{\partial u_\theta}{r}\frac{\partial u_x}{\partial \theta} + u_x\frac{\partial u_x}{\partial x}\right) = -\frac{\partial}{\partial x}(p - \rho g_x x) + \mu\nabla^2 u_x \tag{3.6}$$

The continuity equation takes the form:

$$\frac{\partial \rho}{\partial t} + \frac{1}{r}\frac{\partial}{\partial r}(\rho u_r r) + \frac{1}{r}\frac{\partial}{\partial \theta}(\rho u_\theta) + \frac{\partial}{\partial x}(\rho u_x) = 0 \tag{3.7}$$

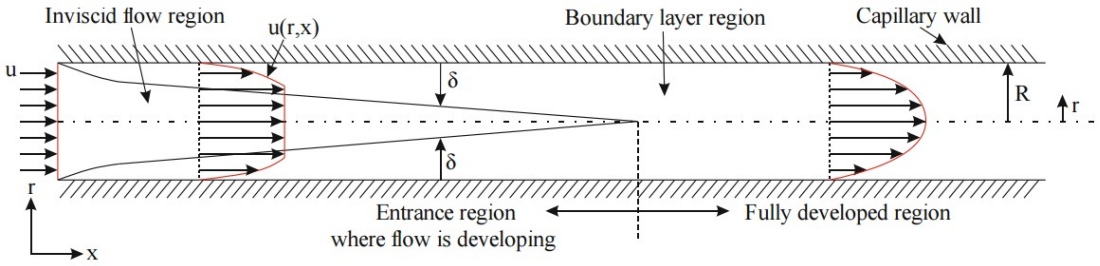

Figure 3.1: Hydrodynamic boundary layer development in laminar circular tube flow Eain (2014)

Assuming steady state, symmetrical on the x-axis and incompressible flow, the continuity and momentum equation can be reduced respectively to:

$$\frac{1}{r}\frac{\partial}{\partial r}(ru_r) = 0 \tag{3.8}$$

$$\rho u_r\left(\frac{\partial u_x}{\partial r}\right) = \mu\frac{1}{r}\frac{\partial}{\partial r}\left(r\frac{\partial u_x}{\partial r}\right) - \left(\frac{dp}{dx}\right) \tag{3.9}$$

Equation 3.8 implies that $u_r = 0$, hence the left hand side of Equation 3.9 is zero as well reducing to:

$$\frac{1}{r}\frac{\partial}{\partial r}\left(r\frac{\partial u_x}{\partial r}\right) = \frac{1}{\mu}\frac{dp}{dx} \tag{3.10}$$

Double integration of Equation 3.10 gives the general solution:

$$U_{(r)} = \frac{1}{4\mu}\frac{\partial P}{\partial x}(r^2) + Cln(r) + D \tag{3.11}$$

where C and D are constants of integration determined by the boundary conditions.

For the case of a non-zero pressure gradient and zero velocity boundary condition at the capillary walls, the velocity $u(r)$, at any given point is defined by:

$$u(r) = \frac{1}{4\mu}\left(\frac{dp}{dx}\right)(R^2 - r^2) \tag{3.12}$$

where μ represents the dynamic viscosity, dp/dx is the pressure gradient, x is the coordinate system in the direction of the flow, R and r are the radius of the capillary and the radial distance from the center of the capillary, respectively.

The presence of a second immiscible phase gives rise to a variety of fluid distributions and flow patterns. The flow behaviour depends on the relative flow rates of the fluid phases involved and the interaction between the gravitational, interfacial, inertial and viscous forces. Such multiphase flows provide several mechanisms for enhancing and improving the performance of single-phase microfluidic systems. Moreover, the dominant interfacial forces combined with the laminar nature of the flow result in a regular shaped interface Kreutzer & Gunther (2009). This characteristic is typically observed in capillary slug flows. Figure 3.2 illustrates a schematic of a slug flow in a capillary represented by a drop suspended in a continuous flow.

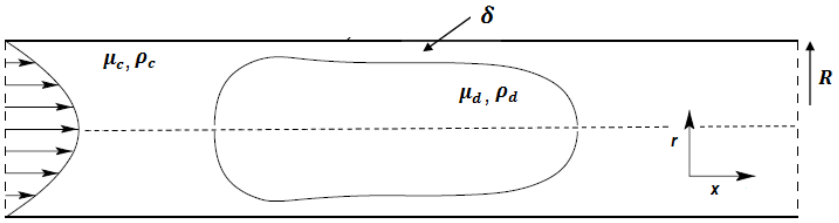

Figure 3.2: Representation of a drop suspended in a continuous flow Lac & Sherwood (2009)

.

Slug flow involves additional complex flow features unique to this type of flow regime as described previously in Section 2.2. Nevertheless, as a first approximation the study can be simplified by considering an infinite long droplet dispersed in a continuous phase and assuming that end effects can be ignored. This flow behaviour is analogous to that corresponding to annular flow and is described in the following sections based on the mathematical models developed by Abiev (2008) and Lac & Sherwood (2009).

3.3 Couette-Pousielle flow in an annulus

The bubble or droplet in a slug flow occupies almost the entire cross-section of the capillary and is separated from the wall by a thin film. So, as a first attempt to describe the two-phase flow behaviour, the bubble can be assumed as an infinitely long cylinder of radius r_1 surrounded by a film with constant thickness δ flowing near the wall of a cylindrical capillary of radius R as illustrated in Figure 3.3.

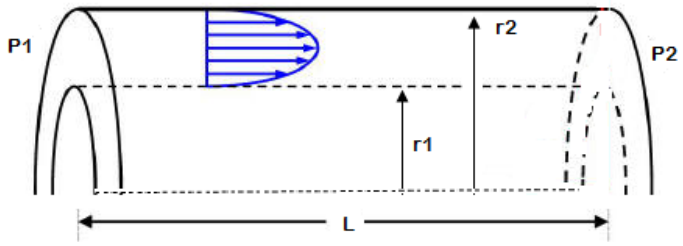

Figure 3.3: Velocity profile of Poiseuille Flow in an Annulus

.

The continuous flow surrounding the droplet of radius r_1 can be first analysed by assuming a solid dispersed phase.

3.3.1 Pousielle flow in an annulus

Considering the case of a non-zero pressure gradient, with zero velocity boundary conditions at both walls:

$$\frac{\partial p}{\partial x} \neq 0 \quad ; \quad U_{(r_1)} = U_{(r_2)} = 0 \tag{3.13}$$

Applying the boundary conditions (3.13) in the Navier-Stokes equation for fully developed flow (3.11) and after simple manipulation, the velocity profile take the form:

$$U_{(r)} = \alpha r^2 + \frac{\alpha}{ln(r_2/r_1)}\left(r_1^2 ln(r/r_2) + r_2^2 ln(r_1/r)\right) \tag{3.14}$$

where $\alpha = \frac{1}{4\mu}\frac{\partial P}{\partial x}$.

3.3.2 Couette Flow in an annulus

Considering the case of zero pressure gradient and non-zero velocity boundary conditions at both capillary walls:

$$\frac{\partial p}{\partial x} = 0 \quad ; \quad U_{(r_1)} = U_1 \quad ; \quad U_{(r_1)} = U_2 \tag{3.15}$$

Thus, Equation 3.11 reduces to:

$$U_{(r)} = Clnr + D \tag{3.16}$$

Applying boundary conditions, the velocity profile of Couette flow in an annulus is given by:

$$U_{(r)} = \frac{U_2 - U_1}{lnr_2 - lnr_1} lnr + \frac{U_1 lnr_2 - U_2 lnr_1}{lnr_2 - lnr_1} \tag{3.17}$$

3.3.3 Couette-Pousielle flow in an annulus

Considering the case of a non-zero pressure gradient, with non-zero velocity boundary conditions at both walls:

$$\frac{\partial p}{\partial x} \neq 0 \quad ; \quad U_{(r_1)} = U_1 \quad ; \quad U_{(r_2)} = U_2 \tag{3.18}$$

Substituting the boundary conditions 3.18 in the general solution described in Equation 3.11, the velocity profile is given by:

$$U(r) = \alpha r_2^2 + \frac{1}{ln(r_2/r_1)} \Big((\alpha r_1^2 - U_1) ln(r/r_2) + (\alpha r_2^2 - U_2) ln(r_1/r) \Big) \tag{3.19}$$

Where: $\alpha = \frac{1}{4\mu} \frac{\partial P}{\partial x}$

Figure 3.4 shows the effect of dragging action of the upper wall exerted on the fluid for different values of pressure gradient. For non-zero pressure $P > 0$ the velocity remains positive along the capillary wall, but for a negative value $P < 0$, there is a positive or adverse pressure gradient in the direction of motion and the velocity can become negative and back flow may occur near the wall at rest Ramamurthi (2012).

Furthermore, Equations 3.14 and 3.15 can be combined to describe the flow of both fluids across the capillary. The relation between the bubble velocity, the velocity in the slug and film regions, and the forces applied to the entire two-phase system are described in the following section for the case of a two-phase flow in the slug flow regime.

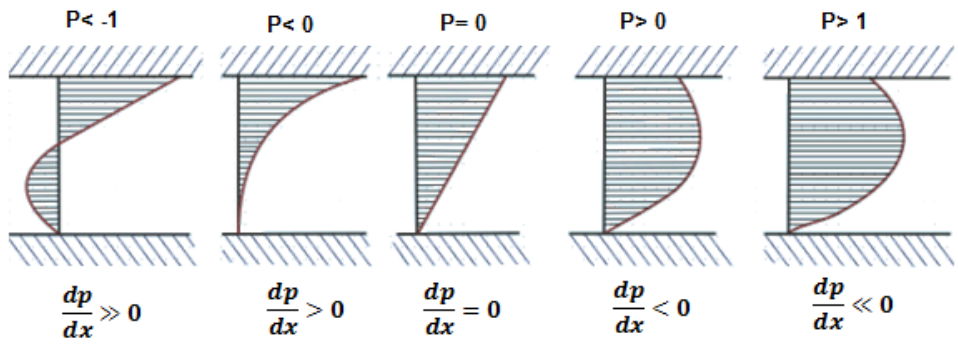

Figure 3.4: Velocity profile for the Couette flow for various values of pressure gradient Ramamurthi (2012)

3.4 Slug Flow in Capillaries

Slug flow is characterised when one of the fluids flows as a continuous phase forming a thin film near the wall and a dispersed phase, with a higher surface tension, travelling in a form of a droplet. The flow is dominated by surface tension forces that allow the two-phase flow to remain stable along the capillary Angeli & Gavriilidis (2008). A representation of slug flow regime in a capillary is shown in Figure 3.5.

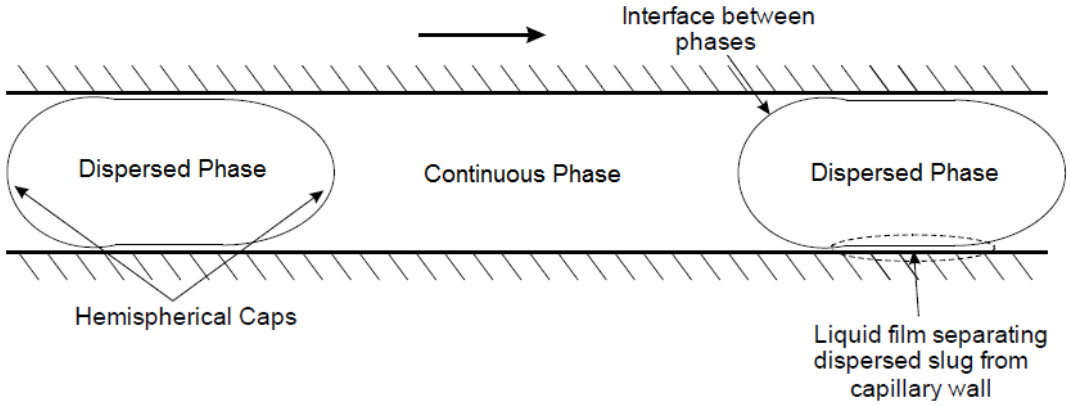

Figure 3.5: Slug flow structure in a capillary Eain (2014)

.

The presence of the liquid film and the hemispherical caps at the rear and

front of the droplets are the main features that affect the hydrodynamics of the slug flow regime Eain *et al.* (2015). For instance, at the capillary cross sections occupied by the two-phase slug flow the velocity profile differs significantly due to the surrounding liquid film.

The velocity profiles in these two regions can be predicted from a momentum balance along the axial direction to evaluate local flow velocity profiles in the film and bubble/droplet regions Abiev (2008); Gupta *et al.* (2013); Howard & Walsh (2013); Lac & Sherwood (2009). Figure 3.6 illustrates a schematic diagram used to formulate the equation of motion for the slug flow regime assuming an infinite droplet.

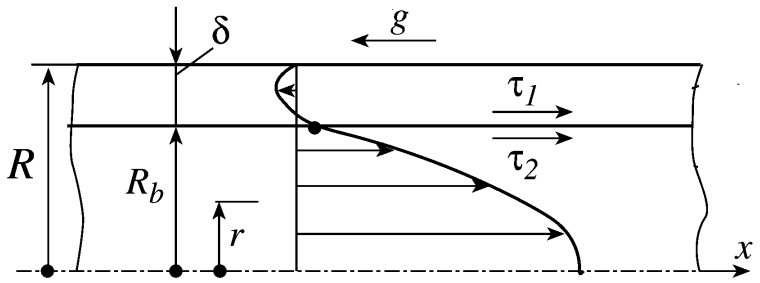

Figure 3.6: Schematic diagram used to formulate the motion equation for the slug flow of a two-phase slug flowAbiev (2008)

Lac & Sherwood (2009), developed a mathematical model to describe the motion of an infinite droplet along a capillary in a pressure driven flow. The velocity profile for the region of the film $r_b \leq r \leq R$ in the limits $\mu_d \to \infty$ or $\mu_d \to 0$ is written as:

$$u_{(r)} = \alpha(r^2 - R^2) \tag{3.20}$$

Where: $\alpha = \frac{1}{4\mu}\frac{\partial P}{\partial x}$

The velocity profile in the region $r_0 \leq r \geq r_1$, corresponding to the droplet take the form:

$$u_{(r)} = \alpha(r^2 + (\lambda - 1)\delta^2 R^2 - \lambda R^2) \tag{3.21}$$

Where: $\lambda = \frac{\mu_d}{\mu_c}$ and δ the non-dimensional film thickness.

The shear stresses at the bubble or droplet surface (r_b) are usually assumed to be negligible when modelling gas-liquid flow systems because the gas viscosity is

very low. However, this feature can not be applied in liquid-liquid systems since the dispersed phase viscosity is not negligible and the effect of shear stresses on the velocity within the film can be considerable Abiev (2009); Abiev & Dymov (2013); Eain *et al.* (2015); Gupta *et al.* (2013); Howard & Walsh (2013).

Abiev (2008) proposed the mathematical model for a gas-liquid slug flow in a capillary assuming ideal annular flow and including the influence of the effective gravitational force as:

$$g_i^{'} = g_x - \frac{1}{\rho}\frac{\partial p}{\partial x} \tag{3.22}$$

where $g_i^{'}$ is the effective gravitational acceleration accounting for the gravitational force and pressure gradient along the x-axis acting on the phase i. Th velocity profiles in the dispersed phase and the liquid film were calculated by taking a momentum balance at the interface between the two phases as:

$$u_1|_{r=r_b} = u_2|_{r=r_b} \quad ; \quad \tau_1|_{r=r_b} = \tau_2|_{r=r_b} \tag{3.23}$$

Thus, the velocity profile in the liquid film is given by:

$$u_1(r) = E_1(R^2 - r^2) - C_1 ln\Big(\frac{R}{r}\Big) \tag{3.24}$$

and the velocity in the dispersed phase take the form:

$$u_2(r) = E_1\big[R^2 - r_d^2\big] + E_2\big[r_d^2 - r^2\big] - C_1 ln\Big(\frac{R}{r_d}\Big) \tag{3.25}$$

where:

$$E_1 = \frac{g_1^{'}}{4\mu_1} = \frac{1}{4\mu_1}\Big(g_x - \frac{1}{\rho_1}\frac{\partial p}{\partial x}\Big) \tag{3.26}$$

$$C_1 = (\rho_1 - \rho_2) g_x \frac{r_d^2}{2\mu_1} \tag{3.27}$$

$$E_2 = \frac{g_2^{'}}{4\mu_2} = \frac{1}{4\mu_2}\Big(g_x - \frac{1}{\rho_2}\frac{\partial p}{\partial x}\Big) \tag{3.28}$$

Similarly, Howard & Walsh (2013) solved for the velocity profiles in the dispersed phase and the liquid film for horizontal slug flow. The velocity profiles for each phase are described as follows:

$$U_{d,(r)} = \left(\frac{2U_m}{1+\frac{r_d^4}{R^4}\left(\frac{\mu_c}{\mu_d}-1\right)}\right)\left(\frac{r_d^2}{R^2}\frac{\mu_c}{\mu_d}\left(1-\frac{r^2}{r_d^2}\right)+1-\frac{r_d^2}{R^2}\right) \tag{3.29}$$

for $r_d > r > 0$

$$U_{f,(r)} = \left(\frac{2U_m}{1+\frac{r_d^4}{R^4}\left(\frac{\mu_c}{\mu_d}-1\right)}\right)\left(1-\frac{r^2}{R}\right) \tag{3.30}$$

for $R > r > r_d$, where the subscripts: c, d, m refers to the slug or continuous phase, dispersed phase and two-phase mixture, respectively.

The influence of the film thickness and curvature interface on the hydrodynamics of a slug flow through a capillary is introduced in the following section.

3.4.1 Film thickness correlations

The first theoretical expression for the film thickness was derived by Bretherton (1961) who applied lubrication theory to the flow in the liquid film surrounding a long inviscid bubble in small tubes, in the absence of gravitational forces. This expression is in the limit of vanishing Ca and is written by:

$$\frac{\delta}{D} = \frac{1}{2}0.643(3Ca)^{\frac{2}{3}} \tag{3.31}$$

Bretherton's correlation assumes negligible inertial effects ($Re < 1$) and a small film thickness (δ) compared to the capillary radius, $\frac{\delta}{R} < 10^{-2}$. Although this correlation has been widely used, its applicability was found to be limited to a small range of Capillary numbers between $10^{-4} \leq Ca \leq 10^{-1}$. A modification to Bretherton's correlation to consider a wider range of Capillary numbers was then proposed by Aussillous & Quere (2000):

$$\frac{\delta}{D} = \frac{1.34(3Ca)^{\frac{2}{3}}}{1+1.34(2.5Ca)^{\frac{2}{3}}} \tag{3.32}$$

The empirical correlation in Equation 3.32 was based on Taylor's experimental data Taylor (1961) and is valid for Ca < 1.4, but only suitable for very low Reynolds number or creeping flows.

Furthermore, Han & Shikazono (2009) developed an extensive experimental work in capillary slug flow and investigated the dependence of the film thickness

on the Reynolds number. A new film thickness correlation was proposed to account for inertial effects. The expression is defined in function of the Reynolds number, Capillary number and Weber number as follows:

$$\frac{\delta}{D} = \frac{0.670Ca^{\frac{2}{3}}}{1 + 3.13Ca^{\frac{2}{3}} + 0.504Ca^{0.672}Re^{0.589} - 0.352We^{0.629}} \tag{3.33}$$

Equation 3.33 is valid between the ranges $0 < Ca < 0.3$ and $0 < Re < 2000$ Howard & Walsh (2013).

Additionally, the CFD study by Langewisch & Buongiorno (2015) proposed a correlation similar in form to Equation 3.33, but includes the inertial effects through the $\phi(Re)$ term described below:

$$\frac{\delta}{D} = \frac{0.670Ca^{\frac{2}{3}}}{1 + 2.86[1 + \phi(Re)] \times Ca^{c}} \tag{3.34}$$

where:

$$\phi(Re) = \left[\frac{32.05}{Re^{0.593}} + 4.56e^{-5}Re^{1.909}\right]^{-1} \tag{3.35}$$

The expression in Equation 3.34 is only suitable for high viscosity and density ratios $\frac{\mu_c}{\mu_d} = 100$ and $\frac{\rho_c}{\rho_d} = 1000$, respectively.

Moreover, Eain *et al.* (2013) developed experimental measurements to investigate the film thickness in liquid-liquid slug flow. The author modified expressions 3.31 and 3.32 and proposed a correlation to describe the film thickness behaviour in the visco-capillary and visco-inertial regimes as follows:

$$\frac{\delta}{R} = \frac{1.34Ca^{\frac{2}{3}}}{1 + 1.34(1.6Ca^{\frac{2}{3}})} \quad ; \quad Ca < Ca^{*} \tag{3.36}$$

$$\frac{\delta}{R} = 0.35Ca^{0.354}We^{0.097} \quad ; \quad Ca > Ca^{*} \tag{3.37}$$

where:

$$Ca^{*} \sim \left(\frac{\mu^2}{\rho R\sigma}\right)^{\frac{3}{4}} \tag{3.38}$$

Equations 3.36 and 3.37 are satisfactory for droplet lengths $L_d > 1.86$.

3.4.2 Pressure drop in slug flow

For fully developed Hagen-Poiseuille flow of a single phase flowing in a capillary, the pressure drop is given by:

$$\frac{\Delta P}{L} = \frac{16}{Re}\Big(\frac{1}{2}\rho U^2\Big)\frac{4}{D} \tag{3.39}$$

where ΔP, L, Re, ρ, U, D refer to the pressure drop, capillary length, Reynolds number, density, mean velocity of the flow and capillary diameter, respectively. The presence of a second immiscible phase into a capillary in order to produce slug flow, results in an increase on the pressure drop over the single phase flow case due to the interfacial shear generated between the phases and the curvature of the bubble. Thus, the total pressure drop in the capillary may now be expressed as the sum of the contribution of the two phases Walsh *et al.* (2009).

$$\Delta P_T = \Delta P_s + \Delta P_b \tag{3.40}$$

Equation 3.40 describes the total pressure drop as the sum of the single phase pressure drop, ΔP_s, and the additional pressure drop ΔP_b caused by the interface between the phases. The total pressure drop can also be written in the non-dimensional form as:

$$fRe_T = fRe_s + fRe_b \tag{3.41}$$

where f corresponds to the friction factor.
One of the earliest studies of capillary slug flow was developed by Bretherton (1961), who presents a theoretical solution for the pressure drop caused by a single bubble in a slug flow regime and is usually given by the following expression:

$$\Delta P_b = 7.16(3Ca^{\frac{2}{3}})\frac{\sigma}{D} \tag{3.42}$$

where σ is the surface tension between the phases. Bretherton's expression was designed to include the changes in curvature due to the presence of a liquid film and the Laplace pressure term. The interfacial pressure drop term ΔP_b can also be described as a function of Capillary number and slug length L_s^* as Walsh *et al.* (2009):

$$fRe_b = \frac{7.16(3Ca)^{\frac{2}{3}}}{2L_s^*Ca} \tag{3.43}$$

In more recent studies, Kreutzer *et al.* (2005) determined that the pressure drop caused by the presence of the bubbles was a function of the slug length L_s^*, Capillary number (Ca) and Reynolds number (Re). The authors examined the contribution of the interface both numerically and experimentally and derived the following expression:

$$fRe_b = \frac{\alpha}{L_s^*}\left(\frac{Re}{Ca}\right)^{\beta} \tag{3.44}$$

where $\alpha = 2.72$, $\beta = 0.33$ are constants and L_s^* is the dimensionless slug length, $L^s = \frac{L_s}{D}$. The same correlation was derived in the experimental work by Walsh *et al.* (2009), but using a different value of $\alpha = 1.92$ which provided a better agreement with the data.

Warnier *et al.* (2010) examined the contribution of the bubble to the pressure drop in a Taylor flow regime. Similar to the work developed by Aussillous & Quere (2000), the authors reworked Bretherton's correlation to incorporate Taylor's Law Taylor (1961) and to account for the presence of the film and its effects on the pressure drop. The correlation was extended for higher Reynolds number $Re < 150$ and Capillary number $Ca < 0.01$. The resultant interfacial pressure drop expression is given by :

$$fRe_b = \left(\frac{7.16\left(3^{\frac{2}{3}}\right)}{32}\frac{1}{L_s^*}\frac{A}{A_B}\frac{1}{Ca^{\frac{1}{3}} + 3.34Ca}\right) \tag{3.45}$$

where A and A_b refer to the capillary and bubble cross sectional areas, respectively. The pressure drop model in Equation 3.45 is analogous to the model proposed by Kreutzer *et al.* (2005); Walsh *et al.* (2009), but additionally considers the velocity of the dispersed phase, thereby increasing the accuracy of the pressure drop along the capillary.

Furthermore, Eain *et al.* (2015) modified this model by normalising the interfacial component in Equation 3.45 by the volume fraction occupied by the continuous phase, $(1 - \alpha)$. The expression is written as:

$$fRe_b = \left(\frac{8.16\left(3^{\frac{2}{3}}\right)}{32}\frac{1}{L_s^*}\frac{A}{A_B}\frac{1}{Ca^{\frac{1}{3}} + 3.34Ca}(1-\alpha)^{\frac{1}{3}}\right) \tag{3.46}$$

where α is the volume fraction of the dispersed phase and can be calculated by:

$$\alpha = \frac{Q_d}{Q_T} \tag{3.47}$$

Equation 3.46 provides an extended range of applicability for the existent gas-liquid models: $1.45 \leq Re \geq 567.59$, $4.5 \times 10^{-5} \leq Ca \geq 0.067$, $0.76 \leq L_s^* \geq 46.83$, $1.05 \leq L_d^* \geq 14.25$ and is also applied for liquid-liquid slug flows in a capillary Eain *et al.* (2015).

Moreover, a computational study for capillary slug flow was developed by Langewisch & Buongiorno (2015) who proposed a new correlation for the pressure drop across a Taylor bubble and is described in Equations 3.48 and 3.49.

$$\frac{\Delta P_b}{\sigma/R} = 3.96 Ca_b^{0.58} \quad ; \quad Ca_b < 0.187 \quad ; \quad Re_b < 5 \tag{3.48}$$

$$\frac{\Delta P_b}{\sigma/R} = 8 Ca_b \quad ; \quad Ca_b \geq 0.187 \tag{3.49}$$

where Ca_b and Re_b refers to the Capillary number and Reynolds number based on the liquid properties and the bubble velocity. Equations 3.48 and 3.49 are valid for high viscosity and density ratios, $\frac{\mu_c}{\mu_d} = 100$ and $\frac{\rho_c}{\rho_d} = 1000$, respectively. The authors created an extensive CFD database of predictions for bubble velocity, film thickness and interfacial pressure drop over a wide range of Reynolds and Capillary numbers, though restricted to the above viscosity and density ratios. The CFD data provided in their work was used for validation in the current study and is presented further in Chapter 5.

3.4.3 Drag Force (C_d)

Recent developments in microfluidic technologies have led to a re-evaluation of the drag force equations that were theoretically derived for ideal cases Hensley & Papavassiliou (2014). The drag force on a spherical particle can be determined by the following expression Stokes (1851):

$$\vec{F}_d = \frac{1}{2} C_d \rho_i A_p \vec{u} |\vec{u}| \tag{3.50}$$

Where A_p is the surface area of the particle ($A_p = \pi d^2/4$), C_d is the drag coefficient and $\vec{u}$ is the relative velocity.

There are many equations relating the drag coefficient C_d to the particle Reynolds number Re_p for spherical particles and also some for the case of non-spherical particles Gabitto & Tsouris (2008).

For low Re_p, the drag force is inversely proportional to the particle Reynolds number and it is referred to as the Stokes regime:

$$C_d = \frac{C_s}{Re_p} \tag{3.51}$$

For high particle Reynolds numbers $Re_p > 10^3$ for sub critical, the drag coefficient is constant and it is known as the Newton regime:

$$C_d = C_N = constant \tag{3.52}$$

The Stokes solution applies for spherical particles in uniform flow in an infinite domain at low Re_p Hensley & Papavassiliou (2014).

3.4.4 Settling Velocity (U_∞)

The prediction of the settling velocity, U_∞, is fundamental for the design of mixing and separation processes. For a single particle, the settling velocity can be calculated from the equilibrium between the gravity and drag forces. The motion of the particle based on the force balance equation can be described as Yam (2012):

$$\rho_p V_p \frac{d\vec{u_p}}{dt} = \Delta\rho V_p \vec{g} - \frac{1}{2} C_d \rho_i A_p |\vec{u}|\vec{u} \tag{3.53}$$

where ρ_p and ρ_i are the particle and fluid densities respectively, and $\Delta\rho = \rho_p - \rho_i$. For a spherical particle and assuming a positive buoyant particle settling under gravity in a stationary fluid, Equation 3.53 may be written as:

$$\frac{\rho_p}{\rho_i} \frac{d\vec{u_p}}{dt} = \vec{g'} - \frac{3}{4} \frac{C_d}{d_p} |\vec{u}_p|^2 \tag{3.54}$$

where $\vec{g'} = \frac{\Delta\rho}{\rho_i}\vec{g}$. Equation 3.54 can be express in non-dimensional form in terms of the particle Reynolds number and Galileo number as follows:

$$\frac{\rho_p}{\rho_i} \frac{d(Re_p)}{dt'} = Ga - \frac{3}{4} C_d Re_p^2 \tag{3.55}$$

Where dt' refers to a non-dimensional time scale relative to the viscous time scale as:

$$t' = t\frac{\nu_f}{d_p^2} \tag{3.56}$$

The settling velocity is achieved when the right hand side of Equation 3.55 is equal to zero. This gives the classical formula for the particle settling Reynolds number:

$$F_d^*(Re_\infty) = Ga \tag{3.57}$$

Thus:

$$Ga = \frac{3}{4} C_d Re_p^2 \tag{3.58}$$

Equation 3.58 can be solved to give an explicit formula for the settling Reynolds number. For instance, in the limit of low Re_p the drag curve for spherical and non-spherical particles obey the Stokes law. In this case, 3.57 is a linear equation, with solution:

$$Re_\infty = \frac{4Ga}{3C_s} \quad , \quad U_\infty = \frac{4g^{'} d_p}{3C_s \nu_f} \tag{3.59}$$

For high Re_p, the drag coefficient is independent of the particle Reynolds number. In this case, 3.57 is a quadratic equation, with solution:

$$Re_\infty = \sqrt{\frac{4Ga}{3C_N}} \quad , \quad U_\infty = \sqrt{\frac{4g^{'} d_p}{3C_N \nu_f}} \tag{3.60}$$

Where C_N is the Newton coefficient and is equal to 0.44 for spherical particles.

In order to quantify for the full range of particle Reynolds number, the two parameter Stokes-Newton drag curve has been suggested to describe the behaviour of low and high particle Reynolds numbers as Cheng (1997):

$$C_d = \frac{C_s}{Re_p} + C_N \tag{3.61}$$

For the Stokes-Newton form of the drag curve, Equation 3.57 is a quadratic equation in Re_∞, with unique positive solution:

$$Re_\infty = \frac{\sqrt{C_s^2 + \frac{16}{3} Ga C_N} - C_s}{2C_N} \tag{3.62}$$

Moreover, a better fit to the drag curve between the Stokes and Newton limits may be obtained with the three parameter Power-Law Stokes Newton drag curve Camenen (2007); Cheng (1997):

$$C_d = \left[\left(\frac{C_s}{Re_p} \right)^p + C_N^p \right]^{\frac{1}{p}} \tag{3.63}$$

In this case, Equation 3.57 can be expressed as a quadratic equation in Re_∞^p, with unique positive solution:

$$Re_\infty^p = \frac{\sqrt{C_s^{2p} + 4(\frac{4}{3}GaC_N)^p} - C_s^p}{2C_N^p} \tag{3.64}$$

The generalised Stokes-Newton drag curve has been proposed to be a good correlation over a wide range of spherical and non-spherical particles Camenen (2007).

A summary of the most relevant expressions to the current study has been presented in this section and are implemented in the following chapters. The understanding of these flow features is a key point for the application of such correlations in microfluidic systems mainly for the prediction of multiphase flow in porous media. The prediction of the drag coefficient in a two-phase flow system when a porous media is present gives a significant suggestion of the flow behaviour in situations when the density and viscosity ratios are relevant (e.g. liquid-liquid systems). Also, the drag coefficient can be use to calculate the settling or rising droplet velocity which is related to the accurate design and performance of mixing and separation processes involving multiphase flows.

3.5 Fundamentals of Porous Media Flow

A porous medium can be defined as a portion of space occupied by heterogeneous or multiphase matter, where at least one of the phases comprising this matter is a solid Bear (1972).

3.5.1 Porosity (γ)

The amount of small spaces or voids within a solid material is known as porosity. It is defined as the ratio of the pore volume to the total volume of the material, which value can vary between 0 and 1. The pores are assumed to be interconnected, so porosity is the physical volume available for fluid to flow. The porosity can be calculated as:

$$\gamma = \frac{V_v}{V_T} = \frac{(1 - V_s)}{V_T} \tag{3.65}$$

where V_v represents the volume of the void space (such as fluid) and V_T is the total volume of the material, including the solid and void components, V_s is the volume of solids within the domain.

3.5.2 Volume Fraction

For a single phase through a porous medium involving a fluid-solid flow with stationary solid, the volume fraction (r_f) of the fluid is equal to the porosity of the domain $\gamma = r_f$ and the solid volume fraction (r_s) can be represented by $r_s = 1 - \gamma$.

3.5.3 Superficial Velocity ($\tilde{u}$)

The porosity is assumed to be an isotropic property (the same in all directions); therefore the interstitial velocity can be related to the superficial velocity. The interstitial velocity (u_f) refers to the actual fluid velocity. For a single phase case the mass flux is given by:

$$Q_f = \gamma \rho_f u_f = \rho_f \tilde{u}_f \tag{3.66}$$

where $\tilde{u}_f$ is the volume flux called the superficial velocity and is defined as:

$$\tilde{u}_f = \gamma u_f = r_f u_f \tag{3.67}$$

3.5.4 Darcy's Law

Darcy's Law is used to describe fluid flow in homogeneous porous media. It is assumed that the fluid mass flux is linearly related to the pressure gradient. Darcy law for a single fluid is represented by:

$$\tilde{u}_f = -\frac{k}{\tilde{u_f}} \nabla p \tag{3.68}$$

where $\tilde{u}_f$ is the superficial velocity, k is the permeability, u_f the dynamic viscosity of the fluid and ∇p is the applied pressure gradient. The inertial and time dependent effects are neglected and the permeability depends only on the geometry of the medium Bear (1972).

In porous materials, the dominant flow regime is laminar. However, different flow regimes have been identified namely: (a) Darcy or creeping flow regime ($Re < 1$); (b) Forchheimer flow regime ($110 < Re < 150$); (c) post-Forchheimer flow regime (unsteady laminar flow, $150 < Re < 300$) and (d) fully turbulent flow ($Re > 300$) Wang *et al.* (2013). Figure 3.7, shows a schematic classification of a single phase flow through a porous media.

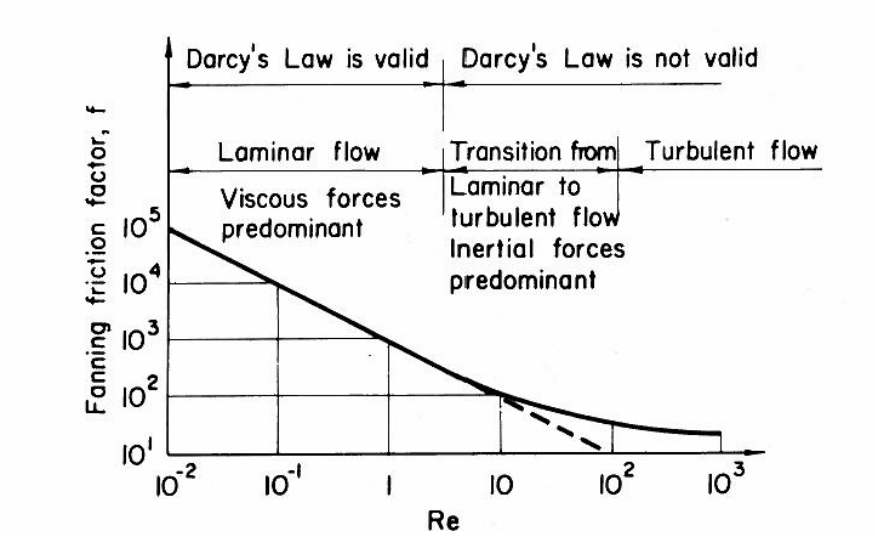

Figure 3.7: Classification of a flow through porous mediaBear (1972)

.

3.5.5 Forchheimer Equation

The Forchheimer equation is used to describe high velocity flows through porous media where inertial effects are taken into account.It includes an additional quadratic term relating the pressure gradient to superficial velocity. If Darcy equation is expressed in function of the superficial velocity, the Forchheimer equation is given as follows:

$$-\nabla p = \frac{\mu}{k}\tilde{u}_f + \beta\tilde{u}_f^2 \tag{3.69}$$

where k represents the permeability, β is the Forchheimer coefficient and has units of L^{-1}. This parameter can be calculated by the following expression proposed

by Joseph (1982):

$$\beta = \frac{C_E}{\sqrt{k}} \tag{3.70}$$

where the dimensionless parameter C_E accounts for the inertial effects and it is strongly dependent on the flow regime. For a wide range of materials, the universal value of $C_E = 0.55$ gives reasonable results Joseph (1982).

3.5.6 Kozeny-Carman Equation

The Kozeny-Carman equation provides a method for predicting the permeability of a packed bed of spherical particles Holdich (2002). This equation assumes that the flow in a porous media can be represented by the flow through many channels and including the definition of superficial velocity. Taking the hydraulic radius, which is the ratio of void volume to particle surface area:

$$d = \frac{AL\gamma}{AL(1-\gamma)S_v} = \frac{\gamma}{(1-\gamma)S_v} \tag{3.71}$$

The Kozeny -Carman equation is written as:

$$\frac{\Delta P}{L} = \mu \left[\frac{A(1-\gamma)^2 S_v^2}{\gamma^3} \right] \tilde{u}_f \tag{3.72}$$

Equation 3.72 includes a factor (A) relating the tortuous flow channel length to the measured bed depth. This constant generally has a value close to 5, but there is evidence that suggests that A is a function of the void fraction Holdich (2002). Darcys Law in Equation 3.68, and the Kozeny-Carman equation, 3.72, can be combined to define an expression for the permeability of a packed bed of spherical particles which can be described by:

$$k = \frac{D_p^2 \gamma^3}{A(1-\gamma)^2} \tag{3.73}$$

where k is the absolute permeability and D_p is the equivalent spherical diameter.

3.5.7 Ergun Equation

The Ergun equation has been preferred for years for modelling flow in porous medium. It is a generalisation of Equation 3.72 based on the pressure losses

caused by simultaneous inertial and viscous losses Macdonald *et al.* (1979). It takes the form:

$$--\frac{dP}{dZ} = \left[A\frac{(1-\epsilon)^2}{\epsilon^3}\frac{\mu}{D_p^2}\right]\tilde{u}_s + \left[B\frac{(1-\epsilon)\rho_f}{\epsilon^3 D_p}\right]\tilde{u}_f^2 \tag{3.74}$$

where ϵ is the void fraction of the bed, μ is the viscosity of the fluid, D_p is the equivalent spherical diameter, $\tilde{u}_s$ is the superficial velocity based on the empty column cross section, ρ_f is the fluid density. The values of $A = 1.75$ and $B = 180$ are recommended but may not be universal Grosser *et al.* (1988); Levec *et al.* (1986); Macdonald *et al.* (1979); Saez & Carbonell (1985).

Since the current study is focused in two-phase flows through a packed bed, the models presented previously must be supplemented with constitutive relationships, which are generally described as closure problems. This refers to the fact that fluid-fluid and fluid-solid boundaries require closure relations that should be specified in order to properly model the phase interaction in the presence of a porous media.

3.6 Two-phase flow in porous media

Considering two-phase flow though a porous media (liquid-gas-solid or liquid-liquid-solid) with stationary solid, each phase can be represented by a physical volume fraction. Let, the volume fraction of the phase α be r_α and a second phase r_β, the volume fraction of the fluid can be represented as:

$$\gamma = r_f = r_\alpha + r_\beta \tag{3.75}$$

In a two-phase flow, the void fraction refers to the fraction of volume of the flow that is occupied by the fluid. It usually varies from the location in the flow depending on the two phase flow pattern.

3.6.1 Saturation(S_i)

The void space of the porous medium is filled by two or more immiscible fluids, the saturation or degree of saturation at a point with respect to a particular fluid

is defined as the fraction of the void volume of the porous medium occupied by the fluid Bear (1972). The saturation of a fluid phase i can be expressed as the ratio of the volume of fluid phase to the volume of pores in the total volume and it is given as:

$$S = \frac{\text{volume of fluid phase}}{\text{volume of pores}} \tag{3.76}$$

The fluid saturation can also be represented in terms of the volume fraction of each fluid phase in the porous medium:

$$r_\alpha = \gamma S_\alpha \quad ; \quad r_\beta = \gamma S_\beta \tag{3.77}$$

So:

$$S_\alpha + S_\beta = 1 \tag{3.78}$$

3.6.2 Superficial velocity

In a multiphase case, each fluid has its own interstitial velocity, so the mass flux for each phase is given by:

$$Q_\alpha = r_\alpha \rho_\alpha \tilde{u}_\alpha = \rho_f \tilde{u}_\alpha \tag{3.79}$$

Where the superficial velocity for each phase is denoted as:

$$\tilde{u}_\alpha = r_\alpha u_\alpha \quad ; \quad \tilde{u}_\beta = r_\beta u_\beta \tag{3.80}$$

3.6.3 Phase Holdup

The prediction of the liquid hold up and pressure drop for two-phase flow in packed bed is of great importance in industrial processes Saez *et al.* (1986). The phase hold up can be defined as the fraction of the void volume in the packed bed occupied by the phase and it is directly related to the drop size and free surface area Rigg & Churchill (1964); Wang *et al.* (2013).

The phase holdup can be either dynamic or static hold up. The latter refers to the amount of fluid that remains in the bed after the two-phase flow through the packed bed. The static hold up (S_α^0) is usually the result from a balance

between surface tension and gravitational forces. It consists basically of stagnant liquid and can be represented as:

$$S_\alpha^0 = \frac{\gamma_\alpha^0}{\gamma} = \frac{r_\alpha}{r_s} \tag{3.81}$$

The static hold up was found to be strongly dependent on the Eötvos number Saez & Carbonell (1985) regardless of the liquid used. It can be described by the following expression:

$$r_\alpha^0 = \frac{0.11}{1 + Eo} \tag{3.82}$$

The correlations proposed for gas-liquid systems have been implemented assuming negligible static hold up for the gas phase Levec *et al.* (1986); Saez & Carbonell (1985). However, this assumption may not apply for the case of liquid-liquid flows in packed beds. For instance, the static hold up in oil-water studies is usually called the irreducible hold up and is typically around 0.2 Dake (1978).

On the other hand, the difference between the actual amount of liquid in the bed and the static holdup (S_α^0) is known as the dynamic hold up Saez & Carbonell (1985). This value can be measured experimentally and is generally expressed in terms of the reduced saturation (δ_α).

3.6.4 Reduced Saturation (δ_α)

The reduced saturation is a measure of the dynamic holdup. This can be normalised as the ratio of the dynamic hold up to the remaining fluid volume by Saez & Carbonell (1985):

$$\delta_\alpha = \frac{r_\alpha - r_\alpha^0}{r_f - r_\alpha^0} = \frac{S_\alpha - S_\alpha^0}{1 - S_\alpha^0} \tag{3.83}$$

3.6.5 Relative Permeability (k'_α)

The relative permeability concept is used to modify the Darcy equation for two-phase flow. The relative permeability defines the ability to flow of one fluid in presence of other fluid Atta *et al.* (2010). For each phase, the absolute permeability (k), is reduced through multiplication by the relative permeabilities k'_α and

k'_β, which are fractions between zero and unity Saez & Carbonell (1985). For a two phase system the flow can be modelled by:

$$Q_\alpha = -k'_\alpha \frac{k}{\mu_\alpha} \nabla P_\alpha \quad ; \quad Q_\beta = -k'_\beta \frac{k}{\mu_\beta} \nabla P_\beta \tag{3.84}$$

Where the relative permeabilities k'_i are usually written as function of saturation for gas-liquid systems Grosser *et al.* (1988); Saez & Carbonell (1985).

A typical example of relative permeability curves can be given by oil-water systems Dake (1978).

3.6.6 Capillary Pressure (P_c)

Dealing with flows in a porous medium at a macroscopic scale requires to consider the effect of fluid dispersion along the porous domain or packing bed. The forces that enhance fluid dispersion are mainly mechanical forces, capillary pressure force and interaction forces. Moreover, when multiple fluid phases are present, it is necessary to account for the pressure jump at the fluid phase boundary which is due to capillary pressure.

Capillary pressure is defined as the difference in pressure across the interface between two immiscible fluids which is generated due to the surface tension or high inertial forces between the fluids Carbonell (2000). Alternatively, it can also be defined as the difference between the pressure of the two fluids at the interface under equilibrium condition as follows:

$$P_c = P_\beta - P_\alpha \tag{3.85}$$

The capillary pressure depends on the average curvature of the fluid interface (r_1, r_2) and the surface tension in the porous medium:

$$P_c = \sigma\Big(\frac{1}{r_1} + \frac{1}{r_2}\Big) \tag{3.86}$$

The average radii of curvature depend on the contact angle at the phases, the pore size and the liquid saturation. Setting a relationship between the pressure of each phase at the interface, the capillary pressure can be modelled as a function of saturation as Leverett (1941):

$$P_c = \Big(\frac{r_f}{k}\Big)^{\frac{1}{2}} \sigma J(S_\alpha) \tag{3.87}$$

where k is the permeability of the packed column and σ the interfacial tension. The J-function depends only on the liquid saturation and ranges from 0 to 1 Carbonell (2000). In gas- liquid systems the experimental $J - values$ are usually limited by the drainage and imbibition curves and the values are different for specific two-phase flow systems. The J-function is not known quantitatively, but the qualitative form can be described as shown in Figure 3.8. This Figure plots the variation of J as a function of the liquid saturation in a gas-liquid packed bed system Grosser *et al.* (1988).

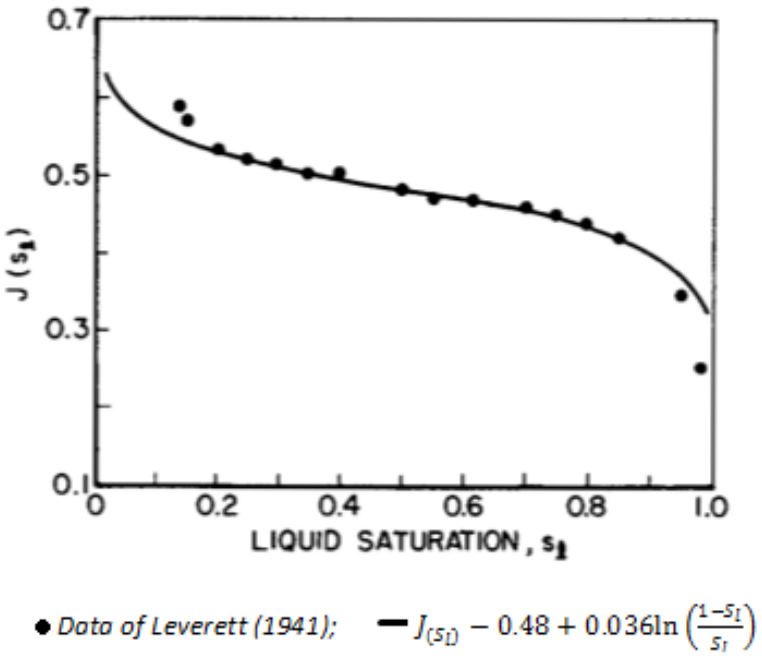

Figure 3.8: Variation of J as function of liquid saturation in a gas-liquid system Grosser *et al.* (1988)

.

The Leverett function described in Equation 3.87 was modified by Jiang *et al.* (2002a) who introduced the particle wetting efficiency, f, to the capillary pressure equation proposed by Grosser *et al.* (1988) leading to the following expression:

$$P_L = P_G - (1 - f)\left(\frac{r_f}{k}\right)^{\frac{1}{2}} \sigma J(S_\alpha) \tag{3.88}$$

Equation 3.88, indicates that the macro-scale capillary effect is negligible when the particles are completely wet externally ($f = 1.0$), whereas this effect is most significant when the particle surfaces tend to be dominantly dry ($f \to 0$) Wang *et al.* (2013).

3.7 Conclusions

This chapter introduced a number of fundamental concepts related to the hydrodynamics in both single and two phase flows in round capillaries. Details of the transport phenomena involved in slug flow through capillaries have been described. There are a series of analytical and empirical expressions that can be used for characterising the liquid film thickness, bubble velocity and pressure drop of slug flow in a capillary. A summary of the most relevant expressions to the current study has been presented in this section and are implemented in the following chapters. The understanding of these flow features is a key point for the application of such correlations in microfluidic systems mainly for the prediction of multiphase flow in porous media. Also, the fundamental concepts of the flow in a porous media were introduced and will be further applied for the development of a pressure drop model for liquid-liquid flow in a packed bed reactor.

Chapter 4

Computational fluid dynamics study of slug flow in a capillary

4.1 Introduction

The complexity of modelling the interface in a two-phase system involving immiscible fluids has lead to the development of several numerical methods for fluid interfaces. Moreover, the prediction of slug flows in capillaries makes such methods difficult to implement due to the high surface tension forces that dominate these type of flows. An efficient method is required to capture the fluid-fluid interactions accurately, mainly when the interface exerts drag between the phases, which is the case of liquid-liquid slug flows. Although the advantages of some numerical techniques, such as moving mesh, front tracking, Diffuse Interface and Level Set methods are that they accurately resolve the shape of the interface and thin film around bubbles and droplets, their application to problems with large interface movement is very complicated and requires high computational efforts. One of the most widely used for simulating two-phase flows is the Volume of Fluid (VOF) method whose advantages are its robustness and the ability to conserve mass and resolve sharp interfaces. However, for surface tension dominated flows it requires a very fine mesh to calculate the curvature of the interface. Also, requires a very small time step to resolve small time scales due to capillary effects, and to prevent numerical instabilities (Hoang *et al.*, 2013). Thus, with the intention to avoid such complex numerical techniques, an alternative approach

to study the interfacial forces in high surface tension flows has been developed in this work.

Computational fluid dynamics (CFD) was used to study the flow behaviour of liquid-liquid slug flow in a circular capillary. The main flow parameters such as, film thickness, droplet and slug lengths, droplet velocity and pressure drops are considered during this study. The role of the interfacial forces was investigated under the limits of high and low viscosity ratios assuming high surface tension in a low Reynolds number flow. As a first attempt, the effect of the drag force in a single droplet freely rising or falling under gravity in a continuous flow was analysed under different operating conditions and geometry configurations.

Then, the motion of a droplet along a capillary in a horizontal pressure driven flow was investigated. The velocity profiles and shear stress profiles across the fluid-fluid interface were calculated and the results were compared with theoretical approaches found in the literature. Also, the hydrodynamic structures obtained in the two-phase flow study, such as the internal recirculation in the dispersed and continuous phase were similar to those observed experimentally and numerically in previous works for slug flow in capillaries.

4.2 Problem description

Considering the regular and periodic characteristic of the slug flow regime, the modelling of a slug flow through a capillary was simplified by defining a periodic unit referred to as a unit cell. This consists of a single droplet with two hemispherical end caps at the rear and front of a cylindrical body, and two adjacent liquid slugs. The assumed droplet shape corresponds to a high surface tension two-phase flow. A schematic representation of the unit cell is illustrated in Figure 4.1. A moving reference framework was adopted in which the droplet remains stationary and the wall moves in the opposite direction to the droplet motion. This configuration allows to simulate the entire flow field (dispersed and continuous phase) with the advantage of a significant reduction in computational resource as demonstrated in the work developed by (Gupta *et al.*, 2009, 2013).

For the first stage of simulations, only the continuous phase was solved and the dispersed phase was represented by a rigid droplet with no-slip and free-slip

boundary conditions at the droplet surface, corresponding to the limits of high and low viscosity ratios: $\frac{\mu_d}{\mu_c} \to \infty$ and $\frac{\mu_d}{\mu_c} \to 0$, respectively. The free-slip case is appropriate to gas-liquid flows and the no-slip case to liquid-liquid flows.

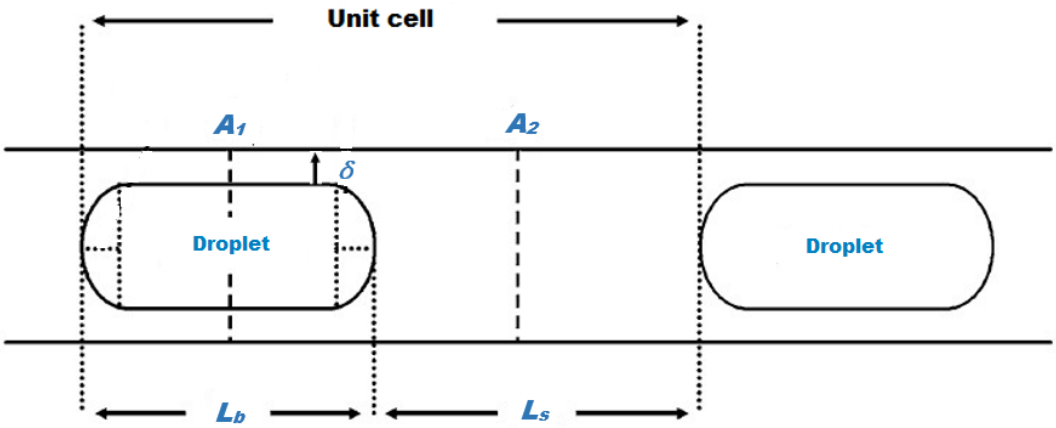

Figure 4.1: Schematic overview of slug flow in a capillary and main flow parameters

.

A number of simulations were developed to study the drag force over an isolated droplet freely rising or falling on a continuous phase. Then, the case of a train of droplets travelling in an horizontal pressure driven flow through a capillary was also simulated. The main parameters of slug flows such as the droplet length (L_d), film thickness (δ) and slug length (L_s) were considered and varied during the study. Furthermore, the droplet velocity in both, vertical and horizontal flow, was calculated under different operating conditions and its influence on the main slug flow parameters was investigated. The methodology followed to predict the droplet velocity in both cases is described further in this chapter.

In the second part of the study, the flow was simulated in both the continuous and dispersed phases. Interfacial boundaries were employed based on continuity of the velocity and shear stresses at the interface. A range of viscosity and density ratios were considered to evaluate the effect of the interfacial shear on the two-phase flow behaviour. The interaction between the two phases allowed a further understanding of the hydrodynamics involved in capillary slug flows.

4.3 CFD Methodology

4.3.1 Geometry and Mesh Generation

The simulations were performed using the commercial CFD package ANSYS CFX 15.0. The geometries and mesh of the unit cell were created in ANSYS ICEM CFD. The geometry consists of a cylindrical capillary of 1 mm in diameter and an idealised slug flow droplet represented by a cylindrical body with hemispherical end caps and two adjacent slugs. Based on the symmetric shape of the droplet and slug region, and to reduce computational time, only a 1 degree angle wedge of the geometry was considered for the study. To model 2D axis-symmetric flows in CFX, the mesh must be one cell thick in the z-direction with symmetry planes specified either side and at an angle to each other. A good representative volume is recommended to be between 1-5 degree angle (ANSYS, 2010b), so different values were tested within the suggested range and the solution was independent of the angle when $\theta \leq 1$. Moreover, the thin edge of the wedge was modified in order to generate a high quality hexahedral and consisted of four end points. Also, this was convenient to define the axis symmetry plane at the centreline corresponding to $du/dr = 0$. Figure 4.2 shows different views of the geometry generated for the current study, highlighting the modified thin end of the wedge in Figure 4.2 (c).

The capillary length was varied until fully developed flow was achieved in the continuous slug region. This allows to prevent the velocity fluid around the droplet to be affected by the wake of another droplet that is located upstream in the periodic computational domain. (Kashid *et al.*, 2010a) suggested a typical capillary length of 10 diameters long which was verified in this study for all cases. The capillary diameter remained constant and the normalised film thickness (δ/r) and droplet lengths were varied in the ranges $0.03 \leq \delta/r \leq 0.15$ and $0.85 \leq L_d^* \leq 10.97$, respectively.

During the mesh generation process in ICEM the block topology and geometry entities were used. After creating a 3D block topology equivalent to the geometry, the blocks were refined through the splitting of edges, faces and blocking. The block topology tool allows rapid generation and manipulation of the block

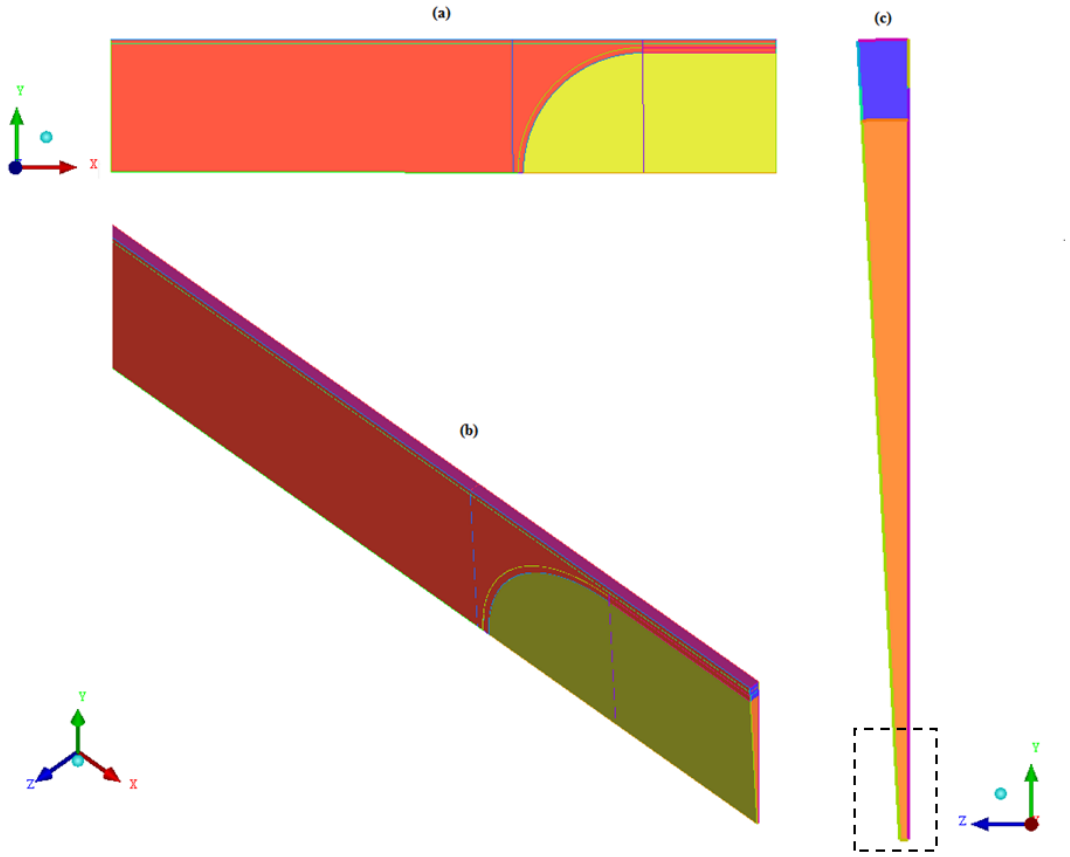

Figure 4.2: Geometry of the wedge used for the 2D simulations in ANSYS CFX a) side view ($+Z$), b) isometric view ($+Y$) and c) front view (-X) showing modified thin edge region.

structure, as well as a rapid generation of hexahedral meshes (ANSYS, 2010b). The mesh for every case was refined gradually in the film region and near the droplet surface to improve accuracy. Each mesh was composed of hexahedral elements and the O-grid option for curved surfaces was implemented to reduce skewness. An example of the mesh used during this study representing a slug flow in a capillary is shown in Figure 4.3.

A method for calculating the grid size to model the film on the wall was proposed by (Gupta *et al.*, 2009), which consists in calculating the film thickness using Bretherton's equation: $\frac{\delta}{r} = 1.34Ca^{\frac{2}{3}}$ and then determine the grid size with the Capillary number and velocity distribution within the film region. Based on

their observations, a minimum of five elements is required across the film to accurately capture the fluid-fluid interface and also they highlighted the importance of having a structured grid in the region of the interface, mainly for flows involving surface tension forces.

Since, in the current study an alternative approach to the Volume of Fluid (VOF) method is implemented. The film thickness was initially defined based on numerical values used in the work by (van Baten & Krishna, 2005) and the grid size was defined following (Gupta *et al.*, 2009) results who suggested a grid size less than 20 μm in the slug region and less than 2 μm along the film surrounding the droplet to achieve grid independence. A sensitivity analysis was developed using different grids having element sizes ranging from 10 μm to 1.4 μm. The velocity profiles in both, the film and slug regions, and also the profile of the total force over the droplet surface were generated until the solution did not change with the number of elements which confirms grid independence.

Moreover, the quality of the mesh was evaluated by the quality values calculated in ANSYS ICEM CFD such as the aspect ratio and the determinant. The aspect ratio of a cell is the ratio of the longest edge length to the shortest edge length. It is used to determine how close to ideal a face or cell is. For instance, for an equilateral cell, the aspect ratio will be 1. Additionally, the quality measure in ICEM is based on the the determinant which is defined as the ratio of the smallest and largest determinant of the Jacobian matrix $J'_{ij} = \frac{\partial x_i}{\partial \varepsilon_j}$, where x_i denotes spatial coordinates, and ε_j denotes local element coordinates. The Jacobian matrix is computed at each node of the element and indicates the deformation of the elements in the mesh. The default range is 0-1 with a determinant value of 1 indicating a perfectly regular mesh element and 0 indicating an element degenerate in one or more edges. Determinant values over 0.3 and aspect ratios over 0.6 are considered as acceptable values (ANSYS, 2010b).

Figure 4.4 shows the quality of the mesh in the form of aspect ratio and the relative determinant represented by an histogram. The minimum quality of the mesh is 0.5, but the majority of elements having quality between 0.8 and 1 which implies uniform square elements. The small values of the determinant refer to the rectangular elements near the interface and thin film region, but overall the

(a)

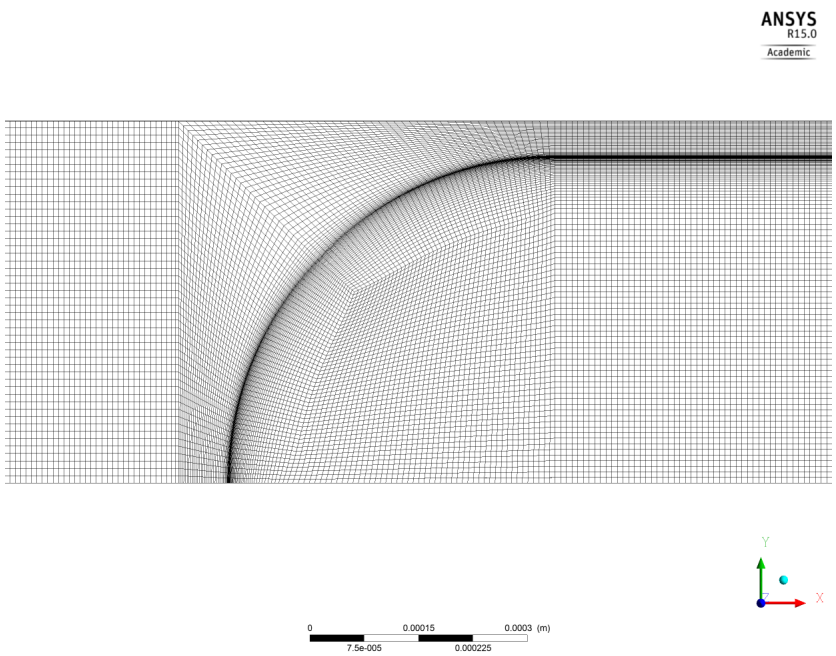

(b)

Figure 4.3: Hexahedral mesh representing the slug flow regime in a capillary as a unit cell (a) continuous slug region (b) Dispersed droplet region

.

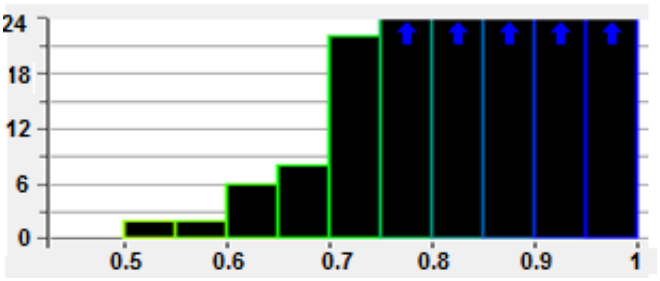

(a)

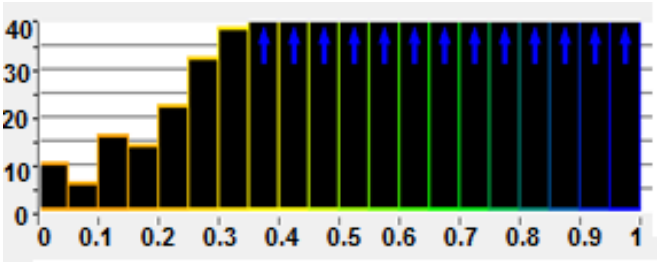

(b)

Figure 4.4: Hexahedral mesh quality values calculated in ANSYS ICEM in the form of (a) Aspect ratio and (b) Determinant of the Jacobian matrix.

structured mesh obtained from grid independence study can be considered as a good quality and optimum for the current study.

4.3.2 Boundary Conditions

Slug flow is considered as a regular and stable flow, so a periodic unit cell was defined comprising of a single droplet with hemispherical caps and two adjacent slugs. A moving reference frame approach was adopted which consists of moving the top wall in the opposite direction to the droplet motion $U_d = -U_w$ while the droplet remains stationary. This configuration allows to simulate the entire flow field (continuous and dispersed phase) with less computational efforts. A no-slip boundary condition was defined on the top wall and symmetry planes were considered accordingly to the geometry. The surface of the droplet was defined as a no-slip boundary condition to simulate the limiting case of low viscosity ratios $\left(\frac{\mu_c}{\mu_d} \to 0\right)$ and a free-slip boundary condition for high viscosity ratios $\left(\frac{\mu_c}{\mu_d} \to \infty\right)$,

e.g. gas-liquid flows. The condition of a rigid droplet is valid for the case of high surface tension two-phase flows, $Ca \rightarrow 0$, where there is no deformation of the droplet. Moreover, periodic pressure boundaries were specified at the inlet and outlet of the domain as $\Delta p_{in} = \Delta p_{out}$ depending on the case under study. For instance, to simulate the case of a droplet suspended in vertical flow the periodic boundaries were specified as $\Delta p_{in} = \Delta p_{out} = 0$ and the hydrostatic pressure drop, ρg, is added to correct the periodic boundary conditions. On the other hand, the pressure drop Δp across the unit cell was defined to study the droplet motion along a capillary in a horizontal pressure driven flow. Figure 4.5 illustrates the boundary conditions applied for the current study.

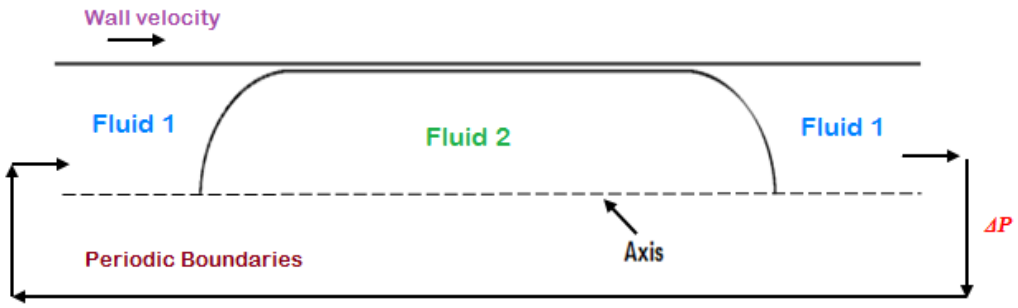

Figure 4.5: Schematic description of computational domain of a unit cell with periodic boundary conditions and moving reference modeling approach

4.3.3 Discretisation Schemes

The commercial CFD package CFX is a finite volume solver, using body-fitted grids and all variables are evaluated at the element vertices. The second order bounded high resolution scheme for advection schemes was used during all the study. CFX is a coupled system solver (solves for all the variables simultaneously), and has the option to solve several different velocity fields when it is required, for example in multiphase problems (ANSYS, 2010a). During every simulation, residual plots were created to monitor the convergence of the solution. Convergence was assumed when changes in the main variables were negligible and reached a target criterion of 1e-08. Monitor points for quantities of interest

namely velocity, total force on the droplet surface and pressure drop across the capillary were displayed until flat profiles were achieved. Also, the mass imbalances which measures the overall conservation of quantity (mass, momentum and energy) in the entire flow domain were monitored to be below 1%.

4.4 Single Phase study

4.4.1 Method for calculating the droplet settling/rising velocity in vertical flow

The drag force over a single droplet was investigated as a first attempt to study the role of the interfacial forces in capillary slug flow. The case of a droplet freely rising or falling under gravity was considered which implies $\Delta p = 0$ at the inlet and outlet boundaries. The droplet was assumed as a rigid solid acting as a surface with a surrounding liquid phase. The liquid flow is driven by the wall velocity $-U_w = -U_d$ and was varied over a range of Reynolds numbers. Also, different droplet lengths, film thickness and slug lengths were defined during the study for each Reynolds number. The non-dimensional parameters and ranges used throughout the study are specified in Table 4.1.

Table 4.1: Details of the non-dimensional ranges used in the simulations of a slug flow through a capillary of 1 mm diameter.

Reynolds	L_d^*	L_s^*	$\frac{\delta}{r}$
$1 \leq Re \leq 12$	0.85-10.97	0.01-10	0.03-0.15
$25 \leq Re \leq 100$	0.85-10.97	0.01-10	0.03-0.15

The total force over the droplet surface (F_d) was monitored during each simulation. The total force is equal to the sum of the pressure and viscous forces on the droplet surface. These forces were directly calculated by the CFX solver as surface integrals and these values were used to calculate the non-dimensional drag coefficient C_d as function of Reynolds number. Then, best fits of the drag curve $C_d(Re)$ were sought for the power-law Stokes -Newton correlation (Equation 3.50), which is applicable for non-spherical drops.

Drag coefficient curves were generated using the optimisation modelling system in Microsoft Excel Solver to calculate the parameters involved in the Stokes-Newton Equation (3.63) such as: the Newton coefficient (C_n), the Stokes coefficient (C_s) and the power value (p). This tool employs the simplex, generalised reduced gradient and branch and bound methods to find an optimal solution.The method to obtain the parameters C_s, C_n and p in the Power-Law Stokes-Newton equation (3.63) is described below:

1. The value of the Stoke coefficient C_s was determined while plotting the logarithmic values of the Reynolds number and the computed drag coefficient. The plots which resulted in a straight line for all cases and the slope which corresponds to the value of C_s varied depending on the case under study.

2. The parameters C_n and p were calculated by giving an initial value to both parameters and implementing the optimisation modelling tool.

3. Most predicted values of p were close to 2. This suggested fixing $p = 2$ and optimising by varying the other parameter C_n.

The prediction of the parameters in the Stokes-Newton equation will allow to identify the influence of various flow conditions and geometry configurations on the drag coefficient. Compared to the traditional study of a flow over an isolated sphere, a different behaviour is in fact expected for non-spherical droplets where the dispersed droplet is expose to confine areas such as the case for capillary slug flows. Also, the drag force and settling velocities will highly influence on the prediction of the mass transfer coefficients in this type of flows which are mainly dominated by viscous forces.

4.4.2 Method for calculating the droplet velocity in horizontal flow

For the case of horizontal flow, gravity has no effect, and the flow is driven instead by a non-zero pressure drop. The droplet initially accelerates, and achieves its final velocity when the total force acting on it is zero. Figure 4.6 illustrates a diagram of the boundary conditions used for this study.

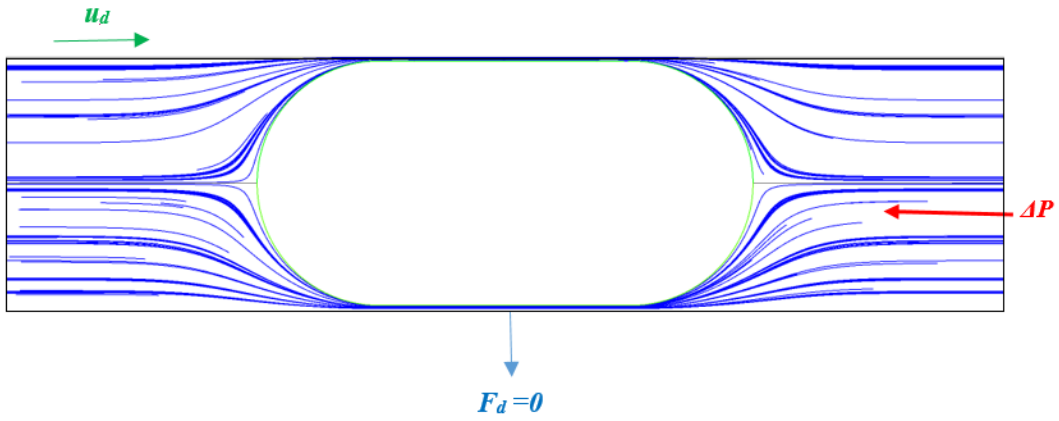

Figure 4.6: Illustration of the boundary conditions to predict the droplet velocity in horizontal flow

.

The droplet velocity is calculated using the secant method to determine the value of the wall velocity $-U_w = U_d$ that yielded zero total force on the droplet surface when a pressure drop $\Delta P > 0$ across the unit cell is specified. This procedure allows to select the normal stress distribution that has a zero mean value over the droplet surface, while the actual velocity of the droplet is determined by the wall velocity. The secant method is applied following the equation for u:

$$u = u_1 - f(u_1)\frac{u_1 - u_0}{f(u_1) - f(u_0)} \tag{4.1}$$

Initially, the top wall is stationary $U_w = u_0 = 0$ and the flow is driven by a given pressure drop defined across the unit cell. The pressure drop was defined based on values reported in the numerical work by (Kashid & Kiwi-Minsker, 2011). The initial simulation generates an average value of the total force F_{d_0} over the droplet and an average velocity of the continuous phase. The latter is used as an initial estimation of the droplet velocity $U_{d1} = -U_w$ and this value is set to the top wall boundary condition. A second simulation is performed and a new value of F_{d_1} is generated. At this time, the two droplet velocity values u_0 and u_{d1} and the two total force values are introduced in equation 4.1 to predict a new value of the droplet velocity which is then used to define the wall velocity and the corresponding total force on the droplet surface. The calculation continuous

until a sufficiently high level of precision (small difference between u_n and $u_{(n-1)}$ has been reached. The same method was used to study the influence of different droplet lengths, film thickness and slug lengths on the droplet velocity. Figure 4.7 illustrates the methodology followed to predict the droplet velocity under different conditions.

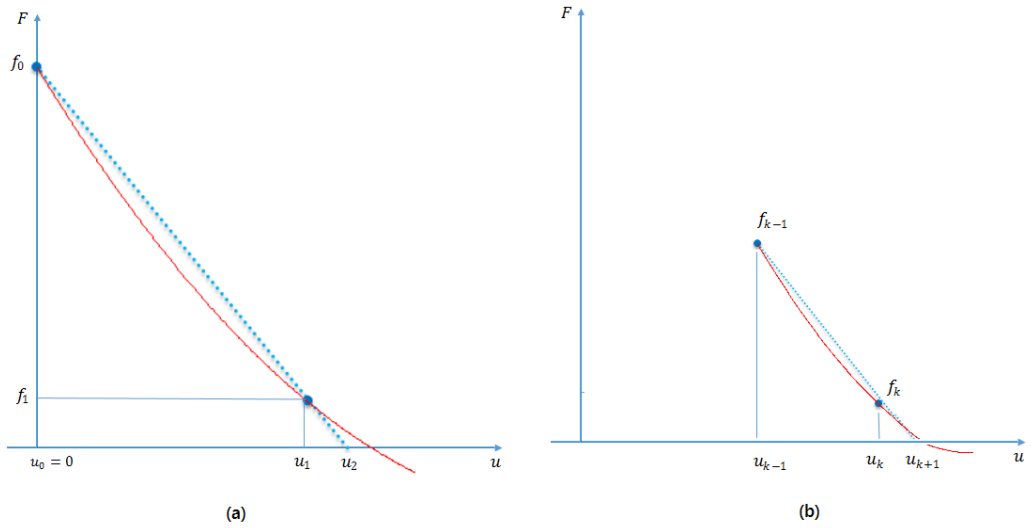

Figure 4.7: Diagram of the secant method to predict the droplet velocity in horizontal pressure driven flow

.

4.5 Two-Phase study

The hydrodynamics study of a slug flow in a capillary was extended to simulate the flow in both phases using interfacial boundary conditions. A detailed understanding of the influence of important flow parameters, such as the viscosity ratio (λ) and the droplet shape is necessary for an accurate prediction of this type of flow, mainly when liquid-liquid systems are involved.

The two-phase study was developed in two stages: the first set of simulations were simplified to the case of an infinite droplet dispersed in a continuous phase in which the influence of the hemispherical caps can be ignored. The film region

is assume to be stable so that the two-phase flow can be analogous to the case of annular flow. This was used to verify the method by comparing with the analytical solutions of Equations 3.20, 3.21, 3.24 and 3.25. The second set of simulations deals with the contribution of the hemispherical caps on the flow field assuming a constant droplet shape during the study which is valid for the case of high surface tension flows $Ca \rightarrow 0$ that prevents the deformation of the droplet. A new methodology for studying interfacial forces in two-phase flows was developed with the advantage of reproducing quick results and evaluating various important parameters to model slug flow in capillaries.

4.5.1 Method for calculating the interfacial velocity and shear stress distribution

The role of the interfacial forces in a liquid-liquid slug flow through a capillary was previously investigated considering the limits of low and high viscosity ratios. Now the effects of finite viscosity ratios are considered which implies a continuous velocity and shear stress boundary condition at the interface.

An alternative approach to the Volume of Fluid (VOF) method has been followed to avoid high computational time and efforts. The study was developed using Python 3.2 and ANSYS CFX 15.0 to generate multiple runs with the intention of communicating information across the domain interface until continuity of the fluid velocity and viscous stresses at the interface has been achieved. In this way, the boundary conditions ($u_c = u_d$) and ($\tau_c = \tau_d$) at the interface are consistent with those described in the mathematical derivation for annular two-phase flows.

During the first set of simulations, annular flow of two liquids driven by a pressure gradient in a capillary was considered. This represents the case of a sufficiently long droplet with a uniform film thickness for which rear and front end caps can be ignored. The inner liquid of viscosity μ_d occupied a cylinder of radius r_1, and the outer liquid of viscosity μ_c, occupied the annular film. The viscosity of the dispersed fluid was varied between the limits of $1 \leq \frac{\mu_c}{\mu_d} \leq 50$. In the second set of simulations, the influence of the gravitational force was considered

for vertical flows and the density ratios were varied between $1 \leq \frac{\rho_c}{\rho_d} \leq 50$ along with the same range of viscosity ratios defined in the previous calculations.

Figure 4.8, illustrates a diagram of the iterative methodology followed to achieve continuity at the interface of the two-phase flow. The iterative procedure was controlled using Python to generate multiple runs in ANSYS CFX. Initially the two phases are separated by a no-slip interface and the flow is driven by a given pressure drop. After a first calculation of the continuous phase flow, a shear profile τ_{c1} is generated in the continuous side of the interface. This profile is transferred to the other side of the interface corresponding to the dispersed phase. A second calculation is performed of the dispersed phase flow and this time a velocity profile u_{d1} at the interface of the dispersed side is generated. This velocity profile is transferred to the continuous side and a third calculation is developed in the continuous phase. The algorithm alternates between the continuous and dispersed phases until the velocity profiles are the same in both sides of the interface, as well as the shear stress profiles which indicates that continuity has been reached, hence a converged solution.

Furthermore, the study was extended to investigate the interface forces of an elongated droplet with spherical shape caps at the rear and front of the droplet. Two different situations were investigated: first, the presence of a high viscous dispersed droplet ($\mu_d \gg \mu_c$) leading to high viscous ratios $\left(\frac{\mu_d}{\mu_c} \to \infty\right)$ and then the case of a low viscous dispersed fluid e.g. gas phase ($\mu_d \ll \mu_c$) which leads to low viscous ratios $\left(\frac{\mu_d}{\mu_c} \to 0\right)$. In both cases, the droplet shape is constant and the stress distribution and the interfacial velocity were calculated during the simulations. At this stage, the calculations in the algorithm required additional efforts due to the presence of the curvature interface. The velocity at the interface was rising rapidly for every iteration and also non-physical pressure jumps across the interface were observed. A relaxation factor was introduced in the algorithm in order to avoid big changes of the variables from one iteration to another. The average of the tangential shear stress and tangential velocity at both sides of droplet surface were monitored during each calculation. Since the simulations involved the presence of the two fluid domains, the grid size was higher and was further refined to capture internal circulations in each region. A full simulation took an average of 4 hours using a High Performance Computer (HPC) and the

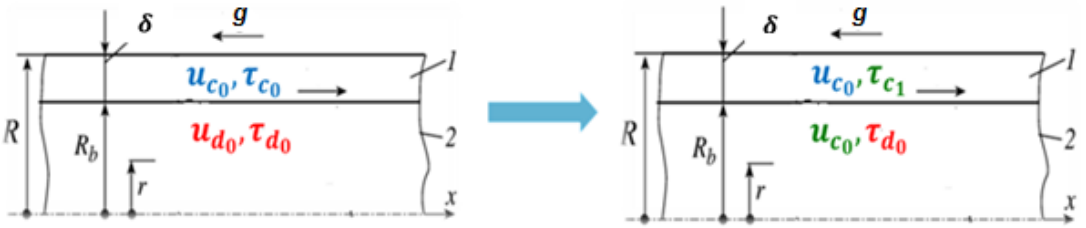

(a)

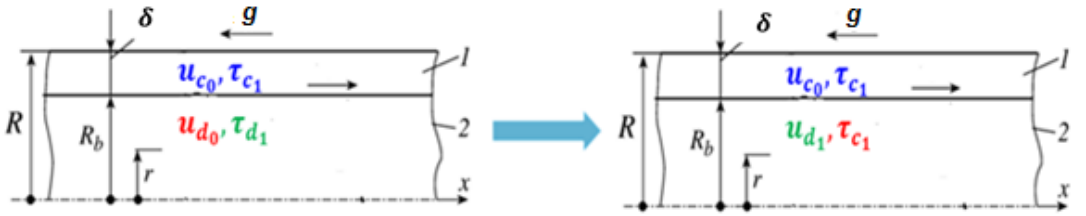

(b)

Figure 4.8: Schematic diagram of the methodology used during the present study (a) Iteration 0 (b) Iteration 1

.

simulation was completed when the difference of the shear stress profiles and velocity profiles in both sides of the interface was less than 1%. A general flow chart for the numerical solution is described in Figure 4.9 and details of the code implemented in this study can be found in Appendix A.

4.6 CFD Results and Discussion

The fluid dynamics study of a slug flow through a capillary was developed in a single phase and two-phase framework. As a first approach, only the continuous phase was solved in the simulations and the dispersed droplet was treated as a solid surface with no-slip and free-slip boundary condition, corresponding to $\left(\frac{\mu_c}{\mu_d} \to 0\right)$ and $\left(\frac{\mu_c}{\mu_d} \to \infty\right)$, respectively. This setup provided an understanding of the role of the interfacial forces and its impact on the flow behaviour along with various slug flow parameters involved in the system. An attempt to predict the

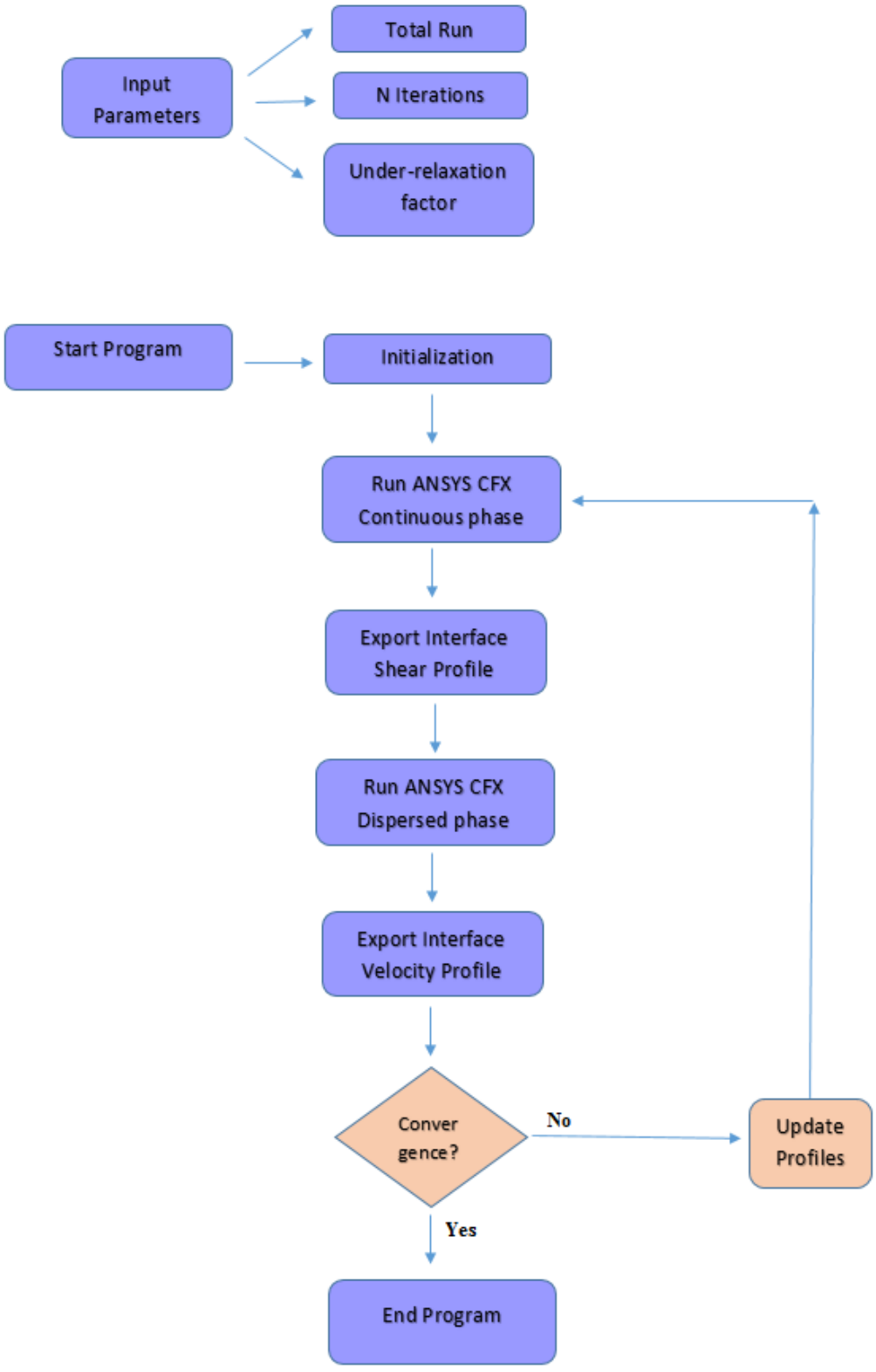

Figure 4.9: Simplified flow chart for numerical solution procedure for interface study of a two-phase flow.

droplet velocity in vertical flow based on a drag force analysis over a single droplet was developed during this study. Also, the motion of a droplet in a horizontal pressure driven flow through a capillary was investigated and different geometry configurations were considered. Moreover, a detailed understanding of the flow characteristics involved in both the continuous and dispersed phases was possible in the two-phase study with the methodology proposed in this work. The role of the viscosity ratio on the flow behaviour and the effects of the film thickness and curvature shape interface on the total pressure drop were investigated. Qualitative results were generated and are analogous to experimental and numerical results found in the literature.

4.6.1 Single Phase Study

Drag force analysis in Vertical Flow

The velocity vectors and contours of the continuous phase over a constant shape droplet are shown in Figure 4.10 considering a moving reference frame for the case of $Re = 1$, $\delta/r = 0.05$, $L_d^* = 2.95$ and $\Delta P = 0$. The velocity profiles in the region of the film varied according to the boundary condition applied on the droplet surface. For instance, considering a no-slip boundary, the flow velocity follows a Couette flow profile, whereas with a free-slip boundary condition a flat velocity profile is generated. Visualisations of these two cases can be observed in Figure 4.10 (a) and (b), respectively. The velocity profile in the slug area is parabolic in shape far away from the droplet when the flow becomes fully developed as shown in Figure 4.10 (c) and follows a Couette-Pousielle flow which can be solved analytically as described in Chapter 3. The purpose of investigating the effect of no-slip and free-slip boundary at the droplet surface relies on the interest of studying interfacial shear on liquid-liquid slug flow, on which influence of the viscosity ratio is relevant. The case of no-slip boundary approximates the presence of a highly viscous dispersed flow ($\mu_d \gg \mu_c$) leading to high viscous ratios $\left(\frac{\mu_d}{\mu_c} \to \infty\right)$. On the other hand, a free-slip boundary approximates a low viscous dispersed fluid e.g. gas phase ($\mu_d \ll \mu_c$) which lead to low viscous ratios $\left(\frac{\mu_d}{\mu_c} \to 0\right)$. Understanding the behaviour of the flow velocity and drag forces under different operating conditions and geometry configurations in these two

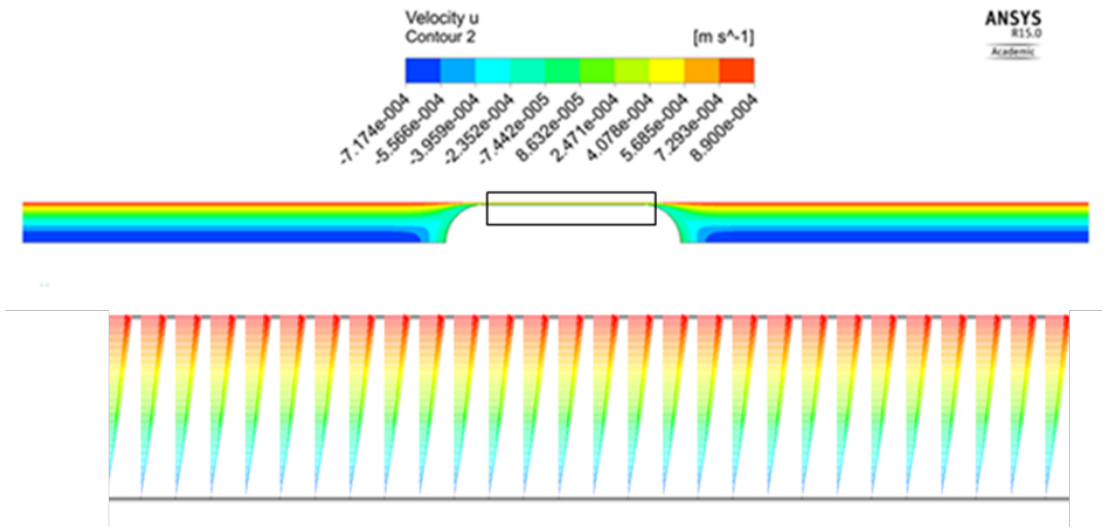

(a)

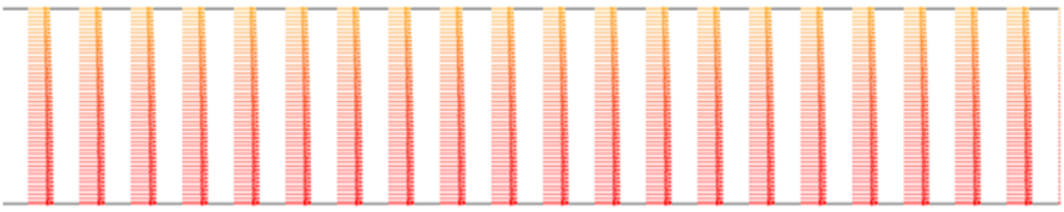

(b)

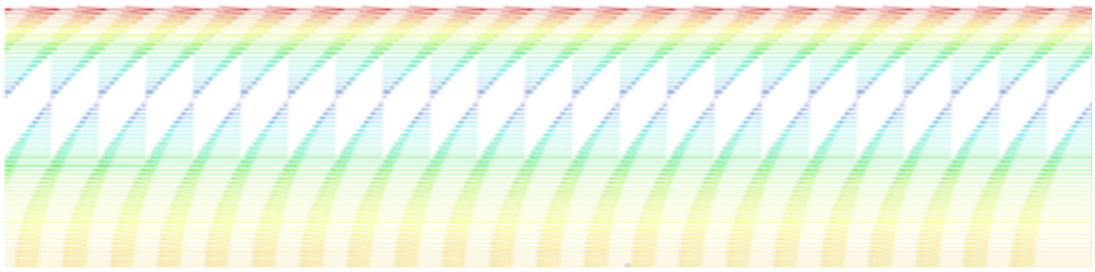

(c)

Figure 4.10: Velocity profiles in the film and slug region of a unit cell considering a single phase framework for $Re = 1$, $\delta/r = 0.05$, $L_d^* = 2.95$ and $\Delta P = 0$ (a) film region with a no-slip droplet (b) film region with a free-slip droplet (c) slug region awa from the droplet.

.

extreme cases, will allow the identification of a range of operability on which the model may be applied.

Moreover, Figure 4.11 shows the pressure distribution along the capillary, including both slug region and film near the droplet for the case of $Re = 1$, $\delta/r = 0.05$, $L_d^* = 2.95$ and $\Delta P = 0$. Different pressure drops between the slug region and film area can be clearly observed. A significant increase in pressure is generated as the flow reaches the front end of the droplet. Along the small film between the droplet surface and the wall the pressure drops linearly until it reaches the other end of the droplet. Also within the continuous phase the pressure decreases linearly due to friction. These features have been investigated by several authors (Gupta *et al.*, 2009, 2013; Jovanovic *et al.*, 2012; Li & Angeli, 2017) who identified three pressure contributions to the total pressure drop in a capillary slug flow. This are the pressure drop in the continuous slug, pressure drop in the film region and the interfacial pressure drop. In the current study, the two first pressure drop contributions were investigated for different droplet lengths and film thickness while varying the Reynolds number.The prediction of the interfacial pressure drop at this stage was not considered as it required knowledge of the curvature at the front and rear ends of the droplet and its relation with the Capillary number. The CFD results showed a significant pressure drop in the film region as the Reynolds number increased. Also, for smaller film thickness and shorter droplets a higher pressure was generated near the droplet surface. To study this aspect more closely, the relation between the Reynolds number and the total drag force over a droplet of different sizes was investigated.

Furthermore, a number of simulations were developed to relate the Reynolds number and the drag coefficient for a droplet freely rising or falling through a capillary using the Power-Law Stokes-Newton equation (Eq.3.63). Firstly, the Stokes (C_s) and Newton coefficients (C_N) were calculated and analysed as described in Section 4.4.1 for different flow conditions. Most predicted values of p were close to 2. This suggested fixing $p = 2$ and optimising by varying the other parameter C_n. Tables 4.2 and 4.3 display the final values of C_n and p for different drop lengths and film thickness. Plots of the Stokes coefficient for different droplet lengths and film thickness are shown in Figure 4.12 when a no-slip and free-slip boundary condition is applied at the droplet surface. From Figure 4.12 (a), it

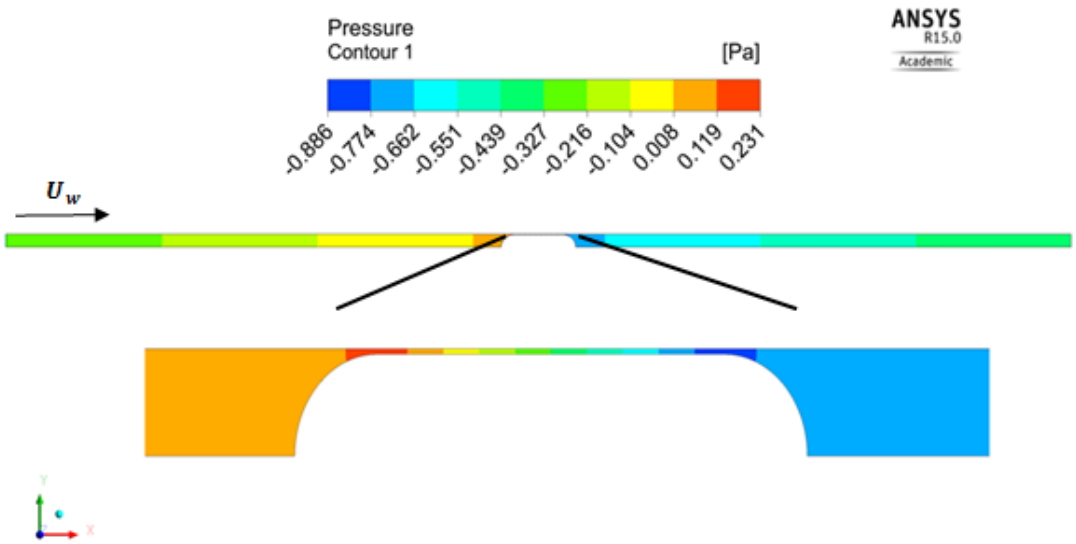

Figure 4.11: Pressure distribution in a unit cell for the case of $Re = 1$, $\delta/r = 0.05$, $L_d^* = 2.95$ and $\Delta P = 0$ for a single phase framework.

can be seen that C_s increases linearly with the droplet length when a no-slip boundary is used and higher values of C_s are achieved when reducing the film thickness. It is interesting to note the big gap between $\delta/r = 0.03$ and $\delta/r = 0.05$ for a small increase in the film thickness, which indicates a high sensibility of the Stokes coefficient to small changes of the film region. On the other hand, with a free-slip boundary condition as shown in Figure 4.12 (b), C_s increases rapidly with the droplet length and then stabilises for longer droplets. A similar behaviour is observed when the film thickness was varied and C_s increases as the film area is reduced. With respect to the Newton coefficient, a lack of consistency was observed when varying the drop length and film thickness as the range of C_N values oscillated from 0-3 depending on the initial value given in the optimisation model approach. The independent behaviour of the parameter C_N suggests that the Stokes-Law is sufficient for describing the flow behaviour under the conditions used in the current case study.

Theoretical drag coefficient curves were calculated for different drop lengths, film thickness and slug lengths. Figure 4.13 depicts the variation of C_d according to Equation 3.63 in the range $0.1 \leq Re \leq 100$ for the case of $\delta/r = 0.05$ and

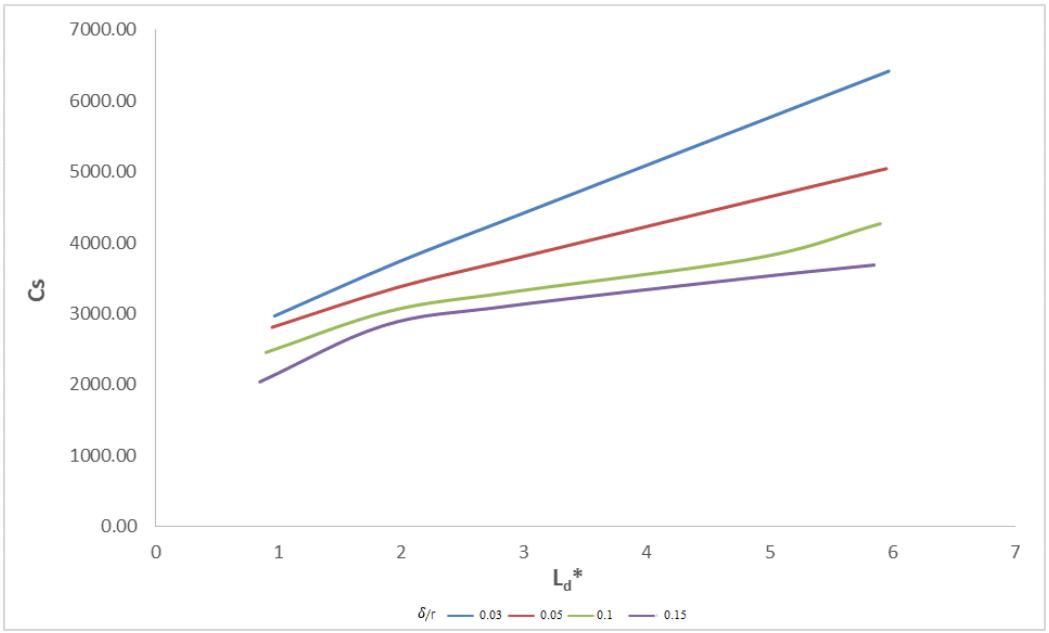

(a)

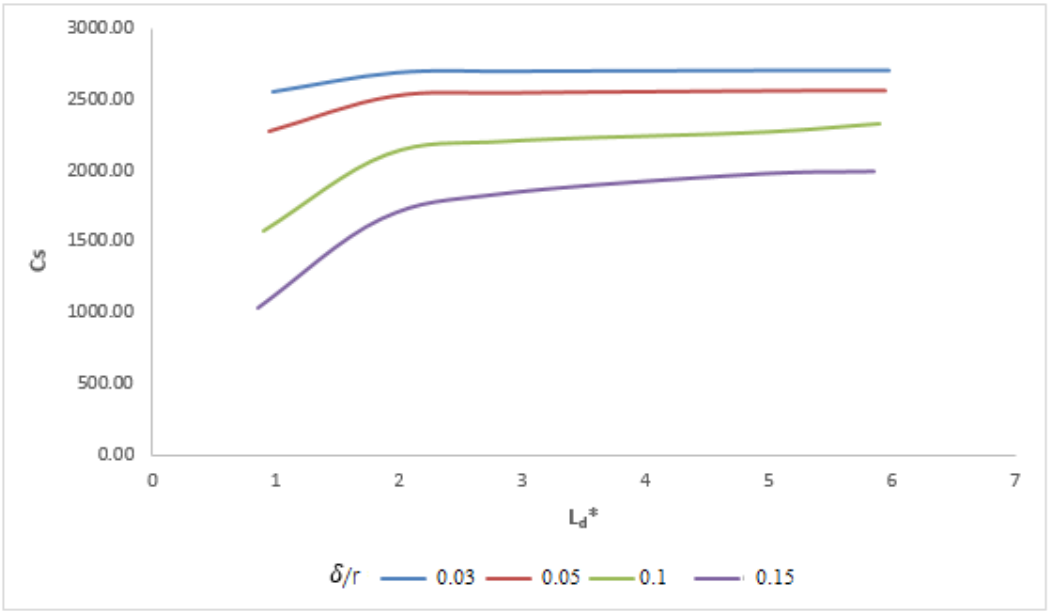

(b)

Figure 4.12: Influence of the drop length (L_d^*) and non-dimensional film thickness (δ/r) on the Stokes coefficient with (a) no-slip (b) free-slip boundary condition at the droplet surface for vertical slug flow

.

Table 4.2: Calculated values of the parameters C_s, C_n and p from the Generalised Stokes-Newton equation with a no-slip boundary condition at the droplet surface

	$\delta = 0.01$			
L_d^*	C_s	C_n	p	Relative Error
1	3362.42	1.98	2.09	1.93e-4
2	5367.75	1.40	1.85	1.41e-04
4	7321.11	2.02	1.93	2.11e-04
5	11223.79	1.47	1.91	1.18e-04
6	13161.44	2.17	1.87	8.75e-05
	$\delta = 0.03$			
1	2968.29	0.08	1.25	3.11e-04
2	3723.89	2.75	2.24	2.04e-04
4	4401.82	2.40	2.11	1.97e-04
5	5747.36	1.12	1.74	2.99e-04
6	6419.7	5.08	2.40	2.11e-04
	$\delta = 0.05$			
1	2808.52	3.11	2.55	3.58e-04
2	3360.18	1.94	2.11	2.63e-04
4	3788.51	2.10	2.08	2.57e-04
5	4628.22	2.03	2.08	1.63e-04
6	5044.35	1.98	2.08	6.53e-04
	$\delta = 0.55$			
1	2453.41	3.11	2.77	5.75e-05
2	3034.03	1.94	2.23	2.21e-04
4	3306.30	2.10	2.24	3.71e-04
5	3787.52	2.03	2.35	3.27e-04
6	4268.74	1.98	2.37	2.56e-04
	$\delta = 0.1$			
1	2038.50	0.26	1.45	2.56e-04
2	2828.18	3.11	2.49	3.30e-04
4	3103.14	1.93	2.26	2.50e-04
5	3505.02	0.23	1.55	2.26e-04
6	3906.90	0.80	1.80	2.30e-04

Table 4.3: Calculated values of the parameters C_s, C_n and p from the Generalised Stokes-Newton equation with a free-slip boundary condition at the droplet surface

	$\delta = 0.01$			
L_d^*	C_s	C_n	p	Relative Error
1	2897.7	2.84	2.50	1.30e-4
2	2972.1	2.07	2.19	3.69e-04
4	2975.2	1.70	1.68	2.17e-03
5	2976.9	1.92	2.20	2.02e-04
6	2976.5	1.96	2.21	2.97e-04
	$\delta = 0.03$			
1	2552.3	3.07	2.91	3.83e-04
2	2686.5	1.82	2.31	2.48e-04
4	2696.2	2.04	2.31	2.03e-04
5	2701.6	1.91	2.40	5.70e-04
6	2702.1	1.26	2.19	4.14e-04
	$\delta = 0.05$			
1	2272.1	1.08	1.30	5.31e-04
2	2521.4	1.98	2.34	2.06e-04
4	2545.7	0.27	1.57	3.05e-04
5	2559.8	1.27	2.38	2.72e-04
6	2561.8	1.13	2.30	1.46e-04
	$\delta = 0.055$			
1	1570.98	2.97	2.08	3.66e-04
2	2112.42	2.01	2.61	5.97e-04
4	2207.74	1.48	2.33	3.64e-04
5	2269.22	1.92	2.33	4.27e-04
6	2330.70	1.60	2.34	3.80e-04
	$\delta = 0.1$			
1	1030.95	3.46	2.02	2.67e-04
2	1654.83	1.66	2.05	3e-04
4	1833.23	2.31	2.39	1.97e-04
5	1966.94	3.62	2.89	2.90e-04
6	1988	3.50	2.92	2.30e-04

$L_d^* = 2.95$. It can be observed that the drag coefficient decreases as the Reynolds number increases, as expected. Also, for higher Reynolds numbers the drag coefficient achieved a constant value which may correspond to the actual value of the Newton coefficient for the specified drop length. Similar drag curves were obtained for the other cases, with the difference that the C_d values were smaller with larger film thickness and higher for longer droplets. The drag coefficient C_d can then be used to compute the terminal velocity of the droplet (U_∞) using the expression in Equation 3.63 which relates the Galileo number and the drag coefficient when the balance of gravitational forces has been reached. The terminal velocity will greatly depend on the relative densities of the dispersed and continuous phases when balancing gravity. The prediction of the settling or rising velocities using the current CFD model requires the densities of both the continuous and dispersed phases to be known, hence further validation with a specific two-phase system is necessary to extend its applicability. Nevertheless, the drag force analysis developed in this study under the limits of low and high viscosity ratios gives a significant suggestion of the behaviour expected in situations when the density and viscosity ratios are relevant. Such is the case during biodiesel production where the continuous phase is denser than the dispersed phase, and this much more viscous than the continuous phase.

The interest for predicting the drag coefficients and terminal velocities is therefore related to the importance of design parameters in mixing or separation processes. The performance of several technologies involving dispersed two-phase flow can be significantly affected by a reliable interfacial drag correlation.

4.6.2 Prediction of the droplet velocity in horizontal flow

The predictions of the droplet velocity in a pressure driven horizontal flow were developed using a single-phase framework for convenience. Preliminary two-phase flow results for a high viscosity ratio showed similar velocity profiles in the continuous phase to those observed in a single phase set-up when a no-slip droplet is defined. Also, the predictions of the droplet velocity obtained from the two-phase set-up for a high viscosity ratio were less than 5% different form the ones

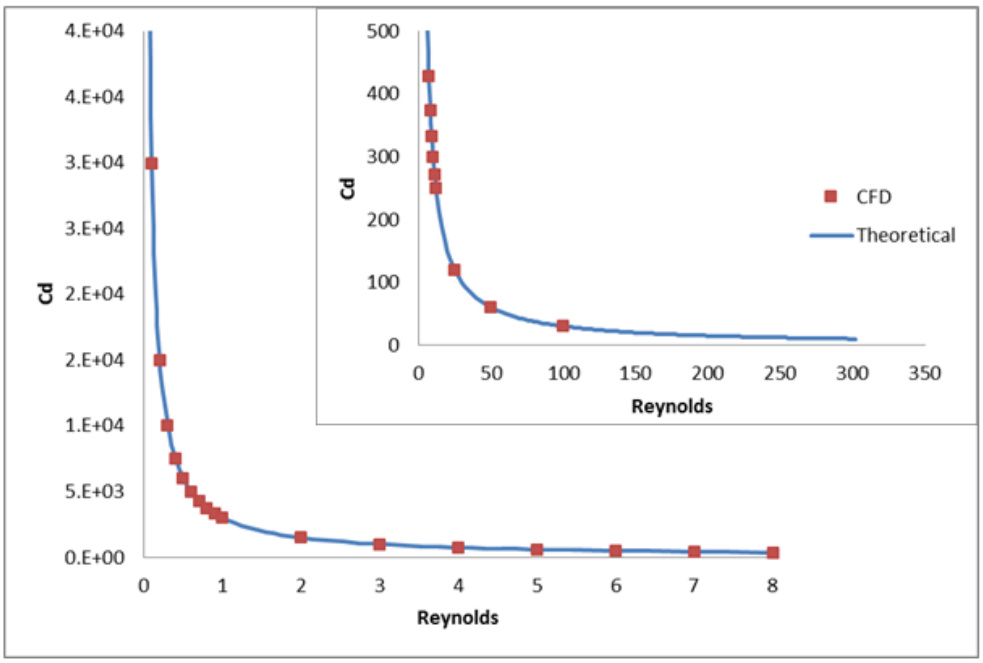

Figure 4.13: Comparison of numerical and theoretical C_d curves for the case of $Re = 1$, $\delta/r = 0.05$, $L_d^* = 2.95$ in a vertical flow

found in a single-phase framework. This configuration allowed to reduce computational time significantly and to investigate the influence of the main slug flow parameters on the droplet velocity more efficiently.

The dependence of the drop length on the droplet velocity with a constant film thickness and pressure boundary condition $\Delta P = 100\ Pa$ is depicted in Figure 4.14. The slug length L_s^* was long enough to achieve fully developed flow in this region. The CFD results show that shorter droplets will travel quicker through the continuous phase and in turn will possibly generate a greater number of segments along the capillary. The predictions for the droplet velocity varied between 0.04-0.14 m/s for drop lengths $1.97 \leq L_p^* \leq 10.97$ and the assumption of a uniform film thickness is valid for drop lengths greater than $L_p^* > 1.82$ as observed in the experimental work by (Li & Angeli, 2017). The authors identified a variation on the film thickness for shorter drop lengths in the range $1.14 \leq L_p^* \leq 1.82$ and

a uniform film thickness always present between the hemispherical caps of the droplet between $1.82 \leq L_p^* \leq 2.31$. Also, an effect of the Capillary number and flow ratio on the drop length was observed in their work. This feature depends on the inlet configuration, e.g. Y-junction, T-junction; and is not considered in the current study. However, the numerical predictions obtained for the droplet velocity fall within the range specified in their experimental work.

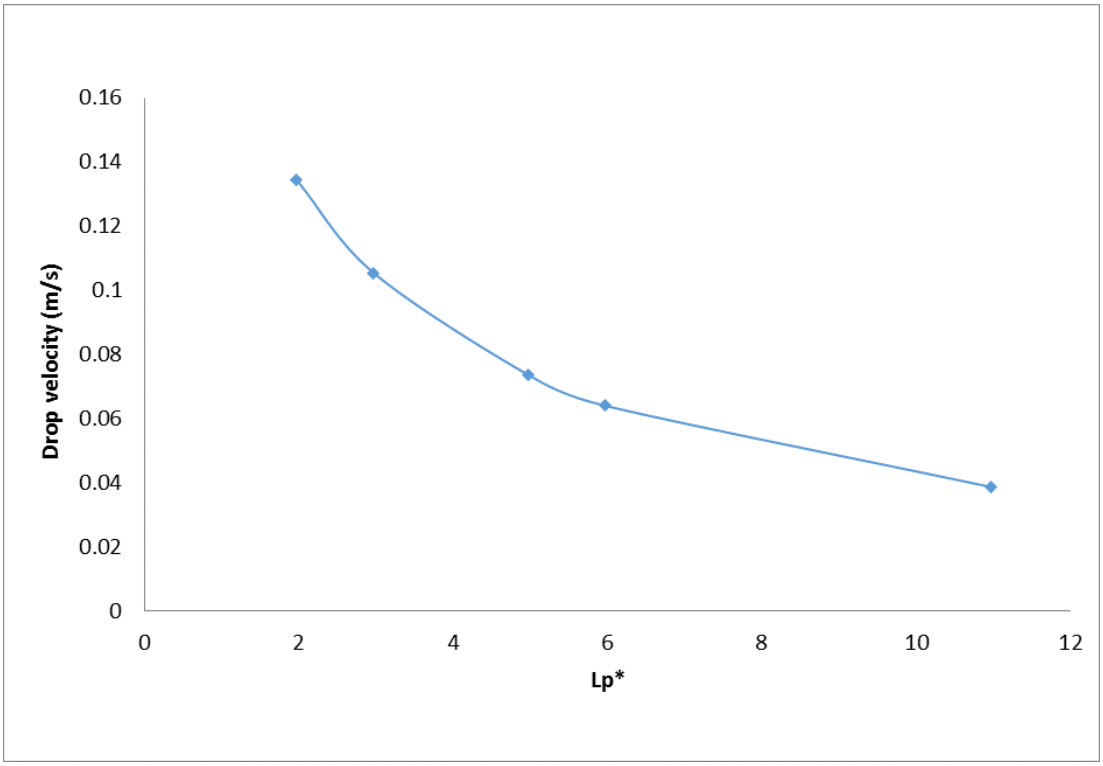

Figure 4.14: Dependence of the drop length on the droplet velocity in horizontal flow with a constant film thickness $\delta/r = 0.05$ and slug length $L_s^* = 10$.

Figure 4.15, shows the CFD predictions of the droplet velocity with different slug lengths and constant drop length $L_d^* = 5.95$ with a uniform film thickness $\delta/r = 0.05$. The dependence of the slug length on the droplet velocity simulates the case of a train of droplets travelling through a capillary. The CFD results show that as the slug length increases the droplet velocity is lower which implies that a train of droplets separated by a very short slug length will move faster along the capillary. The reason for this is that the flow in the slug region is not yet fully

developed, hence the interfacial forces at the front or rear of the droplet are easier to overcome. Likewise, short slug lengths will generated an increase on the total pressure drop since the interfacial pressure will be higher compared to the case of a very long slug where the flow behaves as Poiseuille flow. The influence of the slug length to the total pressure drop in capillary slug flow has been investigated by (Eain *et al.*, 2015; Kreutzer *et al.*, 2005; Walsh *et al.*, 2009) and is further analysed in the next Chapter. Also, the slug length will have a greater impact when dealing with mass transfer between the dispersed and continuous phases as presented in the experimental work by (Jovanovic *et al.*, 2011b; Xu *et al.*, 2013).

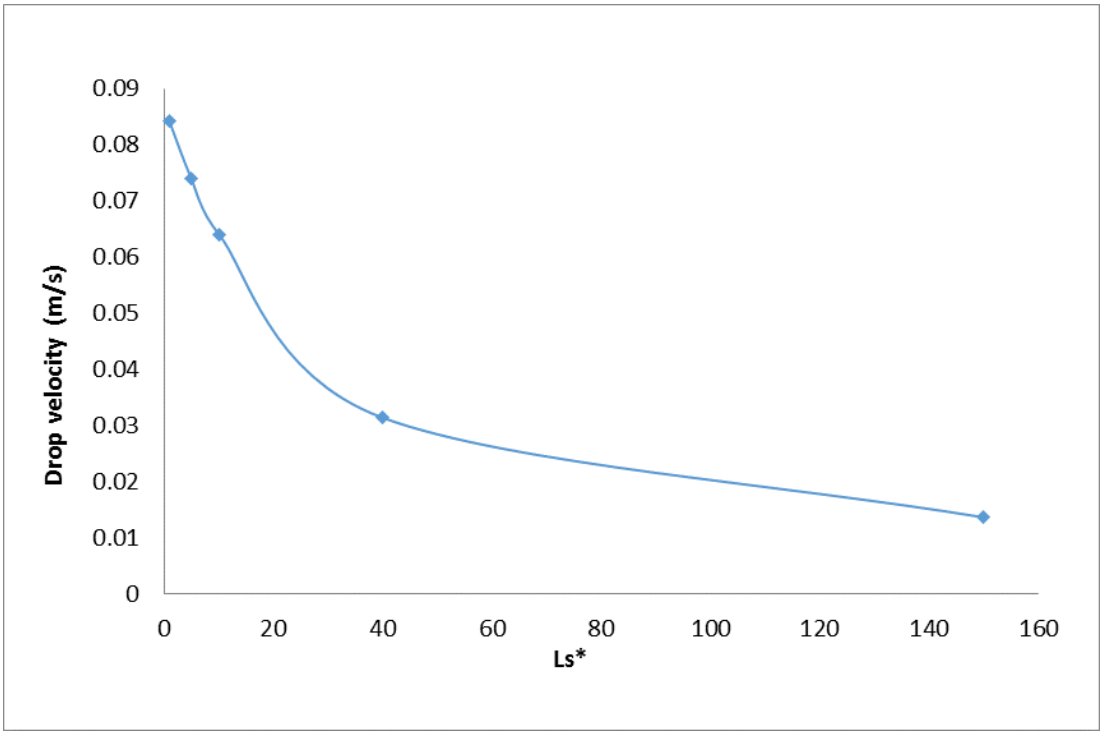

Figure 4.15: Dependence of slug length on the droplet velocity in horizontal flow with a constant film thickness $\delta/r = 0.05$ and drop length $L_d^* = 5.95$.

Moreover, Figure 4.16 shows the CFD predictions of the droplet velocity for different film thickness and a constant droplet length. The results revealed the significance of the film thickness on the droplet velocity since it increases rapidly for a greater film thickness. The validation of the predicted droplet velocity with experimental data is necessary in order to evaluate the dependence of the film

thickness with the Capillary number for the current flow conditions. For instance, a liquid-liquid system involving a very high viscous dispersed phase should satisfy the current CFD predictions.

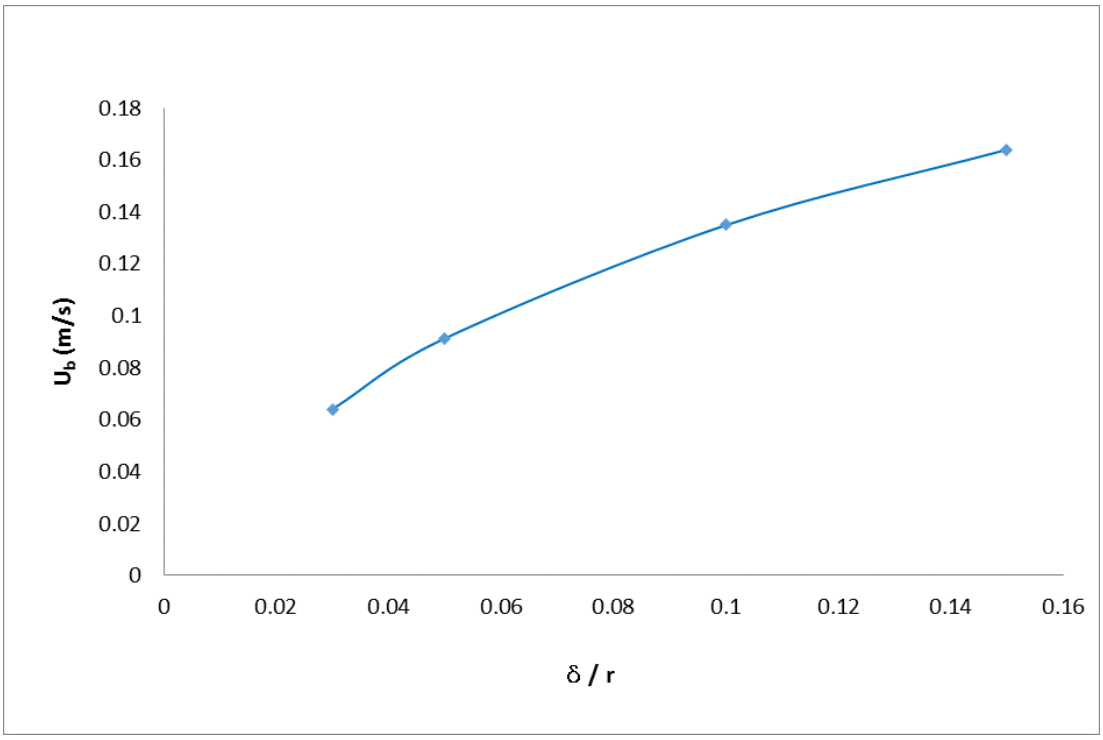

Figure 4.16: Dependence of the non-dimensional film thickness on the droplet velocity in horizontal flow with a constant drop length $L_d^* = 5.95$.

Although, the validation to experimental data is still required at this stage, the CFD methodology developed in this study can also be useful for the predictions of mass transfer coefficients in two-phase slug flows. The film thickness in liquid-liquid slug flows plays an important role in preventing the saturation in this area which would limit the mass transfer between the two phase. The current CFD approach could provide insight into mass transfer mechanisms involving this type of flow conditions.

4.6.3 Two-Phase Study in horizontal flow

The hydrodynamics of a slug flow through capillary was investigated in more detail for further understanding of the flow field characteristics in both dispersed and continuous phases. An alternative approach to the most common methods applied for two-phase studies, e.g Volume of Fluid method, was implemented in this study to investigate the influence of the viscosity ratio and geometry configuration on the flow dynamics of a slug flow through a capillary.

The two-phase study was developed in two stages: first, the assumption of an infinite droplet dispersed in a continuous phase with a constant film thickness was considered. Then, the contribution of the hemispherical end caps was included. In both cases the boundary conditions at the interface $u_d = u_c$ and $\tau_d = \tau_c$ were applied to conserve continuity across the two-phases.

Interfacial velocity and shear stress distribution in liquid-liquid slug flow

The numerical results for an infinitely long droplet dispersed in a continuous phase in a capillary, revealed that the flow behaviour can be described by the analytical solution of a two-phase annular flow driven by a pressure gradient. The velocity profiles in both the film and droplet regions for a viscosity ratio $\frac{\mu_d}{\mu_c} = 2$ are shown in Figure 4.17. As can be seen, there is a good agreement between the CFD simulations and the velocity profiles predicted by Equations 3.20 and 3.21. The velocity profile in the film is shown in Figure 4.17(a), where the CFD predictions are compared against Equation 3.20. The results follow a Couette velocity profile on which the maximum velocity occurs at the droplet surface. This indicate the effect of the shear exerted by the dispersed phase on the velocity field, hence the velocity of the film can not be ignored in the modelling of liquid-liquid flows. Moreover, the velocity profile in the droplet region is shown in Figure 4.17(b) and is also in good agreement with the velocity profile predicted by Equation 3.21. The maximum velocity within the dispersed region is much higher than the film maximum velocity. Also, the viscosity ratio was varied within the range $1 \leq \frac{\mu_d}{\mu_c} \leq 50$. The results show that as the viscosity ratio increases the maximum velocity in the dispersed phase decreases, as expected for very viscous droplets.

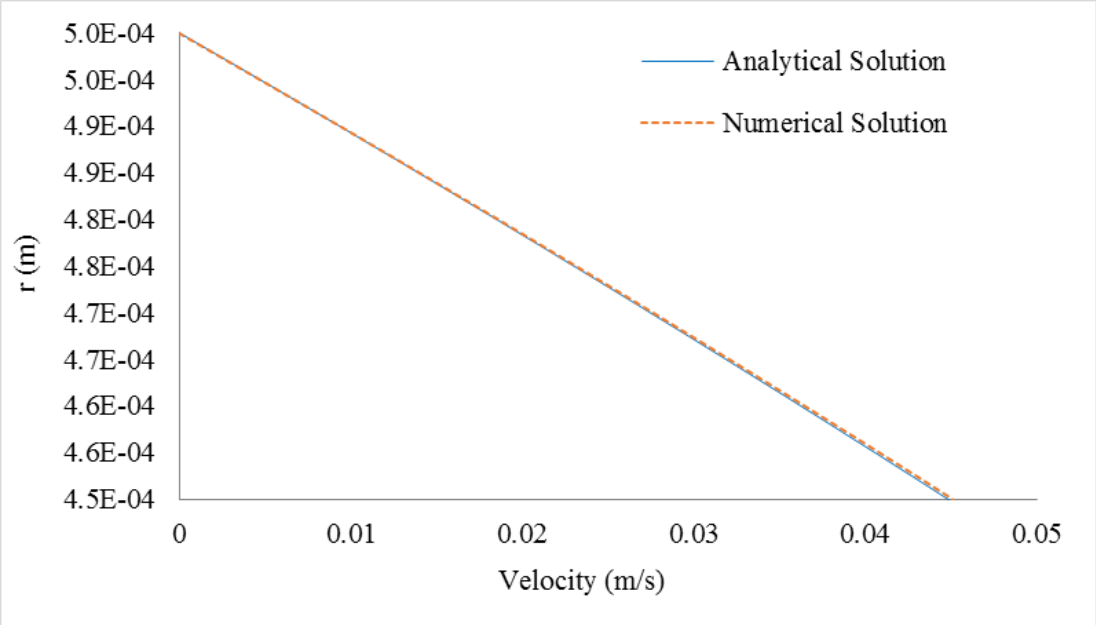

(a)

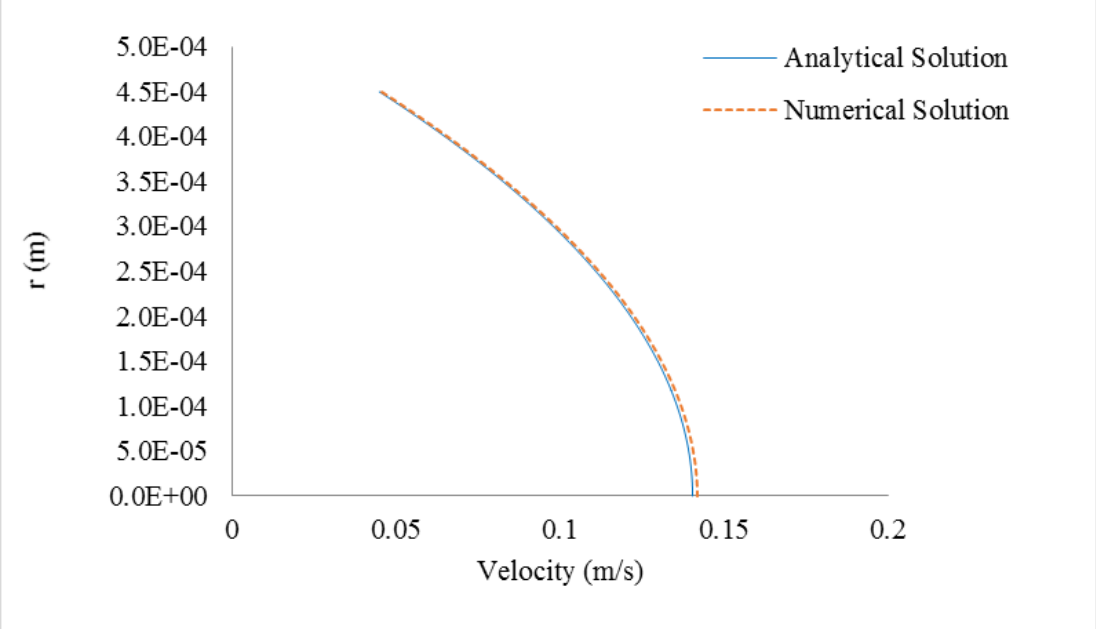

(b)

Figure 4.17: Numerical and analytical profiles of an infinite drop in a continuous flow through a capillary (a) film region (b) droplet region

.

Furthermore, for a known and finite droplet shape, the average interfacial velocity and shear stress at the interface were calculated. Figure 4.18 shows the shear distribution and velocity profile at the interface of the continuous and dispersed side after a complete simulation.

Convergence was achieved in every case, however some discrepancies with the analytical solution for an ideal annular flow were observed. The velocity profiles obtained from the CFD simulations corresponding to a low viscosity ratio $\frac{\mu_d}{\mu_c} = 2$, are about a 5.2% different than the equation for annular flow. The differences from Equation 3.21 might indicate that the droplet in this case is not long enough for the velocity to become fully developed in the middle of the domain. On the other hand, for a high viscosity ratio $\frac{\mu_d}{\mu_c} = 50$ the CFD results on the film area were in good agreement with the velocity profile predicted by Equation 3.20, but, a considerably disagreement was found in the region inside the droplet. The results demonstrate that for a low viscous dispersed phase (e.g. gas phase) the shear produced by the curvature region is almost negligible since using the velocity profile correlations by (Gupta *et al.*, 2013; Lac & Sherwood, 2009), Equations 3.20 and 3.21 for the central region of the droplet, the flow field can be satisfactorily described. Nevertheless, a significant influence from the curvature region to the velocity field inside the droplet was observed. The velocity profiles in the middle of the domain in both the film and droplet regions for a viscosity ratio $\frac{\mu_d}{\mu_c} = 2$ and considering an enclosed droplet are shown in Figure 4.19.

The hydrodynamic structures obtained in the current two-phase flow study are analogous to those experimentally and numerically observed in previous studies of liquid-liquid slug flow in capillaries (Gupta *et al.*, 2013; Jovanovic *et al.*, 2010; Kashid *et al.*, 2005; Li & Angeli, 2017; Raimondi *et al.*, 2008, 2014). Visualisation of the two-phase flow velocity fields are illustrated in Figure 4.20. As can be observed, three different circulation zones are generated inside the droplet region, a large one in the middle and two small ones at the front and rear of the droplet. Compared to gas-liquid systems, the re-circulation in the droplet and slugs in liquid-liquid slug flow will make a significant contribution to mass transfer and heat transfer enhancement as demonstrated in previous experimental work by (Jovanovic *et al.*, 2012; Raimondi *et al.*, 2014). Although, mass transfer mechanisms are not covered in this work, this study can be use as a first approach

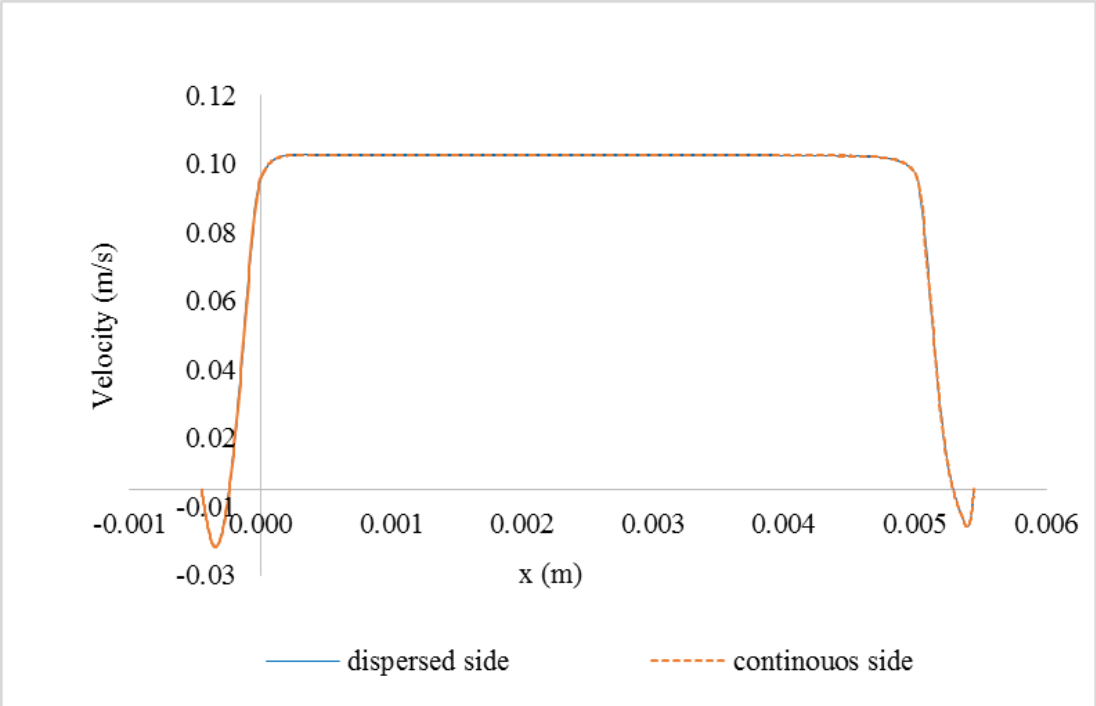

(a)

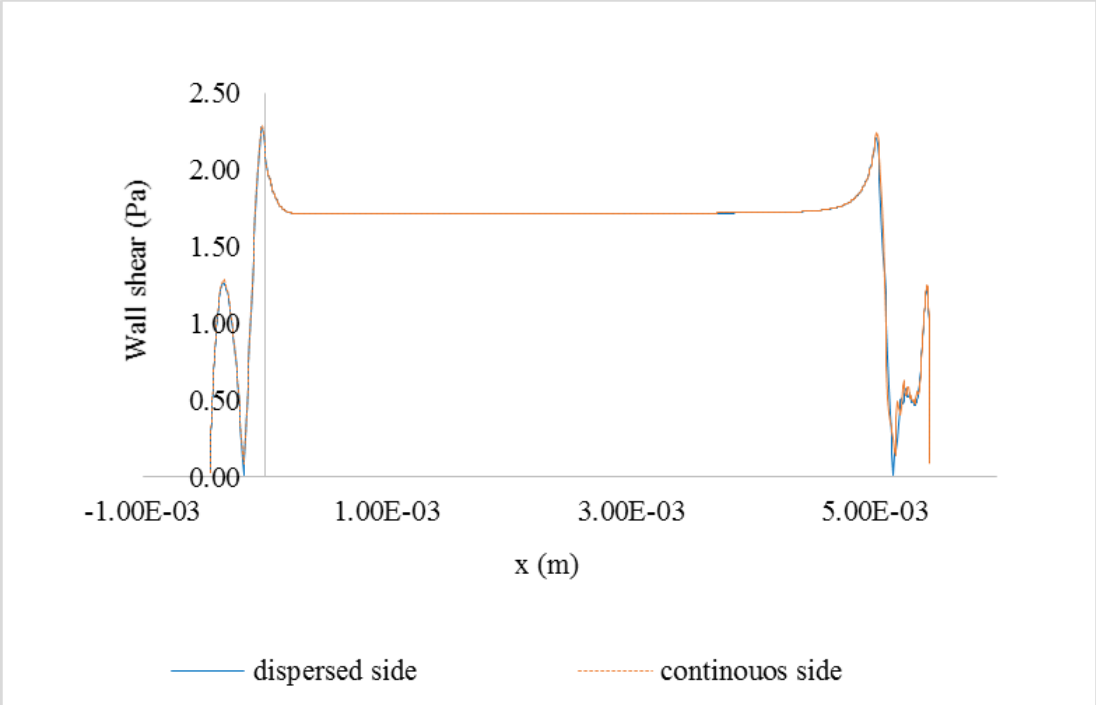

(b)

Figure 4.18: Numerical interfacial profiles of a liquid-liquid slug flow system in a capillary (a) velocity profile (b) shear profile

.

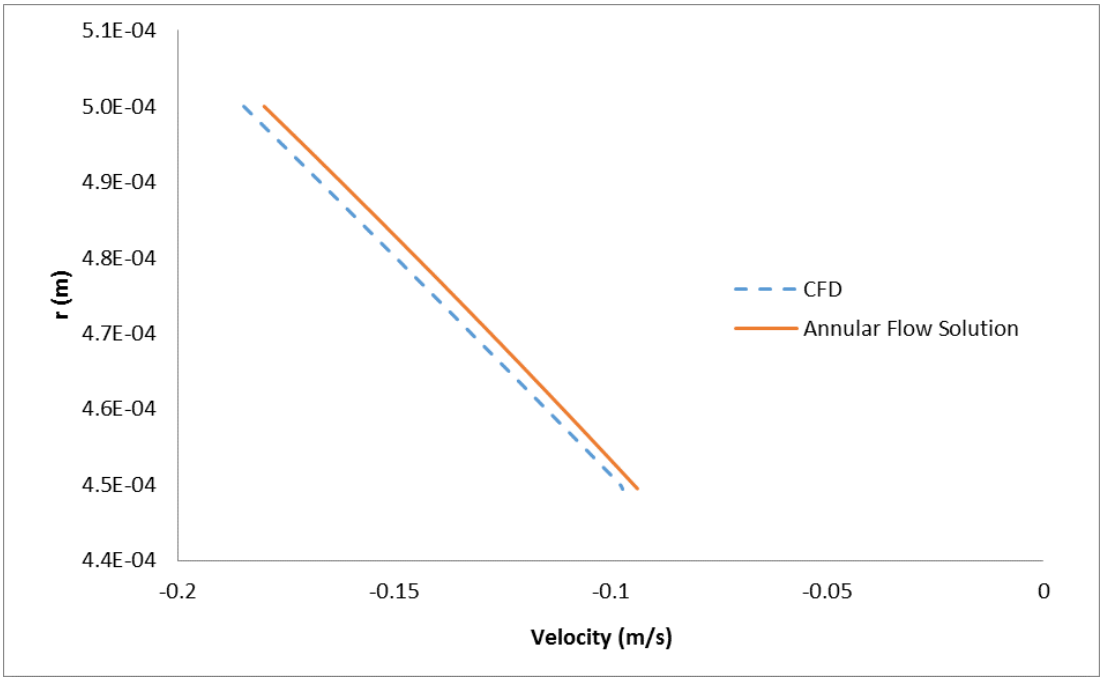

(a)

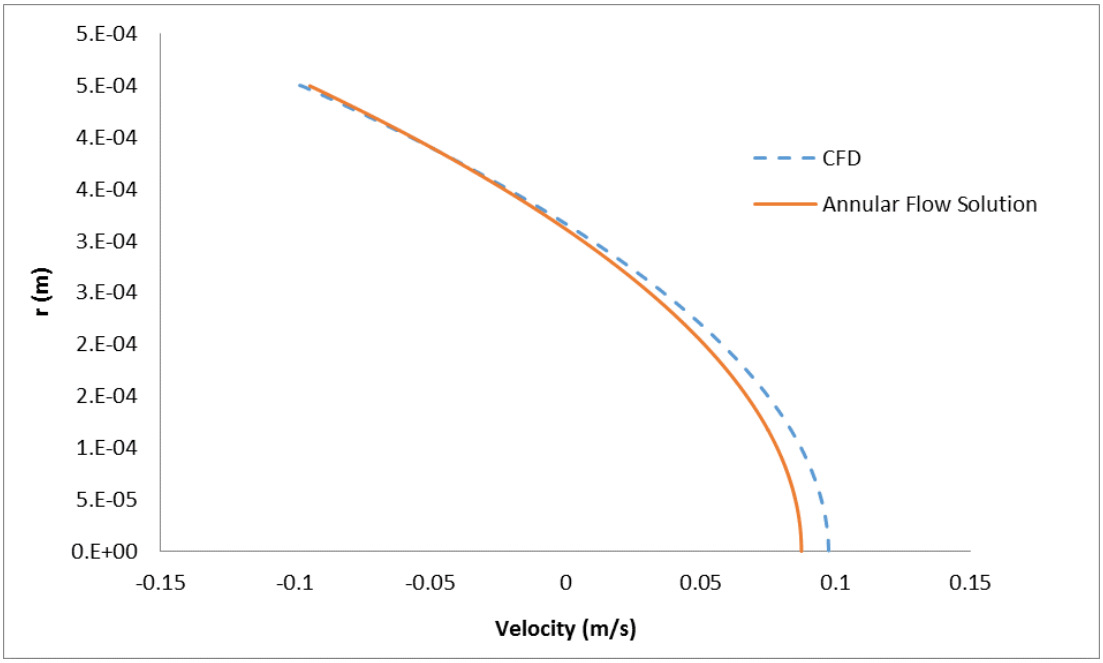

(b)

Figure 4.19: Velocity profiles at the center of the dispersed and continuous phase with a viscosity ratio $\frac{\mu_c}{\mu_d} = 2$ (a) film region (b) droplet region

.

for further development of mass transfer in liquid-liquid slug flows since the wall shear stress and droplet velocities are related to the mass transfer coefficient.

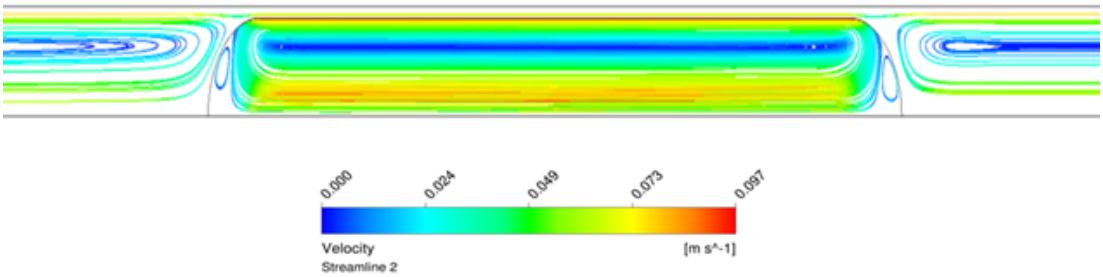

Figure 4.20: Velocity streamlines of liquid-liquid slug flow for a $\frac{\mu_c}{\mu_d} = 2$, $L_d^* = 5.95$, $and \delta/r = 0.05$.

4.6.4 Pressure distribution

The pressure distribution along the capillary together with the pressure gradient at the interface for a viscosity ratio of $\frac{\mu_c}{\mu_d} = 50$ is shown in Figure 4.21. The results clearly show a linear pressure drop in the slug flow region, thin film area and inside the droplet. These three contributions to the overall pressure drop across the capillary were also observed in experimental and numerical studies by (Gupta *et al.*, 2013; Jovanovic *et al.*, 2011b; Kashid *et al.*, 2010a). The CFD results show that the pressure within the continuous phase decreases linearly because of friction and when the interface at the rear of the droplet is reached the pressure increases rapidly and then decreases slightly through the film region. The pressure gradient at the interface is identical in the film area, as shown in Figure 4.21, hence the assumption of annular flow is valid. Also, within a short distance away from the front of the droplet the pressure drops significantly and the behaviour can be described by the Hagen-Poiseuille law in the slug region.

The comparison between the CFD results and the theoretical slug flow models for the total pressure drop was difficult to achieve since the hemispherical caps depend on the surface tension of the two-phase flow. This aspect was initially intended to be overcome by the assumption of a very viscous droplet with a

no-slip boundary condition at the droplet surface and a constant droplet shape which is valid when $Ca \to 0$. Thus the current CFD methodology is satisfactory to a certain extend and can be used to study the flow behaviour of high surface tension flows, having the advantage of generating efficient results and avoiding complex interfacial numerical techniques.

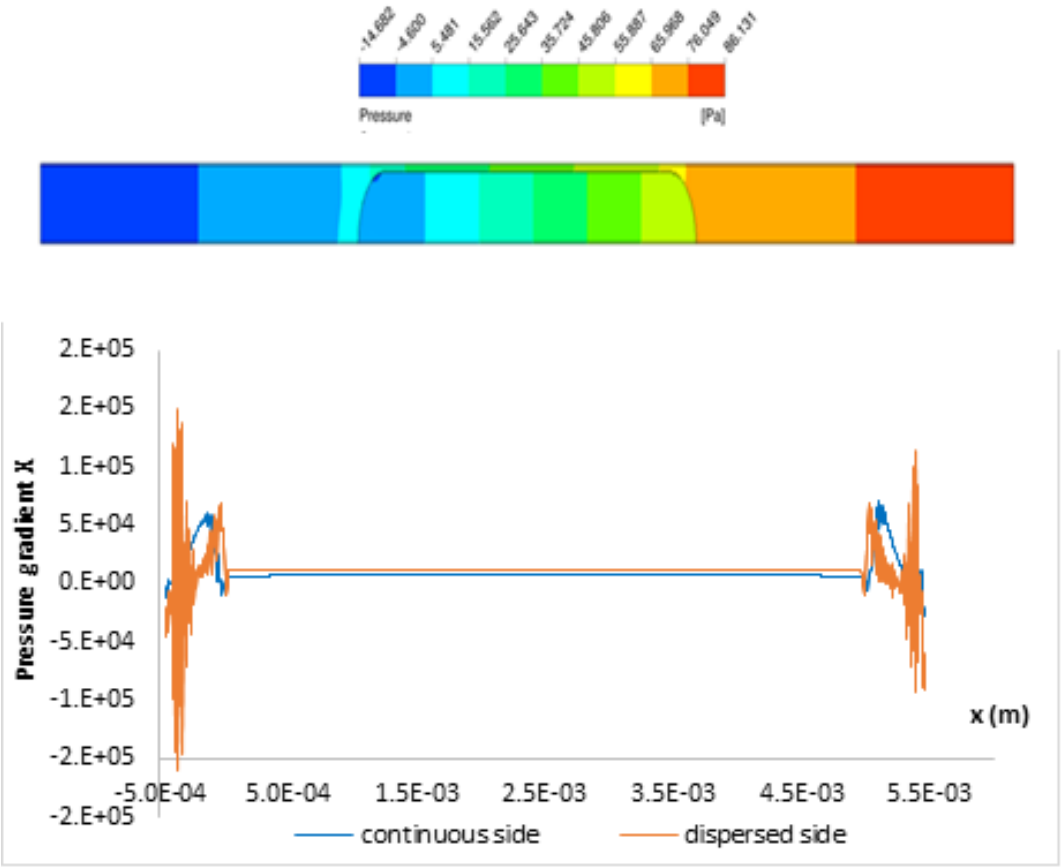

Figure 4.21: Pressure drop and pressure gradient of liquid-liquid slug flow in a unit cell.

Overall, the results from the two-phase study confirm the significance of the interfacial forces for an accurate modelling of liquid-liquid slug flow in a capillary. The velocity field inside the droplet was observed to be greatly affected by the curvature shape. This suggests that additional parameters such as the surface tension are necessary for a reliable prediction of this type of flows. Hence, the

complexity of modelling liquid-liquid slug flow in capillaries is still a big challenge,

4.7 Conclusions

A CFD model has been developed to study the hydrodynamics of liquid-liquid slug flow in a circular capillary. The CFD methodology proposed in this chapter is an alternative to the Volume of Fluid Method (VOF) with the advantage of achieving a faster convergence and to generate parametric studies more efficiently.

As a first attempt, the relationship between the drag coefficient and the Reynolds number was investigated for a free-slip and no-slip droplet of different sizes. The purpose of analysing this effect was attributed to the interest of studying interfacial shear on liquid-liquid slug flow, on which influence of the viscosity ratio is relevant. The case of no-slip boundary approximated the presence of a highly viscous dispersed flow ($\mu_d \gg \mu_c$) leading to high viscous ratios $\left(\frac{\mu_d}{\mu_c} \rightarrow \infty\right)$. On the other hand, a free-slip boundary approximated a low viscous dispersed fluid e.g. gas phase ($\mu_d \ll \mu_c$) which lead to low viscous ratios $\left(\frac{\mu_d}{\mu_c} \rightarrow 0\right)$.

The drag force analysis for various geometry configurations and flow conditions was possible using the Power-Law Stokes-Newton equation. The results show that the drag coefficient depends upon the droplet length, film thickness and Reynolds number. Also, in the limit of low Reynolds number the drag curves for this type of flow obey the Stokes law and the Stokes coefficient (C_s) was greatly influenced by the droplet length, film thickness and the type of boundary condition applied at the droplet surface. The drag coefficients obtained in this study can then be used to predict the terminal velocity of a single droplet freely rising or falling using the definition of the Galileo number and the Generalised Stokes-Newton equation. This requires the densities of both the continuous and dispersed phases to be known. The main limitation of the current CFD approach is that the predictions of the drag coefficient C_d and the settling velocities are functions of the geometric parameters L_d^* and δ/r, while experimental results are for fluid pairs of known surface tension. The CFD analysis needs to be supplemented by models for how film thickness depends on the surface tension.

Moreover, the interfacial forces were investigated in the cases of low and high viscosity ratio. The results confirm that for a large droplet volume for which a sufficiently long uniform thickness film region exists, the velocity profile at the centre of the dispersed and continuous phase can be characterised by an ideal annular flow. The numerical velocity profiles for different viscosity and density ratios were in good agreement with the analytical solution for a Couette-Posiuelle flow of two fluids driven by a pressure gradient. Some discrepancies were found for finite viscous droplets which suggests that additional parameters such as the droplet curvature and surface tension must be included in the model. However, the hydrodynamic structures obtained in the two-phase flow study, such as the internal re-circulation in the dispersed and continuous phase are analogous with those experimentally and numerically observed in previous works found in the literature for slug flow in capillaries.

Additionally, the simulations performed with the proposed CFD methodology took an average of 5 hours for each geometry configuration resulting as an advantage over the VOF method which can take over 24 hours to achieve a converged solution in similar two-phase flow problems.

The results in this study along with previous similar observations revealed the complexity of estimating accurately the interfacial pressure drop in liquid-liquid slug flows. The main difficulty is that the dependence of δ/r on the surface tension is through the Capillary number, which also depends on the droplet velocity. This feature made it difficult to combine the CFD results with the correlations for δ/r, but could be overcome by further improvements on the CFD model developed in this work.

The CFD model proposed in the present study allows to analyse efficiently the effect of viscosity and density ratios for annular flow. Also, the CFD model is predictive for the case of sufficiently high surface tension where the end caps can be assumed to be hemi-spherical. The proposed CFD methodology and configuration can be used as an efficient approach to investigate mass transfer mechanisms in gas-liquid and liquid-liquid slug flows.

The experienced acquired from the previous study led to the development of a different approach which is presented in the following chapter. The proposed methodology considers all the fluid properties of a certain two-phase flow and its

ability to predict film thickness, droplet velocity and pressure drops without a prior knowledge of any of these parameters. A critical review and detail understanding of recent correlations that have been used for the prediction of the main slug flow parameters was convenient in order to develop an efficient predictive tool that can be useful for design purposes of technologies involving this type of flows.

Chapter 5

Prediction of film thickness, bubble velocity and pressure drop in capillary slug flow

5.1 Introduction

Although, a rapid development of several techniques has emerged to investigate the flow behaviour in micro-scale devices and numerous efforts have been undertaken to describe the flow patterns and mass transfer mechanisms in slug flows through capillaries, there are still gaps in understanding some of the fundamental physics in liquid-liquid slug flows compared to gas-liquid systems Bandara *et al.* (2015).

One of the main limitations with the application of the film thickness and bubble velocity expressions that have been used for the modelling of such systems is their coupled dependency Howard & Walsh (2013). For this reason, a computationally efficient process model has been developed in this work to predict important modelling parameters for slug flow in capillaries. The approach is based on theoretical and empirical models found in the literature with the advantage that no-prior knowledge of the bubble's velocity is required. This offers convenience for modelling applications for which this information is difficult to measure or not known. The method consists of an iterative calculation of the film thickness and bubble velocity based on fluid properties and inlet flow conditions.

The algorithm also allows to predict the total pressure drop along a capillary for a given slug and bubble length. The results are validated with experimental and numerical data from the literature and can be useful as a design tool for applications where micro-capillaries are used for process intensification and further scaling up of such systems.

5.2 Method for predicting the film thickness and bubble velocity

The implementation of existing correlations for the prediction of the film thickness and bubble velocity in slug flows is limited to the coupled dependency among these two parameters. With the intention of providing an efficient tool to determine the main slug flow parameters from known information such as the fluid properties and inlet flow rates, a methodology has been developed based on empirical and theoretical correlations found in the literature. The method consists of an iterative calculation based on a system of non-linear equations corresponding to existing correlations used for the modelling of slug flow through capillaries and whose main characteristics were described in Chapter 3. The calculations were performed between a wide range of Reynolds and Capillary numbers. The procedure is described in the following guidelines:

1. The two-phase velocity (U_m) at the inlet is determined from the total volumetric flow rate (Q_t) as: $U_m = \frac{Q_t}{A_c}$, where A_c is the area of the capillary.

2. The flow rate of each phase, Q_d and Q_c is determined from a desired inlet flow ratio.

3. The volume fraction of the dispersed phase is calculated by: $\alpha = \frac{Q_d}{Q_t}$.

4. The Reynolds, Capillary and Weber numbers are calculated using the two-phase velocity (U_m).

5. An approximated film thickness is determined selecting a film thickness expression described in Table 5.1:

Table 5.1: Film thickness correlations used in the current study

Reference	Film thickness correlation
Bretherton (1961)	$\frac{\delta}{D} = \frac{1}{2}0.643(3Ca)^{\frac{2}{3}}$
Aussillous & Quere (2000)	$\frac{\delta}{D} = \frac{1.34(3Ca)^{\frac{2}{3}}}{1+1.34(2.5Ca)^{\frac{2}{3}}}$
Han & Shikazono (2009)	$\frac{\delta}{D} = \frac{0.670Ca^{\frac{2}{3}}}{1+3.13Ca^{\frac{2}{3}}+0.504Ca^{0.672}Re^{0.589}-0.352We^{0.629}}$
Eain *et al.* (2013)	$\frac{\delta}{R} = \frac{1.34Ca^{\frac{2}{3}}}{1+1.34(1.6Ca^{\frac{2}{3}})}$
	$\frac{\delta}{R} = 0.35Ca^{0.354}We^{0.097}$
Langewisch & Buongiorno (2015)	$\frac{\delta}{D} = \frac{0.670Ca^{\frac{2}{3}}}{1+2.86[1+\phi(Re)]\times Ca^{c}}$
Li & Angeli (2017)	$\frac{\delta}{R} = 0.385Ca^{0.265}We^{0.098}$

6. An initial value of the bubble velocity (U_b) is predicted using the approximated film thickness value and a bubble velocity expression from Table 5.2. The expression proposed by Howard & Walsh (2013) was used to evaluate the influence of the viscosity ratio on the bubble velocity. This equation relates the bubble velocity to the mean two phase velocity and can be expressed in terms of the film thickness after simple manipulation as:

$$\frac{U_b}{U_m} = \frac{\left(1-\frac{\delta}{r}\right)^2\left(\frac{\mu_c}{\mu b}-2\right)+2}{\left(1-\frac{\delta}{r}\right)^4\left(\frac{\mu_c}{\mu_b}-1\right)+1} \tag{5.1}$$

7. The bubble Reynolds (Re_b) and Capillary (Ca_b) numbers are determined with the actual bubble velocity U_b.

8. Steps 4-7 are repeated until error of the bubble velocity between iterations is below 1%.

During the first part of the study the film thickness and bubble velocity correlations proposed by Langewisch & Buongiorno (2015) were implemented to validate the performance of the current methodology. The calculations were developed between the ranges $0 \leq Ca \geq 2$ and $0 \leq Re \geq 2000$, which corresponds

Table 5.2: Bubble velocity correlations for two-phase slug flows

Reference	Correlation	Parameters	Flow
Bretherton (1961)	$\frac{U_b - U_s}{U_b} = 1.29(Ca)^{\frac{2}{3}}$	$Ca < 0.03$	G-L
Liu *et al.* (2005)	$\frac{U_b}{U_m} = \frac{1}{1-0.61Ca^{0.33}}$	$2 \times 10^{-4} < Ca < 0.39$	G-L
Kashid *et al.* (2005)	$\frac{U_b}{U_m} = \frac{2}{1+(R_b/R)^2}$	$0 < U_m < 0.2m/s$	L-L
Howard & Walsh (2013)	$\frac{U_b}{U_m} = \frac{\left(\frac{R_b}{R}\right)^2\left(\frac{\mu_c}{\mu_d}-2\right)+2}{\frac{R_b}{R}^2\left(\frac{\mu_c}{\mu_d}-2\right)+1}$	$0.0045 < Ca < 0.0089$	L-L
Langewisch & Buongiorno (2015)	$\frac{U_b}{U_m} = (1-2\frac{\delta}{D})^{-2}$	$0.005 < Ca < 2,$ $0 < Re < 900$	G-L

to the case of high viscosity ratios ($\frac{\mu_c}{\mu_d} \geq 100$) and density ratios ($\frac{\rho_c}{\rho_d} \geq 1000$), namely gas-liquid systems.

The second part of the study uses experimental data extracted from Eain *et al.* (2013) including gas-liquid-and liquid-liquid systems. Details of the fluid properties and two-phase flow combinations are provided in Table 5.3 and 5.4, respectively. The predictions of the film thickness were carried out using different film thickness correlations described in Table 5.1 for comparison and the bubble velocity was calculated using Equation 5.1.

Finally, further analysis of the bubble velocity for an independent data set from Li & Angeli (2017) and Dai *et al.* (2015) was developed using the correlations from gas-liquid and liquid-liquid systems summarised in Table 5.2.

For the case of gas-liquid flow, air was considered as the dispersed phase, and in liquid-liquid flows the properties of the water were used.

Table 5.3: Properties of the fluids used during the current study.

Fluid	Density (kg/m^3)	Viscosity (kg/ms)
Air	1.2	1.84×10^{-5}
Water	996.6	8.68×10^{-4}
Pd5	911.8	3.58×10^{-3}
Ethylene Glycerol (EG)	1112	18.9×10^{-3}
FC40	1854.1	3.91×10^{-3}
AR20	1142.2	20.91×10^{-3}
Dodecane	754.3	1.39×10^{-3}
Hexadecane	767	2.67×10^{-3}

Table 5.4: Two-phase flow properties.

Fluid system	Viscosity ratio $\left(\frac{\mu_c}{\mu_d}\right)$	Density ratio $\left(\frac{\rho_c}{\rho_d}\right)$	Surface tension (N/m)
Water/air	54	830.5	0.073
Pd5/air	190	759.8	0.024
EG/air	953	926.6	0.048
Pd5/water	4.1	0.91	0.039
Dodecane/water	1.5	0.76	0.051
FC40/water	4.5	1.86	0.030
AR20/water	23	1.15	0.052
Hexadecane/water	3.35	0.77	0.051
HNO3/ionic liquid	40	1.22	0.006

5.3 Method for predicting pressure drop in a capillary

The total pressure drop along a capillary is a function of the Reynolds number, Capillary number, slug length and bubble length as described previously in Chapter 3. However, the slug length and bubble length depend on the inlet configuration that is used to merge the two fluids through the capillary e.g. Y-junction or T-junction. For simplicity, the current pressure drop calculation assumes a well-defined slug flow after the mixing region. So, once the bubble velocity and film thickness are determined for given flow conditions, the pressure drop is calculated as follows:

1. Defining a desired slug length L_s^* and bubble length L_d^*.

2. The non-dimensional pressure drop of the bubble, fRe_b is calculated using an expression described in Table 5.5.

Table 5.5: Non-dimensional pressure drop correlations used in the current study

Author	Interfacial pressure drop correlation
Kreutzer *et al.* (2005)	$fRe_b = \frac{0.17}{L_s^*}\left(\frac{Re}{Ca}\right)^{0.33}$
Walsh *et al.* (2009)	$fRe_b = \frac{1.92}{L_s^*}\left(\frac{Re}{Ca}\right)^{0.33}$
Warnier *et al.* (2010)	$fRe_b = \left(\frac{7.16\left(3^{\frac{2}{3}}\right)}{32}\frac{1}{L_s^*}\frac{A}{A_B}\frac{1}{Ca^{\frac{1}{3}}+3.34Ca}\right)$
Eain *et al.* (2015)	$fRe_b = \left(\frac{8.16\left(3^{\frac{2}{3}}\right)}{32}\frac{1}{L_s^*}\frac{A}{A_B}\frac{1}{Ca^{\frac{1}{3}}+3.34Ca}(1-\alpha)^{\frac{1}{3}}\right)$
Langewisch & Buongiorno (2015)	$\frac{\Delta P_b}{\sigma/R} = 3.96Ca_b^{0.58}$ $\frac{\Delta P_b}{\sigma/R} = 8Ca_b$
Li & Angeli (2017)	$fRe_b = \frac{0.225}{L_s^*}\left(\frac{Re}{Ca}\right)^{0.33}$

3. The non-dimensional pressure drop of the continuous slug phase is considered as $fRe_s = 16$, assuming fully developed flow in this region.

4. The total non-dimensional pressure drop along the capillary is determined as: $fRe_t = fRe_s + fRe_b$.

The range of the flow conditions used during the study are described by non-dimensional parameters in Table 5.6. The predictions of the film thickness and drop velocity involved the complete range of Reynolds and Capillary numbers that are specified for each pair of fluids. For the pressure drop calculations some assumptions were considered since the exact slug length (L_s^*) or bubble length (L_b^*) was not specified for the given flow condition. This aspect made it difficult to determined the exact bubble and slug length that correspond to each Reynolds and Capillary number used during their experiments as this information was not provided in detail. So, three values of slug length L_s^* and bubble length L_b^* were used such as the minimum, maximum and average values of the range specified for each fluid pair. The bubble length was assumed constant during every calculation based on the experimental findings by Eain *et al.* (2013),who stated that the bubble length does not vary after $L_b^* > 0.186$ under certain flow conditions.

Table 5.6: Range of operating conditions in dimensionless parameters

Liquid-gas	Re	Ca	L_s^*	L_b^*
Water/air	56-567	0.0014-0.0067	1.17 -11.34	1.67-11.59
Pd5/air	18-50	0.001-0.034	2.86-46.83	3.84-14.25
EG/air	3-15	0.015 -0.0067	1.18-11.34	1.67 -11.59
Liquid-liquid				
Pd5/water	12-45	0.003-0.0098	1.87-14.12	1.65 -8.10
FC40/water	18-98	0.001-0.007	1.09-9.94	1.09-6.5
AR20/water	1-8	0.012-0.052	1.45-4.54	1.13-1.33
Dodecane/Water	1-87	4.5×10^{-5} - 0.0027	0.76-5.88	1.05-5.12

A general description of the algorithm used for this study is shown in Figure 5.1 and details of the python script can be found in the Appendix B.

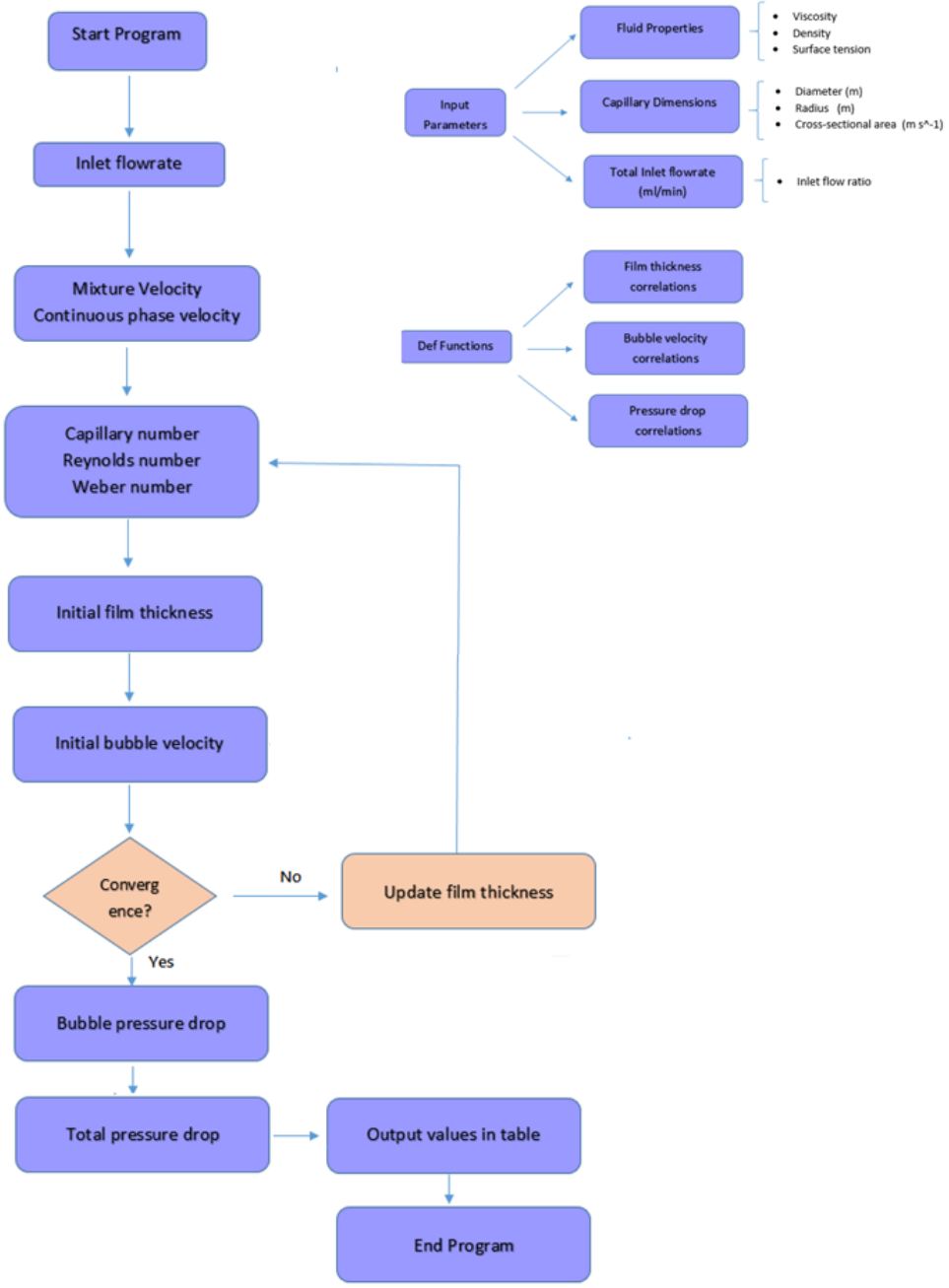

Figure 5.1: Flow chart for the prediction of the film thickness, bubble velocity and pressure drop in capillary slug flow.

.

5.4 Results and Discussion

A number of calculations were developed to predict the film thickness, bubble velocity and pressure drops over a range of Reynolds and Capillary numbers. The first part of the study consisted on the validation of the current model against the CFD database from Langewisch & Buongiorno (2015) which corresponds to a specific density and viscosity ratio namely $\frac{\mu_c}{\mu_d} = 100$ and $\frac{\rho_c}{\rho_d} = 1000$. The second part of the study investigated the behaviour of the film thickness and droplet velocity for a wider range of viscosity and density ratios. The results were validated with experimental data of different pair of fluids including gas-liquid and liquid-liquid systems from the work by Eain *et al.* (2013, 2015). Further analysis of the droplet velocity was developed and compared with an independent data set from Dai *et al.* (2015) and Li & Angeli (2017) including both experimental and numerical predictions. Overall the results show that the current model can be successfully applied to cases when the properties of the fluid pairs and the inlet flow rates are known. The following section describes in detail the results obtained during this study.

5.4.1 Comparison with CFD database

Predictions of the film thickness and bubble velocity over a range of Reynolds and Capillary numbers between $0 < Re < 2000$ and $0.001 < Ca < 2$ were efficiently achieved while using the current method. Figure 5.2 and Figure 5.3 show the predictions of the film thickness and bubble velocity using the correlations from Langewisch & Buongiorno (2015). In both Figures, the y-axis corresponds to the CFD data and the x-axis are the values calculated with the current program using the same equations as in their computational study. As can be seen, the results provide independent validation with those reported in the CFD database by Langewisch & Buongiorno (2015) and show that the model is as good as the database for those ratios and can be applied with some degree of confidence to cases with other density and viscosity ratios.

Figure 5.2 shows the dimensionless film thickness ($\frac{\delta}{d}$) between $0.005 \leq Ca \leq 0.75$ and $0 \leq Re \leq 200$. Clearly, for low Capillary numbers the film is very small. This is due to the surface tension forces dominating in this range, and as

the Capillary number increases the inertial forces begin to overcome generating an increase in the film thickness. A similar behaviour is observed in Figure 5.3 describing the relative velocity $\frac{U_b}{U_m}$ for different Capillary and Reynolds numbers. The velocity of the bubble is higher than the two-phase velocity and also its value increases as inertial effects are higher. These data corresponds to predictions of capillary slug flow with high viscosity and density ratios $\frac{\mu_c}{\mu_d} = 100$ and $\frac{\rho_c}{\rho_d} = 1000$, respectively.

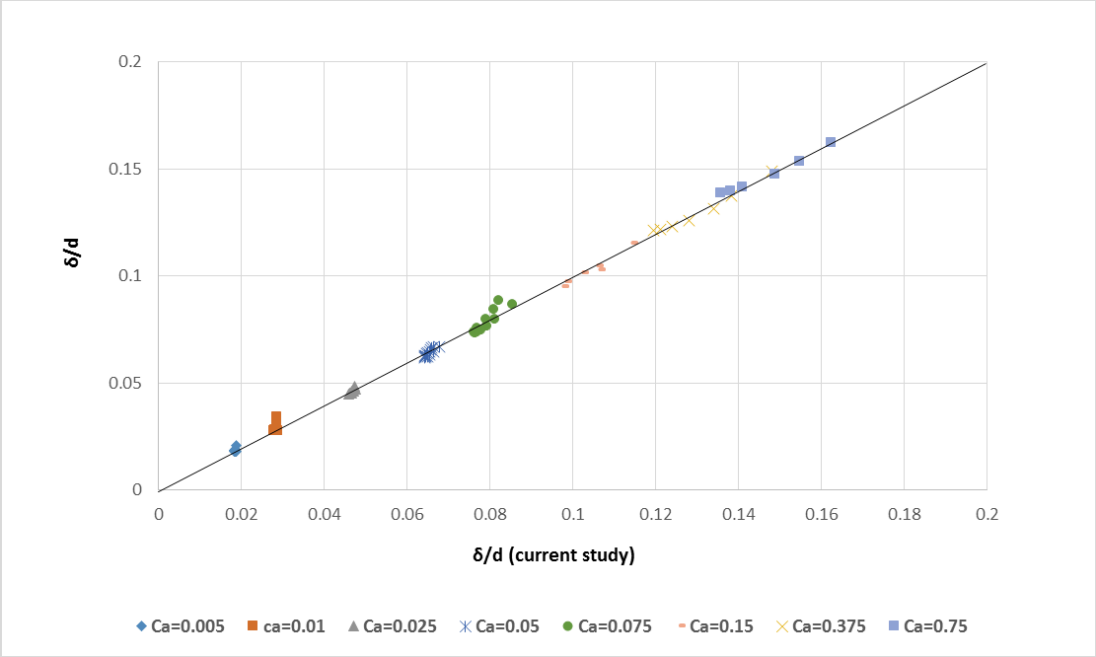

Figure 5.2: Comparison of calculated film thickness values with the CFD data provided by Langewisch & Buongiorno (2015) over a range of Reynolds and Capillary numbers

.

Moreover, the non-dimensional pressure drop of the bubble (ΔP_b^*) in the same range of Reynolds and Capillary numbers was calculated using the pressure drop correlation proposed by Langewisch & Buongiorno (2015)and compared to the CFD database. The results are shown in Figure 5.4 for high and low Capillary numbers using equations 3.48 and 3.49, respectively. The plots contain numerical predictions of ΔP_b^* over a range of Capillary numbers and three different Reynolds

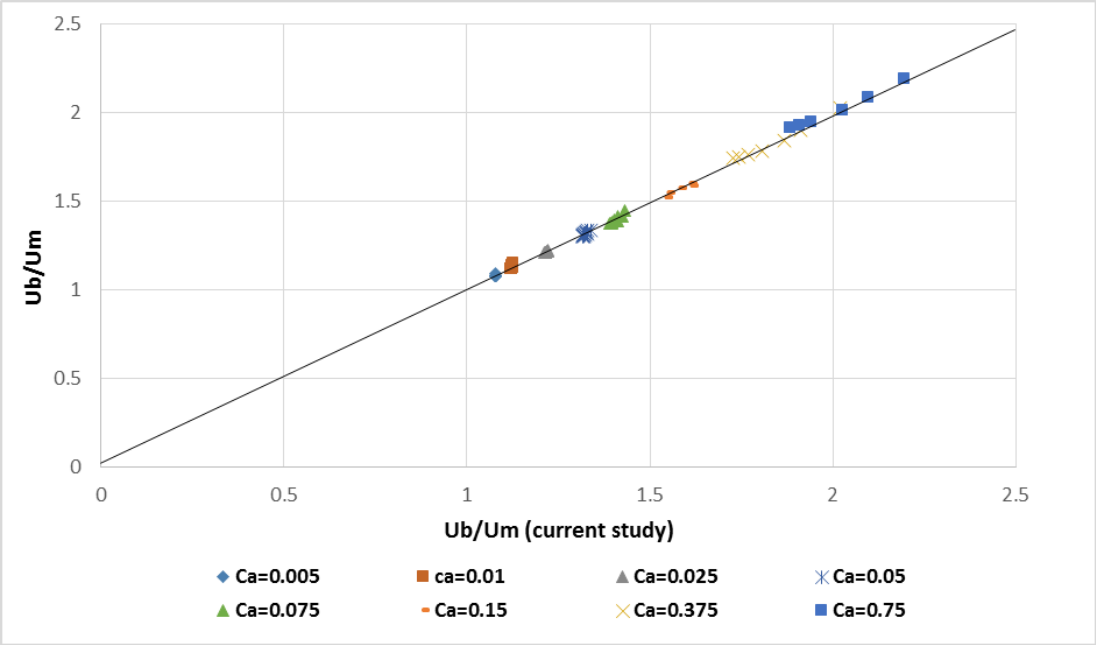

Figure 5.3: Comparison of calculated bubble velocity to mean two phase velocity ratio (U_b/U_m) with the CFD data provided in Langewisch & Buongiorno (2015) over a range of Reynolds and Capillary numbers.

numbers ($Re = 2, 20, 60$). As can be observed in Figure 5.4 (a), the bubble pressure drop is accurately predicted with the current program and agrees with the CFD values when $Ca \leq 0.025$, however some disagreement is identified when $Ca \geq 0.05$ where the pressure drop data appear to be dependent of Re. Consistency with the numerical data using the linear expression proposed by the author in Equation 3.49 was achieved for higher values of Capillary numbers $Ca > 0.187$ and various Reynolds number as shown in Figure 5.4 (b). Possibly, there is some uncertainty on the numerical predictions of ΔP_b^* since the values calculated with the current program using Equation 3.48 agree reasonably for $0.05 < Ca < 0.15$ and $0 < Re < 20$, even though the limit of the Reynolds number is higher than the one established in their study. For instance, in Figure 5.5 (a) the relation between the Capillary number and bubble pressure drop when $Re = 20$ is displayed along with the CFD data and using Bretherton's correlation. It can be seen that the bubble pressure drop increases smoothly with the Capillary number and then

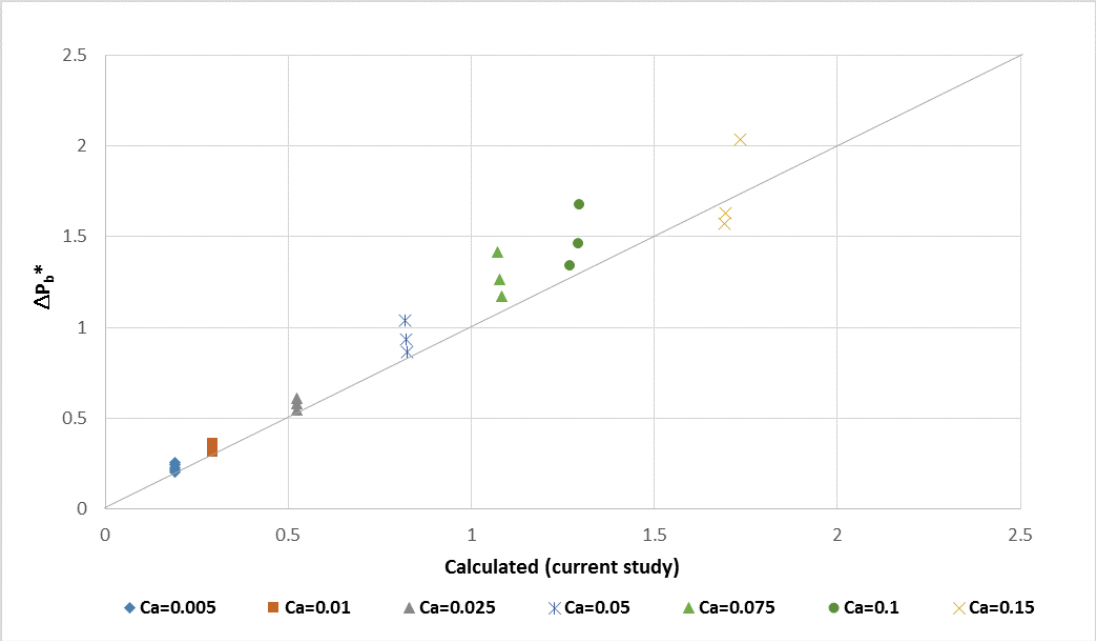

(a)

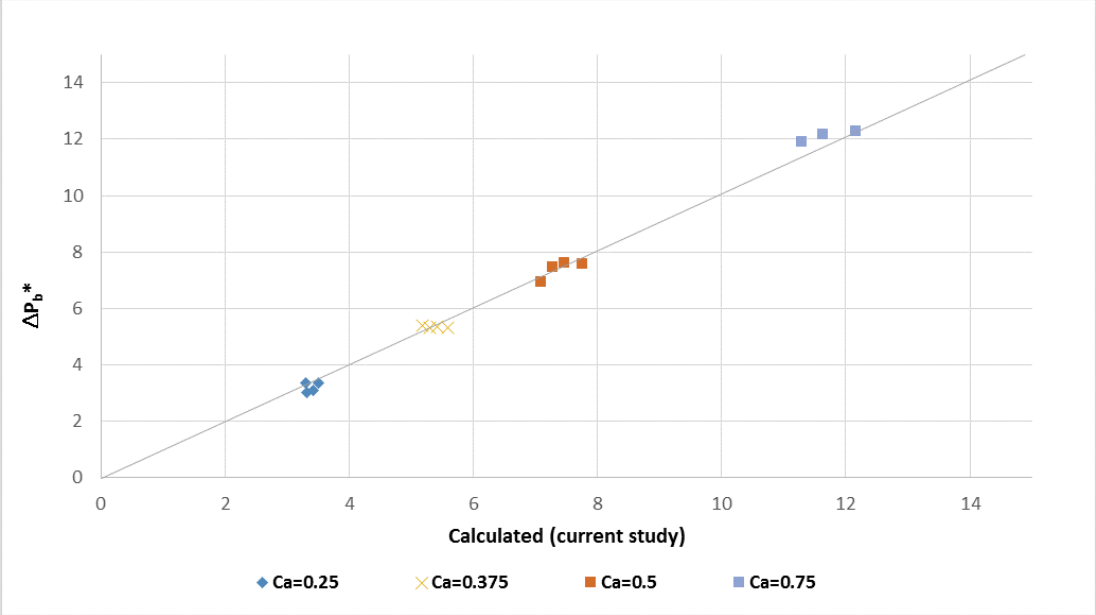

(b)

Figure 5.4: Comparison of calculated bubble pressure drop ΔP_b with that computed in Langewisch & Buongiorno (2015) (*a*) $Ca < 0.187$ and (*b*) $Ca > 0.187$ and different Reynolds number.

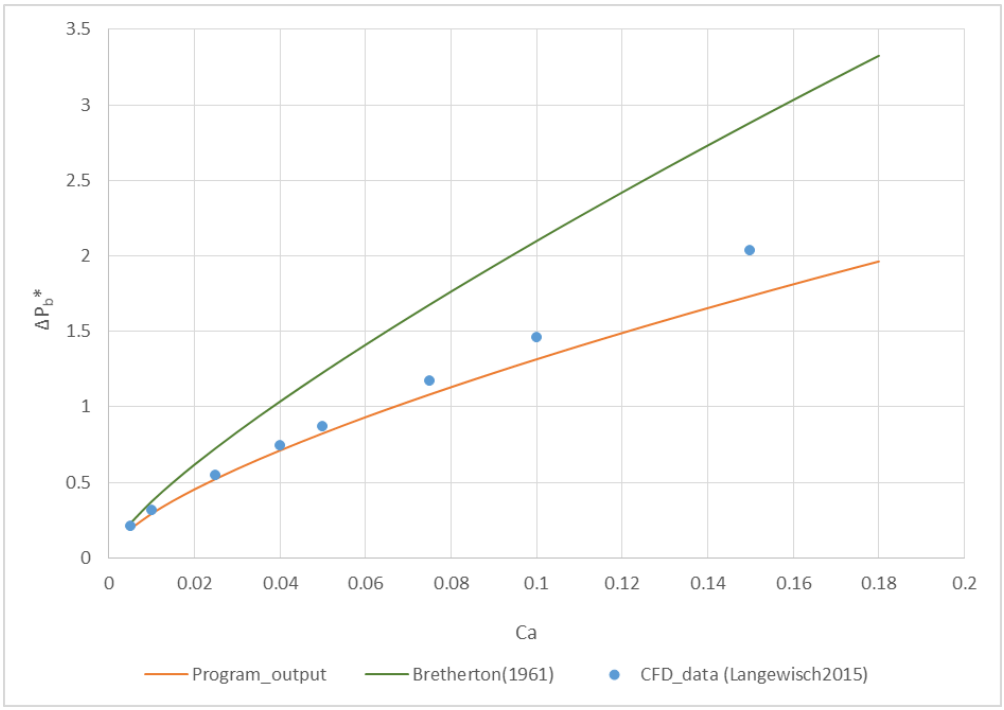

(a)

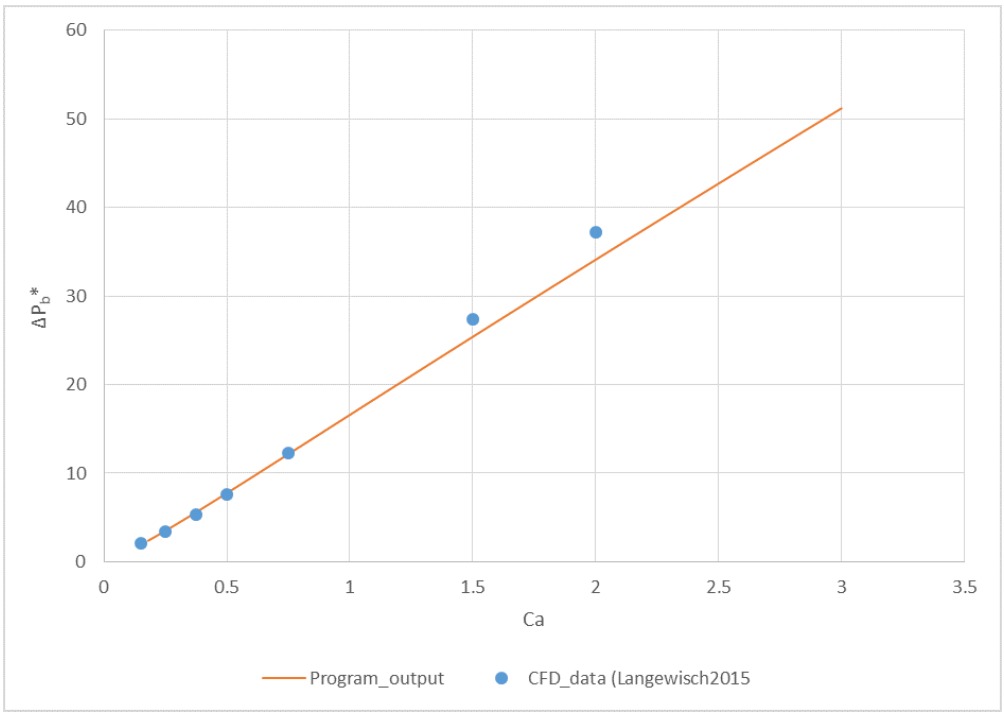

(b)

Figure 5.5: Comparison of calculated bubble pressure drop ΔP_b with that computed in Langewisch & Buongiorno (2015) (*a*) $Ca < 0.187$ and (*b*) $Ca > 0.187$ and predictions using Bretherton's correlation.

follows a linear behaviour for higher values of Ca as shown in Figure 5.5 (b). The results between the CFD data and the calculated data with the current program fall within a mean error less than 1% with respect to the numerical data for all different cases.

5.4.2 Influence of the viscosity and density ratios in capillary slug flow

Subsequently, this study was extended to investigate the case of low viscosity ratio and its influence on the bubble velocity, film thickness and pressure drop. A set of different pairs of fluids was considered over a wide range of Capillary number, Reynolds number and slug lengths. The fluid properties and flow conditions were extracted from the experimental work by Eain *et al.* (2013, 2015).

The effect of the viscosity ratio on the film thickness and Capillary number was investigated using the correlation proposed by Han & Shikazono (2009) (Eq. 3.33). The predictions for each two-phase flow are illustrated in Figure 5.6 (a). As can be seen, the dimensionless film thickness increases non-linearly with increasing the Capillary number. A difference between the results with various viscosity ratios is difficult to be identified when the Capillary number is higher than $Ca > 0.02$, however for low Capillary numbers $Ca < 0.02$, and low viscosity ratios this becomes more prominent and is shown in Figure 5.6 (b). The figure contains experimental measurements of the film thickness for liquid-liquid slug flow extracted from Eain *et al.* (2013) and also plots of literature correlations by Han & Shikazono (2009) (Eq. 3.33) and Eain *et al.* (2013) (Eq. 3.37). The experimental data shows reasonable agreement with Eain *et al.* (2013) as expected. However, the model by Han & Shikazono (2009) underestimates the magnitude of the film measurements and the influence of the viscosity ratio is not appreciable. The reason for this can be attributed to the fact that the correlation by Han & Shikazono (2009) was proposed mainly for gas-liquid flows. In these systems, the shear forces between the phases can be ignored since the gas viscosity is very low and can be assumed negligible. For the case of liquid-liquid flows, the reduced viscosity difference can increase significantly the interfacial shear forces and the velocity of the film will become appreciable. The correlation proposed by Eain

et al. (2013) included in Figure 5.6 reveals an evident influence of the fluid properties in the film as well as a high dependence on the Capillary number. For instance, as the viscosity ratio approaches unity or less, the film thickness tends to be larger as observed for the Pd5-water system. The results confirm that the model proposed by Eain *et al.* (2013) will allow an accurate estimation of the film thickness for various liquid-liquid systems.

Additionally, the relationship between the Reynolds number of the dispersed phase (Re_b) and the two-phase Reynolds number (Re_m) is shown in Figure 5.7 for different two-phase flow properties. In every case, the results show that the bubble velocity is higher than the two-phase velocity and that the relative velocity greatly depend on the viscosity ratio and fluid properties. For instance, the case of an EG-air system involves a very viscous continuous phase that prevents the air bubble from moving faster in comparison to a water-air system. This behaviour is clearly illustrated in Figure 5.7. Also, it can be observed that for a high viscosity ratio; eg. EG-air and AR20-water, a similarity exists regardless of the nature of the two-phase system, but as the viscosity approaches to unity $\left(\frac{\mu_c}{\mu_d}\right) \rightarrow 1$, the behavior is independent for each pair of fluids, e.g. FC40-water system. These results are consistent with those reported by Eain *et al.* (2015) who identified a viscosity ratio threshold of 4.5 $\left(\frac{\mu_c}{\mu_d} = 4.5\right)$. Over this limit, the flow behaviour was accurately modelled using correlations derived from gas-liquid systems. Likewise, the results obtained in this study showed a great influence of the viscosity ratio on the film thickness and bubble velocity in liquid-liquid systems which confirms the significance of this parameter to obtain a reliable prediction of this type of systems.

5.4.3 Comparison with independent CFD and experimental data in a liquid-liquid slug flow

Film thickness predictions

The correlation by Eain *et al.* (2013) was used to compare the experimental data and numerical predictions of the film thickness and droplet velocity from a liquid-liquid study by Dai *et al.* (2015). The two-phase flow consisted of dispersed water droplets in a continuous Hexadecane phase which fluid properties are described

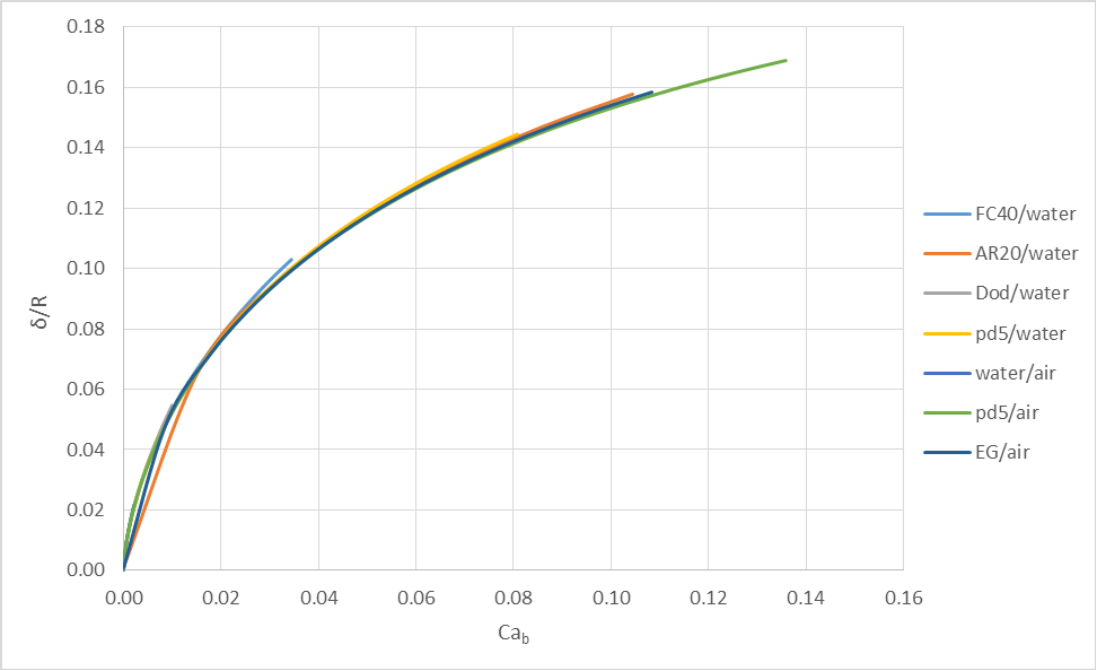

(a)

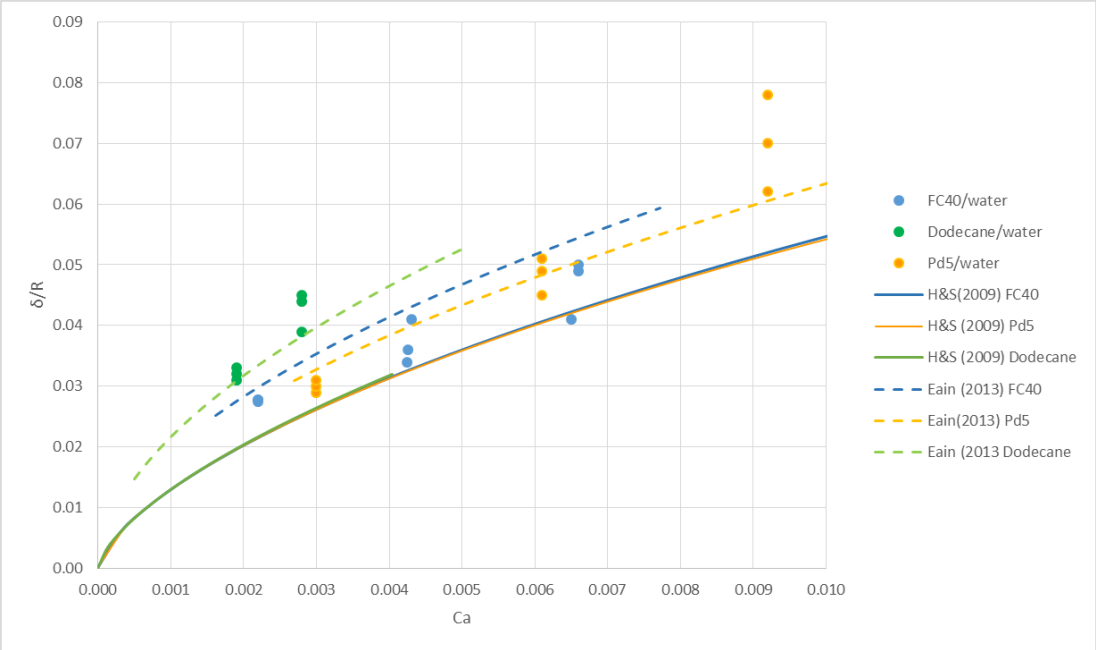

(b)

Figure 5.6: Film thickness predictions for liquid-liquid systems using the models by Eain *et al.* (2013); Han & Shikazono (2009) and compared to experimental data and model from Eain *et al.* (2013)

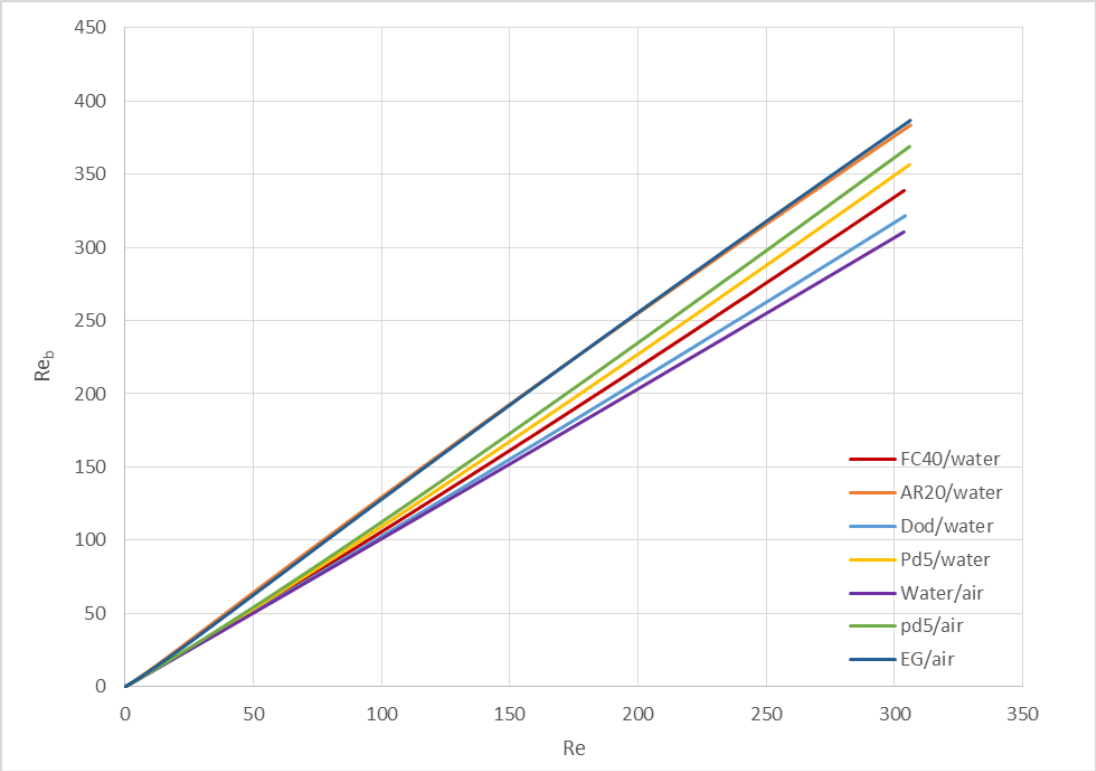

Figure 5.7: Flow diagram for different two-phase flow properties, where $Re_b = \frac{\rho_c U_b D}{\mu c}$ and $Re_m = \frac{\rho_c U_m D}{\mu c}$

.

in Table 5.3. The CFD predictions of film thickness are plotted in Figure 5.8 along with the models by Aussillous & Quere (2000); Eain *et al.* (2013); Han & Shikazono (2009). Also, liquid-liquid experimental data from Eain *et al.* (2013) are included in the graph for comparison. The correlations proposed by Han & Shikazono (2009) and Aussillous & Quere (2000) result in similar predictions of film thickness and fair agreement with the numerical data, whereas the model by Eain *et al.* (2013) over predicts the numerical values. These results indicate some uncertainty with regards to the accuracy of the CFD predictions, which was also revealed in Dai *et al.* (2015) where some cases the experimental data was up to 45% lower than the predicted data. The author stated that such discrepancies could mainly arise from errors in the measurements of the droplet velocity and which values are fed into the simulations to give a film thickness that differs

from that corresponding in the experiments. This observation highlights the importance of the values for the droplet velocity and mixture velocity as they are critical input parameters to achieve accurate numerical predictions. Also, another reason for the discrepancies between the numerical and experimental data might be due to the film thickness correlation used in the CFD study which corresponds to the one proposed by Aussillous & Quere (2000) and which was derived for gas-liquid systems. Therefore, based on the current results in Figure 5.8, the film thickness predictions obtained with the model by Eain *et al.* (2013) may offer a better description of the film behaviour for the Hexadecane-water system. Additionally, as a way to compare with other similar liquid-liquid systems, the experimental data of Dodecane-water and Pd5-water are also included in Figure 5.8 with the corresponding model predictions using Eain *et al.* (2013). It is clearly seen that the film thickness greatly depends on the viscosity ratio of the two-phase system and therefore the prediction of this parameter is necessary for an accurate modelling of liquid-liquid slug flows in capillaries.

Bubble velocity predictions

Moreover, estimations of the bubble velocity for specific liquid-liquid systems were developed using different bubble velocity correlations from the literature. The results were compared to experimental and CFD data reported by Li & Angeli (2017) and Dai *et al.* (2015). The results are shown in Figure 5.9 and correspond to an ionic-liquid and hexadecane-water systems in a capillary diameter of 0.5 mm and 2 mm, respectively.

The predictions of the bubble velocity were determined using the film thickness correlation proposed by Eain *et al.* (2013) and using different bubble velocity correlations for comparison. Overall, the results indicate that the bubble velocity is always higher than the mixture velocity and it is mainly due to the presence of the film surrounding the bubble. The prediction of the bubble velocity corresponding to the ionic-liquid two-phase flow properties using three different models is depicted in Figure 5.9. Discrepancies with the experimental data using the correlation proposed by Langewisch & Buongiorno (2015) can be observed and it is mainly because such correlation was derived for gas-liquid systems, however, the

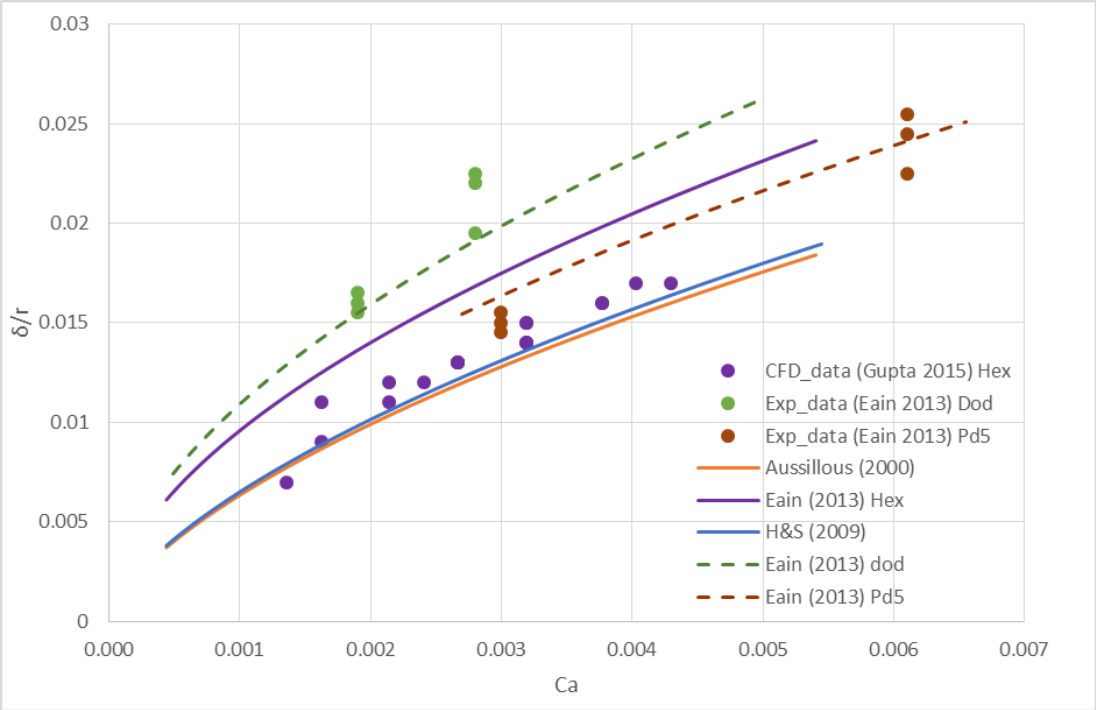

Figure 5.8: Film thickness for liquid-liquid systems compared to numerical data from Dai *et al.* (2015), models by Aussillous & Quere (2000); Han & Shikazono (2009) and experimental data from Eain *et al.* (2013).

predictions with this model seem to be closer to the CFD results obtained in Li & Angeli (2017) for low bubble velocity values. On the other hand, the correlation by Kashid *et al.* (2005) developed for liquid-liquid slug flow under predicts the experimental data from Li & Angeli (2017). This model includes the influence of the film thickness, but not the effect of the Capillary number, which may be the reason for the differences with the experimental data. Nevertheless, the correlation proposed by Howard & Walsh (2013) agrees well with the experimental data from both studies Li & Angeli (2017) and Dai *et al.* (2015). This correlation was derived for liquid-liquid slug flows where the effects of the viscosity ratio and film thickness are combined and determines the influence of the velocity in the film relative to the bubble velocity. Therefore, more accurate predictions of the bubble velocity can be obtained with this correlation for different two-phase systems.

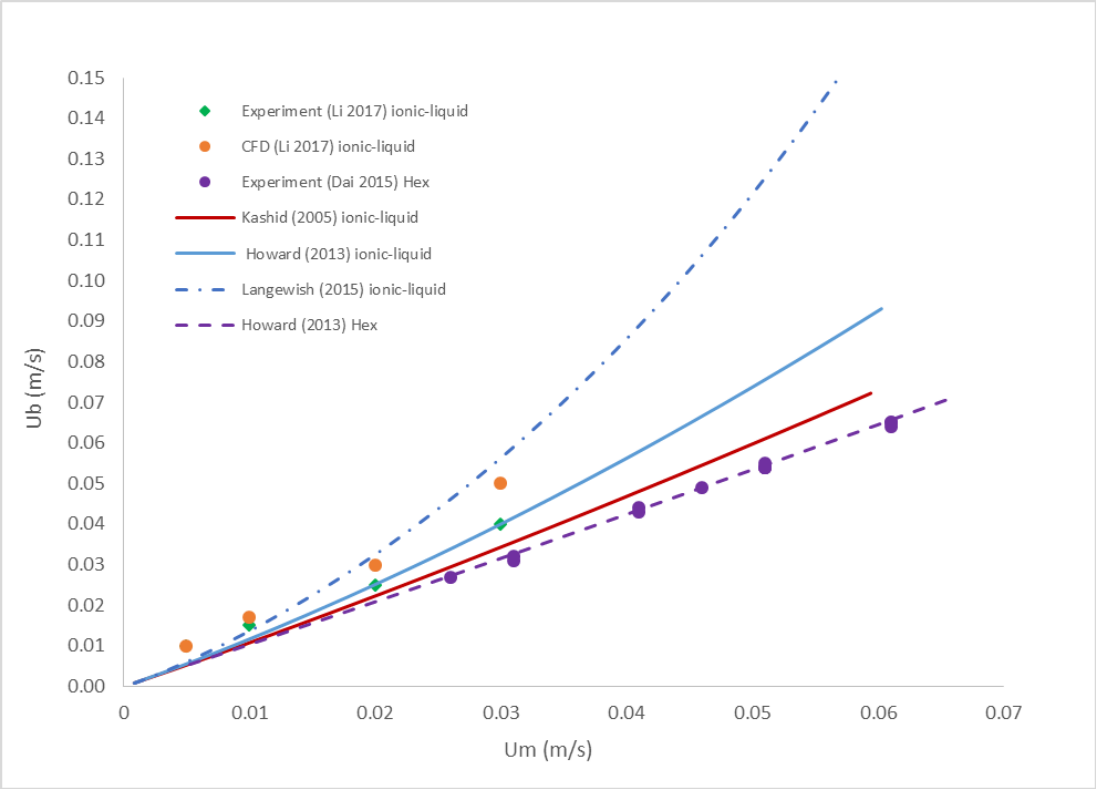

Figure 5.9: Bubble velocity prediction obtained with current program using the correlations by Howard & Walsh (2013); Kashid *et al.* (2005); Langewisch & Buongiorno (2015) compared to the CFD data from Li & Angeli (2017) and experimental data from Dai *et al.* (2015); Li & Angeli (2017).

5.4.4 Study of the pressure drop for different two-phase flows in a capillary

Finally, predictions of the non-dimensional total pressure drop (fRe) were achieved within a range of viscosity ratios and slug lengths. As a first approach, the total pressure drop across the capillary was calculated using a FC40-water system. The predictions for the total pressure drop were in good agreement with the experimental data with a slug length of $L_s = 1.09$. The results are shown in Figure 5.10 for different total flow rates. The graph contains experimentally measured data points by Eain *et al.* (2015) and estimations using the models by Eain *et al.* (2015); Kreutzer *et al.* (2005); Warnier *et al.* (2010) described in Equations 3.44,

3.45 and 3.46, respectively. The predictions from the models by Warnier *et al.* (2010) and Eain *et al.* (2015) are closer to the experimental measurements than Kreutzer *et al.* (2005) model, which appears to be less accurate for such two-phase system, specially with higher volume flow rates.

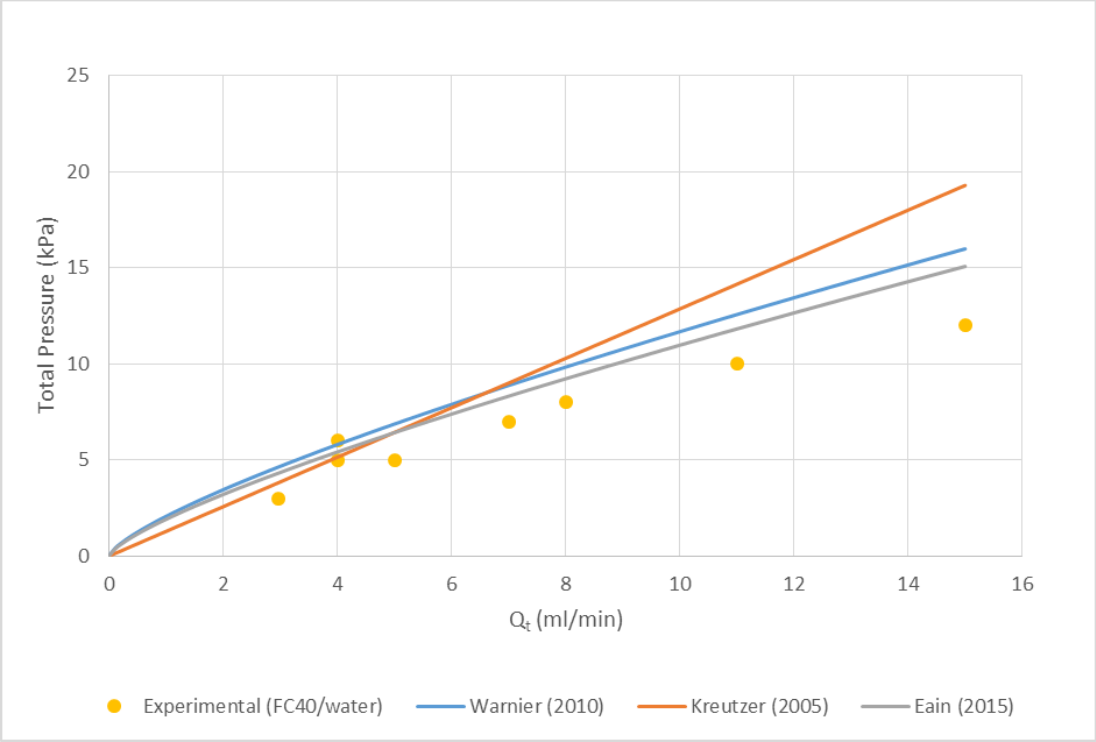

Figure 5.10: Total pressure drop predictions with different flow rates for a FC40/water system using the correlations by Eain *et al.* (2015); Kreutzer *et al.* (2005); Warnier *et al.* (2010) and the experimental data from Eain *et al.* (2015).

Moreover, the predictions of the non-dimensional total pressure drop (fRe) were developed using the flow conditions described in Table 5.6 and the pressure drop correlation by Eain *et al.* (2015). The results for fRe are illustrated in Figure 5.11 with respect to the scale parameter $L_s^* \left(\frac{Ca}{Re}\right)^{0.33}$ proposed by Walsh *et al.* (2009). This parameter indicates the limits of the slug length contribution to the overall pressure drop. For instance, a value over 0.1 refers to a negligible effect of the slug length, so the pressure drop in the flow can be described by Poiseuille flow. This condition can be observed in Figure 5.11 (a) which shows

data points in this region approaching an asymptotic curve where $fRe = 16$, indicating fully developed flow.

On the other hand, values lower than 0.1 imply a great influence of the slug length on the total pressure drop and the presence of a slug flow is expected under this limits, which means that the interfacial pressure drop will contribute significantly to the total pressure drop. This feature can be observed in Figure 5.11 (b) contains data points falling in the region for small slug lengths. The results show higher values of fRe in the region when the scale parameter is less than 0.1 and then the contribution decreases smoothly for longer slug lengths. Overall, the results in Figure 5.11 follow a similar trend of those reported in Eain *et al.* (2015); Walsh *et al.* (2009) as expected, however, it was not possible to achieve an exact comparison with the experimental data. The reason for this is the lack of explicit data information which made difficult to identify the exact slug and bubble length for each pressure drop prediction.

Despite of this, it was possible to investigate the effect of the viscosity ratio on the bubble velocity and pressure drop assuming a constant slug and bubble length. Figure 5.12 describes the non-dimensional total pressure drop (fRe_t) as function of the bubble Reynolds number Re_b for different two-phase flow systems using the pressure drop correlation from Eain *et al.* (2015). It can be observed that the pressure drop along a capillary is greatly influenced by the two-phase system used. In general, the frictional pressure drop decreases as the inertial forces increase and tends to a constant behaviour for all different cases. Also, the pressure drop is relatively low for high viscosity ratios in comparison with a two-phase flows with similar viscosity. The behaviour of these parameters will vary according to the inlet configuration used to generate the slug flow as it is directly related to the slug and bubble lengths which in turn have a significant influence in the overall pressure drop along the capillary.

Besides the geometric characteristics of the slug flow, the prediction of the pressure drop along the capillary is important for the design of pumps, energy loss and for the choice of flow rates which will affect the operation of a specific process. Therefore, it is important to quantitatively analyse pressure drop in two-phase flow systems. Although, various methods have been developed to determine pressure drop slug flows, none have been able to predict over a full range of

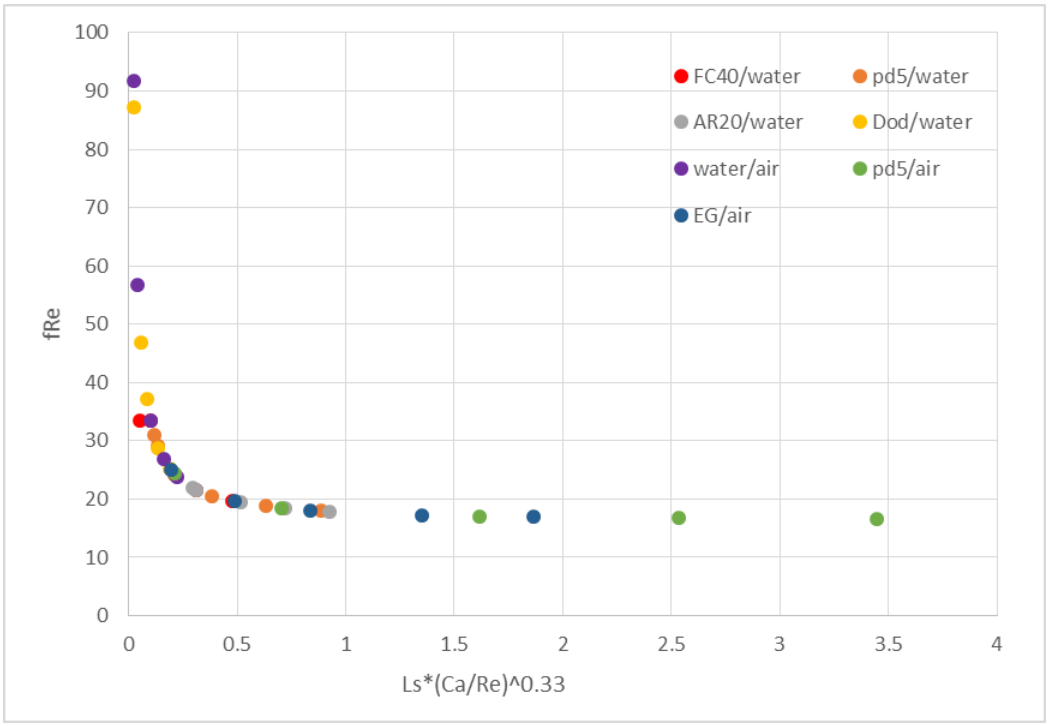

(a)

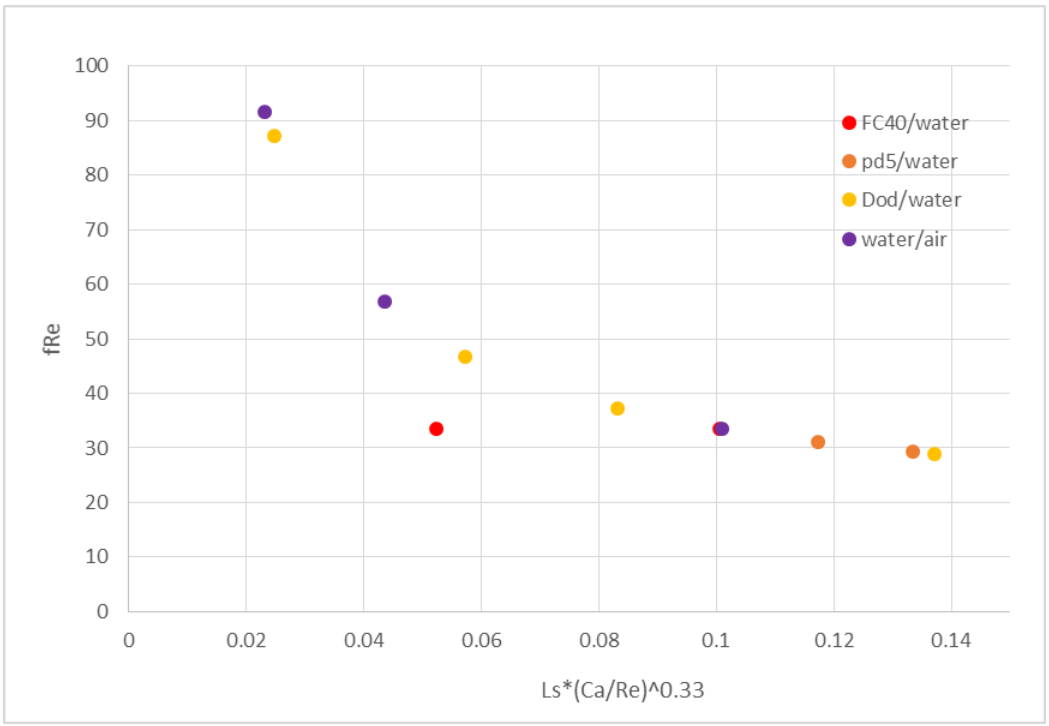

(b)

Figure 5.11: Predictions of non-dimensional pressure drop as a function of dimensionless slug length, Reynolds and Capillary numbers using correlation from Eain *et al.* (2015)

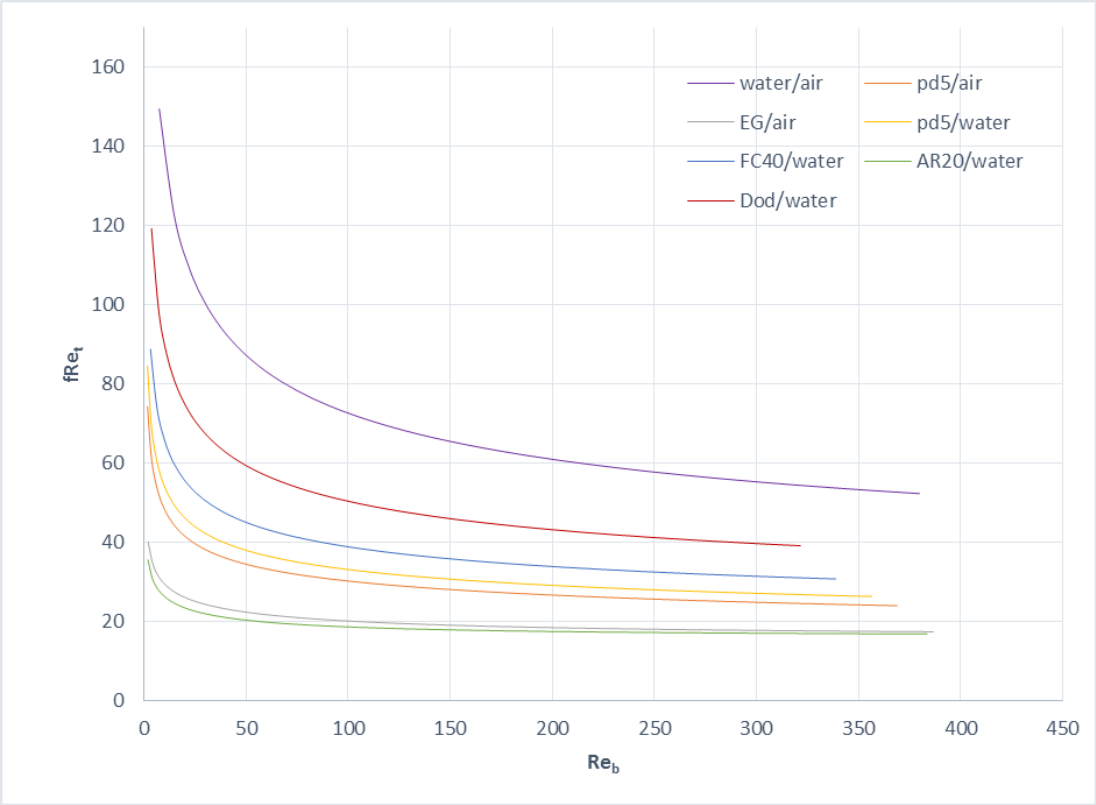

Figure 5.12: Non-dimensional pressure drop as function of the bubble Reynolds number using correlation from Eain *et al.* (2015).

conditions Bandara *et al.* (2015). The current program can be useful to predict the operating ranges of the slug flow regime in a capillary for a given pair of liquids with known density, viscosity and surface tension. This tool can predict non-dimensional film thickness and droplet velocity as function of the non-dimensional inlet flow rates. Also, it can be helpful to explore the most optimum slug flow correlation for a particular two-phase system and to identify if the viscosity ratio will have an influence or not on the flow parameters under study.

5.5 Conclusions

An extensive study of the main slug flow parameters has been presented in this chapter. The approach has been pursued based on the implementation of recent

empirical correlations and considering experimental and numerical data found in the literature. The validation of the current model against the CFD database from Langewisch & Buongiorno (2015) which corresponds to a specific density ratio and viscosity ratio, showed that the model is as good as the database for those ratios and can be applied with some degree of confidence to cases with other density and viscosity ratios. Therefore, predictions of the film thickness, bubble velocity and pressure drop were achieved based on the fluid properties and inlet flow conditions. The study was extended to evaluate the effect of low viscosity ratio on the main slug flow parameters. The study provides significant independent validation of the model proposed by Eain *et al.* (2015) while comparing it to experimental and CFD data for gas-liquid and liquid-liquid systems from the literature. The results demonstrated that accurate predictions of the film thickness for several liquid-liquid slug flows can be achieved with the correlation proposed by Eain *et al.* (2013). As this parameter is related to the bubble velocity, it was possible to predict both, the film thickness and bubble velocity from initial flow conditions and fluid properties. The influence of the viscosity ratio on the bubble velocity was investigated using correlations from the literature. It was found that the model proposed by Abiev (2008) and also implemented by Dai *et al.* (2015) offers accurate predictions of the bubble velocity for different two-phase flow systems. Efforts to predict the pressure drop of liquid-liquid slug flow through a capillary were carried out using the correlation proposed by Eain *et al.* (2015). A direct comparison to experimental data was difficult to obtained because the precise length of the bubble and slug for each operating condition was not specified in the experimental work, however a broad understanding of the frictional pressure drop for various two-phase flow systems was achieved and a similar behaviour to that obtain by Eain *et al.* (2015) regarding the pressure drop over a range of slug lengths was observed in the current study. The results have shown the applicability and efficiency of the current computational process to predict important parameters of two-phase slug flow through capillaries, thus being useful as a design tool for applications involving micro-capillaries technologies. Also, the algorithm can be helpful for predicting initial conditions or input parameters for the development of CFD models, in this case applied to liquid-liquid flows in porous media.

Chapter 6

CFD modelling of liquid-liquid flow in packed bed reactors

6.1 Introduction

Problems involving the flow of two or more fluid phases (liquid or gas) in porous media are widespread in science and engineering. These systems are usually found in several applications, namely biofuel processes, which are limited at industrial scale due to the complex hydrodynamics involved. This in turn makes experimental studies very difficult for characterising such systems, which leaves a wide window for implementing computational fluid dynamics modelling approaches.

The prediction of the flow patterns and mass transfer mechanisms, especially in liquid-liquid flows through a porous media represents a challenge for both experimental and numerical studies. Traditional numerical approaches to these sort of problems ignore important effects such as the fluid-fluid interactions which are usually absorbed into the empiricism of solid-fluid interaction models. The development of a model able to predict accurately the hydrodynamics of a two-phase liquid-liquid flow through a porous media, specially when inertial effects are important, is necessary for an adequate design of such complex systems.

The current work approaches this complex problem by relating the flow of two immiscible liquids through a porous media with a two-phase flow in a capillary under the slug flow regime conditions. The study of liquid-liquid slug flow in

capillaries will provide insight into the effectiveness of packed bed reactors which are commonly found in the chemical industry for mixing purposes.

Moreover, the following chapter intends to extend the work by Figueroa (2013) who developed a CFD modelling approach to predict the two-phase liquid-liquid flow in a packed bed reactor. Further improvement of such CFD model is proposed by implementing the correlations corresponding to liquid-liquid slug flow through a capillary and generalise those derived for two-phase flows in porous systems.

6.2 Liquid-liquid pressure drop model development

For estimations of the pressure drop in two-phase flow in randomly packed bed reactors, an homogeneous model approach is most frequently used. This model estimates the pressure drop of a two-phase system, neglecting surface tension effects which are usually absent in a single phase pressure drop model. Therefore inaccurate predictions of the pressure drop when dealing with two-phase flows are usually achieved Kreutzer *et al.* (2005). This feature was one of the main motivations of the present work and a first approach is proposed in the following section.

Gas-liquid trickle flow model Attou & Ferschneider (1999)

A typical diagram describing a co-current gas-liquid downward flow through the interstitial void space of the packed bed is shown in Figure 6.1.

The mass balance equation of each fluid can be written in the form:

$$\int_{A_s} X_i \rho_i u_i n dS + \int_{A_1} X_i \rho_i u_i n dS + \int_{A_2} X_i \rho_i u_i n dS + \int_{S_i} \rho(u_i - u_{int}) n dS = 0 \quad (6.1)$$

where: A_s is the solid particle wall area, A_1, A_2 represent the inlet and outlet cross sections, S is the surface defined by $S = A_1 \cup A_s \cup A_2$, X_i is the characteristic presence function of the $i-$phase (0 or 1), u_i is the velocity of the phase, u_{int} is the interface velocity, ρ is the density and n is the unit vector normal to the gas-liquid interface S_i.

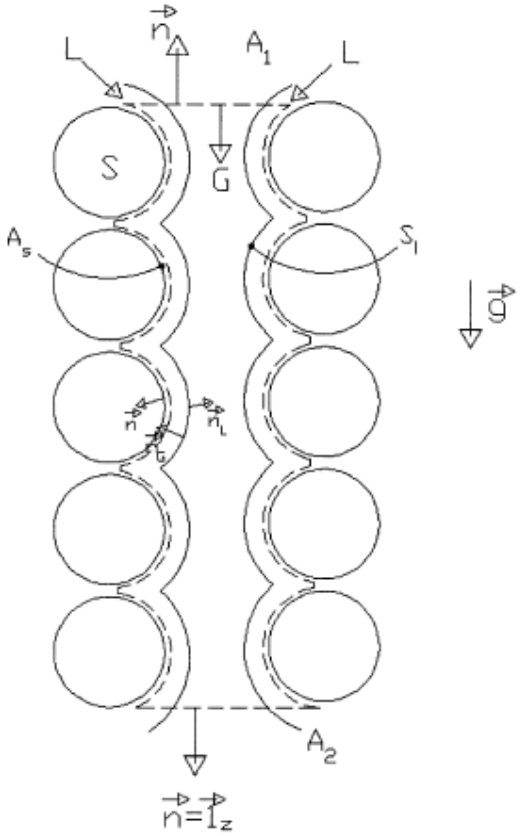

Figure 6.1: Schematic representation of the co-current gas-liquid downward flow through the interstitial void space of the packed bed Attou & Ferschneider (1999)

.

Considering non-porous solid particles and no mass transfer between the fluids, the first and last terms in Equation 6.1 are zero, reducing to:

$$\int_{A_1} X_i \rho_i u_i 1_z dS - \int_{A_2} X_i \rho_i u_i 1_z dS = 0 \tag{6.2}$$

where 1_z is the unit vector in the axial direction z.

Dividing each member in Equation 6.2 by the volume $V = Adz$, where A is the effective cross-sectional area of the void space and dz is the distance between A_1 and A_2, the following mass balance equations are obtained for each phase:

$$\frac{d}{dz}(\alpha \rho_1 u_1) = 0 \tag{6.3}$$

$$\frac{d}{dz}((1-\alpha)\rho_2 u_2) = 0 \tag{6.4}$$

Where the axial velocity of the $i-$phase averaged over the cross-sectional area A_i and the fraction of the effective cross-sectional area occupied by the phase $\alpha_i = \frac{A_1}{A}$ is defined by:

$$u_i = \frac{1}{A_i}\int_{A_i} X_i u_i 1_z dS \tag{6.5}$$

Moreover, each flowing fluid is submitted simultaneously to actions of total stress, inertia and gravity forces. The resultant of the total stress forces involves a contribution due to the shear stress exerted at the surface of the solid particles and another one due to the interaction between the fluid phases. So, the linear momentum balance of each phase can be written in the form:

$$\begin{aligned} &\oint_S (X_i(\rho_i u_i(u_i n) - T_i n)ds + \int_{S_i}(\rho_i u_i(u_i - u_{int})n_i - T_i n_i - \tau_{int} n_i)ds - \\ &\int_{S_i} X_i \tau_i n ds = \int_V X_i \rho_i g dV \end{aligned} \tag{6.6}$$

where τ_{int} is the interfacial shear stress at the gas-liquid (S_i) and liquid-solid A_s interfaces and g is the gravitational acceleration. T_i denotes the total stress tensor of the $i-$phase and can be decomposed into the scalar tensor proportional to the pressure p_i and the viscous stress tensor τ_i as follows:

$$T_i = -p_i + \tau_i \tag{6.7}$$

Since there is no mass transfer between the phases, the condition $\rho_i(u_i - u_{int}) = 0$ is satisfied at the fluid-fluid interface (S_i) in Equation 6.6. Substituting 6.7 in Equation 6.6 along the axial direction z gives:

$$\begin{aligned} &\int_{A_2} X_i(\rho_i(u_i 1_z)^2 + p_i)dS - \int_{A_1} X_i(\rho_i(u_i 1_z)^2 + p_i)ds + \\ &\int_{A_1} X_i \tau_{i_{zz}} dS - \int_{A_2} X_i \tau_{i_{zz}} dS - \int_{A_s} X_i \tau_{i_{nz}} dS - \int_{S_i} \tau_{i_{nz}} dS - \\ &\int_{A_s} X_i \tau_i (n_i 1_z) dS - \int_{S_i} \tau_{i_{nz}}(n_i 1_z) dS + \int_{A_s} X_i p_i (n_i 1_z) dS = \int_V X_i \rho_i g dV \end{aligned} \tag{6.8}$$

where $\tau_{i_{zz}} = 2\mu_i du_i/dz$ is the longitudinal component of the viscous stress tensor and the resultant forces are several orders of magnitude smaller than the pressure forces exerted at the cross-sectional areas A_1 and A_2 Attou & Ferschneider (1999). Hence, these terms can be neglected and Equation 6.8 reduces to:

$$\int_{A_2} X_i(\rho_i(u_i 1_z)^2 + p_i)dS - \int_{A_1} X_i(\rho_i(u_i 1_z)^2 + p_i)dS - \int_{A_s} X_i \tau_{i_{nz}} dS - \int_{S_i} \tau_{i_{nz}} dS - \int_{A_s} X_i \tau_i(n_i 1_z)dS - \int_{S_i} \tau_i(n_i 1_z)dS + \int_{A_s} X_i p_i(n_i 1_z)dS = \int_V X_i \rho_i g dV \tag{6.9}$$

Additionally, in a trickle flow packed bed reactor, the liquid fraction α_i does not change significantly with z for a steady state flow and the capillary pressure gradient dp_c/dz can be neglected with regard to the fluid pressure gradient dp_i/dz. This assumption is acceptable for the modelling of the steady state macroscopic average hydrodynamic bed behaviour since only a small fraction of the reactor volume is submitted to the capillary effects Attou & Ferschneider (1999). Thus, the last term of the LHS in Equation 6.9 can be written as:

$$-\int_{A_s} X_i p_i(n_i 1_z)\frac{dS}{Adz} = p_i \frac{1}{A}\frac{dA_i}{dz} = p_i \frac{\alpha_i}{dz} \tag{6.10}$$

The axial momentum balance equations for the two phases (Fluid 1 and Fluid 2) result from the division of each member of Equation 6.9 by the volume $V = Adz$ of the void space and can be written respectively as follows:

$$\alpha \frac{dp}{dz} = -\phi_1 \frac{d}{dz}(\alpha \rho_1 u_1^2) + \alpha \rho_1 g + F_1 \tag{6.11}$$

$$(1-\alpha)\frac{dp}{dz} = -\phi_2 \frac{d}{dz}((1-\alpha)\rho_2 u_1^2) + (1-\alpha)\rho_2 g + F_2 \tag{6.12}$$

where α is the volume fraction of the dispersed phase and ϕ is the shape factor which characterises the liquid film velocity and usually takes the value of 4/3 for a laminar liquid film Attou & Ferschneider (1999).

The total drag force, F_i in Equations 6.11 and 6.14 determine the fluid-solid and fluid-fluid interactions along the packed bed. For the case of Fluid 1 (dispersed phase), the total drag force F_1 is the contribution of two forces: (a) the

drag force due to the relative motion between the fluids and is opposed to the slip motion, f_{int}, and (b) the force due to the material interface, also interpreted as the fraction of the fluid momentum transferred to the solid across the liquid film and is opposed to the fluid motion, f_{s1} Attou & Ferschneider (1999). Thus, Equation 6.11 can be written as:

$$\alpha\frac{dP}{dz} = -\phi_1(\alpha\rho_1 u_1^2) + \alpha\rho_1 g - (f_{int} + f_{s1}) \tag{6.13}$$

Similarly, the continuous phase (Fluid2) can be described as follows:

$$(1-\alpha)\frac{dp}{dz} = -\phi_2\frac{d}{dz}((1-\alpha)\rho_2 u_1^2) + (1-\alpha)\rho_2 g - (f_{int} + f_{s2}) \tag{6.14}$$

The total drag force F_2 is also constituted by two forces: (a) the drag force due to the shear stress between the fluid and the solid particles, f_{s2}, which is opposite to the fluid motion and (b) the drag force between the fluids, f_{int}.

The model developed by Attou & Ferschneider (1999) for a gas-liquid trickle flow uses the theoretical formulation of Kozeny-Carman's equation on each component of the interaction terms f_{int}, f_{s1} and f_{s2} taking into consideration the physical properties and the superficial velocity of each phase. They found that the interaction terms are proportional to the drag force expression proposed by Kozeny-Carman's equation as it involve a viscous and inertial contribution as follows:

$$f = A\mu_i\tilde{u}_i + B\rho_i\tilde{u}_i^2 \tag{6.15}$$

where f is the fluid-solid drag force per unit volume of void space in the packed bed and $\tilde{u}$ is the superficial velocity of the fluid based on the total cross-sectional area of the reactor. The trickle flow model proposed by Attou & Ferschneider (1999) takes the form:

$$\frac{1}{p}\frac{dp}{dz} + \frac{1}{\alpha}\frac{d\alpha}{dz} + \frac{1}{u_1}\frac{du_1}{dz} = 0 \tag{6.16}$$

$$\frac{1}{1-\alpha}\frac{d(1-\alpha)}{dz} + \frac{1}{u_2}\frac{du_2}{dz} = 0 \tag{6.17}$$

$$\alpha\frac{dp}{dz} = -\frac{\phi_1}{RT}\alpha p u_1\frac{du_1}{dz} - \alpha(A_1\mu_1(\tilde{u}_r + \tilde{u}_1) + B_1\rho_1(\tilde{u}_r^2 + \tilde{u}_2^2)) + \alpha\rho_1 g \tag{6.18}$$

$$(1-\alpha)\frac{dp}{dz} = -\phi(1-\alpha)u_2\frac{du_2}{dz} + \alpha(A_1\mu_1(\tilde{u}_r+\tilde{u}_1) + B_1\rho_1(\tilde{u}_r^2+\tilde{u}_2^2)) - (A_2\mu_2\tilde{u}_2 + B_2\rho_2\tilde{u}_2^2) + \alpha\rho_1 g \tag{6.19}$$

where the coefficients A_i and B_i are functions of the volume fraction and geometrical characteristics of the packed bed.

The trickle flow model described before corresponds to the case of a gas-liquid flow through a packed bed reactor. Here we propose a similar approach to predict the total pressure drop of a liquid-liquid slug flow through a packed bed. The behaviour can be analogous to that of annular flow by assuming an infinite long droplet described by the analytical solution of Couette-Poisiuelle flow as presented in Chapter 4.

The main difference in the model will be identified in the interaction term f_{int} as the slip motion between the liquid-liquid will be higher and therefore a higher drag force is expected. The study will allow to evaluate the effect of the viscosity ratio of a two-phase flow in porous media over the total pressure drop of the packed bed. The CFD case for a free-slip on the droplet surface should give a similar pressure drop when using Attou & Ferschneider (1999) model.

Now, in order to generalise the Kozeny-Carman theoretical formulation to the overall pressure drop of slug flow model, recall the Hagen-Pouiselle flow equation for pipes:

$$\frac{\Delta P}{L} = f\Big(\frac{1}{2}\rho U^2\Big)\frac{4}{d_c} \tag{6.20}$$

The Kozeny-Carman equation to calculate the flow in a porous media was derived from Equation 6.20, defining a hydraulic radius d_c as:

$$d_c = \frac{AL\epsilon}{AL(1-\epsilon)S_p} = \frac{\epsilon}{(1-\epsilon)S_p} \tag{6.21}$$

where ϵ is the porosity and S_p refers to the particle surface area per volume or interfacial area density. Equation 6.21 defines the ratio of void volume in the media to the particle surface area. Substituting Equation 6.21 in Equation 6.20 assuming fully developed flow in the pipe $f = \frac{16}{Re}$ and including the superficial velocity $\tilde{u}_f = \gamma U_f$ leads to the Kozeny-Carman equation as:

$$\frac{\Delta P}{L} = 16\frac{\mu}{\rho U_f d_c}\Big(\frac{1}{2}\rho U^2\Big)\frac{4}{d_c} \tag{6.22}$$

$$\frac{\Delta P}{L} = 32\frac{\mu}{d_c^2}\frac{\tilde{u}_f}{\epsilon} \tag{6.23}$$

$$\frac{\Delta P}{L} = A\left[\mu\frac{(1-\epsilon)^2 S_p^2}{\epsilon^3}\right]\tilde{u}_f \tag{6.24}$$

where A is the Kozeny constant which relates the tortuous flow channel length to the measured bed depth.

Following a similar approach to derive a pressure drop expression for a slug flow in a porous media, but now considering the friction factor corresponding to the slug flow in a capillary suggested by Eain *et al.* (2015) as:

$$fRe_b = \left(\frac{8.16\left(3^{\frac{2}{3}}\right)}{32}\frac{1}{L_s^*}\frac{A}{A_B}\frac{1}{Ca^{\frac{1}{3}} + 3.34Ca}(1-r_i)^{\frac{1}{3}}\right) \tag{6.25}$$

A similar model to Equation 6.25 with constants modified to take into account a more complex geometry is proposed here and takes the following form:

$$f = \frac{16}{Re}\left[1 + \psi\left(\frac{A_c}{A_b}\right)\left(\frac{d_c}{L_s}\right)\left(\frac{1}{Ca_b^{\frac{1}{3}} + \xi Ca_b}\right)(1-r_\alpha)^{\frac{1}{3}}\right] \tag{6.26}$$

Substituting 6.26 in Hagen-Poisuielle equation 6.20 gives:

$$\frac{\Delta P}{L} = \frac{16}{Re}\left[1 + \psi\left(\frac{A_c}{A_b}\right)\left(\frac{d_c}{L_s}\right)\left(\frac{1}{Ca_b^{\frac{1}{3}} + \xi Ca_b}\right)(1-r_\alpha)^{\frac{1}{3}}\right]\left(\frac{1}{2}\rho U^2\right)\frac{4}{d_c} \tag{6.27}$$

where ψ and ξ are fitting parameters to be based on experiments. Let α and β the dispersed and continuous phase respectively:

$$\frac{\Delta P}{L} = 16\frac{\mu_\beta}{\rho_\beta U_f d_c}\left[1 + \psi\left(\frac{A_c}{A_\alpha}\right)\left(\frac{d_c}{L_s}\right)\left(\frac{1}{Ca_\alpha^{\frac{1}{3}} + \xi Ca_\alpha}\right)(1-r_\alpha)^{\frac{1}{3}}\right]\left(\frac{1}{2}\rho_\beta U_f^2\right)\frac{4}{d_c} \tag{6.28}$$

The cross-sectional ratio $\frac{A_c}{A_\alpha}$ can be expressed in terms of the capillary and bubble diameter $\frac{d_c}{d_\alpha}$ so:

$$\frac{\Delta P}{L} = A\frac{\mu_\beta}{d_c}\left[1 + \psi\left(\frac{d_c}{d_\alpha}\right)\left(\frac{d_c}{L_s}\right)\left(\frac{1}{Ca_\alpha^{\frac{1}{3}} + \xi Ca_\alpha}\right)(1-r_\alpha)^{\frac{1}{3}}\right]U_f \tag{6.29}$$

Substituting the hydraulic diameter defined in Equation 6.21 and superficial velocity:

$$\frac{\Delta P}{L} = A\frac{\mu_\beta(1-\epsilon)^2 S_p^2}{\epsilon^3}\left[1+\psi\left(\frac{1}{d_\alpha}\right)\left(\frac{1}{L_s}\right)\left(\frac{\epsilon^2}{(1-\epsilon)^2 S_p^2}\right)\left(\frac{1}{Ca_\alpha^{\frac{1}{3}}+\xi Ca_\alpha}\right)(1-r_\alpha)^{\frac{1}{3}}\right]\tilde{u}_f \tag{6.30}$$

$$\frac{\Delta P}{L} = \left[A\frac{\mu_\beta(1-\epsilon)^2 S_p^2}{\epsilon^3} + A\psi\frac{\mu_\beta}{\epsilon}\left(\frac{1}{d_\alpha}\right)\left(\frac{1}{L_s}\right)\left(\frac{(1-r_\alpha)^{\frac{1}{3}}}{Ca_\alpha^{\frac{1}{3}}+\xi Ca_\alpha}\right)\right]\tilde{u}_f \tag{6.31}$$

$$\frac{\Delta P}{L} = \left[A\frac{\mu_\beta(1-\epsilon)^2 S_p^2}{\epsilon^3}\right]\tilde{u}_f + \left[A\psi\frac{\mu_\beta}{\epsilon}\left(\frac{1}{d_\alpha}\right)\left(\frac{1}{L_s}\right)\left(\frac{(1-r_\alpha)^{\frac{1}{3}}}{Ca_\alpha^{\frac{1}{3}}+\xi Ca_\alpha}\right)\right]\tilde{u}_f \tag{6.32}$$

Equation 6.32 can be written as follows:

$$\frac{\Delta P}{L} = [C_{kk} + C_{slug}]\tilde{u}_f \tag{6.33}$$

Where:

$$C_{kk} = \left[A\frac{\mu_\beta(1-\epsilon)^2 S_p^2}{\epsilon^3}\right] \tag{6.34}$$

and

$$C_{slug} = \left[A\psi\frac{\mu_\beta}{\epsilon}\left(\frac{1}{d_\alpha}\right)\left(\frac{1}{L_s}\right)\left(\frac{(1-r_\alpha)^{\frac{1}{3}}}{Ca_\alpha^{\frac{1}{3}}+\xi Ca_\alpha}\right)\right] \tag{6.35}$$

C_{kk} represents the term describing a single phase flow through a porous domain and C_{slug} describes the contribution of a second immiscible phase in the medium. Additionally, the ratio between C_{slug} and C_{kk} gives a non-dimensional parameter in function of the Capillary number (Ca), porosity (ϵ) and the volume fraction of the dispersed phase (r_α). This ratio is given by:

$$\frac{C_{slug}}{C_{kk}} = \frac{1}{W}\left(\frac{\epsilon}{1-\epsilon}\right)^2\left(\frac{(r_\beta)^{\frac{1}{3}}}{Ca^{\frac{1}{3}} + \xi Ca}\right) \tag{6.36}$$

Where $W = S_p^2 d_\alpha L_s$ is a non-dimensional shape parameter that depends on the inlet flow conditions and the fluids properties and the precise numerical value of the parameters ψ and ξ will depend on the complexity of the pores, hence these would have to be estimated from comparison with experimental data.

6.3 Results and Discussion

An early stage pressure drop model to predict liquid-liquid slug flow along a packed bed column has been proposed in in this chapter based on the Karman-Cozeny equation and semi-empirical correlation for liquid-liquid slug flow in capillaries. As described earlier in Chapter 2, a two-phase system e.g gas-liquid with similar inlet velocities and a low Capillary number, will flow through the porous media in the form of pulses or slugs. Compared to trickle flow, the prediction of this type of flow behaviour is more complicated and especially if one deals with immiscible liquid-liquid systems. Although, the suggested pressure drop model presented in Equation 6.32 requires calibration of the constants from experimental measurements, the non-dimensional expression in Equation 6.36 can be used to evaluate the influence of important modelling parameters such as the Capillary number, volume fraction and the porosity on the slug flow regime along a packed bed column.

For instance, the effect of the Capillary number and the volume fractions of the continuous phase is shown in Figure 6.2. The Figure plots the behaviour of the last term in Equation 6.36 for Capillary numbers ranging from Ca=0 to Ca=0.2 and different volume fraction of the continuous phase r_c. Overall, the results show a decrease as the Capillary number increases indicating the presence of slugs when surface tension forces are greater (low Capillary numbers) and smooths down as inertial forces overcome. The effect of the volume fraction r_c comes into consideration for values between $0.8 < r_c > 0.1$, where $r_c = 1$ indicates the limit of a continuous flow along the packed bed (no droplets) or very long

slug lengths and $r_c = 0$ the limit where the presence of bubbles/droplets fill the void spaces and are separated by a very short slug length.

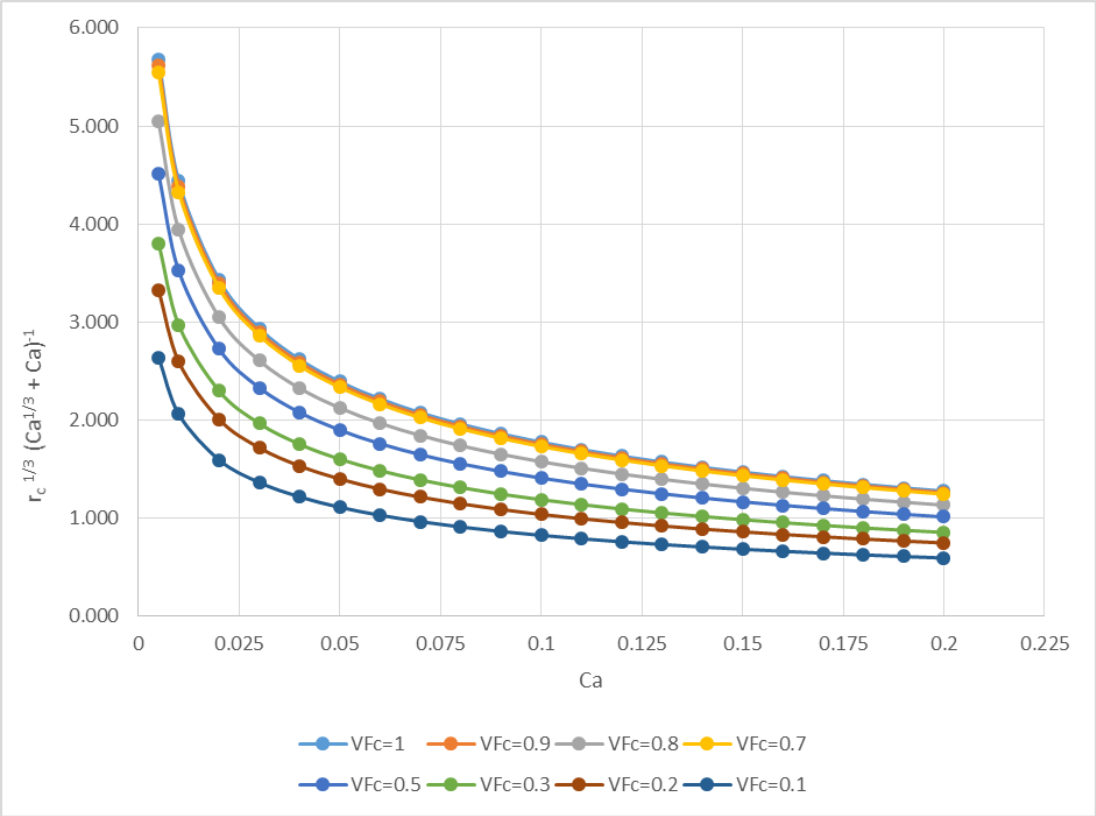

Figure 6.2: Effect of the Capillary number for different volume fractions of the continuous phase.

Moreover, the influence of the Capillary number on the parameter $\frac{C_{slug}}{C_{kk}}$ for different volume fractions of the continuous phase and a porosity of $\epsilon = 0.4$ are shown in Figure 6.3. It can be observed that the ratio $\frac{C_{slug}}{C_{kk}}$ increases with the volume fraction r_c. Also, an evident influence of the Capillary number can be identified suggesting that for large ratios of $\frac{C_{slug}}{C_{kk}} > 1$ the presence of the interfacial forces are dominant and therefore important to be considered in the pressure drop calculations; whereas for smaller ratios $\frac{C_{slug}}{C_{kk}} \leq 1$ it suggests that a very little influence of the presence of the slugs in the domain can be expected and the flow may be treated as single phase flow for the case of a two-phase system with low viscous ratios $\left(\frac{\mu_d}{\mu_c} \rightarrow 0\right)$. For large viscosity ratios, additional

parameters must be considered in the model to represent the flow behaviour along the packed bed more accurately such as the relative permeability concept and capillary pressure effects.

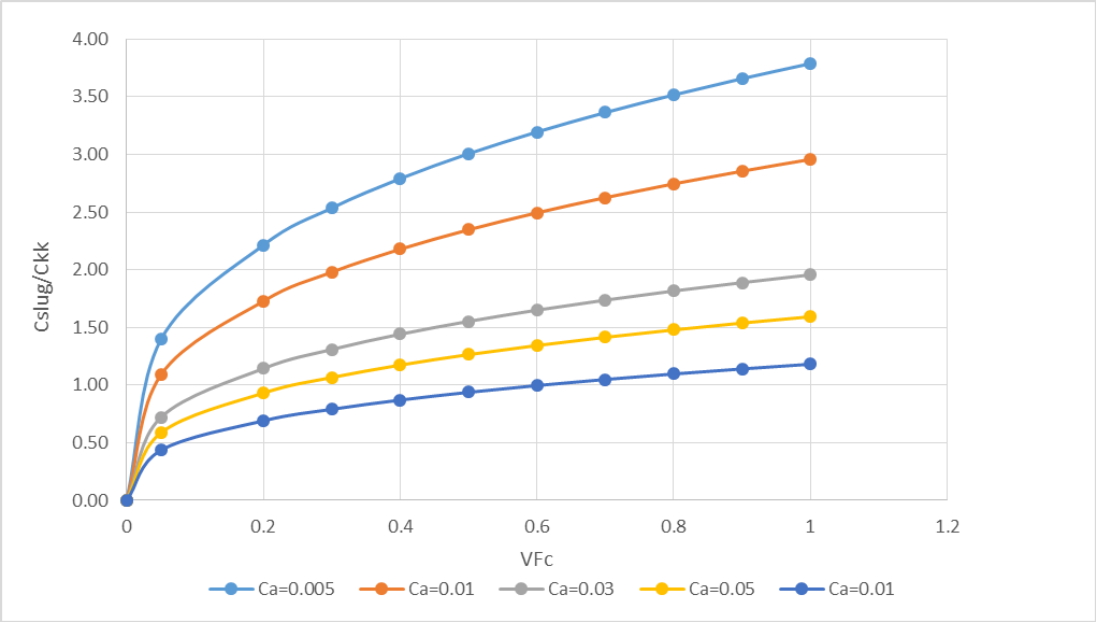

Figure 6.3: Effect of the Capillary number on the parameter $\frac{C_{slug}}{C_{kk}}$ for different volume fractions of the continuous phase and porosity $\epsilon = 0.4$

.

Furthermore, Figure 6.4 describes the effect of the porosity on the parameter $\frac{C_{slug}}{C_{kk}}$ for different volume fractions and a Capillary number of Ca=0.05. The graph reveals that a high impact on the overall pressure drop may be expected when the bed porosity is between $1 < \epsilon < 0.7$ and will be higher for low Capillary numbers. An optimum bed size porosity will be required to avoid blockage of the two-phase flow under study and to prevent bubble breakage. Detail values of $\frac{C_{slug}}{C_{kk}}$ for different porosity and Capillary numbers are available in Tables 6.1 and for further parametric studies.

Table 6.1: Calculated values of $\frac{C_{slug}}{C_{kk}}$ for different volume fractions and Capillary numbers.

Ca=0.005								
$\epsilon = 0.1$	$\epsilon = 0.2$	$\epsilon = 0.3$	$\epsilon = 0.4$	$\epsilon = 0.5$	$\epsilon = 0.6$	$\epsilon = 0.7$	$\epsilon = 0.8$	$\epsilon = 0.9$
0.63	1.42	2.44	3.79	5.68	8.52	13.26	22.73	51.14
0.61	1.37	2.35	3.66	5.49	8.23	12.80	21.94	49.37
0.59	1.32	2.26	3.52	5.27	7.91	12.31	21.10	47.47
0.56	1.26	2.16	3.36	5.04	7.57	11.77	20.18	45.40
0.53	1.20	2.05	3.19	4.79	7.19	11.18	19.17	43.13
0.50	1.13	1.93	3.01	4.51	6.76	10.52	18.04	40.59
0.47	1.05	1.79	2.79	4.19	6.28	9.77	16.75	37.68
0.42	0.95	1.63	2.54	3.80	5.71	8.88	15.21	34.23
0.83	1.42	2.22	3.32	4.98	7.75	13.29	29.91	
0.23	0.52	0.90	1.40	2.09	3.14	4.88	8.37	18.84
	$Ca = 0.01$							
0.49	1.11	1.90	2.96	4.44	6.65	10.35	17.74	39.92
0.48	1.07	1.84	2.86	4.28	6.42	9.99	17.13	38.54
0.46	1.03	1.76	2.75	4.12	6.18	9.61	16.47	37.06
0.44	0.98	1.69	2.63	3.94	5.91	9.19	15.75	35.45
0.42	0.94	1.60	2.49	3.74	5.61	8.73	14.96	33.67
0.39	0.88	1.51	2.35	3.52	5.28	8.21	14.08	31.69
0.36	0.82	1.40	2.18	3.27	4.90	7.63	13.07	29.41
0.33	0.74	1.27	1.98	2.97	4.45	6.93	11.88	26.72
0.29	0.65	1.11	1.73	2.59	3.89	6.05	10.38	23.35
0.18	0.41	0.70	1.09	1.63	2.45	3.81	6.54	14.71
	$Ca = 0.03$							
0.33	0.73	1.26	1.96	2.93	4.40	6.85	11.74	26.41
0.31	0.71	1.21	1.89	2.83	4.25	6.61	11.33	25.50
0.30	0.68	1.17	1.82	2.72	4.09	6.36	10.90	24.52
0.29	0.65	1.12	1.74	2.61	3.91	6.08	10.42	23.45
0.28	0.62	1.06	1.65	2.48	3.71	5.78	9.90	22.28
0.26	0.58	1.00	1.55	2.33	3.49	5.44	9.32	20.97
0.24	0.54	0.93	1.44	2.16	3.24	5.05	8.65	19.46
0.22	0.49	0.84	1.31	1.96	2.95	4.58	7.86	17.68
0.19	0.43	0.74	1.14	1.72	2.57	4.00	6.87	15.45
0.12	0.27	0.46	0.72	1.08	1.62	2.52	4.32	9.73

Table 6.2: Calculated values of $\frac{C_{slug}}{C_{kk}}$ for different volume fractions and Capillary numbers.

Ca=0.05								
$\epsilon = 0.1$	$\epsilon = 0.2$	$\epsilon = 0.3$	$\epsilon = 0.4$	$\epsilon = 0.5$	$\epsilon = 0.6$	$\epsilon = 0.7$	$\epsilon = 0.8$	$\epsilon = 0.9$
0.27	0.60	1.02	1.59	2.39	3.59	5.58	9.56	21.51
0.26	0.58	0.99	1.54	2.31	3.46	5.38	9.23	20.77
0.25	0.55	0.95	1.48	2.22	3.33	5.18	8.87	19.97
0.24	0.53	0.91	1.41	2.12	3.18	4.95	8.49	19.10
0.22	0.50	0.86	1.34	2.02	3.02	4.70	8.06	18.14
0.21	0.47	0.81	1.26	1.90	2.85	4.43	7.59	17.07
0.20	0.44	0.75	1.17	1.76	2.64	4.11	7.04	15.85
0.18	0.40	0.69	1.07	1.60	2.40	3.73	6.40	14.40
0.16	0.35	0.60	0.93	1.40	2.10	3.26	5.59	12.58
0.10	0.22	0.38	0.59	0.88	1.32	2.05	3.52	7.92
	$Ca = 0.1$							
0.20	0.44	0.76	1.18	1.77	2.66	4.14	7.09	15.95
0.19	0.43	0.73	1.14	1.71	2.57	3.99	6.85	15.40
0.18	0.41	0.71	1.10	1.65	2.47	3.84	6.58	14.81
0.17	0.39	0.67	1.05	1.57	2.36	3.67	6.30	14.16
0.17	0.37	0.64	1.00	1.50	2.24	3.49	5.98	13.46
0.16	0.35	0.60	0.94	1.41	2.11	3.28	5.63	12.66
0.15	0.33	0.56	0.87	1.31	1.96	3.05	5.22	11.75
0.13	0.30	0.51	0.79	1.19	1.78	2.77	4.75	10.68
0.12	0.26	0.44	0.69	1.04	1.55	2.42	4.15	9.33
0.07	0.16	0.28	0.44	0.65	0.98	1.52	2.61	5.88

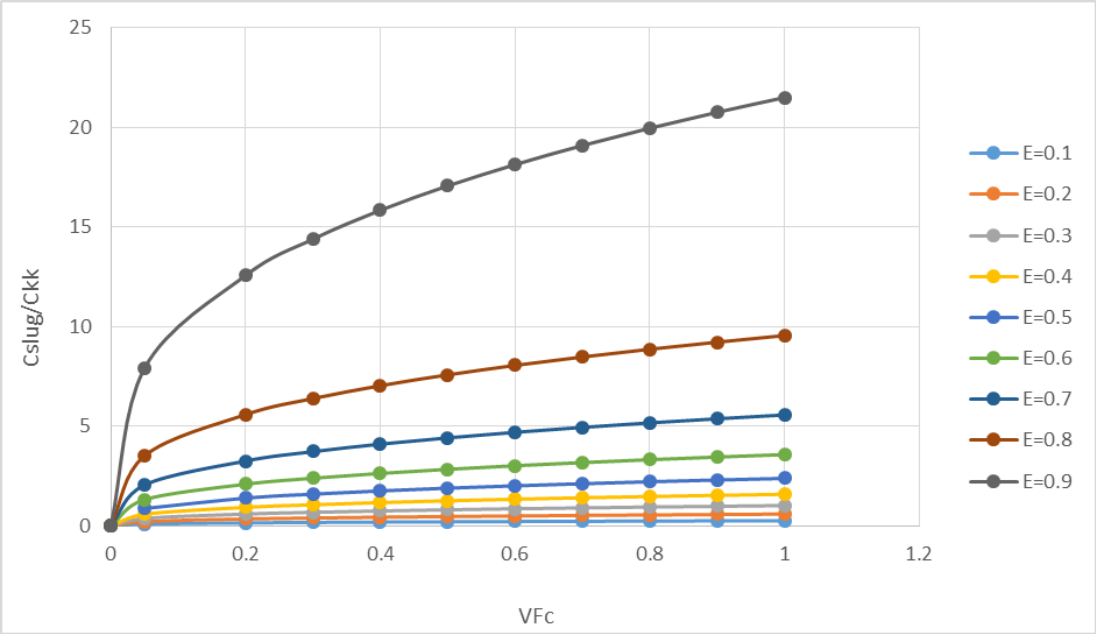

Figure 6.4: Effect of the porosity on the parameter $\frac{C_{slug}}{C_{kk}}$ for different volume fractions and Capillar number Ca=0.05

6.4 Conclusions

Based on the slug flow study presented in the previous chapters, the correlations corresponding to liquid-liquid slug flow through a capillary were used to generalise the Kozeny-Carman equation and applied it for two-phase liquid-liquid systems in porous media. The proposed model includes the influence of the interfacial shear forces and inertial effects in a porous media. This model may provide insight on the hydrodynamics of liquid-liquid flows though packed bed reactors and can be further implemented in biodiesel production process. A non-dimensional parameter $\frac{C_{slug}}{C_{kk}}$ has been introduced to evaluate the influence of important modelling parameters of slug flow through a porous media such as the Capillary number, volume fraction and the porosity. Generic plots of this new parameter were created and can be used as a measure to indicate the conditions when slug flow characteristics are necessary for an accurate prediction of the two-phase system or whether a single phase flow along the porous domain may be assumed. Nevertheless, the most suitable model parameters must be determined

from experiments for the system in question and to validate the proposed model. Also, limited experimental data regarding liquid-liquid slug flow in a packed bed was identified during this work.

Chapter 7

Conclusions and Future work

7.1 Conclusions

The hydrodynamic study of a two-phase slug flow in a capillary was developed throughout this work, motivated by the application in packed bed reactors as an alternative mixing technology for biodiesel production and process optimisation. The CFD approach developed in this work provided an understanding of the influence of the interfacial forces in capillary slug flows and also facilitated the analysis of various parameters in high surface tension flows more efficiently compared to other interface capturing techniques. For instance, using the Volume of Fluid (VOF) method a typical slug flow simulation can take from 24 hours to 1 or 2 weeks. Whereas, with the proposed CFD model the simulations took an average of 6 hours for each geometry configuration. Also, the CFD results were validated with theoretical models and the hydrodynamics structures were compared with similar studies in the literature to a certain extent. Some limitations in the CFD model were identified which made it difficult to compare the numerical results with experimental data. Mainly, the CFD predictions are functions of the geometric parameters and assumes a known particle shape while experimental results are for fluid pairs of known surface tension. Thus, the CFD methodology requires additional models for how film thickness depends on the surface tension. For instance, a correlation describing the variation of the droplet shape with the Capillary number.

The prediction of the main slug flow parameters such as the film thickness, bubble velocity and pressure drop for different pair of fluids over a wide range of inlet flow rates was successfully achieved through the implementation of an iterative method based on correlations from the literature. The results were in agreement with experimental and CFD data found in the literature for gas-liquid and liquid-liquid slug flows in capillaries. This tool offers convenience when the film thickness or droplet velocity are not known a priori, hence being useful for design purposes where two-phase flows in capillaries is desired. Also, predictions of the film thickness and bubble velocity can be successfully achieved in less than 1 hour without the necessity of implementing complex CFD simulations.

Finally, the first stage of a pressure drop model for predicting liquid-liquid flow in packed bed reactors has been proposed. The model includes the influence of the interfacial shear forces and inertial effects in a porous media. A non-dimensional parameter has been introduced to describe the influence of the Capillary number, volume fraction and the porosity on the slug flow regime through a packed bed. However, further calibration of the parameters and validation from experiments is required. Nevertheless, this model may provide insight on the hydrodynamics of liquid-liquid flows though packed bed reactors and can be further implemented in biodiesel production process.

7.2 Thesis summary

An overview of hydrodynamics studies including gas-liquid and liquid-liquid slug flow through capillaries were presented in Chapter 2. The existing knowledge from both experimental and computational studies, were reviewed and summarised involving available correlations to model slug flow in capillaries. Plenty of work has been developed in gas-liquid slug flows, but there are some gaps about the accurate prediction of pressure drops and mass transfer mechanisms in liquid-liquid slug flow in capillaries. Moreover, a summary of experimental and numerical studies for two-phase flow problems involving porous domains, mainly packed bed reactors was presented in this chapter. Details of important modelling parameters such as relative permeability, capillary pressure and liquid saturation

were discussed. Also, recent applications of packed bed reactors for biodiesel production were briefly described.

Chapter 3 presented the fundamental concepts of single and two phase flows in circular pipes. Details of the the most widely used correlations to model capillary slug flows were described and correspond mainly to gas-liquid flows. Also, recent empirical correlations from the literature to model liquid-liquid slug flow were defined and are suitable for a wide range of viscosity ratios. The aim of this chapter was to understand the transport phenomena in capillaries and then incorporate it into microfluidic systems applications, such as the flow in catalytic monoliths and multi-phase flow in porous media. Additionally, relevant theoretical concepts for modelling single and two phase flows in a porous media were also introduced in this chapter.

Chapter 4 introduced a computational fluid dynamic (CFD) approach for a liquid-liquid slug flow in a capillary. Firstly, the study of the interfacial forces was addressed by a drag force analysis over a single droplet of different sizes dispersed in a continuous phase. The Stokes-Newton equation was used to investigate the influence of the film thickness, droplet and slug length on the drag force coefficient. The results showed that this parameter can be characterised by the Stokes Law and the Stokes coefficient was highly influenced by the film thickness for different drop lengths. The results obtained in this study can be use to predict the settling or rising droplet velocity in two-phase capillary flows which is a significant parameter for an accurate design of mixing and separation processes.

Also, the motion of an elongated droplet in horizontal pressure driven flow in a capillary was evaluated. Predictions of the droplet velocity with different film thickness, droplet lengths and slug lengths were achieved. The results showed a significant effect of the film thickness on the droplet velocity and their relationship followed a similar behaviour as described by several authors in the literature.

The study was extended to investigate the influence of the interfacial forces on the flow in both continuous and dispersed phases. It was found that for an infinite long droplet the flow can be described by the analytical solution of two-phase annular flow through a circular capillary. For finite length droplets assuming high surface tension, the curvature shape of the end caps greatly affect the dispersed phase flow behaviour. The velocity profile corresponding to low

viscous finite droplet showed good agreement with the annular flow solution. However, discrepancies were observed for the case of a high viscous droplet. The main reason for this is that the CFD predictions are functions of the geometric parameters L_d^* and δ/r, while experimental results are for fluid pairs of known surface tension. Thus, the CFD analysis needs to be supplemented by models for how film thickness depends on the surface tension. Nevertheless, the CFD model proposed in the present study allows to analyse efficiently the effect of viscosity and density ratios for annular flow and is predictive for the case of sufficiently high surface tension. Additionally, the CFD methodology and configuration can be used as an efficient approach to investigate mass transfer mechanisms in gas-liquid and liquid-liquid slug flows.

Chapter 5 described an efficient tool to predict the film thickness and droplet velocity of two-phase slug flows in capillaries. The algorithm consisted of an iterative method based on existing correlations used to model slug flow through capillaries. The prediction of these two parameters was achieved from known fluid properties and inlet flow rates. The results have shown the applicability and efficiency of the current computational process to predict important parameters of two-phase slug flow through capillaries, thus being useful as a design tool for applications involving micro-capillaries technologies and to formulate guidelines for their design. Also, the algorithm can be helpful for predicting initial conditions or input parameters for the development of CFD models, in this case applied to liquid-liquid flows in porous media.

Finally, an early stage approach to predict the pressure drop of a liquid-liquid slug flow along a packed bed reactor has been proposed in Chapter 6 based on the Karman-Cozeny equation and semi-empirical correlation for liquid-liquid slug flow in capillaries. The proposed model includes the influence of the interfacial shear forces and inertial effects in a porous media. This model may provide insight on the hydrodynamics of liquid-liquid flows though packed bed reactors. The most suitable model parameters must be determined from experiments for the system in question and to validate the proposed model. Limited experimental data regarding liquid-liquid slug flow in a packed bed was identified during this work.

7.3 Suggestions for further research

The prediction of the settling or rising velocity of a droplet in a capillary slug flow can be computed using the expression defined in Chapter 3, Equation 3.63, which relates the Galileo number and the drag coefficient when the balance of gravitational forces has been reached. This calculation requires the densities of both the continuous and dispersed phases to be known, hence further validation with a specific two-phase system is necessary to extend its applicability. The drag forces and terminal velocities may highly influence on the predictions on the mass transfer coefficients in this type of flows, thus being a significant parameter for an accurate design of mixing and separation processes.

Moreover, an improvement of the CFD model developed in Chapter 4 can be achieved by considering a moving mesh approach and including the dependence of the film thickness on the surface tension using the Laplace pressure or the film evolution theory. Also, the secant method to predict the droplet velocity for a range of total pressure drops along the capillary can be incorporated in the model. Additionally, the study of the mass transfer mechanisms for a particular gas-liquid and liquid-liquid slug flow systems can be developed and estimations of the mass transfer coefficients under different operating conditions and geometry configurations can be efficiently achieved with the proposed two-phase slug flow CFD model.

The coupling of the hydrodynamics in capillary slug flow with chemical reactions can then be considered in the model. For instance, the reaction kinetics in biodiesel production can be incorporated to predict the formation of the different phases occurring during the reaction, since the droplet size reduces in size as it progresses down the channel. Thus, being the pressure drop an important parameter in function of the droplet size.

The algorithm presented in Chapter 5 for the prediction of the main slug flow parameters in a capillary can be improved by including the bubble frequency based on (Warnier *et al.*, 2010) correlation. This feature may improve the pressure drop predictions of a particular two-phase system and can be extended to study the influence of different inlet configurations for slug flow generation.

Ultimately, calibrate the parameters involved in the pressure drop model proposed in Chapter 5 using experimental data of liquid-liquid flow in packed bed reactors. Additional parameters such as relative permeability and capillary effects can be incorporated in the model to characterise the flow distribution inside the packed bed. Also, a detailed analysis of the interfacial forces within the fluid domains should be developed, for instance drag force studies taking into account various shapes of the droplets along the porous domain and effect of turbulence dispersion forces. With these modifications, the CFD model can be adapted to compute improved predictions of the operating conditions in packed bed reactors for biodiesel production.

Appendix A

Code sample A

A.1 Interface study of a two-phase flow in a capillary

The program allows multiple runs between Python and ANSYS CFX to communicate information across a two-phase interface

```
import csv
import math
import subprocess
from sys import argv
from sys import exit
from os import system
from glob import glob
import shutil

input parameters:
velocity=[]
TotalRuns =60
m=0.3 #under-relaxing factor
m1 = 1 - m

input def functions:
```

```
def read_table_from_file( csv_filename ):
    table = []
    with open( csv_filename , "rt") as csvfile:

         for N in range(8):  # skip header lines
            csvfile.readline()

         for record in csv.reader(csvfile):
              table.append( [ float(record[0]),
                              float(record[1]),
                              float(record[2]),
                              float(record[3]),
                              float(record[4]),
                              float(record[5])
                            ]
                          ) #Reads and record Velocity U,V,W
    return table

def read_tangential_unit_vectors_from_file( csv_filename ):
    table = []
    with open( csv_filename , "rt") as csvfile:

         for N in range(1):  # skip header line
            csvfile.readline()

         for record in csv.reader(csvfile):
              table.append( [ float(record[0]),
                              float(record[1]),
                              float(record[2])])
    return table

def write_shear_table_to_file( table, csv_filename ):
    with open( csv_filename, "w" ) as csvfile:
        csvwriter = csv.writer(csvfile)
```

```
        #csvwriter.writerow( [] )
        csvwriter.writerow( [ "[Name]" ] )
        csvwriter.writerow(["wallshear"])
        csvwriter.writerow([])
        csvwriter.writerow(["[Spatial Fields]"])
        csvwriter.writerow("xyz")
        csvwriter.writerow([])
        csvwriter.writerow(["[Data]"])
        csvwriter.writerow(["x" "[ m ]","y" "[ m ]","z" "[ m ]",
        "Wall Shear X" " [Pa]","Wall Shear Y" " [Pa]",
        "Wall Shear Z" " [Pa]"])

        for record in table:
            csvwriter.writerow(record)

def write_velocity_table_to_file( table, csv_filename ):
        with open( csv_filename, "w" ) as csvfile:
            csvwriter = csv.writer(csvfile)
            #csvwriter.writerow( [] )
            csvwriter.writerow( [ "[Name]" ] )
            csvwriter.writerow(["velocity"])
            csvwriter.writerow([])
            csvwriter.writerow(["[Spatial Fields]"])
            csvwriter.writerow("xyz")
            csvwriter.writerow([])
            csvwriter.writerow(["[Data]"])
            csvwriter.writerow(["x" "[ m ]","y" "[ m ]","z" "[ m ]",
                                "Velocity u" " [m s^-1]","Velocity v" " [m s^-1]
                                "Velocity w" " [m s^-1]"])
            for record in table:
                 csvwriter.writerow( record )

    #Calculate under relaxing values
```

```
def generate_under_relaxing_table( table1, table2 ):
    table3 = []
    for recnum in range( len(table1) ):
        newA = (m * table2[recnum][3]) + (m1 * table1[recnum][3])
        newB = (m * table2[recnum][4]) + (m1 * table1[recnum][4])
        newC = (m * table2[recnum][5]) + (m1 * table1[recnum][5])
        table3.append([table1[recnum][0],table1[recnum][1],table1[recnum][2],
                       newA,newB,newC])
    return table3

    #Calculate Tangential velocity vector

def generate_vel_dot_tangential_table ( tableA, tableB ):
    if not(len(tableA) == len( tableB)):
        print( "Error in generate_vel_dot_tangential_table: tables are not same
        return( "ERROR" )
    prod_table = []
    for recnum in range(len(tableA)):
        Udot =[(tableA[recnum][3])*(tableB[recnum][0])+
               (tableA[recnum][4])*(tableB[recnum][1])+
               (tableA[recnum][5])*(tableB[recnum][2])]
        prod_table.append(Udot)
    return prod_table

def generate_tangential_velocity_vector_table ( tableA, tableB ):
    if not(len(tableA) == len( tableB)):
        print( "Error in generate_vel_dot_tangential_table: tables are not same
        return( "ERROR" )
    prod_table = []
    for recnum in range(len(tableA)):
        newA=(tableA[recnum][0])*(tableB[recnum][3])
        newB=(tableA[recnum][0])*(tableB[recnum][4])
        newC=(tableA[recnum][0])*(tableB[recnum][5])
```

```
#        prod_vector =[(tableA[recnum][0])*(tableB[recnum][3]),
#                      (tableA[recnum][0])*(tableB[recnum][4]),
#                      (tableA[recnum][0])*(tableB[recnum][5])]
        prod_table.append([tableB[recnum][0],tableB[recnum][1],
tableB[recnum][2], newA,newB,newC])
    return prod_table

def show_table( table ):
    for record in table:
        print( record )

def get_output_file_of_dispersed_phase():
       files = glob('filename1.csv')
       if not(len(files) == 2):
           print( "WARNING: more than one dispersed_phase output file was found!
       return files [0]

def get_output_file_of_cont_phase():
       files = glob('/filename2.csv')
       if not(len(files) == 2):
           print( "WARNING: more than one cont_phase output file was found!!!" )
       return files [0]

def generate_and_return_new_table_dispersed():
       new_output_file_dispersed = get_output_file_of_dispersed_phase()
       print("Found output file", new_output_file_dispersed_phase)
       print("Reading output file into table")
       return read_table_from_file( new_output_file_dispersed_phase )

       new_table =  generate_and_return_new_table_dispersed()
       show_table( new_table )

def delete_all_output_files():
        dispersed_directories = glob('*.csv')
```

```
        for directory in dispersed_directories:
            subprocess.call( ["rm", "-r", directory])

            print( "Deleting dispersed output files" )
            #delete_all_dispersed_output_files()

def setup_initial_tables():
    print("Reading initial previous_shear_table" )
    table1 = read_table_from_file( "table1.csv" )
    print("Reading initial shear_table" )
    table2 = read_table_from_file( "table2.csv" )

    print("Reading initial previous_velocity_table" )
    table3 = read_table_from_file( "table3.csv" )

    return (table1, table2, table3)

def get_unit_vectors_table():
    print("Reading unit vectors" )
    table =read_tangential_unit_vectors_from_file("table4.csv")
    return (table)

def copy_results_files():
        csv_files=glob('table_*')
        for files in csv_files:
            subprocess.call(["cp", "-r", files, 'filename'])
            print("Copy csv files")

def get_previous_shear_table():
     csv_files = glob('filename1.csv')
     return csv_files [0]
     print("Getting previous shear table")

def get_previous_velocity_table():
```

```
     csv_files = glob('filename2.csv')
     return csv_files [0]
     print("Getting previous velocity table")


print( "\n----------Starting Program to find Convergence----------\n" )

print( "Initialising Tables" )
( previous_shear_table, new_shear_table, previous_velocity_table) =
setup_initial_tables()
unit_vectors_table = get_unit_vectors_table()
print( "\nStarting Iteration" )
for Nrun in range( TotalRuns ):
    print("Loop Iteration:", Nrun)
    print(" Generating new under-relaxing shear table" )
    ur_shear_table =
   generate_under_relaxing_table( previous_shear_table, new_shear_table )
    write_shear_table_to_file( "filename.csv" )

    print("running cfx5solve two_phase.def / contphase domain")
    subprocess.call(["cfx5solve", "-def", "filename.def"])

    print("Getting velocity table filename" )
    contout_filename = get_output_file_of_cont_phase()
    new_velocity_table = read_table_from_file( contout_filename )

    print("Calculating Tangential Velocity Vectors")
    vel_dot_table=
    generate_vel_dot_tangential_table ( new_velocity_table, unit_vectors_table )
    tangential_vector_table=
    generate_tangential_velocity_vector_table(vel_dot_table, new_velocity_table)
    new_velocity_table=tangential_vector_table
    write_velocity_table_to_file("filename.csv" )
```

```
print("Writing Tangential velocity vectors table")
write_velocity_table_to_file( new_velocity_table, "filename.csv" )

copy_results_files()
delete_all_output_files()

print("Generating new under-relaxing velocity table" )
ur_velocity_table =
generate_under_relaxing_table( previous_velocity_table, new_velocity_table )
write_velocity_table_to_file( ur_velocity_table, "filename.csv" )

print("running cfx5solve two_phase.def / dispersed phase domain")
subprocess.call(["cfx5solve", "-def", "two_phase_zero deltaP.def"])

print("Getting dispersed output filename" )
dispersed_out_filename =
get_output_file_of_dispersed_phase()
new_shear_table =
 read_table_from_file( dispersed_out_filename )
write_shear_table_to_file( new_shear_table, "filename.csv" )

#show_table(new_shear_table)
copy_results_files()
delete_all_output_files()
print("progressing shear tables" )
new_previous_shear_table = get_previous_shear_table()
previous_shear_table=
read_table_from_file(new_previous_shear_table)
print("progressing velocity tables" )
new_previous_velocity_table =
get_previous_velocity_table()
previous_velocity_table=
read_table_from_file(new_previous_velocity_table)
print("End of Run")
```

Appendix B

Code sample B

B.1 Prediction of slug flow parameters

This program predicts the film thickness, bubble velocity and pressure drop in a capillary for a given fluid properties and inlet flow rates operating in slug flow conditions.

```
import csv
import math
import pylab as pl

input fluid density:
air_{den}=1.2
water_{den}=996.6
pd5_{den}=911.8
EG_{den}=1112
FC40_{den}=1854.1
AR20_{den}=1142.2
Dod_{den}=754.3
Hex_{den}=767
HN03_{den}=1030
TBP_{den}=1259

input fluid viscosity:
```

```
air_{vis}=1.84e-05
water_{vis}=8.68e-4
pd5_{vis}=3.58e-03
EG_{vis}=1.89e-02
$FC40_{vis}=3.91e-03
AR20_{vis}=2.09e-02
Dod_{vis}=1.39e-03
Hex_{vis}=2.67e-03
HN03_{vis}=7.5e-04
TBP_{vis}=0.03

input surface tension:
Dod_water=0.052
pd5_water=0.039
FC40_water=0.051
AR20_water=0.03
water_air=0.073
pd5_air=0.024
EG_air=0.048
Hex_water=0.051
TBP_HN03=0.0067

input fluid pair properties:
viscosity_cont=Hex_vis
density_cont=Hex_den
viscosity_disp=water_visdensity_disp=water_den
surface_tension=Hex_water
viscosity_ratio=viscosity_cont/viscosity_disp
density_ratio=density_cont/density_disp

input capillary dimensions (m):
capillary_diameter=0.0005
radius=capillary_diameter/2
area=math.pi*(capillary_diameter**2)/4
```

```
input constants in correlations:
a=0.6667
b=0.672
c=0.589
d=0.629

A=32.05
B=4.564e-5
C=2.860
aa=0.593
bb=1.909
cc=0.764

input  def functions:
```

(i) film thickness correlations

```
def calculate_film_thickness_HS(value1,value2):
     delta=(float((1.34*(value1**a))/(1+(3.13*(value1**a))
            +(0.504*(value1**b)*(value2**c))-(0.352*((value1*value2)**d)))))
     return delta

def calculate_expression(value1):
     phi=(1+((A/(value1**aa)+(B*(value1**bb))))**(-1))
     return phi

def calculate_film_thickness_cfd(value1,value3):
     delta=(float((0.67*(value1**a))/(1+(value3*C)*(value1**cc))))
     return delta

def calculate_film_thickness_eain(value1,value2):
     delta=0.35*(value1**(0.354))*(value2**(0.097))
    return delta
```

```
def calculate_film_thickness_angeli(value1,value2):
      delta=0.385*(value1**(0.265))*(value2**(0.098))
     return delta
```

(ii) pressure drop correlations

```
def calculate_pressure_bubble_walsh(value1,value2, value3):
     fReb=1.92*(capillary_diameter/value1)*((value2/value3)**0.33)
     return fReb

def calculate_pressure_bubble_cfd(value1,value2):
     fReb=float(3.96*((value1)**0.58))/(value2)
     return fReb

def calculate_pressure_bubble_bretherton(value1, value2):
     fReb=float(7.16*((3*value1)**a))/(2*value2*value1)
     return fReb

def calculate_pressure_bubble_warnier(value1,value2, value3):
     fb=0.3875*(area/value1)*(capillary_diameter/value2)*(1/((value3**(0.33))
+3.34*value3))
     return fb

def calculate_slug_pressure(value1):
     fs=(32*viscosity_cont*value1)/(capillary_diameter**2)
     return fs

def calculate_pressure_bubble_kreutzer(value1, value2, value3):
     fb=0.11*(capillary_diameter/value1)*((value2/value3)**0.33)
     return fb

def calculate_fReb_general(value1):
     fReb=7.16*((surface_tension*(3*value1**0.66))/
(capillary_diameter*((1+3.34*value1)**0.66)))
     return fReb
```

```
def calculate_fRem(value1, value2,value3):
     fsRem=16*(1+1.92*(capillary_diameter/value1)*(value2/value3)**0.33)
     return fsRem

def calculate_pressure_bubble_warnier(value1, value4, value5):
   fb=0.465*(capillary_diameter*value5/value1)*(1/((value4**(0.33)
+3.34*value4)))
     return fb

def calculate_pressure_bubble_eain(value1,value2,value3,value4):
      fReb=0.4416*(area/value2)*(capillary_diameter/value1)*(1/
((value3**(0.33))+3.34*value3))*((1-value4)**0.33)
     return fReb
```

(iii) bubble velocity correlations

```
def calculate_velocity_ratio(value1): #(Langewish correlation)
     ub_um=(1-(2*value1))**(-2)
     return ub_um

def calculate_bubble_velocity(value1,value2):
     Ub=value1*value2
     return Ub

def calculate_velocity_general(value1): #(Fletcher, Abiev correlation)
     ub_um=(((1-value1)**2)*(viscosity_ratio-2)+2)/
(((1-value1)**4)*(viscosity_ratio-1)+1)
     return ub_um

def calculate_velocity_kashid(value1): #(Kashid correlation}
     ub_um=2/(1+(1-value1)**2)
     return ub_um
```

generate data table

```
def write_to_file( table, csv_filename):
    with open( csv_filename, "a" ) as csvfile:
        data = csv.writer(csvfile, lineterminator='\n')
        for record in table:
                data.writerow(record)

def generate_final_data_table(value):
    table=[]
    final_table=value
    table.append(final_table)

    return table

def write_headings_to_file( csv_filename):
    with open( csv_filename, "w" ) as csvfile:
        data = csv.writer(csvfile, lineterminator='\n')
        data.writerow( ["Re", "Ca",  "Ub/Um", "delta/r","DeltaPb","fReb1",
"fRet1", "fReb*_Walsh", "fRet_Walsh",
"delta_HS", "Uwalsh"])
        data.writerow( [])

def write_headings2_to_file( csv_filename):
    with open( csv_filename, "w" ) as csvfile:
        data = csv.writer(csvfile, lineterminator='\n')
        data.writerow( ["Visc Ratio","Qt (ml/min)", "Um (m/s)", "Re", "Ca",
"h/r", "Ub/Um", "Reb", "Cab", "fReb_Warnier*",
"fReb_Kreutzer", "fReb_Walsh","fReb_Eain",
"Pt_Warnier (kPa)", "Pt_Kreutzer (kPa)",
 "Pt_Walsh(kPa)","Pt_Eain(kPa)", "Warnier2_Freq (kPa)"])
        data.writerow( [])


  print ("\n-----Starting Program to Calculate slug flow parameters------\n")
N_it=10
Ls=5.88*capillary_diameter
```

```
Lb=1.09*capillary_diameter
inlet_flow_ratio=0.5
data_table=[]

print "Viscosity ratio:","\%.2f" \% viscosity_ratio

for Qt in pl.frange(0.05,20,0.1):
    print "Qt (ml/min)=" , Qt

    Qc=Qt/(inlet_flow_ratio+1)
    Qd=inlet_flow_ratio*Qc
    print "Qd (ml/min)=" , Qd
    print "Qc (ml/min)=" , Qc

    VFd=Qd/Qt
    VFc=1-VFd

    Um=(Qt/area)*(0.000001/60) # m/s
    print "Um (m/s)=", Um

    Uc=(Qc/area)*(0.000001/60)
    print "Uc (m/s):", Uc

#Calculate Capillary number
    cap_num=viscosity_cont*Um/surface_tension

#Calculate Reynolds number
    re_num=density_cont*Um*capillary_diameter/viscosity_cont

    Re=re_num
    print "Re=", Re
    Ca=cap_num
    print "Ca=", Ca
    We=Ca*Re
```

```
delta_HS=calculate_film_thickness_HS(Ca,Re)
print "Film_initial:" , delta_HS

delta_eain=calculate_film_thickness_eain(Ca,We)
delta_angeli=calculate_film_thickness_angeli(Ca,We)

U_HS=calculate_velocity_general(delta_eain)
U_HS=calculate_velocity_general(delta_eain)
print "Ub/Um_initial:", U_HS

Ub=calculate_bubble_velocity(U_HS, Um)
print "Ub_initial:", Ub

print ("\n-------------- Starting iteration ------------------\n")

for N in range(N_it):
    print "Iteration:", N
    Reb=density_cont*Ub*capillary_diameter/viscosity_cont
    print "Reb:", Reb

    Cab=viscosity_cont*Ub/surface_tension
    print "Cab:", Cab

    Web=Reb*Cab
    #calculate film thickness
    deltab_HS=calculate_film_thickness_HS_modified(Cab,Reb)
    print "delta:", deltab_HS

    deltab_eain=calculate_film_thickness_eain(Cab,Web)
    deltab_eain=calculate_film_thickness_eain(Cab,Web)
    print "delta/r:", deltab_eain
    film=deltab_eain*radius
    print "film [m]:", film
```

```
#calculate bubble velocity
    Ub_HS=calculate_velocity_general(deltab_eain)
        print "Ub/HS_new:", Ub_HS
        new_Ub=calculate_bubble_velocity(Ub_HS, Um)
        print "Ub_new:", new_Ub
        Ub=new_Ub

#calculate bubble pressure drop
        dpb_eain=calculate_pressure_bubble_eain(area_bubble,Ls,Cab,VFd)
        print "dpb_eain", dpb_eain

        dpb_warnier=(calculate_pressure_bubble_warnier(area_bubble,Ls,Cab))
        print "dpb_warnier:", dpb_warnier

        dpb_kreutzer=calculate_pressure_bubble_kreutzer(Ls,Re,Ca)
        print "dpb_kreutzer:", dpb_kreutzer

#calculate slug pressure drop
        dp_slug=calculate_slug_pressure(Um)
        dp_slug=16
        print "dp_slug:", dp_slug

#calculate total pressure drop

        tp_warnier=(dp_slug*(1+dpb_warnier))/1000
        print "Total pressure warnier (kPa):", tp_warnier

        tp_kreutzer=(dp_slug*(1+dpb_kreutzer))/1000
        print "Total pressure kreutzer (kPa):", tp_kreutzer

        tp_walsh=(dp_slug*(1+dpb_walsh))/1000
        print "Total pressure walsh (kPa):", tp_walsh
```

```
        tp_eain=(dp_slug*(1+dpb_eain))/1000
        print "Total pressure eain (kPa):", tp_eain

#Non-dimensional pressure drop fRe
        fRe_eain=16*(1+dpb_eain)
        print "fRet_eain=", fRe_eain

        fRe_warnier1=16*(1+dpb_warnier)
        print "fRet_warnier1=", fRe_warnier1

        fRe_kreutzer=16*(1+dpb_kreutzer)
        print "fRet_kreutzer=", fRe_kreutzer

        fRe_walsh=16*(1+dpb_walsh)
        print "fRet_walsh=", fRe_walsh

    #parameter for Warnier Equation
        radius_bubble=radius-film
        diam_bubble=2*radius_bubble
        area_bubble=math.pi*(radius_bubble**2)
        print "radius bubble:", radius_bubble

        length_unitcell=Ls+Lb
        print "Length unitecell:", length_unitcell

        pb_slug2=calculate_slug_pressure(Uc)
        print "Ps:", pb_slug2

        dpdz_warnier=(calculate_slug_pressure(Uc)*(1+pb_f))/1000
        print "dpdz:", dpdz_warnier

        ftotal_Re=16*(1+pb_f)
        print "fRet_warnier2:", ftotal_Re
```

Export final values in table

```
write_headings2_to_file("filename.csv")

data_table=generate_final_data_table((float(viscosity_ratio),float(Qt),
 float(Um), float(Re),float(Ca),float(delta_eain),
float(U_HS), float(Reb), float(Cab), float(fRe_warnier1),
 float(fRe_kreutzer), float(fRe_walsh), float(fRe_eain),
float(tp_warnier), float(tp_kreutzer), float(tp_walsh),
float(tp_eain), float(dpdz_warnier)))

 write_to_file(data_table, "filename.csv")
```

References

Abiev, R.S. (2008). Simulation of the slug flow of a gas-liquid system in capillaries. *Theoretical Foundations of Chemical Engineering*, **42**, 105–117, iSI Document Delivery No.: 297BK Times Cited: 13 Cited Reference Count: 23 Abiev, R. Sh. Maik nauka/interperiodica/springer New york. xvi, 28, 29, 33, 36, 61, 65, 66, 147

Abiev, R.S. (2009). Circulation and bypass modes of the slug flow of a gas-liquid mixture in capillaries. *Theoretical Foundations of Chemical Engineering*, **43**, 298–306, iSI Document Delivery No.: 461GP Times Cited: 7 Cited Reference Count: 16 Abiev, R. Sh. Hydrodynamics of a gas-liquid system The important problems of the hydrodynamics of a gas-liquid system in the capillaries of monolith catalysts are as follows: Maik nauka/interperiodica/springer New york. 66

Abiev, R.S. (2010). Method for calculating the void fraction and relative length of bubbles under slug flow conditions in capillaries. *Theoretical Foundations of Chemical Engineering*, **44**, 86–101, iSI Document Delivery No.: 563JN Times Cited: 5 Cited Reference Count: 30 Abiev, R. Sh. Maik nauka/interperiodica/springer New york. 28

Abiev, R.S. (2013). Bubbles velocity, taylor circulation rate and mass transfer model for slug flow in milli- and microchannels. *Chemical Engineering Journal*, **227**, 66–79, iSI Document Delivery No.: 189WQ Times Cited: 3 Cited Reference Count: 29 Abiev, R. Sh. 12th International Conference on Microreaction Technology Feb 20-22, 2012 Sch Chem, Engn & Phys Lyon (CPE Lyon), Lyon, FRANCE Elsevier science sa Lausanne. 29, 35, 39

Abiev, R.S. (2015). Effect of contact-angle hysteresis on the pressure drop under slug flow conditions in minichannels and microchannels. *Theoretical Foundations of Chemical Engineering*, **49**, 414–421, iSI Document Delivery No.: CP3SX Times Cited: 0 Cited Reference Count: 30 Abiev, R. Sh. Maik nauka/interperiodica/springer New york. 39

Abiev, R.S. & Dymov, A.V. (2013). Modeling the hydrodynamics of slug flow in a minichannel for liquid-liquid two-phase system. *Theoretical Foundations of Chemical Engineering*, **47**, 299–305, iSI Document Delivery No.: 204MR Times Cited: 0 Cited Reference Count: 7 Abiev, R. Sh Dymov, A. V. Maik nauka/interperiodica/springer New york. 21, 30, 66

Akbar, M.K. & Ghiaasiaan, S.M. (2006). Simulation of taylor flow in capillaries based on the volume-of-fluid technique. *Industrial & Engineering Chemistry Research*, **45**, 5396–5403, iSI Document Delivery No.: 062VL Times Cited: 28 Cited Reference Count: 34 Akbar, M. K. Ghiaasiaan, S. M. Amer chemical soc Washington. 13, 22

Al-Dahhan, M.H. & Dudukovic, M.P. (1994). Pressure drop and liquid holdup in high pressure trickle-bed reactors. *Chemical Engineering Science*, **49**, 5681 – 5698. 51

Al-Dahhan, M.H., Khadilkar, M.R., Wu, Y. & Dudukovi, M.P. (1998). Prediction of pressure drop and liquid holdup in high-pressure trickle-bed reactors. *Industrial & Engineering Chemistry Research*, **37**, 793–798. 51

Anan, N. & Danisman, A. (2007). Alkali catalyzed transesterification of cottonseed oil by microwave irradiation. *Fuel*, **86**, 2639–2644, iSI Document Delivery No.: 235ZT Times Cited: 2 Cited Reference Count: 17 Anan, Nezhe Danisman, Aysegul Elsevier sci ltd Oxford. 8

Angeli, P. & Gavriilidis, A. (2008). Hydrodynamics of taylor flow in small channels: a review. *Proceedings of the Institution of Mechanical Engineers Part C-Journal of Mechanical Engineering Science*, **222**, 737–751, iSI Document Delivery No.: 318IU Times Cited: 48 Cited Reference Count: 58 Angeli, P. Gavriilidis, A. Colloquium on Micro- and Nano-Scale Flows - Advancing the

Engineering Science and Design Dec 07-08, 2006 Glasgow, SCOTLAND Sage publications ltd London. 21, 64

ANSYS (2010a). *Academic Research, Release 14.0 Help System, CFX-Modeling Guide. ANSYS Inc.* 92

ANSYS (2010b). *Academic Research, Release 14.0 Help System, ICEM User Manual. ANSYS Inc.* 87, 88, 89

Arsenjuk, L., Kaske, F., Franzke, J. & Agar, D.W. (2016). Experimental investigation of wall film renewal in liquid-liquid slug flow. *International Journal of Multiphase Flow*, **85**, 177–185, iSI Document Delivery No.: DU1EM Times Cited: 0 Cited Reference Count: 28 Arsenjuk, Linda Kaske, Florian Franzke, Joachim Agar, David W. Pergamon-elsevier science ltd Oxford. 35, 39

Asadolahi, A.N., Gupta, R., Fletcher, D.F. & Haynes, B.S. (2011). Cfd approaches for the simulation of hydrodynamics and heat transfer in taylor flow. *Chemical Engineering Science*, **66**, 5575–5584, iSI Document Delivery No.: 831IW Times Cited: 11 Cited Reference Count: 46 Asadolahi, Azadeh N. Gupta, Raghvendra Fletcher, David F. Haynes, Brian S. University of Sydney; Australian Research Council [DP0985453]; Heatric Division of Meggitt (UK) Azadeh N. Asadolahi was supported through the University of Sydney Postgraduate Award. The work was supported under Australian Research Council Discovery Grant DP0985453. The financial support of the Heatric Division of Meggitt (UK) is also gratefully acknowledged. Pergamon-elsevier science ltd Oxford. 25, 29

Asadolahi, A.N., Gupta, R., Leung, S.S.Y., Fletcher, D.F. & Haynes, B.S. (2012). Validation of a cfd model of taylor flow hydrodynamics and heat transfer. *Chemical Engineering Science*, **69**, 541–552, iSI Document Delivery No.: 865QQ Times Cited: 8 Cited Reference Count: 27 Asadolahi, Azadeh N. Gupta, Raghvendra Leung, Sharon S. Y. Fletcher, David F. Haynes, Brian S. University of Sydney; Endeavour International Postgraduate Research Scholarship; Australian Government; Australian Research Council [DP0985453];

Heatric Division of Meggitt (UK) A.N. Asadolahi was supported through a University of Sydney Postgraduate Award. S. Leung was supported through the Endeavour International Postgraduate Research Scholarship funded by the Australian Government. The work was supported under Australian Research Council Discovery Grant DP0985453. The financial support of the Heatric Division of Meggitt (UK) is also gratefully acknowledged. Pergamon-elsevier science ltd Oxford. 21

Ataya, F., Dube, M.A. & Ternan, M. (2008). Transesterification of canola oil to fatty acid methyl ester (fame) in a continuous flow liquid-liquid packed bed reactor. *Energy & Fuels*, **22**, 3551–3556, iSI Document Delivery No.: 350DK Times Cited: 10 Cited Reference Count: 22 Ataya, Fadi Dube, Marc A. Ternan, Marten BIOCAP Canada Foundation; Natural Sciences and Engineering Research Council (NSERC) of Canada The authors acknowledge the BIOCAP Canada Foundation and the Natural Sciences and Engineering Research Council (NSERC) of Canada for financial support of this research. Amer chemical soc Washington. 2

Atta, A., Roy, S. & Nigam, K. (2007). Prediction of pressure drop and liquid holdup in trickle bed reactor using relative permeability concept in cfd. *Chemical Engineering Science*, **62**, 5870 – 5879. 50, 52

Atta, A., Roy, S. & Nigam, K. (2010). A two-phase eulerian approach using relative permeability concept for modeling of hydrodynamics in trickle-bed reactors at elevated pressure. *Chemical Engineering Research and Design*, **88**, 369 – 378, special Issue in Honour of Professor Klaas Roelof Westerterp on the occasion of his 80th birthday. 50, 52, 80

Attou, A. & Ferschneider, G. (1999). A two-fluid model for flow regime transition in gas-liquid trickle-bed reactors. *Chemical Engineering Science*, **54**, 5031–5037, iSI Document Delivery No.: 229NG Times Cited: 26 Cited Reference Count: 12 Attou, A Ferschneider, G 4th International Conference on Gas-Liquid and Gas-Liquid-Solid Reactor Engineering Aug 23-25, 1999 Delft, netherlands Kramers Lab Fysische Technol Pergamon-elsevier science ltd Oxford. xix, 49, 51, 52, 53, 149, 150, 152, 153, 154

Attou, A. & Ferschneider, G. (2000). A two-fluid hydrodynamic model for the transition between trickle and pulse flow in a cocurrent gasliquid packed-bed reactor. *Chemical Engineering Science*, **55**, 491 – 511. 52

Aussillous, P. & Quere, D. (2000). Quick deposition of a fluid on the wall of a tube. *Physics of Fluids*, **12**, 2367–2371, iSI Document Delivery No.: 351RB Times Cited: 151 Cited Reference Count: 7 Aussillous, P Quere, D Amer inst physics Melville. xix, 21, 28, 31, 35, 67, 70, 125, 139, 140, 141

Aydin, B. & Larachi, F. (2005). Trickle bed hydrodynamics and flow regime transition at elevated temperature for a newtonian and a non-newtonian liquid. *Chemical Engineering Science*, **60**, 6687–6701, iSI Document Delivery No.: 969OQ Times Cited: 24 Cited Reference Count: 41 Aydin, B Larachi, F Pergamon-elsevier science ltd Oxford. 48, 49

Bandara, T., Nguyen, N.T. & Rosengarten, G. (2015). Slug flow heat transfer without phase change in microchannels: A review. *Chemical Engineering Science*, **126**, 283 – 295. 123, 146

Barnard, T.M., Leadbeater, N.E., Boucher, M.B., Stencel, L.M. & Wilhite, B.A. (2007). Continuous-flow preparation of biodiesel using microwave heating. *Energy Fuels, 21(3), pp 1777-1781*. 8

Bear, J. (1972). *Dynamics of Fluids in Porous Media*. AMERICAN ELSEVIER PUBLISHING COMPANY, INC, 52 Vanderbilt Avenue, New York, N.Y. xvi, 74, 75, 76, 79

Biardi G., B.G. (1999). Three-phase catalytic reactors. *Catalysis Today-ELSEVIER*. 48

Biswas, K.G., Patra, R., Das, G., Ray, S. & Basu, J.K. (2015). Effect of flow orientation on liquidliquid slug flow in a capillary tube. *Chemical Engineering Journal*, **262**, 436 – 446. 21, 37, 39

Boer (2009). Investigation of liquid-liquid two phase flow in biodiesel production. *Seventh International Conference on CFD in the Minerals and Process Industries*. xiv, 3, 4, 42, 54, 55

Boyer, C., Koudil, A., Chen, P. & Dudukovic, M. (2005). Study of liquid spreading from a point source in a trickle bed via gamma-ray tomography and cfd simulation. *Chemical Engineering Science*, **60**, 6279 – 6288, 7th International Conference on Gas-Liquid and Gas-Liquid-Solid Reactor Engineering. 52

Boyer, C., Volpi, C. & Ferschneider, G. (2007). Hydrodynamics of trickle bed reactors at high pressure: Two-phase flow model for pressure drop and liquid holdup, formulation and experimental validation. *Chemical Engineering Science*, **62**, 7026 – 7032, 8th International Conference on Gas-Liquid and Gas-Liquid-Solid Reactor Engineering. 49, 51

Bretherton, F.P. (1961). The motion of long bubbles in tubes. *Journal of Fluid Mechanics*, **10**, 166–188, iSI Document Delivery No.: WT930 Times Cited: 988 Cited Reference Count: 12 Bretherton, fp Cambridge univ press New york. 21, 27, 28, 30, 31, 35, 36, 67, 69, 125, 126

Burns, J.R. & Ramshaw, C. (1999). Development of a microreactor for chemical production. *Chemical Engineering Research & Design*, **77**, 206–211, iSI Document Delivery No.: 216PN Times Cited: 62 Cited Reference Count: 6 Burns, JR Ramshaw, C International Conference on Process Innovation and Intensification Oct 21-22, 1998 Manchester, england 218l Inst chemical engineers Rugby. 21

Burton, K.J.J.M. (2007). U.s. and tennessee biodiesel production-2007 industry update. Tech. rep., Department of Agricultural Economics, The University of Tennessee, Knosxville, Tennessee. 1

Camenen, B. (2007). Simple and general formula for the settling velocity of particles. *Journal of Hydraulic Engineering-Asce*, **133**, 229–233, iSI Document Delivery No.: 126WY Times Cited: 18 Cited Reference Count: 26 Camenen, Benoit Asce-amer soc civil engineers Reston. 73, 74

Cao, P.G., Dube, M.A. & Tremblay, A.Y. (2008). High-purity fatty acid methyl ester production from canola, soybean, palm, and yellow grease lipids by means of a membrane reactor. *Biomass & Bioenergy*, **32**, 1028–1036, iSI

Document Delivery No.: 354UZ Times Cited: 47 Cited Reference Count: 33 Cao, Peigang Dube, Marc A. Tremblay, Andre Y. Natural Sciences and Engineering Research Council of Canada (NSERC); Ford Foundation The authors would like to thank the Natural Sciences and Engineering Research Council of Canada (NSERC) and the Ford Foundation for financial support. Pergamon-elsevier science ltd Oxford. xiv, 10

Carbonell, R.G. (2000). Multiphase flow models in packed beds. *Oil & Gas Science and Technology-Revue D Ifp Energies Nouvelles*, **55**, 417–425, iSI Document Delivery No.: 431BG Times Cited: 25 Cited Reference Count: 50 Carbonell, RG Editions technip Paris 15 Si. 81, 82

Chen, Y., Enearu, O., Montalvao, D. & Sutharssan, T. (2016). A review of computational fluid dynamics simulations on pefc performance. *Journal of Applied Mechanical Engineering*. 54

Chen, Y.H., Wang, L.C., Tsai, C.H. & Shang, N.C. (2010). Continuous-flow esterification of free fatty acids in a rotating packed bed. *Industrial & Engineering Chemistry Research*, **49**, 4117–4122, iSI Document Delivery No.: 588BR Times Cited: 2 Cited Reference Count: 34 Chen, Yi-Hung Wang, Liang-Chi Tsai, Cheng-Hsien Shang, Neng-Chou National Science Council of Taiwan [NSC 98-2622-E-027-025-CC3, NSC 98-3114-E-007-013, NSC 98-3114-E-002-011] This study was supported by the National Science Council of Taiwan under Grant Nos. NSC 98-2622-E-027-025-CC3, NSC 98-3114-E-007-013, and NSC 98-3114-E-002-011. Amer chemical soc Washington. xiv, 9

Cheng, N.S. (1997). Simplified settling velocity formula for sediment particle. *Journal of Hydraulic Engineering-Asce*, **123**, 149–152, iSI Document Delivery No.: WF419 Times Cited: 137 Cited Reference Count: 14 Cheng, NS Asce-amer soc civil engineers New york. 73

Dai, J.Y., Li, D.Y., Zhao, Y.C. & Xiu, Z.L. (2014). Statistical optimization for biodiesel production from soybean oil in a microchannel reactor. *Industrial & Engineering Chemistry Research*, **53**, 9325–9330, iSI Document Delivery No.: AI6WP Times Cited: 0 Cited Reference Count: 23 Dai, Jian-Ying

Li, Dong-Yuan Zhao, Yu-Chao Xiu, Zhi-Long Fundamental Research Funds for the Central Universities [DUT11NY02] This work was supported by the Fundamental Research Funds for the Central Universities (No. DUT11NY02). Amer chemical soc Washington. 1, 45

Dai, Z., Guo, Z., Fletcher, D.F. & Haynes, B.S. (2015). Taylor flow heat transfer in microchannelsunification of liquidliquid and gasliquid results. *Chemical Engineering Science*, **138**, 140 – 152. xix, 33, 126, 131, 137, 139, 140, 141, 142, 147

Dake, L. (1978). *Fundamentals of Reservoir Engineering*. Elsevier. 54, 80, 81

Demirbas, A. (2009). Progress and recent trends in biodiesel fuels. *Energy Conversion and Management*, **50**, 14–34, iSI Document Delivery No.: 400SY Times Cited: 331 Cited Reference Count: 156 Demirbas, Ayhan Pergamon-elsevier science ltd Oxford. 40

Dessimoz, A.L., Cavin, L., Renken, A. & Kiwi-Minsker, L. (2008). Liquid-liquid two-phase flow patterns and mass transfer characteristics in rectangular glass microreactors. *Chemical Engineering Science*, **63**, 4035–4044, iSI Document Delivery No.: 346NW Times Cited: 69 Cited Reference Count: 33 Dessimoz, Anne-Laure Cavin, Laurent Renken, Albert Kiwi-Minsker, Lioubov Swiss National Science Foundation; Swiss Commission for Technology and Innovation (CH) Financial support by the Swiss National Science Foundation and the Swiss Commission for Technology and Innovation (CH) is gratefully acknowledged. Pergamon-elsevier science ltd Oxford. 21, 22

Di Serio, M., Mallardo, S., Carotenuto, G., Tesser, R. & Santacesaria, E. (2012). Mg/al hydrotalcite catalyst for biodiesel production in continuous packed bed reactors. *Catalysis Today*, **195**, 54–58, iSI Document Delivery No.: 030KT Times Cited: 2 Cited Reference Count: 27 Di Serio, Martino Mallardo, Salvatore Carotenuto, Giuseppina Tesser, Riccardo Santacesaria, Elio EU Large-Scale Project COPIRIDE [CP-IP 228853]; MIPAF Finanziamento AGROPROM (Bando Bioenergetico) [DM 246/2007] Funding by EU Large-Scale Project COPIRIDE (funding number CP-IP 228853) and

by MIPAF Finanziamento AGROPROM (Bando Bioenergetico DM 246/2007 del 23/10/2007) are acknowledged. Sasol Germany GmbH is thanked for the providing of the PURAL (R) MG76. Elsevier science bv Amsterdam. 45

Dore, V., Tsaoulidis, D. & Angeli, P. (2012). Mixing patterns in water plugs during water/ionic liquid segmented flow in microchannels. *Chemical Engineering Science*, **80**, 334 – 341. 30, 33, 35, 38

Dub, M., Tremblay, A. & Liu, J. (2007). Biodiesel production using a membrane reactor. *Bioresource Technology*, **98**, 639 – 647. 9

e Silva, W.C., Teixeira, L.F., Carvalho, A.K., Mendes, A.A. & de Castro, H.F. (2014). Influence of feedstock source on the biocatalyst stability and reactor performance in continuous biodiesel production. *Journal of Industrial and Engineering Chemistry*, **20**, 881 – 886. 55

Eain, M.M., Egan, V. & Punch, J. (2013). Film thickness measurements in liquid-liquid slug flow regimes. *International Journal of Heat and Fluid Flow*, **44**, 515–523, eain, Marc Mac Giolla Egan, Vanessa Punch, Jeff. xix, 21, 35, 39, 68, 125, 126, 129, 131, 136, 137, 138, 139, 140, 141, 147

Eain, M.M.G. (2014). *On the thermal and hydrodynamic characteristic of liquid-liquid Taylor flows*. Ph.D. thesis, Department of Mechanical, Aeronautical and Biomedical Engineering, University of Limerick. xvi, 60, 64

Eain, M.M.G., Egan, V., Howard, J., Walsh, P., Walsh, E. & Punch, J. (2015). Review and extension of pressure drop models applied to taylor flow regimes. *International Journal of Multiphase Flow*, **68**, 1–9, iSI Document Delivery No.: AX8CA Times Cited: 3 Cited Reference Count: 40 Eain, Marc Mac Giolla Egan, Vanessa Howard, James Walsh, Patrick Walsh, Edmond Punch, Jeff Irish Research Council through the Embark Initiative; Science Foundation Ireland [10/CE/I1883] The authors gratefully acknowledge the financial support of the Irish Research Council through the Embark Initiative. The involvement of Jeff Punch is supported by Science Foundation Ireland under Grant No. 10/CE/I1883. Pergamon-elsevier science ltd Oxford. xix, 21, 22, 30, 36, 39, 65, 66, 70, 71, 111, 128, 131, 136, 137, 142, 143, 144, 145, 146, 147, 155

Fairbrother, F. & Stubbs, A.E. (1935). Studies in electro-endosmosis. part vi. the bubble-tube method of measurement. *Journal of the Chemical Society*. 27, 28, 31

Figueroa, J.A. (2013). *CFD Simulation of Liquid-Liquid Flow in a Packed Bed Reactor*. Master's thesis, School of Chemical and Process Engineering, University of Leeds. 54, 149

Freund, H., Bauer, J., Zeiser, T. & Emig, G. (2005). Detailed simulation of transport processes in fixed-beds. *Industrial & Engineering Chemistry Research*, **44**, 6423–6434, iSI Document Delivery No.: 950AA Times Cited: 21 Cited Reference Count: 65 Freund, H Bauer, J Zeiser, T Emig, G Amer chemical soc Washington. xvi, 46

Gabitto, J. & Tsouris, C. (2008). Drag coefficient and settling velocity for particles of cylindrical shape. *Powder Technology*, **183**, 314 – 322. 71

Ghaini, A., Kashid, M.N. & Agar, D.W. (2010). Effective interfacial area for mass transfer in the liquid-liquid slug flow capillary microreactors. *Chemical Engineering and Processing*, **49**, 358–366, iSI Document Delivery No.: 606HP Times Cited: 19 Cited Reference Count: 28 Ghaini, A. Kashid, M. N. Agar, D. W. German Research Funding Organization (Deutsche Forschungsgesellschaft, DFG) [0611011105/095] The authors would like to thank the German Research Funding Organization (Deutsche Forschungsgesellschaft, DFG) for the financial support (Project. 0611011105/095). Elsevier science sa Lausanne. 38

Ghaini, A., Mescher, A. & Agar, D.W. (2011). Hydrodynamic studies of liquid-liquid slug flows in circular microchannels. *Chemical Engineering Science*, **66**, 1168–1178, iSI Document Delivery No.: 716MR Times Cited: 15 Cited Reference Count: 24 Ghaini, Aras Mescher, Axel Agar, David W. German Research Funding Organization (Deutsche Forschungsgesellschaft, DFG) [0611011105/095] The authors would like to thank the Institute for Analytical Sciences Dortmund (ISAS Dortmund) for the cooperation and the German Research Funding Organization (Deutsche Forschungsgesellschaft, DFG)

for financial support (Project: 0611011105/095). Pergamon-elsevier science ltd Oxford. 30, 38

Gonzalez, A., Nada, E.O. & Castellanos, A.M. (2011). Packed bed reactor for biodiesel production. *Tecnologia, Ciencia y Educacion*. 55

Grosser, K., Carbonell, R.G. & Sundaresan, S. (1988). Onset of pulsing in 2-phase cocurrent downflow through a packed-bed. *Aiche Journal*, **34**, 1850–1860, iSI Document Delivery No.: Q8433 Times Cited: 100 Cited Reference Count: 45 Grosser, k carbonell, rg sundaresan, s Amer inst chemical engineers New york. xvi, 52, 78, 81, 82

Gupta, R., Fletcher, D.F. & Haynes, B.S. (2009). On the cfd modelling of taylor flow in microchannels. *Chemical Engineering Science*, **64**, 2941–2950, iSI Document Delivery No.: 513BW Times Cited: 62 Cited Reference Count: 63 Gupta, Raghvendra Fletcher, David F. Haynes, Brian S. Australian Research Council (ARC) [DP0559516] RG acknowledges the University of Sydney's Henry Bettie and Florence Mabel Gritton research scholarship foundation. This work was supported by an Australian Research Council (ARC) Discovery Grant (DP0559516). Pergamon-elsevier science ltd Oxford. 21, 25, 29, 31, 85, 88, 89, 103

Gupta, R., Fletcher, D.F. & Haynes, B.S. (2010). Cfd modelling of flow and heat transfer in the taylor flow regime. *Chemical Engineering Science*, **65**, 2094–2107, iSI Document Delivery No.: 574KP Times Cited: 29 Cited Reference Count: 60 Gupta, Raghvendra Fletcher, David F. Haynes, Brian S. Heatric division of Meggitt (UK) Ltd; Australian Research Council; University of Sydney's Henry Bertie; Florence Mabel Gritton Research Scholarship Foundation The authors acknowledge Chidambaram Narayanan from TransAT for his technical support. The Heatric division of Meggitt (UK) Ltd and the Australian Research Council are thanked for their financial support of this work. R. Gupta also acknowledges the University of Sydney's Henry Bertie and Florence Mabel Gritton Research Scholarship Foundation. Pergamon-elsevier science ltd Oxford. 21, 25, 28, 29

Gupta, R., Leung, S.S.Y., Manica, R., Fletcher, D.F. & Haynes, B.S. (2013). Hydrodynamics of liquid-liquid taylor flow in microchannels. *Chemical Engineering Science*, **92**, 180–189, iSI Document Delivery No.: 113LW Times Cited: 2 Cited Reference Count: 35 Gupta, Raghvendra Leung, Sharon S. Y. Manica, Rogerio Fletcher, David F. Haynes, Brian S. Australian Research Council [DP120103235] The work was supported under Australian Research Council Discovery Grant DP120103235. R. Gupta and R. Manica would like to thank Evert Klaseboer for his insightful comments and suggestions to improve the manuscript. Pergamon-elsevier science ltd Oxford. xv, 21, 22, 30, 32, 33, 39, 65, 66, 85, 103, 115, 118

Haase, S. (2016). Characterisation of gas-liquid two-phase flow in minichannels with co-flowing fluid injection inside the channel, part i: unified mapping of flow regimes. *International Journal of Multiphase Flow*, **87**, 197–211, times Cited: 0. 21, 22

Haase, S., Murzin, D.Y. & Salmi, T. (2016). Review on hydrodynamics and mass transfer in minichannel wall reactors with gasliquid taylor flow. *Chemical Engineering Research and Design*, **113**, 304 – 329. 21, 31

Han, Y. & Shikazono, N. (2009). Measurement of liquid film thickness in micro square channel. *International Journal of Multiphase Flow*, **35**, 896–903, iSI Document Delivery No.: 504NM Times Cited: 57 Cited Reference Count: 19 Han, Youngbae Shikazono, Naoki MEXT, Japan [20560179] We thank Prof Kasagi, Prof Suzuki and Dr. Hasegawa for the fruitful discussions and suggestions. This work is supported through Grant in Aid for Scientific Research (No. 20560179) by MEXT, Japan. Pergamon-elsevier science ltd Oxford. xix, 28, 30, 31, 67, 125, 136, 138, 139, 141

Harvey, K.B. & Adam (2013). *Process Intensification For Green Chemistry*. John Wiley & Sons, Ltd, School of Chemical Engineering and Advanced Materials, Newcastle University, UK. 1, 6, 11

He, B.B., Singh, A.P. & Thompson, J.C. (2006). A novel continuous-flow reactor using reactive distillation for biodiesel production. *Transactions of the*

Asabe, **49**, 107–112, iSI Document Delivery No.: 057LB Times Cited: 33 Cited Reference Count: 25 He, BB Singh, AP Thompson, JC Amer soc agricultural & biological engineers St joseph. xiv, 11

Hensley, Z.D. & Papavassiliou, D.V. (2014). Drag coefficient correction for spherical and nonspherical particles suspended in square microducts. *Industrial & Engineering Chemistry Research*, **53**, 10465–10474, iSI Document Delivery No.: AK1OG Times Cited: 0 Cited Reference Count: 27 Hensley, Zachary D. Papavassiliou, Dimitrios V. Advanced Energy Consortium Part of this work was done while D.V.P. was serving at the National Science Foundation (NSF). Any opinion, findings, conclusions, or recommendations expressed in this material are those of the authors and do not necessarily reflect the views of the NSF. This work was supported by the Advanced Energy Consortium (http://www.beg.utexas.edu/aec/). Member companies include BP America Inc., BG Group, Petrobras, Schlumberger, Statoil, Shell, Repsol, and Total. Amer chemical soc Washington. 71, 72

Hessel, V., A.Renken, Schouten, J. & Yoshida, J.I. (2009). *Chemical Micro Process Engineering: Processing and Plants*. WILEY-VCH Verlag GmbH & Co. KGaA, Weinheim. 6

Hoang, D.A., van Steijn, V., Portela, L.M., Kreutzer, M.T. & Kleijn, C.R. (2013). Benchmark numerical simulations of segmented two-phase flows in microchannels using the volume of fluid method. *Computers & Fluids*, **86**, 28–36, times Cited: 18. 28, 84

Holdich, R. (2002). *Fundamentals of Particle Technology*. Midland Information Technology and Publishing, United Kingdom. 77

Holub, R., Dudukovi, M. & Ramachandran, P. (1992). A phenomenological model for pressure drop, liquid holdup, and flow regime transition in gas-liquid trickle flow. *Chemical Engineering Science*, **47**, 2343 – 2348, twelfth International Symposium on Chemical Reaction Engineering Today. 49, 50

Howard, J.A. & Walsh, P.A. (2013). Review and extensions to film thickness and relative bubble drift velocity prediction methods in laminar taylor or slug

flows. *International Journal of Multiphase Flow*, **55**, 32–42, iSI Document Delivery No.: 191SC Times Cited: 11 Cited Reference Count: 43 Howard, James A. Walsh, Patrick A. IRCSET 'Embark Initiative' The authors acknowledge the financial support of IRCSET 'Embark Initiative' for supporting this research. Pergamon-elsevier science ltd Oxford. xv, xix, 31, 36, 37, 65, 66, 68, 123, 125, 126, 141, 142

Iliuta, I. & Larachi, F. (1999). The generalized slit model: Pressure gradient, liquid holdup & wetting efficiency in gasliquid trickle flow. *Chemical Engineering Science*, **54**, 5039 – 5045. 51

Iliuta, I. & Larachi, F. (2004). Onset of pulsing in gasliquid trickle bed filtration. *Chemical Engineering Science*, **59**, 1199 – 1211. 53

Iliuta, I., Larachi, F. & Al-Dahhan, M.H. (2000). Double-slit model for partially wetted trickle flow hydrodynamics. *AIChE Journal*, **46**, 597–609. 49

Iordanidi, A. (2002). *Mathematical modeling of catalytic fixed bed reactors*. Ph.D. thesis, Netherlands. 45

Irandoust, S. & Andersson, B. (1989). Liquid film in taylor flow through a capillary. *Industrial & Engineering Chemistry Research*, **28**, 1684–1688. 31, 33, 35

Jacob A. Moulijnn, A.S. & Kapeteijn, F. (2003). The potential of structured reactors in process intensification. *Chemistry for Sustainable Development*, **11**, 3–9. 13

Jiang, Y., Khadilkar, M., Al-Dahhan, M. & Dudukovic, M. (1999). Two-phase flow distribution in 2d trickle-bed reactors. *Chemical Engineering Science*, **54**, 2409 – 2419. 52

Jiang, Y., Khadilkar, M.R., Al-Dahhan, M.H. & Dudukovic, M.P. (2001). Cfd modeling of multiphase flow distribution in catalytic packed bed reactors: scale down issues. *Catalysis Today*, **66**, 209–218, iSI Document Delivery No.: 429FH Times Cited: 19 Cited Reference Count: 42 Jiang, Y Khadilkar,

MR Al-Dahhan, MH Dudukovic, MP 3rd International Symposium on Catalysis in Multiphase Reactors May 29-31, 2000 Naples, italy Elsevier science bv Amsterdam. 48

Jiang, Y., Khadilkar, M.R., Al-Dahhan, M.H. & Dudukovic, A.P. (2002a). Cfd of multiphase flow in packed-bed reactors: I. k-fluid modeling issues. *Aiche Journal*, **48**, 701–715, iSI Document Delivery No.: 544XT Times Cited: 48 Cited Reference Count: 65 Jiang, Y Khadilkar, MR Al-Dahhan, MH Dudukovic, AP Amer inst chemical engineers New york. 52, 82

Jiang, Y., Khadilkar, M.R., Al-Dahhan, M.H. & Dudukovic, M.P. (2002b). Cfd of multiphase flow in packed-bed reactors: I. k-fluid modeling issues. *AIChE Journal*, **48**, 701–715. 52

Joseph, D. (1982). Nonlinear equation governing flow in a saturated porous medium. *Water Resources research*, **18**, 1049–1052. 77

Jovanovic, J., Rebrov, E.V., Nijhuis, T.A., Hessel, V. & Schouten, J.C. (2010). Phase-transfer catalysis in segmented flow in a microchannel: Fluidic control of selectivity and productivity. *Industrial & Engineering Chemistry Research*, **49**, 2681–2687, iSI Document Delivery No.: 566NO Times Cited: 17 Cited Reference Count: 49 Jovanovic, Jovan Rebrov, Evgeny V. Nijhuis, T. A. (Xander) Hessel, Volker Schouten, Jaap C. Netherlands Organisation of Scientific Research The financial support by The Netherlands Organisation of Scientific Research (NWO/CW, TOP Grant of JCS) is gratefully acknowledged. Amer chemical soc Washington. 6, 21, 30, 115

Jovanovic, J., Zhou, W.Y., Rebrov, E.V., Nijhuis, T.A., Hessel, V. & Schouten, J.C. (2011a). Liquid-liquid slug flow: Hydrodynamics and pressure drop. *Chemical Engineering Science*, **66**, 42–54, iSI Document Delivery No.: 678GS Times Cited: 18 Cited Reference Count: 53 Jovanovic, Jovan Zhou, Wenya Rebrov, Evgeny V. Nijhuis, T. A. Hessel, Volker Schouten, Jaap C. Netherlands Organisation of Scientific Research (NWO/CW); JCS The financial support by The Netherlands Organisation of Scientific Research

(NWO/CW, TOP Grant of JCS) was gratefully acknowledged. Pergamon-elsevier science ltd Oxford. 21

Jovanovic, J., Zhou, W.Y., Rebrov, E.V., Nijhuis, T.A., Hessel, V. & Schouten, J.C. (2011b). Liquid-liquid slug flow: Hydrodynamics and pressure drop. *Chemical Engineering Science*, **66**, 42–54, iSI Document Delivery No.: 678GS Times Cited: 15 Cited Reference Count: 53 Jovanovic, Jovan Zhou, Wenya Rebrov, Evgeny V. Nijhuis, T. A. Hessel, Volker Schouten, Jaap C. Netherlands Organisation of Scientific Research (NWO/CW); JCS The financial support by The Netherlands Organisation of Scientific Research (NWO/CW, TOP Grant of JCS) was gratefully acknowledged. Pergamon-elsevier science ltd Oxford. 30, 32, 36, 39, 111, 118

Jovanovic, J., Rebrov, E.V., Nijhuis, T.A., Kreutzer, M.T., Hessel, V. & Schouten, J.C. (2012). Liquid-liquid flow in a capillary microreactor: Hydrodynamic flow patterns and extraction performance. *Industrial & Engineering Chemistry Research*, **51**, 1015–1026, iSI Document Delivery No.: 882UG Times Cited: 9 Cited Reference Count: 38 Jovanovic, Jovan Rebrov, Evgeny V. Nijhuis, T. A. (Xander) Kreutzer, M. T. Hessel, Volker Schouten, Jaap C. Amer chemical soc Washington. 21, 103, 115

Kashid, M. & Kiwi-Minsker, L. (2011). Quantitative prediction of flow patterns in liquid-liquid flow in micro-capillaries. *Chemical Engineering and Processing*, **50**, 972–978, iSI Document Delivery No.: 877PC Times Cited: 5 Cited Reference Count: 19 Kashid, Madhvanand Kiwi-Minsker, Lioubov 7th European Framework Program PILLS Project [CP-FP 214599]; Swiss National Science foundation The authors acknowledge the financial support from the 7th European Framework Program PILLS Project (Grant agreement number: CP-FP 214599) and the Swiss National Science foundation. Elsevier science sa Lausanne Si. xv, 21, 23, 24, 30, 38, 95

Kashid, M.N. & Agar, D.W. (2007). Hydrodynamics of liquid-liquid slug flow capillary microreactor: Flow regimes, slug size and pressure drop. *Chemical Engineering Journal*, **131**, 1–13, iSI Document Delivery No.: 177XZ Times

Cited: 68 Cited Reference Count: 11 Kashid, Madhvanand N. Agar, David W. Elsevier science sa Lausanne. 21, 30, 32, 35, 36, 38

Kashid, M.N., Gerlach, I., Goetz, S., Franzke, J., Acker, J.F., Platte, F., Agar, D.W. & Turek, S. (2005). Internal circulation within the liquid slugs of a liquid-liquid slug-flow capillary microreactor. *Industrial & Engineering Chemistry Research*, **44**, 5003–5010, iSI Document Delivery No.: 944NN Times Cited: 93 Cited Reference Count: 27 Kashid, MN Gerlach, I Goetz, S Franzke, J Acker, JF Platte, F Agar, DW Turek, S Amer chemical soc Washington. xix, 21, 31, 38, 115, 126, 141, 142

Kashid, M.N., Agar, D.W. & Turek, S. (2007a). Cfd modelling of mass transfer with and without chemical reaction in the liquid-liquid slug flow microreactor. *Chemical Engineering Science*, **62**, 5102–5109, iSI Document Delivery No.: 212DB Times Cited: 30 Cited Reference Count: 12 Kashid, M. N. Agar, D. W. Turek, S. 19th International Symposium on Chemical Reaction Engineering (ISCRE 19) Sep, 2006 Potsdam, GERMANY BASF, Bayer Healthcare AG, Cargill bvba, Clariant Produkte GmbH, Degussa AG, Schering AG, Siemens AG, SOLVAY GmbH, UHDE GmbH, UHDE Inventa Fischer GbbH Pergamon-elsevier science ltd Oxford Si. 21, 31, 32

Kashid, M.N., Harshe, Y.M. & Agar, D.W. (2007b). Liquid-liquid slug flow in a capillary: An alternative to suspended drop or film contactors. *Industrial & Engineering Chemistry Research*, **46**, 8420–8430, iSI Document Delivery No.: 235OT Times Cited: 47 Cited Reference Count: 19 Kashid, M. N. Harshe, Y. M. Agar, D. W. Joint 6th International Symposium on Catalysis in Multiphase Reactors/5th International Symposium on Multifunctional Reactors (CAMURE-6/ISMR-5-) Jan 14-17, 2007 Pune, INDIA Amer chemical soc Washington. 21, 31, 32

Kashid, M.N., Gupta, A., Renken, A. & Kiwi-Minsker, L. (2010a). Numbering-up and mass transfer studies of liquid-liquid two-phase microstructured reactors. *Chemical Engineering Journal*, **158**, 233–240, iSI Document Delivery No.: 584FV Times Cited: 25 Cited Reference Count: 18 Kashid, M.

N. Gupta, A. Renken, A. Kiwi-Minsker, L. Elsevier science sa Lausanne. 21, 32, 87, 118

Kashid, M.N., Renken, A. & Kiwi-Minsker, L. (2010b). Cfd modelling of liquid-liquid multiphase microstructured reactor: Slug flow generation. *Chemical Engineering Research & Design*, **88**, 362–368, iSI Document Delivery No.: 586CH Times Cited: 13 Cited Reference Count: 23 Kashid, M. N. Renken, A. Kiwi-Minsker, L. Inst chemical engineers Rugby Si. xv, 32

Kashid, M.N., Renken, A. & Kiwi-Minsker, L. (2011). Influence of flow regime on mass transfer in different types of microchannels. *Industrial & Engineering Chemistry Research*, **50**, 6906–6914, iSI Document Delivery No.: 767GS Times Cited: 14 Cited Reference Count: 19 Kashid, Madhvanand N. Renken, Albert Kiwi-Minsker, Lioubov 7th European Framework Program PILLS Project [CP-FP 214599]; Swiss National Science foundation The authors acknowledge the financial support from the 7th European Framework Program PILLS Project (Grant Agreement No. CP-FP 214599) and the Swiss National Science foundation. The authors also thank Patrick Lob and Rami Haidar (Institut fur Mikrotechnik Mainz GmbH (IMM), Main; Germany) for providing caterpillar microchannels, as a part of the PILLS project. Amer chemical soc Washington. 21

Kashid, M.N., Kowalinski, W., Renken, A., Baldyga, J. & Kiwi-Minsker, L. (2012). Analytical method to predict two-phase flow pattern in horizontal micro-capillaries. *Chemical Engineering Science*, **74**, 219–232, times Cited: 2. 11

Kraai, G., vanZwol, F., Schuur, B., Heeres, H. & deVries, J. (2008). Two-phase (bio)catalytic reactions in a table-top centrifugal contact separator. *Angewandte Chemie International Edition*, **47**, 3905–3908. 11

Kralisch, D., Staffel, C., Ott, D., Bensaid, S., Saracco, G., Bellantoni, P. & Loeb, P. (2013). Process design accompanying life cycle management and risk analysis as a decision support tool for sustainable biodiesel production. *Green Chemistry*, **15**, 463–477, iSI Document Delivery

No.: 079QH Times Cited: 7 Cited Reference Count: 101 Kralisch, Dana Staffel, Christin Ott, Denise Bensaid, Samir Saracco, Guido Bellantoni, Pierluigi Loeb, Patrick Eu [cp-ip 228853] The financial support of the EU Seventh Framework Programme for Research and Technological Development (CP-IP 228853, COPIRIDE) is gratefully acknowledged. Royal soc chemistry Cambridge. 1

Kreutzer, M.T. (2003). *Hydrodynamics of Taylor Flow in Capillaries and Monolithic Reactors*. Ph.D. thesis. 21

Kreutzer, M.T. & Gunther, A. (2009). *Micro Process Engineering, Vol. 1: Fundamentals, Operations and Catalysts*. WILEY-VCH Verlag GmbH & Co. KGaA, Weinheim. 61

Kreutzer, M.T., Kapteijn, F., Moulijn, J.A., Kleijn, C.R. & Heiszwolf, J.J. (2005). Inertial and interfacial effects on pressure drop of taylor flow in capillaries. *Aiche Journal*, **51**, 2428–2440, iSI Document Delivery No.: 955PB Times Cited: 126 Cited Reference Count: 46 Kreutzer, MT Kapteijn, F Moulijn, JA Kleijn, CR Heiszwolf, JJ John wiley & sons inc Hoboken. xix, 13, 15, 27, 29, 30, 34, 70, 111, 128, 142, 143, 149

Kundu, A., Saroha, A.K. & Nigam, K.D.P. (2001). Liquid distribution studies in trickle-bed reactors. *Chemical Engineering Science*, **56**, 5963–5967, iSI Document Delivery No.: 503AP Times Cited: 20 Cited Reference Count: 9 Kundu, A Saroha, AK Nigam, KDP 5th International Conference on Gas-Liquid and Gas-Liquid-Solid Reactor Engineering Sep 23-27, 2001 Melbourne, australia Australian Res Council Special Res Ctr Multiphase Processes, Univ Newcastle Pergamon-elsevier science ltd Oxford. 48

Kundu, A., Nigam, K.D.P. & Verma, R.P. (2003). Catalyst wetting characteristics in trickle-bed reactors. *AIChE Journal*, **49**, 2253–2263. 51

Lac, E. & Sherwood, J.D. (2009). Motion of a drop along the centreline of a capillary in a pressure-driven flow. *Journal of Fluid Mechanics*, **640**, 27–54, iSI Document Delivery No.: 538LH Times Cited: 22 Cited Reference Count: 30 Lac, Etienne Sherwood, J. D. E.U. Marie Curie fellowship [IEF-041766] This work was partially funded by an E.U. Marie Curie fellowship awarded to E.L.,

contract IEF-041766 (EOTIP). Cambridge univ press New york. xvi, 29, 61, 65, 115

Lakota, A., Levec, J. & Carbonell, R.G. (2002). Hydrodynamics of trickling flow in packed beds: Relative permeability concept. *AIChE Journal*, **48**, 731–738. 50

Langewisch, D.R. & Buongiorno, J. (2015). Prediction of film thickness, bubble velocity, and pressure drop for capillary slug flow using a cfd-generated database. *International Journal of Heat and Fluid Flow*, **54**, 250–257, iSI Document Delivery No.: CO0CM Times Cited: 1 Cited Reference Count: 36 Langewisch, D. R. Buongiorno, J. AREVA Doctoral Fellowship program We are grateful to the AREVA Doctoral Fellowship program for supporting this research. Elsevier science inc New york. xviii, xix, 29, 31, 68, 71, 125, 126, 128, 131, 132, 133, 134, 135, 140, 142, 147

Lappalainen, K., Gorshkova, E., Manninen, M. & Alopaeus (2009). Cfd modeling of radial spreading of flow in trickle-bed reactors due to mechanical and capillary dispersion. *Chemical Engineering Science 64, 207-218*. 52

Lappalainen, K., Gorshkova, E., Manninen, M. & Alopaeus (2011). Characteristics of liquid and tracer dispersion in trickle-bed reactors: Effect on cfd modeling and experimental analyses. *Computers & Chemical Engineering, 35, 41-49.*. 52

Leung, S.S.Y., Liu, Y., Fletcher, D.F. & Haynes, B. (2010). Heat transfer in well-characterised taylor flow. *Chemical Engineering Science*, **65**, 6379–6388, iSI Document Delivery No.: 678GG Times Cited: 17 Cited Reference Count: 30 Leung, Sharon S. Y. Liu, Yang Fletcher, David F. Haynes, Brian S. Australian Government; Australian Research Council [DP0559516, DP0985453]; Heatric Division of Meggitt (UK) S. Leung was supported through the Endeavour International Postgraduate Research Scholarship funded by the Australian Government. The authors are thankful to R. Gupta for his fruitful discussions. This work was supported under Australian Research Council Discovery Grants DP0559516 and DP0985453. The financial support of the Heatric

Division of Meggitt (UK) is gratefully acknowledged. Pergamon-elsevier science ltd Oxford. xiv, 3

Leung, S.S.Y., Gupta, R., Fletcher, D.F. & Haynes, B.S. (2012). Gravitational effect on taylor flow in horizontal microchannels. *Chemical Engineering Science*, **69**, 553–564, iSI Document Delivery No.: 865QQ Times Cited: 4 Cited Reference Count: 30 Leung, Sharon S. Y. Gupta, Raghvendra Fletcher, David F. Haynes, Brian S. Endeavor International Postgraduate Research Scholarship; Australian Government; Australian Research Council [DP0985453]; Heatric Division of Meggitt (UK) S. Leung was supported through the Endeavor International Postgraduate Research Scholarship funded by the Australian Government. The work was supported under Australian Research Council Discovery Grant DP0985453. The financial support of the Heatric Division of Meggitt (UK) is also gratefully acknowledged. Pergamon-elsevier science ltd Oxford. 21, 28

Levec, J., Saez, A.E. & Carbonell, R.G. (1986). The hydrodynamics of trickling flow in packed-beds .2. experimental-observations. *Aiche Journal*, **32**, 369–380, iSI Document Delivery No.: A5792 Times Cited: 91 Cited Reference Count: 21 Levec, j saez, ae carbonell, rg Amer inst chemical engineers New york. 49, 50, 78, 80

Leverett, M. (1941). Capillary behaviour in porous solids. *Transactions of the AIME (142): 159172*. 51, 52, 81

Li, Q. & Angeli, P. (2017). Experimental and numerical hydrodynamic studies of ionic liquid-aqueous plug flow in small channels. *Chemical Engineering Journal*, **328**, 717 – 736. xv, xix, 21, 30, 34, 39, 103, 109, 115, 125, 126, 128, 131, 140, 141, 142

Liu, H., Vandu, C.O. & Krishna, R. (2005). Hydrodynamics of taylor flow in vertical capillaries: Flow regimes, bubble rise velocity, liquid slug length, and pressure drop. *Industrial & Engineering Chemistry Research*, **44**, 4884–4897, iSI Document Delivery No.: 944NN Times Cited: 94 Cited Reference Count: 43 Liu, H Vandu, CO Krishna, R Amer chemical soc Washington. 28, 37, 126

Liu, X.J., Piao, X.L., Wang, Y.J. & Zhu, S.L. (2010). Model study on transesterification of soybean oil to biodiesel with methanol using solid base catalyst. *Journal of Physical Chemistry A*, **114**, 3750–3755, iSI Document Delivery No.: 570WA Times Cited: 8 Cited Reference Count: 26 Liu, Xuejun Piao, Xianglan Wang, Yujun Zhu, Shenlin National Basic Research Plan [2007CB714302]; China Postdoctoral Science Foundation [20080440365] This research has been supported by the National Basic Research Plan (No 2007CB714302) and China Postdoctoral Science Foundation (Grant Number: 20080440365). Amer chemical soc Washington. 3

Liu, Y., Lotero, E. & Goodwin, J.G. (2006). A comparison of the esterification of acetic acid with methanol using heterogeneous versus homogeneous acid catalysis. *Journal of Catalysis*, **242**, 278 – 286. 54

Lopes, R.J., de Sousa, V.S. & Quinta-Ferreira, R.M. (2011). Cfd and experimental studies of reactive pulsing flow in environmentally-based trickle-bed reactors. *Chemical Engineering Science*, **66**, 3280 – 3290, 10th International Conference on GasLiquid and GasLiquidSolid Reactor Engineering. 53

Lopez-Guajardo, E., Ortiz-Nadal, E., Montesinos-Castellanos, A. & Nigam, K.D.P. (2017). Process intensification of biodiesel production using a tubular micro-reactor (tmr): Experimental and numerical assessment. *Chemical Engineering Communications*, **204**, 467–475. xiv, xvi, 5, 43, 44

Lui, D. (2012). Dielectrophoresis-based micropumping and self-assembly of nanostructures. *International Journal of Micro-Nanoscale Thermal Fluid Transport Phenomena*. xiv, 22

Macdonald, I.F., Elsayed, M.S., Mow, K. & Dullien, F.A.L. (1979). Flow through porous-media - ergun equation revisited. *Industrial & Engineering Chemistry Fundamentals*, **18**, 199–208, iSI Document Delivery No.: HD935 Times Cited: 374 Cited Reference Count: 20 Macdonald, if elsayed, ms mow, k dullien, fal Amer chemical soc Washington. 49, 78

Muradoglu, M. & Tryggvason, G. (2008). A front-tracking method for computation of interfacial flows with soluble surfactants. *Journal of Computational Physics*, **227**, 2238 – 2262. 28

Nakahara, M. & Sano, Y. (2009). Uranium, plutonium and neptunium corecovery with high nitric acid concentration in extraction section by simplified solvent extraction process. *Radiochimica Acta*, **97**, 727–731, iSI Document Delivery No.: 538JM Times Cited: 2 Cited Reference Count: 8 Nakahara, M. Sano, Y. Oldenbourg verlag Munich. xiv, 12

Narasimhan, C.S.L., Verma, R.P., Kundu, A. & Nigam, K.D.P. (2002). Modeling hydrodynamics of trickle-bed reactors at high pressure. *AIChE Journal*, **48**, 2459–2474. 49, 51

Nemec, D. & Levec, J. (2005). Flow through packed bed reactors: 2. two-phase concurrent downflow. *Chemical Engineering Science*, **60**, 6958 – 6970. 49, 50

Nemec, D., Beri, G. & Levec, J. (2001). The hydrodynamics of trickling flow in packed beds operating at high pressures. the relative permeability concept. *Chemical Engineering Science*, **56**, 5955 – 5962, proceedings of the 5th International Conference on Gas-Liquid and Gas-Liquid-Solid Reactor Engineering. 50

Olabi, A.G. (2013). State of the art on renewable and sustainable energy. *Energy*, **61**, 2–5, iSI Document Delivery No.: 261SN Times Cited: 0 Cited Reference Count: 45 Olabi, A. G. Pergamon-elsevier science ltd Oxford. 1

Omota, F., Dimian, A.C. & Bliek, A. (2003). Fatty acid esterification by reactive distillation. part 1: equilibrium-based design. *Chemical Engineering Science*, **58**, 3159 – 3174. 10

Qiao, B., Zhou, D., Li, G., Yin, J., Xue, S. & Liu, J. (2016). Process enhancement of supercritical methanol biodiesel production by packing beds. *Bioresource Technology*. 1, 14

Qiu, Z.Y., Zhao, L.N. & Weather, L. (2010). Process intensification technologies in continuous biodiesel production. *Chemical Engineering and Processing*, **49**, 323–330, iSI Document Delivery No.: 606HP Times Cited: 37 Cited Reference Count: 42 Qiu, Zheyan Zhao, Lina Weather, Laurence Elsevier science sa Lausanne. 6, 7, 10, 15, 40

Raimondi, N.D., Prat, L., Gourdon, C. & Cognet, P. (2008). Direct numerical simulations of mass transfer in square microchannels for liquid-liquid slug flow. *Chemical Engineering Science*, **63**, 5522–5530, iSI Document Delivery No.: 381VS Times Cited: 17 Cited Reference Count: 26 Raimondi, Nathalie Di Miceli Prat, Laurent Gourdon, Christophe Cognet, Patrick 6th Framework EU [NMP2-CF-2005-011816]; Institut National Polytechnique of Toulouse This work has been supported by 6th Framework EU under Grant IMPULSE no: NMP2-CF-2005-011816 and the Institut National Polytechnique of Toulouse (see http://www.inp-toulouse.fr). Experiments presented in this paper were carried out using the Grid'5000 experimental testbed, an initiative from the French Ministry of Research through the ACI GRID incentive action, INRIA, CNRS and RENATER and other contributing partners (see http://www.grid5000.fr). Pergamon-elsevier science ltd Oxford. 21, 22, 115

Raimondi, N.D., Prat, L., Gourdon, C. & Tasselli, J. (2014). Experiments of mass transfer with liquid-liquid slug flow in square microchannels. *Chemical Engineering Science*, **105**, 169–178, iSI Document Delivery No.: 274BN Times Cited: 0 Cited Reference Count: 43 Raimondi, N. Di Miceli Prat, L. Gourdon, C. Tasselli, J. EU [NMP2-CT-2005-011816]; Institut National Polytechnique of Toulouse This work has been supported by the 6th Framework EU under Grant IMPULSE no NMP2-CT-2005-011816 and the Institut National Polytechnique of Toulouse. Other contributing partners are CNRS, the University of Toulouse and LAAS. Pergamon-elsevier science ltd Oxford. 21, 30, 115

Ramamurthi, K.B. (2012). Viscous incompressible flows (chapter 8). xvi, 63, 64

Rase, H.F. (1990). *Fixed-Bed Reactor Design and Diagnostics*. Butterworth Publishers. 14

Rebrov, E.V. (2010). Two-phase flow regimes in microchannels. *Theoretical Foundations of Chemical Engineering*, **44**, 355–367. 25

Reinecke, N. & Mewes, D. (1997). Investigation of the two phase flow in trickle-bed reactors using capacitance tomography. *Chemical Engineering Science*, **52**, 2111–2127, iSI Document Delivery No.: XJ036 Times Cited: 42 Cited Reference Count: 34 Reinecke, N Mewes, D International Conference on Frontiers in Industrial Process Tomography Oct 29-nov 03, 1995 San luis obispo, ca Engn Fdn, Amer Inst Chem Engineers, Engn & Phys Sci Res Council (UK), Natl Sci Fdn, Unilever Res, Port Sunlight, UK, Inst Chem Engineers, Particle Technol Subject Grp Pergamon-elsevier science ltd Oxford. xiv, xvi, 13, 14, 47

Rigg, R.G. & Churchill, S.W. (1964). The behavior of immiscible liquids in concurrent flow through packed beds. *Aiche Journal*, **10**, 810–816, iSI Document Delivery No.: WW633 Times Cited: 7 Cited Reference Count: 17 Rigg, rg churchill, sw Amer inst chemical engineers New york. 79

Saez, A.E. & Carbonell, R.G. (1985). Hydrodynamic parameters for gas-liquid cocurrent flow in packed-beds. *Aiche Journal*, **31**, 52–62, iSI Document Delivery No.: AAC15 Times Cited: 191 Cited Reference Count: 41 Saez, ae carbonell, rg Amer inst chemical engineers New york. 49, 50, 52, 78, 80, 81

Saez, A.E., Carbonell, R.G. & Levec, J. (1986). The hydrodynamics of trickling flow in packed-beds .1. conduit models. *Aiche Journal*, **32**, 353–368, iSI Document Delivery No.: A5792 Times Cited: 36 Cited Reference Count: 25 Saez, ae carbonell, rg levec, j Amer inst chemical engineers New york. 79

Santacesaria, E., Di Serio, M., Tesser, R., Tortorelli, M., Turco, R. & Russo, V. (2011). A simple device to test biodiesel process intensification. *Chemical Engineering and Processing*, **50**, 1085–1094, iSI Document Delivery No.: 877PC Times Cited: 6 Cited Reference Count: 20 Santacesaria, E. Di Serio, M. Tesser, R. Tortorelli, M. Turco, R. Russo, V. EC [CP-IP 228853-2]; MIPAF (Italian Ministry of Agricultural, Food and Forest Policies) [246/2007,

16912/7303/10] Thanks are due to EC VII Framework Programme CP-IP 228853-2 COPIRIDE and to MIPAF (Italian Ministry of Agricultural, Food and Forest Policies) "Project AGROPROM - New technologies for the production of biodiesel from waste oil and fats sources" D.M. 246/2007 (23/10/2007) and 16912/7303/10 (23/7/2010) for the financial support. Elsevier science sa Lausanne Si. 2, 15, 40, 42

Santacesaria, E., Di Serio, M., Tesser, R., Turco, R., Tortorelli, M. & Russo, V. (2012a). Biodiesel process intensification in a very simple microchannel device. *Chemical Engineering and Processing*, **52**, 47–54, iSI Document Delivery No.: 918TT Times Cited: 2 Cited Reference Count: 29 Santacesaria, E. Di Serio, M. Tesser, R. Turco, R. Tortorelli, M. Russo, V. EC VII Framework Programme [CP-IP 228853-2 COPIRIDE]; MIPAF (Italian Ministry of Agricultural, Food and Forest Policies) [D.M. 246/2007, 16912/7303/10] Thanks are due to EC VII Framework Programme CP-IP 228853-2 COPIRIDE and to MIPAF (Italian Ministry of Agricultural, Food and Forest Policies) "Project AGROPROM - New technologies for the production of biodiesel from waste oil and fats sources" D.M. 246/2007 (23/10/2007) and 16912/7303/10 (23/7/2010) for the financial support. Elsevier science sa Lausanne. xv, 40, 42, 43

Santacesaria, E., Turco, R., Tortorelli, M., Russo, V., Di Serio, M. & Tesser, R. (2012b). Biodiesel process intensification by using static mixers tubular reactors. *Industrial & Engineering Chemistry Research*, **51**, 8777–8787, iSI Document Delivery No.: 967BB Times Cited: 2 Cited Reference Count: 22 Santacesaria, E. Turco, R. Tortorelli, M. Russo, V. Di Serio, M. Tesser, R. EC VII Framework Programme [CP-IP 228853-2 COPIRIDE]; MIPAF (Italian Ministry of Agricultural, Food and Forest Policies) "Project AGROPROM - New technologies for the production of biodiesel from waste oil and fats sources" [D.M. 246/2007, 16912/7303/10] Thanks are due to EC VII Framework Programme CP-IP 228853-2 COPIRIDE and to MIPAF (Italian Ministry of Agricultural, Food and Forest Policies) "Project AGROPROM - New technologies for the production of biodiesel from waste oil and fats sources"

D.M. 246/2007 (23/10/2007) and 16912/7303/10 (23/7/2010) for the financial support. Amer chemical soc Washington. 2, 3, 54

Shao, N., Gavriilidis, A. & Angeli, P. (2009). Flow regimes for adiabatic gas-liquid flow in microchannels. *Chemical Engineering Science*, **64**, 2749–2761, iSI Document Delivery No.: 452IV Times Cited: 44 Cited Reference Count: 53 Shao, N. Gavriilidis, A. Angeli, P. Pergamon-elsevier science ltd Oxford. xv, 21, 22, 23, 25

Shao, N., Gavriilidis, A. & Angeli, P. (2010). Mass transfer during taylor flow in microchannels with and without chemical reaction. *Chemical Engineering Journal*, **160**, 873–881, iSI Document Delivery No.: 617QL Times Cited: 26 Cited Reference Count: 32 Shao, N. Gavriilidis, A. Angeli, P. 10th International Conference on Microreaction Technology (IMRET 10) Apr, 2008 New Orleans, LA Amer Chem Soc, Amer Inst Chem Engineers, AIChE Elsevier science sa Lausanne Si. 29

Sharma, Y.C., Singh, B. & Korstad, J. (2011). Latest developments on application of heterogenous basic catalysts for an efficient and eco friendly synthesis of biodiesel: A review. *Fuel*, **90**, 1309 – 1324. 54

Shuit, S.H., Ong, Y.T., Lee, K.T., Subhash, B. & Tan, S.H. (2012). Membrane technology as a promising alternative in biodiesel production: A review. *Biotechnology Advances*, **30**, 1364–1380, iSI Document Delivery No.: 047RQ Times Cited: 10 Cited Reference Count: 143 Shuit, Siew Hoong Ong, Yit Thai Lee, Keat Teong Subhash, Bhatia Tan, Soon Huat Ministry of Higher Education of Malaysia; USM Membrane Cluster Grant; Fundamental of Research Grant Scheme (FRGS); Universiti Sains Malaysia Research University (RU) grant; Postgraduate Research Grant Scheme (PRGS) Shuit, S. H. and Ong, Y. T. acknowledge the MyPhD fellowship support from the Ministry of Higher Education of Malaysia. This research work is supported by USM Membrane Cluster Grant, the Fundamental of Research Grant Scheme (FRGS), Universiti Sains Malaysia Research University (RU) grant and the Postgraduate Research Grant Scheme (PRGS). Pergamon-elsevier science ltd Oxford. 10

Silva, C. & Oliveira, J.V. (2014). Biodiesel production through non-catalytic supercritical transesterification: current state and perspectives. *Brazilian Journal of Chemical Engineering*. 55

Solomenko, Z., Haroun, Y., Fourati, M., Larachi, F., Boyer, C. & Augier, F. (2015). Liquid spreading in trickle-bed reactors: Experiments and numerical simulations using eulerianeulerian two-fluid approach. *Chemical Engineering Science*, **126**, 698 – 710. xvi, 53

Somnuk, K., Smithmaitrie, P. & Prateepchaikul, G. (2013). Optimization of continuous acid-catalyzed esterification for free fatty acids reduction in mixed crude palm oil using static mixer coupled with high-intensity ultrasonic irradiation. *Energy Conversion and Management*, **68**, 193–199, iSI Document Delivery No.: 117AZ Times Cited: 5 Cited Reference Count: 19 Somnuk, Krit Smithmaitrie, Pruittikorn Prateepchaikul, Gumpon Higher Education Research Promotion and National Research University Project of Thailand; Office of the Higher Education Commission; Energy Policy and Planning Office of Thailand (EPPO); Faculty of Engineering, Prince of Songkla University This work was supported by the Higher Education Research Promotion and National Research University Project of Thailand, Office of the Higher Education Commission, the Energy Policy and Planning Office of Thailand (EPPO), and the Faculty of Engineering, Prince of Songkla University for providing research funds. Special thanks go to a senior lecturer Mr. Wiwat Sutiwipakorn for reviewing and correcting the English of this paper. Pergamon-elsevier science ltd Oxford. 6

Stanek, V. (1994). *FIXED BED OPERATIONS:Flow Distribution and Efficiency*. ELLIS HORWOOD, Market Cross House, Cooper Street, Chichester, West Sussex, PO19 1EB, England. 46

Stokes, G.G. (1851). On the effect of the internal friction of fluids on the motion of pendulums. *Transactions of the Cambridge Philosophical Society, Part II, 9, 8-106.*. 71

Taitel, Y., Sarica, C. & Brill, J.P. (2000). Slug flow modeling for downward inclined pipe flow: theoretical considerations. *International Journal of Multiphase Flow*, **26**, 833–844, iSI Document Delivery No.: 308JA Times Cited: 9 Cited Reference Count: 23 Taitel, Y Sarica, C Brill, JP Pergamon-elsevier science ltd Oxford. 21

Taylor, G.I. (1961). Deposition of a viscous fluid on the wall of a tube. *Journal of Fluid Mechanics*, **10**, 161–165, iSI Document Delivery No.: WT930 Times Cited: 446 Cited Reference Count: 1 Taylor, gi Cambridge univ press New york. 21, 28, 67, 70

Thulasidas, T.C., Abraham, M.A. & Cerro, R.L. (1995). Bubble-train flow in capillaries of circular and square cross-section. *Chemical Engineering Science*, **50**, 183–199, iSI Document Delivery No.: QG082 Times Cited: 151 Cited Reference Count: 34 Thulasidas, tc abraham, ma cerro, rl Pergamon-elsevier science ltd Oxford. 29

Tice, J.D., Lyon, A.D. & Ismagilov, R.F. (2004). Effects of viscosity on droplet formation and mixing in microfluidic channels. *Analytica Chimica Acta*, **507**, 73 – 77, microfluidics and Lab - On - a - Chip. 32

Triplett, K.A., Ghiaasiaan, S.M., Abdel-Khalik, S.I., LeMouel, A. & McCord, B.N. (1999). Gas-liquid two-phase flow in microchannels - part ii: void fraction and pressure drop. *International Journal of Multiphase Flow*, **25**, 395–410, iSI Document Delivery No.: 188MG Times Cited: 192 Cited Reference Count: 26 Triplett, KA Ghiaasiaan, SM Abdel-Khalik, SI LeMouel, A McCord, BN Pergamon-elsevier science ltd Oxford. 21

Tsaoulidis, D. & Angeli, P. (2016). Effect of channel size on liquid-liquid plug flow in small channels. *AIChE Journal*, **62**, 315–324. 21, 35, 39

Tsaoulidis, D., Dore, V., Angeli, P., Plechkova, N.V. & Seddon, K.R. (2013). Flow patterns and pressure drop of ionic liquid-water two-phase flows in microchannels. *International Journal of Multiphase Flow*, **54**, 1–10, iSI Document Delivery No.: 170BZ Times Cited: 0 Cited Reference Count: 32

Tsaoulidis, Dimitrios Dore, Valentina Angeli, Panagiota Plechkova, Natalia V. Seddon, Kenneth R. Pergamon-elsevier science ltd Oxford. 21, 30, 33, 39

Urseanu, M.I., Boelhouwer, J.G., Bosman, H.J.M., Schroijen, J.C. & Kwant, G. (2005). Estimation of trickle-to-pulse flow regime transition and pressure drop in high-pressure trickle bed reactors with organic liquids. *Chemical Engineering Journal*, **111**, 5–11, iSI Document Delivery No.: 957TM Times Cited: 9 Cited Reference Count: 16 Urseanu, MI Boelhouwer, JG Bosman, HJM Schroijen, JC Kwant, G Elsevier science sa Lausanne. xvi, 48

van Baten, J.M. & Krishna, R. (2004). Cfd simulations of mass transfer from taylor bubbles rising in circular capillaries. *Chemical Engineering Science*, **59**, 2535–2545, iSI Document Delivery No.: 827TU Times Cited: 90 Cited Reference Count: 28 van Baten, JM Krishna, R Pergamon-elsevier science ltd Oxford. 28

van Baten, J.M. & Krishna, R. (2005). Cfd simulations of wall mass transfer for taylor flow in circular capillaries. *Chemical Engineering Science*, **60**, 1117–1126, iSI Document Delivery No.: 894DD Times Cited: 33 Cited Reference Count: 18 van Baten, JM Krishna, R Pergamon-elsevier science ltd Oxford. 21, 89

Vandu, C.O., Liu, H. & Krishna, R. (2005). Mass transfer from taylor bubbles rising in single capillaries. *Chemical Engineering Science*, **60**, 6430–6437, iSI Document Delivery No.: 958ZO Times Cited: 51 Cited Reference Count: 13 Vandu, CO Liu, H Krishna, R 7th International Conference on Gas-Liquid and Gas-Liquid-Solid Feb, 2005 Strasbourg, FRANCE Chem Engn Grp Nancy Pergamon-elsevier science ltd Oxford Si. 21, 28

Walsh, E., Muzychka, Y., Walsh, P., Egan, V. & Punch, J. (2009). Pressure drop in two phase slug/bubble flows in mini scale capillaries. *International Journal of Multiphase Flow*, **35**, 879 – 884. 30, 34, 36, 69, 70, 111, 128, 143, 144

Wang, Y., Chen, J. & Larachi, F. (2013). Modelling and simulation of trickle-bed reactors using computational fluid dynamics: A state-of-the-art review. *The Canadian Journal of Chemical Engineering*, **91**, 136–180. 48, 50, 52, 53, 76, 79, 83

Wang, Y., Shu, C., Huang, H. & Teo, C. (2015a). Multiphase lattice boltzmann flux solver for incompressible multiphase flows with large density ratio. *Journal of Computational Physics*, **280**, 404 – 423. 28

Wang, Y., Shu, C., Shao, J., Wu, J. & Niu, X. (2015b). A mass-conserved diffuse interface method and its application for incompressible multiphase flows with large density ratio. *Journal of Computational Physics*, **290**, 336 – 351. 28

Warnier, M.J.F., de Croon, M., Rebrov, E.V. & Schouten, J.C. (2010). Pressure drop of gas-liquid taylor flow in round micro-capillaries for low to intermediate reynolds numbers. *Microfluidics and Nanofluidics*, **8**, 33–45, iSI Document Delivery No.: 524WM Times Cited: 35 Cited Reference Count: 25 Warnier, M. J. F. de Croon, M. H. J. M. Rebrov, E. V. Schouten, J. C. Springer heidelberg Heidelberg. xix, 30, 36, 70, 128, 142, 143, 168

Wen, Z.Z., Yu, X.H., Tu, S.T., Yan, J.Y. & Dahlquist, E. (2009). Intensification of biodiesel synthesis using zigzag micro-channel reactors. *Bioresource Technology*, **100**, 3054–3060, iSI Document Delivery No.: 435HR Times Cited: 36 Cited Reference Count: 26 Wen, Zhenzhong Yu, Xinhai Tu, Shan-Tung Yan, Jinyue Dahlquist, Erik Swedish Research Links Programme by Swedish Research Council; China Natural Science Foundation [20606011] This study has been financially supported by the Swedish Research Links Programme by Swedish Research Council (VR) and the China Natural Science Foundation (contract No. 20606011). Elsevier sci ltd Oxford. 42

Xie, T.M., Zhang, L.X. & Xu, N.P. (2012). Biodiesel synthesis in microreactors. *Green Processing and Synthesis*, **1**, 61–70, iSI Document Delivery No.: V31MC Times Cited: 2 Cited Reference Count: 49 Xie, Tianming Zhang, Lixiong Xu, Nanping Walter de gruyter gmbh Berlin. xv, 41

Xu, B.J., Cai, W.F., Liu, X.L. & Zhang, X.B. (2013). Mass transfer behavior of liquid-liquid slug flow in circular cross-section microchannel. *Chemical Engineering Research & Design*, **91**, 1203–1211, iSI Document Delivery No.: 174KV Times Cited: 0 Cited Reference Count: 30 Xu, Bujian Cai, Wangfeng Liu, Xiaolei Zhang, Xubin Inst chemical engineers Rugby. 30, 111

Yagodnitsyna, A.A., Kovalev, A.V. & Bilsky, A.V. (2016). Flow patterns of immiscible liquid-liquid flow in a rectangular microchannel with t-junction. *Chemical Engineering Journal*, **303**, 547 – 554. xv, 21, 23, 26, 31

Yam, K.S. (2012). *Physical and Computation Modelling of Turbidity Currents: The Role of Turbulence-Particles Interactions and Interfacial Forces*. Ph.D. thesis, School of Earth & Environment, University of Leeds. 72

Yong, Y., Yang, C., Jiang, Y., Joshi, A., Shi, Y. & Yin, X. (2011). Numerical simulation of immiscible liquid-liquid flow in microchannels using lattice boltzmann method. *Science China Chemistry*, **54**, 244–256. 28

Yuan, H.Z., Shu, C., Wang, Y. & Shu, S. (2018). A simple mass-conserved level set method for simulation of multiphase flows. *Physics of Fluids*, **30**, 040908. 28

Zelic, A.S. & Bruno (2011). Microreactors-portable factories for biodiesel fuel production. *goriva i maziva*, **50**, 85–110. 40

Zhao, W., Zhang, S., Lu, M., Shen, S., Yun, J., Yao, K., Xu, L., Lin, D.Q., Guan, Y.X. & Yao, S.J. (2014). Immiscible liquidliquid slug flow characteristics in the generation of aqueous drops within a rectangular microchannel for preparation of poly(2-hydroxyethylmethacrylate) cryogel beads. *Chemical Engineering Research and Design*, **92**, 2182 – 2190. xv, 25, 26